

---

**FINAL REPORT**

**U.F. Project No: 00088115**  
**FDOT Project No: BDK75 977-34**

---

**USE OF RECLAIMED ASPHALT PAVEMENT  
IN CONCRETE PAVEMENT SLABS**

---

**Mang Tia**  
**Nabil Hossiney**  
**Yu-Min Su**  
**Yu Chen**  
**Tu Anh Do**

---

**October 2012**

**Department of Civil and Coastal Engineering**  
**Engineering School of Sustainable Infrastructure and Environment**  
**College of Engineering**  
**University of Florida**  
**Gainesville, Florida 32611-6580**

---

## **DISCLAIMER**

The opinions, findings, and conclusions expressed in this publication are those of the authors and not necessarily those of the State of Florida Department of Transportation or the U.S. Department of Transportation.

Prepared in cooperation with the State of Florida Department of Transportation and the U.S. Department of Transportation.

## SI (MODERN METRIC) CONVERSION FACTORS (from FHWA)

### APPROXIMATE CONVERSIONS TO SI UNITS

SYMBOL	WHEN YOU KNOW	MULTIPLY BY	TO FIND	SYMBOL
<b>LENGTH</b>				
<b>in</b>	inches	25.4	millimeters	mm
<b>ft</b>	feet	0.305	meters	m
<b>yd</b>	yards	0.914	meters	m
<b>mi</b>	miles	1.61	kilometers	km

SYMBOL	WHEN YOU KNOW	MULTIPLY BY	TO FIND	SYMBOL
<b>AREA</b>				
<b>in<sup>2</sup></b>	square inches	645.2	square millimeters	mm <sup>2</sup>
<b>ft<sup>2</sup></b>	square feet	0.093	square meters	m <sup>2</sup>
<b>yd<sup>2</sup></b>	square yard	0.836	square meters	m <sup>2</sup>
<b>ac</b>	acres	0.405	hectares	ha
<b>mi<sup>2</sup></b>	square miles	2.59	square kilometers	km <sup>2</sup>

SYMBOL	WHEN YOU KNOW	MULTIPLY BY	TO FIND	SYMBOL
<b>VOLUME</b>				
<b>fl oz</b>	fluid ounces	29.57	milliliters	mL
<b>gal</b>	gallons	3.785	liters	L
<b>ft<sup>3</sup></b>	cubic feet	0.028	cubic meters	m <sup>3</sup>
<b>yd<sup>3</sup></b>	cubic yards	0.765	cubic meters	m <sup>3</sup>

NOTE: volumes greater than 1000 L shall be shown in m<sup>3</sup>

SYMBOL	WHEN YOU KNOW	MULTIPLY BY	TO FIND	SYMBOL
<b>MASS</b>				
<b>oz</b>	ounces	28.35	grams	g
<b>lb</b>	pounds	0.454	kilograms	kg
<b>T</b>	short tons (2000 lb)	0.907	megagrams (or "metric ton")	Mg (or "t")

SYMBOL	WHEN YOU KNOW	MULTIPLY BY	TO FIND	SYMBOL
<b>TEMPERATURE (exact degrees)</b>				
<b>°F</b>	Fahrenheit	5 (F-32)/9 or (F-32)/1.8	Celsius	°C

SYMBOL	WHEN YOU KNOW	MULTIPLY BY	TO FIND	SYMBOL
<b>ILLUMINATION</b>				
<b>fc</b>	foot-candles	10.76	lux	lx
<b>fl</b>	foot-Lamberts	3.426	candela/m <sup>2</sup>	cd/m <sup>2</sup>

SYMBOL	WHEN YOU KNOW	MULTIPLY BY	TO FIND	SYMBOL
<b>FORCE and PRESSURE or STRESS</b>				
<b>lbf</b>	poundforce	4.45	newtons	N
<b>kip</b>	kilo poundforce	4.45	kilo newtons	kN
<b>lbf/in<sup>2</sup></b>	poundforce per square inch	6.89	kilopascals	kPa

**APPROXIMATE CONVERSIONS TO SI UNITS**

SYMBOL	WHEN YOU KNOW	MULTIPLY BY	TO FIND	SYMBOL
<b>LENGTH</b>				
<b>mm</b>	millimeters	0.039	inches	in
<b>m</b>	meters	3.28	feet	ft
<b>m</b>	meters	1.09	yards	yd
<b>km</b>	kilometers	0.621	miles	mi

SYMBOL	WHEN YOU KNOW	MULTIPLY BY	TO FIND	SYMBOL
<b>AREA</b>				
<b>mm<sup>2</sup></b>	square millimeters	0.0016	square inches	in <sup>2</sup>
<b>m<sup>2</sup></b>	square meters	10.764	square feet	ft <sup>2</sup>
<b>m<sup>2</sup></b>	square meters	1.195	square yards	yd <sup>2</sup>
<b>ha</b>	hectares	2.47	acres	ac
<b>km<sup>2</sup></b>	square kilometers	0.386	square miles	mi <sup>2</sup>

SYMBOL	WHEN YOU KNOW	MULTIPLY BY	TO FIND	SYMBOL
<b>VOLUME</b>				
<b>mL</b>	milliliters	0.034	fluid ounces	fl oz
<b>L</b>	liters	0.264	gallons	gal
<b>m<sup>3</sup></b>	cubic meters	35.314	cubic feet	ft <sup>3</sup>
<b>m<sup>3</sup></b>	cubic meters	1.307	cubic yards	yd <sup>3</sup>

SYMBOL	WHEN YOU KNOW	MULTIPLY BY	TO FIND	SYMBOL
<b>MASS</b>				
<b>g</b>	grams	0.035	ounces	oz
<b>kg</b>	kilograms	2.202	pounds	lb
<b>Mg (or "t")</b>	megagrams (or "metric ton")	1.103	short tons (2000 lb)	T

SYMBOL	WHEN YOU KNOW	MULTIPLY BY	TO FIND	SYMBOL
<b>TEMPERATURE (exact degrees)</b>				
<b>°C</b>	Celsius	1.8C+32	Fahrenheit	°F

SYMBOL	WHEN YOU KNOW	MULTIPLY BY	TO FIND	SYMBOL
<b>ILLUMINATION</b>				
<b>lx</b>	lux	0.0929	foot-candles	fc
<b>cd/m<sup>2</sup></b>	candela/m <sup>2</sup>	0.2919	foot-Lamberts	fl

SYMBOL	WHEN YOU KNOW	MULTIPLY BY	TO FIND	SYMBOL
<b>FORCE and PRESSURE or STRESS</b>				
<b>N</b>	newtons	0.225	poundforce	lbf
<b>kPa</b>	kilopascals	0.145	poundforce per square inch	lbf/in <sup>2</sup>

\*SI is the symbol for International System of Units. Appropriate rounding should be made to comply with Section 4 of ASTM E380. (Revised March 2003)

## TECHNICAL REPORT DOCUMENTATION PAGE

1. Report No. 00088115	2. Government Accession No.	3. Recipient's Catalog No.	
4. Title and Subtitle  Use of Reclaimed Asphalt Pavement in Concrete Pavement Slabs		5. Report Date October 2012	
		6. Performing Organization Code	
7. Author(s) Mang Tia, Nabil Hossiney, Yu-Min Su, Yu Chen & Tu Ahn Do		8. Performing Organization Report No. 00088115	
9. Performing Organization Name and Address Department of Civil and Coastal Engineering Engineering School of Sustainable Infrastructure & Environment University of Florida 365 Weil Hall – P.O. Box 116580 Gainesville, FL 32611-6580		10. Work Unit No. (TR AIS)	
		11. Contract or Grant No.  BDK75 977-34	
12. Sponsoring Agency Name and Address  Florida Department of Transportation 605 Suwannee Street, MS 30 Tallahassee, FL 32399		13. Type of Report and Period Covered Final Report 5/13/10 – 10/30/12	
		14. Sponsoring Agency Code	
15. Supplementary Notes Prepared in cooperation with the U.S. Department of Transportation and the Federal Highway Administration			
16. Abstract <p>This study evaluated the feasibility of using RAP as aggregate replacement in concrete for use in pavement. Four different RAPs from FDOT approved RAP sources were used. Concrete mixtures with 0%, 20%, 40%, 70% and 100% aggregate replacement by RAP were produced and evaluated.</p> <p>The compressive strength, modulus of elasticity, splitting tensile strength and flexural strength of concrete were observed to decrease as the percentage of RAP increased in the concrete mix. The reduction in flexural strength was 10% to 20% lower than the corresponding reduction in compressive strength. The percent reduction in modulus of elasticity of the concrete was much higher than the corresponding reduction in compressive strength. The failure strain and toughness of concrete increased as the percentage of RAP increased in the mix.</p> <p>When a finite element analysis was performed to determine the maximum stresses in a typical concrete pavement in Florida under critical temperature and load conditions, the maximum computed stresses decreased as the RAP content of the mix increased, due to decrease in the elastic modulus of the concrete. Though the flexural strength of the concrete with RAP was lower than that of the conventional concrete, the computed stress to strength ratio for some of the RAP concrete was lower than that for the conventional concrete. The results of analysis of ultimate failure loads of concrete pavement slabs show that, on the average, the pavement slabs using RAP concrete have higher failure load than that of the slab using the conventional concrete.</p> <p>The results of this study indicate that the use of RAP as aggregate replacement in pavement concrete appears to be not only feasible but also offers the possibility of improving the performance of concrete pavement. A recommended mix design procedure for concrete containing RAP is provided. It is recommended that a concrete pavement test section using RAP concrete be constructed within an existing highway to perform field validation.</p>			
17. Key Words Reclaimed Asphalt Pavement (RAP), Concrete Pavement, FEACONS, Critical Stress Analysis, X-Ray CT, Superpave IDT, Flexural Strength, Elastic Modulus, Coefficient of Thermal Expansion, Toughness, Ultimate Failure Load		18. Distribution Statement  No restrictions.	
19. Security Classif. (of this report) Unclassified	20. Security Classif. (of this page) Unclassified	21. No. of Pages 321	22. Price

## **ACKNOWLEDGMENTS**

A compilation of this nature could not have been completed without the help and support of others. The Florida Department of Transportation (FDOT) is gratefully acknowledged for providing the financial support for this study. The FDOT Materials Office provided the additional testing equipment, materials, and personnel needed for this investigation. Sincere thanks and appreciation are extended to the Project Manager, Mr. Michael Bergin, for providing his technical coordination and expert advice throughout the project. Sincere gratitude is extended to FDOT personnel, particularly to Messrs. Richard DeLorenzo, Harvey DeFord, David Webb, Patrick Upshaw, Patrick Carlton and Joseph Fitzgerald for their invaluable help on this project.

# TABLE OF CONTENTS

	<u>page</u>
DISCLAIMER .....	ii
SI (MODERN METRIC) CONVERSION FACTORS (from FHWA) .....	iii
TECHNICAL REPORT DOCUMENTATION PAGE .....	v
ACKNOWLEDGMENTS .....	vi
LIST OF TABLES .....	x
LIST OF FIGURES .....	xiv
TECHNICAL SUMMARY .....	xxii
CHAPTER	
1 BACKGROUND AND RESEARCH OBJECTIVE .....	1
1.1 Problem Statement.....	1
1.2 Research Objectives.....	1
1.3 Scope of the Research.....	1
1.4 Research Approach.....	2
2 LITERATURE REVIEW .....	3
2.1 Characterization of Aggregate Gradation in Concrete .....	3
2.1.1 Maximum Density Method.....	3
2.1.2 Fineness Modulus .....	4
2.1.3 Surface Area and Particle Interface Method .....	5
2.1.4 Coarseness Factor .....	6
2.1.5 Individual Percent Retained .....	8
2.1.6 0.45 Power Chart.....	10
2.2 Effect of Aggregate Gradation on Concrete Properties .....	12
2.3 Properties of Recycled Asphalt Pavement.....	14
2.4 Concrete Properties Containing Recycled Asphalt Pavement.....	16
3 MATERIALS AND EXPERIMENTAL PROGRAM .....	22
3.1 Introduction.....	22
3.2 Selection of Materials .....	22
3.3 Material Properties.....	23
3.3.1 Cement.....	23
3.3.2 Fine Aggregate .....	24

3.3.3	Coarse Aggregate .....	26
3.3.4	Recycled Asphalt Pavement (RAP).....	27
3.4	Concrete Mix Proportions.....	31
4	EVALUATION OF AGGREGATE GRADATIONS OF CONCRETE CONTAINING RAP.....	35
4.1	Combined Aggregate Gradation .....	35
4.2	Evaluation of Aggregate Gradations .....	35
4.2.1	Coarseness Factor of Combined Aggregate .....	37
4.2.2	Individual Percentage Retained of Combined Aggregate .....	40
4.2.3	0.45 Power Chart of Combined Aggregate .....	45
4.3	Summary of Findings .....	50
5	CONCRETE PRODUCTION AND TEST METHODS .....	51
5.1	Introduction.....	51
5.2	Fabrication and Curing of Concrete Specimens .....	51
5.2.1	Concrete Preparation .....	51
5.2.2	Specimen Preparation.....	53
5.3	Tests on Fresh Concrete.....	55
5.4	Tests on Hardened Concrete.....	57
5.4.1	Compressive Strength Test.....	57
5.4.2	Young's Modulus and Poisson's Ratio Test .....	58
5.4.3	Flexural Strength Test .....	60
5.4.4	Splitting Tensile Strength Test .....	63
5.4.5	Drying Shrinkage Test.....	64
5.4.6	Coefficient of Thermal Expansion Test .....	65
6	CONCRETE TEST RESULTS AND ANALYSIS.....	69
6.1	Introduction.....	69
6.2	Results of Fresh Concrete Properties.....	69
6.3	Analysis of Strength Test Results.....	71
6.3.1	Compressive Strength Test Results .....	71
6.3.2	Modulus of Elasticity Test Results.....	76
6.3.3	Poisson's Ratio Test Results .....	77
6.3.4	Flexural Strength Test Results.....	83
6.3.5	Modulus of Toughness Test Results.....	88
6.3.6	Splitting Tensile Strength Test Results .....	91
6.3.7	Coefficient of Thermal Expansion Test Results.....	96
6.3.8	Drying Shrinkage Test Results.....	102
6.4	Relationship among the Concrete Properties.....	108
6.4.1	Relationship between Compressive Strength and Flexural Strength .....	108
6.4.2	Relationship between Compressive Strength and Modulus of Elasticity.....	109
6.4.3	Relationship between Compressive Strength and Splitting Tensile Strength .....	111
6.4.4	Relationship between Splitting Tensile Strength and Flexural Strength.....	112

6.5 Summary of Findings .....	113
7 EVALUATION OF POTENTIAL PERFORMANCE IN CONCRETE PAVEMENT SLABS .....	114
7.1 Introduction.....	114
7.2 Critical Stress Analysis Using FEACONS IV Program .....	114
7.3 Analysis Using Mechanistic Empirical Pavement Design Guide.....	115
7.4 Analysis of Ultimate Load to Cause Failure of Pavement Slab .....	124
7.4.1 Finite Element Model .....	124
7.4.2 Modeling of Critical Loading Condition .....	126
7.4.3 Modeling of Stress-Strain Behavior of Concrete Material.....	127
7.4.4 Analysis to Determine Failure Load of Pavement Slab Containing RAP.....	127
7.5 Summary of Findings .....	130
8 DEVELOPMENT OF CRITERIA FOR RAP CONCRETE.....	131
8.1 Development of Stress-Strength Ratio Charts.....	131
9 SUMMARY OF FINDINGS, CONCLUSIONS AND RECOMMENDATIONS.....	137
9.1 Findings from This Study .....	137
9.1.1 Mechanical and Thermal Properties of Concrete Containing RAP.....	137
9.1.2 Combined Aggregate Gradation of Concrete Containing RAP .....	137
9.1.3 Stress Analysis of Concrete Containing RAP .....	138
9.2 Conclusions and Recommendations .....	138
REFERENCES .....	140
APPENDIX	
A STRENGTH TEST DATA.....	144
B STRESS-STRAIN PLOT OF RAP CONCRETE .....	205
C MEPDG INPUT DATA .....	210
D CHARACTERIZATION OF CONCRETE CONTAINING RECLAIMED ASPHALT PAVEMENT BY SUPERPAVE INDIRECT TENSILE TEST AND X-RAY COMPUTED TOMOGRAPHY .....	215

## LIST OF TABLES

<u>Table</u>	<u>page</u>
3-1. Details of the RAP material selected for this research study .....	22
3-2. Physical and chemical properties of Portland cement .....	23
3-3. Specific gravity and water absorption of fine aggregate .....	24
3-4. Gradation of fine aggregate #1 .....	24
3-5. Gradation of fine aggregate #2 .....	25
3-6. Specific gravity and water absorption of coarse aggregate (Florida limestone) .....	26
3-7. Gradation of coarse aggregate #1 (Florida Limestone) .....	26
3-8. Gradation of coarse aggregate #2 (Florida Limestone) .....	26
3-9. Properties of recovered asphalt binder from RAP .....	28
3-10. Specific gravity and water absorption of fine RAP .....	29
3-11. Specific gravity and water absorption of coarse RAP .....	29
3-12. Gradation of fine RAP .....	29
3-13. Gradation of coarse RAP .....	29
3-14. Concrete mixtures containing RAP to be evaluated .....	33
3-15. Mix proportions of concrete mixtures used in this research study .....	34
4-1. Combined gradation of fine aggregate with various percentages of RAP .....	36
4-2. Combined gradation of coarse aggregate with various percentages of RAP .....	36
5-1. Standard tests on fresh and hardened concrete .....	51
5-2. Fresh and hardened concrete tests run per batch of concrete .....	56
6-1. Fresh concrete properties of the mixtures evaluated in this research study .....	70
6-2. Compressive strength of concrete mixtures evaluated .....	72
6-3. Modulus of elasticity of concrete mixtures evaluated .....	77
6-4. Poisson's ratio of concrete mixtures evaluated .....	81

6-5. Flexural Strength of concrete mixtures evaluated .....	84
6-6. Flexural toughness of concrete containing RAP .....	89
6-7. Splitting tensile strength of concrete containing RAP.....	92
6-8. Actual Coefficient of thermal expansion of concrete containing RAP .....	97
6-9. Adjusted coefficient of thermal expansion of concrete containing RAP .....	98
6-10. Drying shrinkage strain of concrete containing RAP after air curing .....	103
6-11. Drying shrinkage strain of concrete containing RAP after moisture curing .....	104
7-1. Performance criteria used in the MEPDG model .....	116
7-2. Results of critical stress analysis using concrete properties at 7 days curing.....	117
7-3. Results of critical stress analysis using concrete properties at 14 days curing.....	118
7-4. Results of critical stress analysis using concrete properties at 28 days curing.....	119
7-5. Results of critical stress analysis using concrete properties at 90 days curing.....	120
7-6. Traffic information used in the MEPDG model.....	122
7-7. Predicted terminal IRI from MEPDG analysis of pavements using concrete containing RAP.....	122
7-8. Predicted mean terminal joint faulting from MEPDG analysis of pavements using concrete containing RAP .....	122
7-9. Predicted terminal transverse cracking from MEPDG analysis of pavement using concrete containing RAP .....	123
7-10. Failure Loading Pressure and Toughness of Concrete Containing RAP.....	128
8-1. Stress analysis for concrete mixtures with a coefficient of thermal expansion of $4.5 \times$ $10^{-6}/^{\circ}\text{F}$ .....	132
8-2. Stress analysis for concrete mixtures with a coefficient of thermal expansion of $5.0 \times$ $10^{-6}/^{\circ}\text{F}$ .....	133
8-3. Stress analysis for concrete mixtures with a coefficient of thermal expansion of $5.5 \times$ $10^{-6}/^{\circ}\text{F}$ .....	133
8-4. Stress analysis for concrete mixtures with a coefficient of thermal expansion of $6.0 \times$ $10^{-6}/^{\circ}\text{F}$ .....	133

A-1. Compressive strength test results for concrete containing no RAP.....	144
A-2. Compressive strength test results for concrete containing RAP-1 .....	146
A-3. Compressive strength test results for concrete containing RAP-2 .....	149
A-4. Compressive strength test results for concrete containing RAP-3 .....	152
A-5. Compressive strength test results for concrete containing RAP-4 .....	155
A-6. Modulus of elasticity and poison’s ratio test results for concrete containing no RAP .....	157
A-7. Modulus of elasticity and poison’s ratio test results for concrete containing RAP-1 .....	159
A-8. Modulus of elasticity and poison’s ratio test results for concrete containing RAP-2 .....	160
A-9. Modulus of elasticity and poison’s ratio test results for concrete containing RAP-3 .....	162
A-10. Modulus of elasticity and poison’s ratio test results for concrete containing RAP-4 .....	163
A-11. Splitting tensile strength test results for concrete containing no RAP .....	165
A-12. Splitting tensile strength test results for concrete containing RAP-1 .....	166
A-13. Splitting tensile strength test results for concrete containing RAP-2 .....	167
A-14. Splitting tensile strength test results for concrete containing RAP-3 .....	168
A-15. Splitting tensile strength test results for concrete containing RAP-4.....	170
A-16. Flexural strength test data for concrete containing no RAP .....	171
A-17. Flexural strength test data for concrete containing RAP-1.....	172
A-18. Flexural strength test data for concrete containing RAP-2.....	174
A-19. Flexural strength test data for concrete containing RAP-3.....	176
A-20. Flexural strength test data for concrete containing RAP-4.....	177
A-21. Modulus of toughness data for concrete containing no RAP .....	178
A-22. Modulus of toughness data for concrete containing RAP-1 .....	179
A-23. Modulus of toughness data for concrete containing RAP-2.....	179
A-24. Modulus of toughness data for concrete containing RAP-3.....	181
A-25. Modulus of toughness data for concrete containing RAP-4.....	182

A-26. Shrinkage test data for concrete containing no RAP after air curing .....	184
A-27. Shrinkage test data for concrete containing RAP-1 after air curing.....	185
A-28. Shrinkage test data for concrete containing RAP-2 after air curing.....	186
A-29. Shrinkage test data for concrete containing RAP-3 after air curing.....	187
A-30. Shrinkage test data for concrete containing RAP-4 after air curing.....	189
A-31. Shrinkage test data for concrete containing no RAP after moist curing.....	190
A-32. Shrinkage test data for concrete containing RAP-1 after moist curing.....	191
A-33. Shrinkage test data for concrete containing RAP-2 after moist curing .....	193
A-34. Shrinkage test data for concrete containing RAP-3 after moist curing .....	194
A-35. Shrinkage test data for concrete containing RAP-4 after moist curing .....	195
A-36. Coefficient of thermal expansion test data for concrete containing no RAP .....	197
A-37. Coefficient of thermal expansion test data for concrete containing RAP-1 .....	198
A-38. Coefficient of thermal expansion test data for concrete containing RAP-2 .....	199
A-39. Coefficient of thermal expansion test data for concrete containing RAP-3 .....	201
A-40. Coefficient of thermal expansion test data for concrete containing RAP-4.....	202
D-1. Results of indirect tension test (using peak stress) .....	237
D-2. Results of indirect tension test (using failure stress) .....	239
D-3. Results of elastic modulus, Poisson’s ratio, and toughness (using peak stress).....	236
D-4. Results fracture energy (using failure stress).....	239
D-5. Load/unload pattern used in Superpave IDT strength test.....	266
D-6. Average air voids under different load levels.....	267

## LIST OF FIGURES

<u>Figure</u>	<u>page</u>
2-1. Representation of aggregate particles in paste (Koehler and Fowler, 2007).....	4
2-2. Examples of mixtures with insufficient paste volume (left) and sufficient paste volume (right) for filling ability (Koehler and Fowler, 2007).....	4
2-3. Coarseness factor chart proposed by Shilstone. ....	8
2-4. Shilstone 8-18 band chart .....	9
2-5. Ideal plot on individual percentage retained chart.....	9
2-6. Problematic plot on individual percentage retained chart .....	10
2-7. 0.45 power chart for a well graded mix .....	11
2-8. 0.45 power chart for a gap graded mix. ....	11
2-9. Individual percent retained for optimized mix .....	13
2-10. 0.45 power chart for optimized mix .....	13
2-11. Coarseness factor chart for optimized mix .....	14
2-12. Gradation of aggregates and RAP (Huang, et al. 2006) .....	15
2-13. Grain size distribution for aggregate and RAP (Al-Oraimi, et al. 2007).....	15
2-14. Particle size distribution of RAP and virgin aggregates (Kang, et al. 2011).....	16
2-15. Propagation of crack through aggregate with and without asphalt film (Huang, et al. 2006). ....	17
2-16. Compressive strength of concrete containing RAP (Al-Oraimi, et al. 2009).....	18
2-17. Reduction in compressive strength of concrete containing RAP (Al-Oraimi, et al. 2009) .....	18
3-1. Gradation chart for virgin fine aggregate .....	25
3-2. Gradation chart for virgin coarse aggregate .....	27
3-3. Gradation chart for fine RAP aggregate .....	30
3-4. Gradation chart for coarse RAP aggregate .....	31

4-1. Coarseness factor chart for concrete mixtures containing 20% RAP.....	38
4-2. Coarseness factor chart for concrete mixtures containing 40% RAP.....	39
4-3. Coarseness factor chart for concrete mixtures containing 70% RAP.....	39
4-4. Coarseness factor chart for concrete mixtures containing 100% RAP.....	40
4-5. Individual percentage retained chart for concrete mixtures containing 20% RAP-1 and 20% RAP-2 .....	41
4-6. Individual percentage retained chart for concrete mixtures containing 20% RAP-3 and 20% RAP-4 .....	42
4-7. Individual percentage retained chart for concrete mixtures containing 40% RAP-1 and 40% RAP-2 .....	42
4-8. Individual percentage retained chart for concrete mixtures containing 40% RAP-3 and 40% RAP-4 .....	43
4-9. Individual percentage retained chart for concrete mixtures containing 70% RAP-1 and 70% RAP-2 .....	43
4-10. Individual percentage retained chart for concrete mixtures containing 70% RAP-3 and 70% RAP-4 .....	44
4-11. Individual percentage retained chart for concrete mixtures containing 100% RAP-1 and 100% RAP-2 .....	44
4-12. Individual percentage retained chart for concrete mixtures containing 100% RAP-3 and 100% RAP-4 .....	45
4-13. 0.45 power chart for gradation of concrete mixtures containing RAP-1.....	46
4-14. 0.45 power chart for gradation of concrete mixtures containing RAP-2.....	47
4-15. 0.45 power chart for gradation of concrete mixtures containing RAP-3.....	48
4-16. 0.45 power chart for gradation of concrete mixtures containing RAP-4.....	49
5-1. Scale used for weighing materials .....	52
5-2. Drum mixer used for mixing concrete.....	52
5-3. Specimens covered with polyethylene sheets.....	54
5-4. Moisture room used for curing specimens .....	54
5-5. Hardened surface of concrete containing RAP.....	55

5-6. Compressive strength test equipment .....	58
5-7. Modulus of elasticity and Poisson's ratio test apparatus .....	60
5-8. Samples tested in flexural strength .....	62
5-9. Flexural strength test apparatus .....	62
5-10. Splitting tensile strength test apparatus .....	64
5-11. Concrete specimens before and after splitting tensile strength test .....	64
5-12. Drying shrinkage extensometer .....	65
5-13. Grinding machine used to grind concrete specimens .....	67
5-14. Coefficient of thermal expansion test equipment .....	67
6-1. Compressive strength of concrete mixtures containing RAP .....	73
6-2. Development of compressive strength at different curing times relative to the strength at 28 days curing time .....	74
6-3. Percentage reduction in compressive strength of concrete containing RAP .....	75
6-4. Modulus of elasticity of concrete mixtures containing RAP .....	78
6-5. Development of modulus of elasticity at different curing times relative to the elastic modulus at 28 days curing time .....	79
6-6. Percentage reduction in modulus of elasticity of concrete mixtures containing RAP .....	80
6-7. Poisson's ratio of concrete mixtures containing RAP .....	82
6-8. Flexural strength of concrete mixtures containing RAP .....	85
6-9. Development of flexural strength at different curing times relative to the flexural strength at 28 days curing time .....	86
6-10. Percentage reduction in flexural strength of concrete mixtures containing RAP .....	87
6-11. Stress strain plots for concrete containing RAP-2 at 7 days of curing time .....	88
6-12. Stress strain plots for concrete containing RAP-3 at 14 days of curing time .....	89
6-13. Stress strain plots for concrete containing RAP-4 at 28 days of curing time .....	90
6-14. Stress strain plots for concrete containing RAP-1 at 90 days of curing time .....	90

6-15. Modulus of toughness for concrete mixtures containing different RAP's at 90 days of curing time. ....	91
6-16. Splitting tensile strength of concrete mixtures containing RAP.....	93
6-17. Development of splitting tensile strength at different curing times compared to that of 28 days curing time.....	94
6-18. Percentage reduction in splitting tensile strength at 90 days of curing relative to the control mix.....	95
6-19. Adjusted coefficient of thermal expansion for RAP-1 at 90 days of curing time .....	97
6-20. Adjusted coefficient of thermal expansion for RAP-2 at 90 days of curing time .....	98
6-21. Adjusted coefficient of thermal expansion for RAP-3 at 90 days of curing time .....	99
6-22. Adjusted coefficient of thermal expansion for RAP-4 at 90 days of curing time .....	99
6-23. Coefficient of thermal expansion of concrete mixtures containing RAP-1.....	100
6-24. Coefficient of thermal expansion of concrete mixtures containing RAP-2.....	100
6-25. Coefficient of thermal expansion of concrete mixtures containing RAP-3.....	101
6-26. Coefficient of thermal expansion of concrete mixtures containing RAP-4.....	101
6-27. Drying shrinkage of concrete mixtures with RAP-1 after air curing .....	104
6-28. Drying shrinkage of concrete mixtures with RAP-2 after air curing. ....	105
6-29. Drying shrinkage of concrete mixtures with RAP-3 after air curing .....	105
6-30. Drying shrinkage of concrete mixtures with RAP-4 after air curing .....	106
6-31. Drying shrinkage of concrete mixtures with RAP-1 after moisture curing.....	106
6-32. Drying shrinkage of concrete mixtures with RAP-2 after moisture curing.....	107
6-33. Drying shrinkage of concrete mixtures with RAP-3 after moisture curing.....	107
6-34. Drying shrinkage of concrete mixtures with RAP-4 after moist curing .....	108
6-35. Relationship between compressive strength and flexural strength.....	109
6-36. Relationship between compressive strength and elastic modulus .....	110
6-37. Relationship between compressive strength and splitting tensile strength.....	111

6-38. Relationship between splitting tensile strength and flexural strength .....	112
7-1. Stress-strength ratio of concrete mixtures containing RAP at 28 days of curing time.....	121
7-2. Stress-strength ratio of concrete mixtures containing RAP at 90 days of curing time.....	121
7-3. Modeling of slab on spring foundation.....	124
7-4. Eight-node isoparametric brick element.....	125
7-5. Force-displacement relationship of the springs .....	125
7-6. Single axle load of equal-weight tires placed at the mid-edge of slab .....	126
7-7. Examples of stress-strain diagrams of concrete containing RAP.....	127
7-8. Failure loading pressure vs. toughness. ....	129
8-1. Stress-strength ratio chart for concrete with a CTE of $4.5 \times 10^{-6}/^{\circ}\text{F}$ .....	134
8-2. Stress-strength ratio chart for concrete with a CTE of $5.0 \times 10^{-6}/^{\circ}\text{F}$ .....	135
8-3. Stress-strength ratio chart for concrete with a CTE of $5.5 \times 10^{-6}/^{\circ}\text{F}$ .....	135
8-4. Stress-strength ratio chart for concrete with a CTE of $6.0 \times 10^{-6}/^{\circ}\text{F}$ .....	136
B-1. Stress-strain plot for concrete mixtures with RAP-2 at 14 days of curing time .....	205
B-2. Stress-strain plot for concrete mixtures with RAP-2 at 28 days of curing time .....	205
B-3. Stress-strain plot for concrete mixtures with RAP-2 at 90 days of curing time .....	206
B-4. Stress-strain plot for concrete mixtures with RAP-3 at 7 days of curing time .....	206
B-5. Stress-strain plot for concrete mixtures with RAP-3 at 28 days of curing time .....	207
B-6. Stress-strain plot for concrete mixtures with RAP-3 at 90 days of curing time .....	207
B-7. Stress-strain plot for concrete mixtures with RAP-4 at 7 days of curing time .....	208
B-8. Stress-strain plot for concrete mixtures with RAP-4 at 14 days of curing time .....	208
B-9. Stress-strain plot for concrete mixtures with RAP-4 at 90 days of curing time .....	209
C-1. Traffic volume adjustment factors, vehicle class distribution, and hourly truck traffic distribution .....	210
C-2. Traffic growth factor, general traffic inputs, and axle configuration .....	211
C-3. Layer 2 input parameters .....	212

C-4. Layer 3 input parameters .....	212
C-5. Layer 4 input parameters .....	214
D-1. Tensile stresses in a diametrically loaded specimen (after Buttlar et al., 1996).....	220
D-2. Example of strength results by using Superpave IDT (after Buttlar et al., 1996) .....	221
D-3. Gage point mounting system (Photo courtesy of Yu-Min Su) .....	223
D-4. ESPEC environment chamber (Photo courtesy of Yu-Min Su) .....	224
D-5. Thin concrete specimen on the load frame with strain gages (Photo courtesy of Yu- Min Su) .....	226
D-6. Example of determining the failure load on PCC with w/c=0.50 .....	229
D-7. Example of (A) secant modulus and (B) stress—strain curve of PCC and concrete containing 70% RAP.....	231
D-8. Examples of stress—strain plots with two horizontal strain gages in the Superpave IDT test under force-control load rate .....	235
D-9. Comparison of Indirect tensile strength results in PCC control mixes (using peak stress) .....	237
D-10. Comparison of Indirect tensile strength results in concrete mixes containing RAP-3 (using peak stress).....	238
D-11. Comparison of Indirect tensile strength results in PCC control mixes (using failure stress) .....	239
D-12. Comparison of Indirect tensile strength results in concrete mixes containing RAP (failure stress).....	240
D-13. Comparison of elastic modulus in PCC and concrete containing RAP.....	237
D-14. Comparison of Poisson’s ratio in PCC and concrete containing RAP .....	237
D-15. Comparison of toughness in PCC and concrete containing RAP-3 (force-control) .....	238
D-16. Comparison of Fracture energy in PCC and concrete containing RAP-3 (using failure stress) .....	240
D-17. Examples of stress—strain plots with two horizontal strain gages in the Superpave IDT test under displacement-control load rate.....	241
D-18. Comparison of tensile strength obtained from force-control versus displacement control tests .....	242

D-19. Comparison of Poisson’s ratio between conventional test in compression versus force-control and displacement-control in the Superpave IDT strength tests.....	243
D-20. Comparison of toughness obtained from force-control versus displacement control tests .....	244
D-21. Correlation of tensile strength between splitting and Superpave IDT strength test under 23°C .....	245
D-22. Correlation of elastic modulus between conventional and the Superpave IDT strength tests .....	246
D-23. Correlation of Poisson’s ratio between conventional and the Superpave IDT strength tests .....	247
D-24. Major components of X-ray CT facility at UF .....	249
D-25. Diagonal plan view of CT scan chamber.....	249
D-26. Acquisition of spatial information by 3-D calibration tool .....	253
D-27. 3-D reconstructed model of a concrete specimen.....	254
D-28. (A) A cross-sectional image of reconstructed 3-D model in concrete after process of window-leveling on Z-axis (B) Histogram of the 3-D model.....	255
D-29. The load frame set-up under Superpave IDT apparatus (Photo courtesy of Yu-Min Su) .....	259
D-30. DR image of the Superpave IDT concrete specimen with strain gages .....	260
D-31. Cropping the interested area from a virtual slice.....	262
D-32. Cropped image 1.5 inches square on each slice .....	263
D-33. Cropped image after binary process (threshold=87) .....	264
D-34. Air void distribution of w/c=0.45 PCC mix .....	269
D-35. Air void distribution of w/c=0.55 PCC mix .....	270
D-36. Air void distribution of concrete mix containing 20% RAP .....	271
D-37. Air void distribution of concrete mix containing 40% RAP .....	272
D-38. Air void distribution of concrete mix containing 70% RAP .....	273
D-39. Air void distribution of concrete mix containing 100% RAP .....	274

D-40. Voids distributions after fracture of w/c=0.45 and 0.55 PCC mixes.....	275
D-41. Voids distributions after fracture of concrete mixes containing 40% and 100% RAP ....	276
D-42. Air voids distribution in w/c=0.45 PCC with locations of interest .....	278
D-43. Air voids at the location of 0.069 inches .....	279
D-44. Air voids at the location of 0.15 inches .....	280
D-45. Air voids at the location of 0.32 inches .....	281
D-46. Air voids at the location of 0.52 inches .....	282
D-47. Air voids at the location of 0.72 inches .....	283
D-48. Air voids at the location of 1.00 inches .....	284
D-49. Air voids at the location of 0.60 inches .....	285
D-50. Air voids at the location of 0.09 inches of 100% RAP-3 (voids reduction).....	285
D-51. Air voids at the location of 0.60 inches of 100% RAP-3 (voids dull).....	286
D-52. Air voids at the location of 1.00 inches of 100% RAP-3 (voids growing).....	286
D-53. Fracture pattern in w/c=0.45 PCC mix .....	288

## **TECHNICAL SUMMARY**

### **Background and Research Objective**

Reclaimed or recycled asphalt pavement (RAP) materials have been used in recycled asphalt pavement mixtures in Florida, resulting in substantial savings in cost and conservation of aggregates and asphalt. However, with the adoption of the more stringent Superpave mix design method in Florida in recent years, a smaller percentage of RAP is now being used in the recycled asphalt mixtures. This has resulted in an excess of RAP which needs to be put into good use. The possible use of RAP in concrete pavement not only would help to dispose of our excess RAP, but could provide us with a concrete which could improve the performance and cost effectiveness of our pavements.

The main objective of this research project was to evaluate the feasibility of using RAP as aggregate replacement in concrete for use in pavement. The potential performance of typical Florida concrete pavement slabs made with concrete containing RAP was assessed.

### **Scope of the Research**

Four different RAPs were obtained from FDOT approved RAP sources and used for this research project. Concrete mixtures with 0%, 20%, 40%, 70% and 100% aggregate replacement by RAP for both coarse portion and fine portion were produced and evaluated. All the concrete mixtures had a fixed proportion of fine to coarse aggregate ratio and a fixed water to cement ratio of 0.5. Mechanical properties and thermal properties of the concrete mixtures were determined at different curing periods of 7 days, 14 days, 28 days and 90 days. Analysis for the maximum load-temperature induced stresses in typical concrete pavement made with these concretes was performed using FEACONS IV program under critical loading conditions in Florida. Analysis for the ultimate loads to cause failure of typical concrete pavement slabs made with these concretes was performed using ADINA software.

## **Main Findings**

The compressive strength, modulus of elasticity, splitting tensile strength and flexural strength of concrete containing RAP were observed to decrease as the percentage of RAP increased in the concrete mix. With the incorporation of RAP in concrete, the reduction in flexural strength was 10% to 20% lower than the corresponding reduction in compressive strength. The percent reduction in modulus of elasticity of the concrete with the incorporation of RAP was much higher than the corresponding reduction in compressive strength. The failure strain and toughness of concrete increased as the percentage of RAP increased in the mix. The Poisson's ratio, drying shrinkage, and coefficient of thermal expansion increased slightly as the percentage of RAP increased in the mix. Based on the data obtained in this study, regression equations relating compressive strength to flexural strength and elastic modulus of concrete containing RAP were developed.

The results of critical stress analysis show that the maximum stresses in pavement decreases as the RAP content of the mix increases, due to decrease in the elastic modulus of the concrete. Though the flexural strength of the concrete with RAP was lower than that of the conventional concrete, the computed stress to strength ratio for some of the RAP concrete was lower than that for the conventional concrete in some cases. The results of analysis of ultimate failure load of concrete pavement slab show that, on the average, the pavement slabs using RAP concrete have higher failure load than that of the slab using the conventional concrete. These results indicate that the RAP concrete can have better performance than a conventional concrete when used in concrete pavement slabs.

Stress-strength ratio tables and charts were developed for convenient determination of stress-strength ratios for different RAP concrete mixes with different combinations of flexural

strength, elastic modulus and coefficient of thermal expansion. The optimum concrete mix to be adopted for concrete pavement application should be the mix with lowest stress-strength ratio.

### **Conclusions and Recommendations**

The results of the laboratory testing program and finite element analysis indicate that the use of RAP as aggregate replacement in pavement concrete appears to be not only feasible but also offers the possibility of improving the performance of concrete pavement. A recommended mix design procedure for concrete containing RAP is provided.

Since the findings from this research has been based mainly on the results of laboratory study and theoretical finite element analysis, the actual performance of concrete containing RAP needs to be validated by field testing. It is recommended that a concrete pavement test section be constructed within an existing highway to perform this field validation. The recommended experimental parameters to be included in this test section are also provided.

# **CHAPTER 1 BACKGROUND AND RESEARCH OBJECTIVE**

## **1.1 Problem Statement**

Reclaimed or recycled asphalt pavement (RAP) materials have been used in recycled asphalt pavement mixtures in Florida, resulting in substantial savings in cost and conservation of aggregates and asphalt. However, with the adoption of the more stringent Superpave mix design method in Florida in recent years, a smaller percentage of RAP is now being used in the recycled asphalt mixtures. This has resulted in an excess of RAP which needs to be put into good use. The possible use of RAP in concrete pavement not only would help to dispose of our excess RAP, but could provide us with a concrete which could improve the performance and cost effectiveness of our pavements.

## **1.2 Research Objectives**

The main objectives of this research project are as follows:

- To characterize the mechanical and thermal properties of concrete containing RAP as affected by its mix ingredients, production methods, curing conditions and other relevant factors, in order to have a better understanding of the behavior of this type of concrete.
- To evaluate the gradation of concrete mixtures containing RAP.
- To study the stress-strain behavior of concrete containing RAP.
- To evaluate the performance of a hypothetical concrete pavement with the determined properties of concrete containing RAP using critical stress analysis.

## **1.3 Scope of the Research**

Four different FDOT RAP sources were used to acquire four different RAPs for this research project. Concrete mixtures with 0%, 20%, 40%, 70% and 100% aggregate replacement by RAP for both coarse portion and fine portion were produced and evaluated. All the concrete mixtures had a fixed proportion of fine to coarse aggregate ratio and a fixed water to cement ratio of 0.5. Mechanical properties and thermal properties of the concrete mixtures were

determined according to ASTM and AASHTO standard methods at different curing periods of 7 days, 14 days, 28 days and 90 days. Analysis for the maximum load-temperature induced stresses in typical concrete pavement was performed using FEACONS IV program under critical loading conditions in Florida.

#### **1.4 Research Approach**

The following approach was taken to study the properties of concrete containing RAP and the feasibility of using this type of concrete in concrete pavement slabs.

- Literature Review: 1) Characterization of aggregate gradation in concrete; 2) Properties of concrete containing recycled asphalt pavement.
- Selection of RAP material: Four different FDOT approved RAP sources were used for this research project. The selected RAP's had different properties in terms of recovered binder viscosity and aggregate properties.
- Mix design for concrete containing RAP: All the mix designs had fixed water to cement ratio. Concrete mixtures with 0%, 20%, 40%, 70% and 100% RAP as aggregate replacement were produced in laboratory.
- The following tests were performed at different curing periods of 7 days, 14 days, 28 days and 90 days according to ASTM and AASHTO standards: 1) Compressive strength; 2) Splitting tensile strength; 3) Modulus of elasticity and Poisson's ratio; 4) Flexural strength; 5) Drying shrinkage; 6) Coefficient of thermal expansion.
- Evaluation of the gradation of the combined aggregate of the concrete containing RAP.
- Evaluation of performance for rigid pavements with incorporation of RAP: FEACONS IV program was used to evaluate the performance of a hypothetical concrete pavement using the determined properties of concrete containing RAP.

## CHAPTER 2 LITERATURE REVIEW

### 2.1 Characterization of Aggregate Gradation in Concrete

#### 2.1.1 Maximum Density Method

Early work by Fuller and Thompson showed the importance of aggregate combined gradation on the workability and strength of concrete. They also developed an ideal shape of the combined gradation curve (Fuller and Thompson, 1907). They concluded that the concrete mixtures with densely graded aggregates had the highest strength. But some researchers concluded that concrete produced with aggregate gradation of maximum density would be harsh and difficult to use (Talbot and Richart, 1923). The equation for Fuller's maximum density curve is as follows:

$$P = \left(\frac{d}{D}\right)^n (100) \quad (2-1)$$

Where,

P = percent finer than an aggregate size

d = aggregate size taken for consideration

D = maximum aggregate size

n = parameter that controls fineness and coarseness of the curve (0.5 for maximum particle density)

The use of well graded and well-shaped aggregate with high packing density can significantly reduce the volume of the paste required, thus improving the properties of hardened concrete. Figure 2-1 shows the conceptual representation of aggregate particles in concrete. Apart from the paste required to fill up the voids between the aggregate, additional paste is required to separate the aggregate and make the concrete flowable (Koehler and Fowler, 2007)

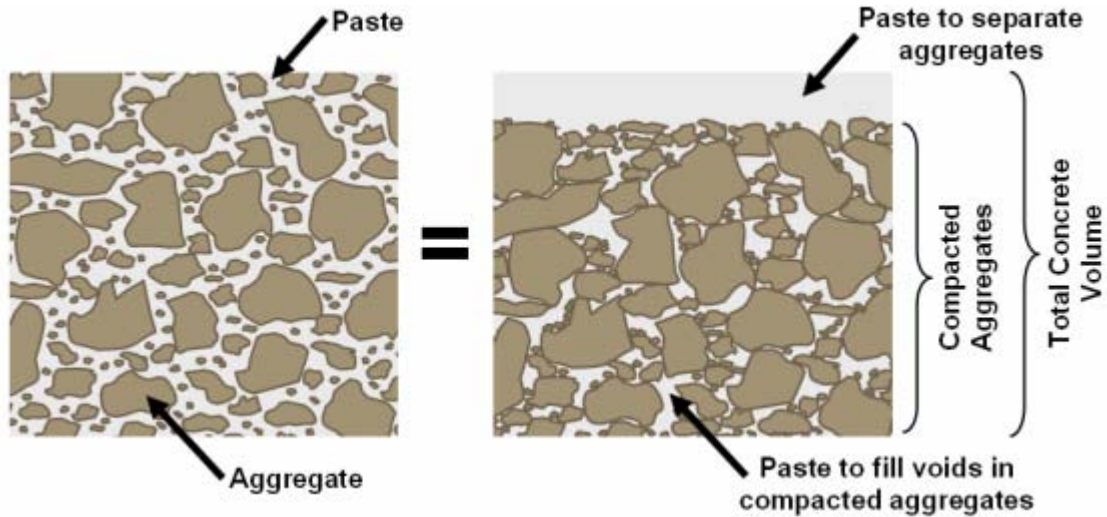


Figure 2-1. Representation of aggregate particles in paste (Koehler and Fowler, 2007)



Figure 2-2. Examples of mixtures with insufficient paste volume (left) and sufficient paste volume (right) for filling ability (Koehler and Fowler, 2007)

### 2.1.2 Fineness Modulus

Fineness modulus was used as an index of coarseness or fineness of an aggregate. Fineness modulus was determined as follows:

$$FM = \frac{\text{Cumulative percentage retained}}{100} \quad (2-2)$$

The sieves selected by Abrams were 11/2", 3/4", 3/8", #4, #8, #14, #28, #48 and #100. The #14, #28 and #48 sieves were later replaced by #16, #30 and #50 sieves. Abrams found that grading of the mixtures was affected by fineness modulus of the aggregate. He stated that for any

concrete mix with aggregate that gives the same fineness modulus, the same quantity of water would be needed to produce a mix of same plasticity and strength.

### 2.1.3 Surface Area and Particle Interface Method

Edward, 1918 and Young, 1919, used the method of proportioning aggregate based on the surface area of the aggregate. They concluded that less water is required for the aggregate with lower surface area. When less water is used, it results in a lower water to cement ratio and a stronger concrete.

Particle interface method was proposed by Weymouth in 1933. In order to determine satisfactory gradation, he determined the volumetric relationship between the successive size groups of particles. It was based on the assumption that the particles of each group are distributed throughout the mass in such a way that the distance between them is equal to the mean diameter of the particles of the smaller size group plus the thickness of the cement film between them. Between two successive sizes, the particle interference occurred when the distance between the particles is not sufficient to allow free passage of the smaller particles. This method results in gradings finer than necessary for satisfactory workability. The equation for the distance between the particles by Weymouth is as follows:

$$t = \left[ \left( \frac{d_o}{d_a} \right)^{1/3} - 1 \right] \times D \quad (2-3)$$

Where,

t = average distance between particles of diameter D

d<sub>o</sub> = density of the size group (the solids present in a unit volume alone, secured by a unit weight and specific gravity test)

$d_a$  = ratio of the absolute volume of a size group to the space available to that size in concrete

$D$  = average diameter of the particles in the size group

#### 2.1.4 Coarseness Factor

Shilstone came up with a concept called coarseness factor chart from the aggregate gradation, which could be used to predict the workability of the concrete mixtures. The coarseness factor chart is a method of analyzing the size and uniformity of the combined aggregate particle distribution, instead of considering the coarse and fine aggregate separately. The equation for coarseness factor chart is as follows,

$$CF = \left[ \frac{Q}{Q+I} \right] \quad (2-4)$$

Where,  $Q$  = Coarse particles which is plus 3/8", and  $I$  = Coarse particles on #4 and #8 sieve. Thus a coarseness factor (CF) with a value of 100 would represent a gap-graded aggregate blend with no material between 3/8" and #8, while a coarseness factor (CF) of zero would be an aggregate that has no material retained on the 3/8" sieve. Another term on the coarseness factor chart is the workability factor 'W'. It is the percentage of material passing #8 sieve. Figure 2-3 shows the coarseness factor chart that was proposed by Shilstone. The x-axis of the chart is the coarseness factor (CF) and the y-axis is the workability (W) as discussed above. A trend bar was included in order to use it as a reference and to find the optimal region based on the trial batches performed for different concrete mixtures. In general, the concrete mixtures that fall above the trend bar are considered to be sandy mixtures, and the mixtures below the trend line were considered to be rocky mixtures. The mixtures that fall in the trend bar will require least amount of water for a given slump, but the concrete can be difficult to pump or even have poor finishability. In a modified coarseness factor chart the entire chart area was divided into five

zones which will be used to study the concrete mixtures containing RAP. In the coarseness factor chart, we have five zones with the roman letters I to V as shown in the figure.

Zone I, is the condition of a gap-graded mixture and will encounter potential problems of segregation or unnecessary consolidation due to lack of intermediate particles. These mixtures will not be cohesive, and so a clear separation between the coarse particles and the mortar will be observed.

Zone II, is the condition of an optimum mixture. Mixtures that fall in this zone are well graded and excellent for regular production use. High quality concrete can be produced when the coarseness factor is approximately 60 and the workability is around 35. Zone II is also divided into five regions. Depending on the applications, each of these small regions in Zone II can be beneficial. Zone III is the extension of Zone II and is for aggregates with smaller maximum aggregate size (approximately 1/2").

Zone IV is the condition of excessive fines that can lead to segregation. Mixtures in zone IV can also cause high permeability, shrinkage, cracking, curling, spalling and scaling. Zone V is the condition of very coarse mix with lack of fines making the mixtures nonplastic. Mixtures in this zone will require high amount of fine aggregate to make the mix workable.

The coarseness factor chart can also be used to maintain the mix characteristic with the changing aggregate gradation. For example, as the amount of intermediate particles increases in the mix, the coarseness factor decreases. In this case, more fines should be added to make the mix workable.

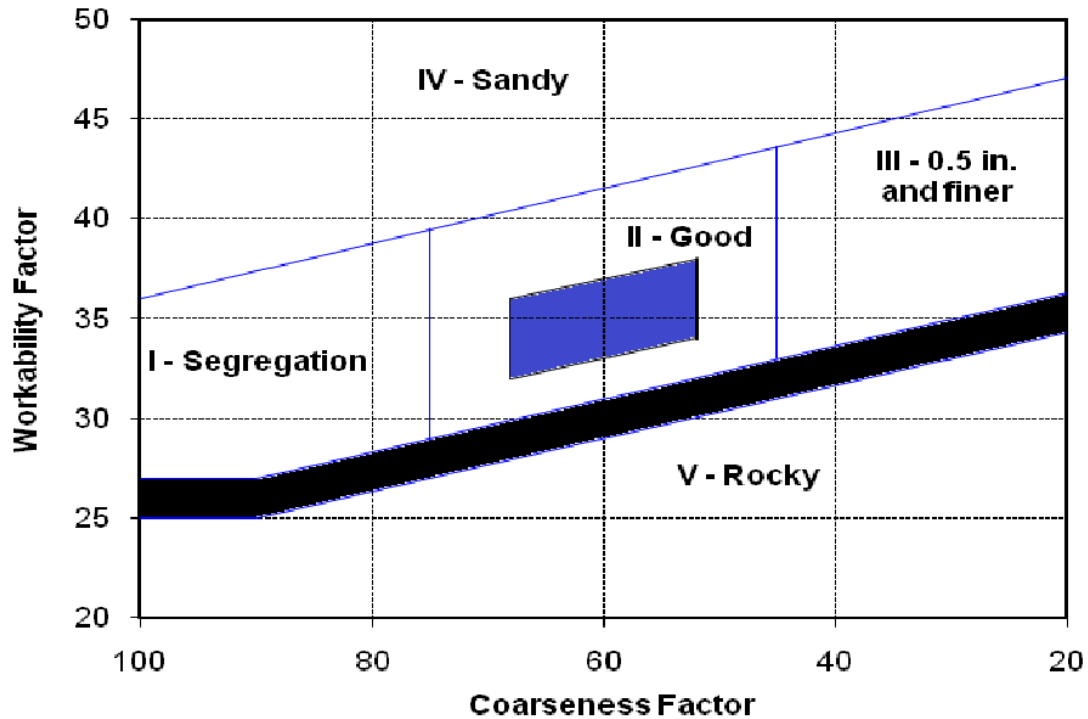


Figure 2-3. Coarseness factor chart proposed by Shilstone

### 2.1.5 Individual Percent Retained

The individual percent retained chart provides a method for graphing the distribution of different sizes of aggregates in a combined aggregate plot. It helps to reveal the lack of aggregate on specific sieves as gaps on the chart. The “8-18” band on this chart is the region where the ideal aggregate gradation should be. It is the limitations on the minimum and maximum of the amount of aggregate fractions proposed by Shilstone as shown in Figure 2-4. Figure 2-5 shows the ideal individual percentage retained curve that must be achieved. However with the current ASTM C33 aggregate specification, #57 aggregate and ASTM C33 sand, there is a deficit in particles retained on the #8 and #16 sieves, and excess of particles retained on the #30 and #50 sieves as shown in Figure 2-6. Such kinds of gradation lead to problems like cracking, spalling, and blistering of concrete. If there is a deficit on one sieve and the adjacent sieve has an excess, the two sieves can balance one another. However, it will not be desirable to have three adjacent deficient sieve sizes.

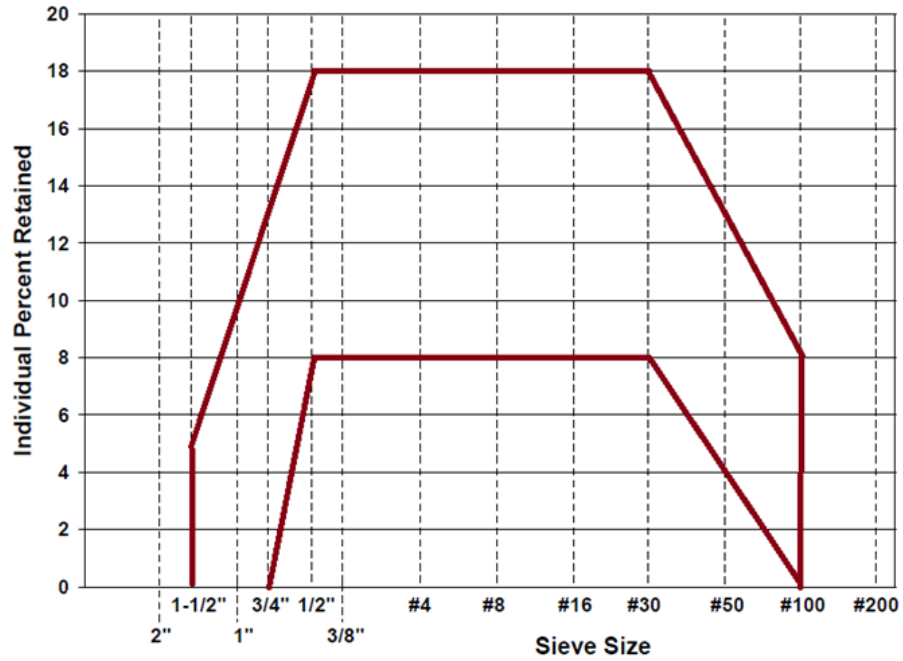


Figure 2-4. Shilstone 8-18 band chart

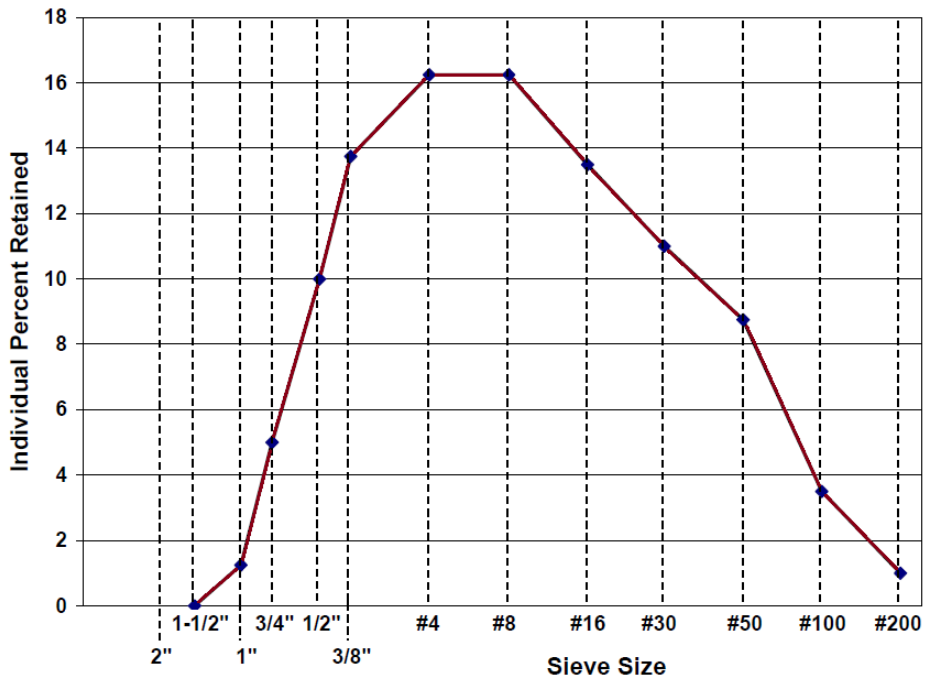


Figure 2-5. Ideal plot on individual percentage retained chart

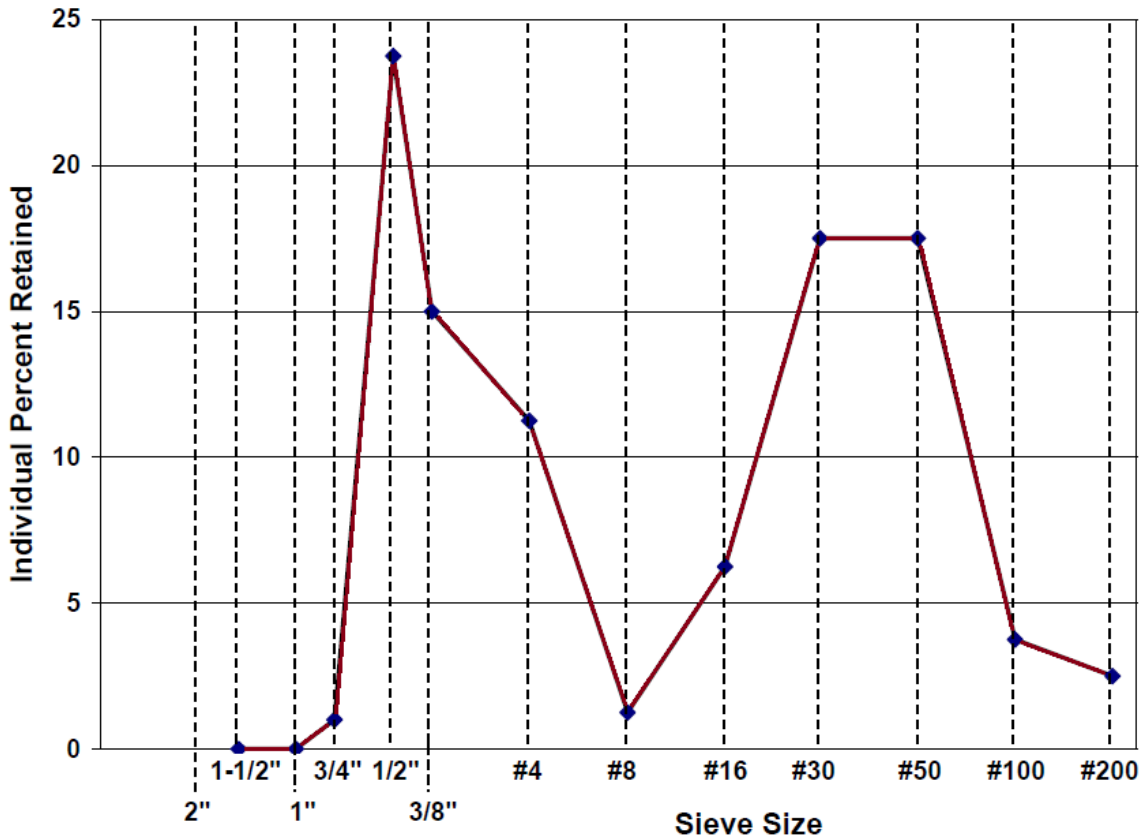


Figure 2-6. Problematic plot on individual percentage retained chart

### 2.1.6 0.45 Power Chart

The 0.45 power chart is similar to semi-log graph, with the exception that the x-axis is the sieve opening plotted on a 0.45 power scale. The 0.45 power chart is widely used in the asphalt industry to reduce the voids of the combined aggregate, and the amount of asphalt in the asphalt mixture design. The optimum line on the 0.45 power chart is the straight line, which will give the least amount of voids and best packing in the combined aggregate. The deviations from the optimum line helps to identify the location of grading problems as shown in Figure 2-8. Gradings should be close to the optimum line with very little deviation and zigzag patterns as shown in Figure 2-7. S-shaped curve will usually form in the case of a gap graded mix (ACI.302.1R-04, 2004)

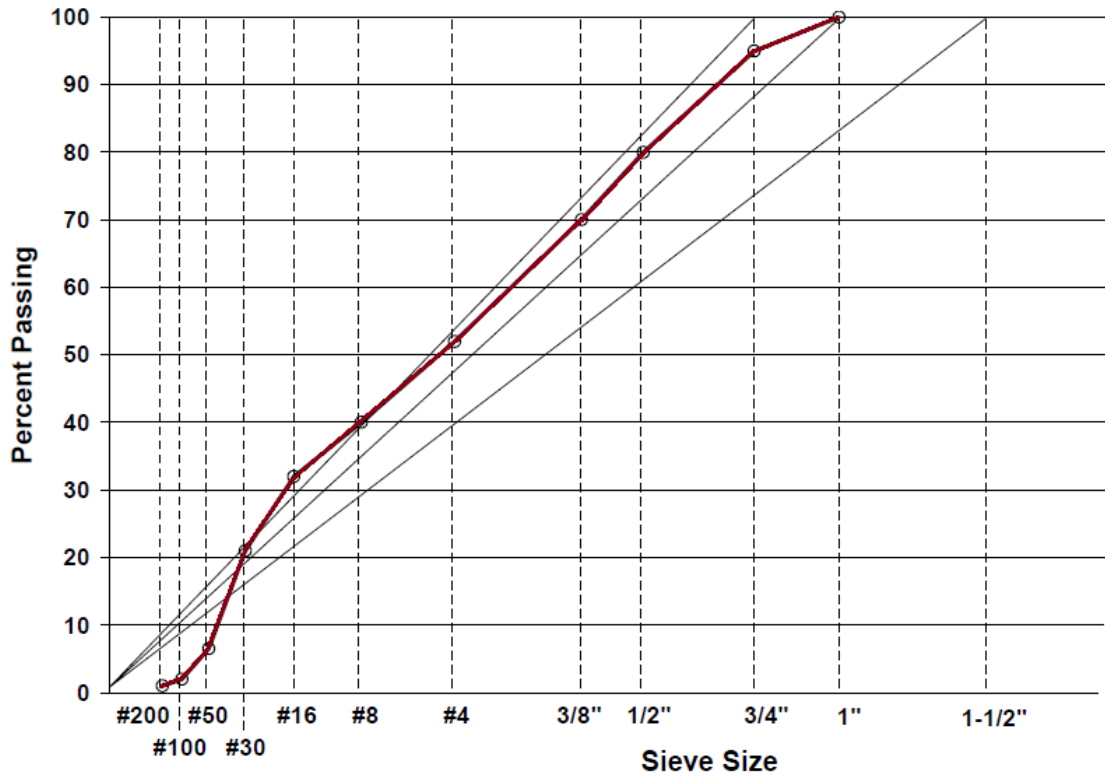


Figure 2-7. 0.45 power chart for a well graded mix

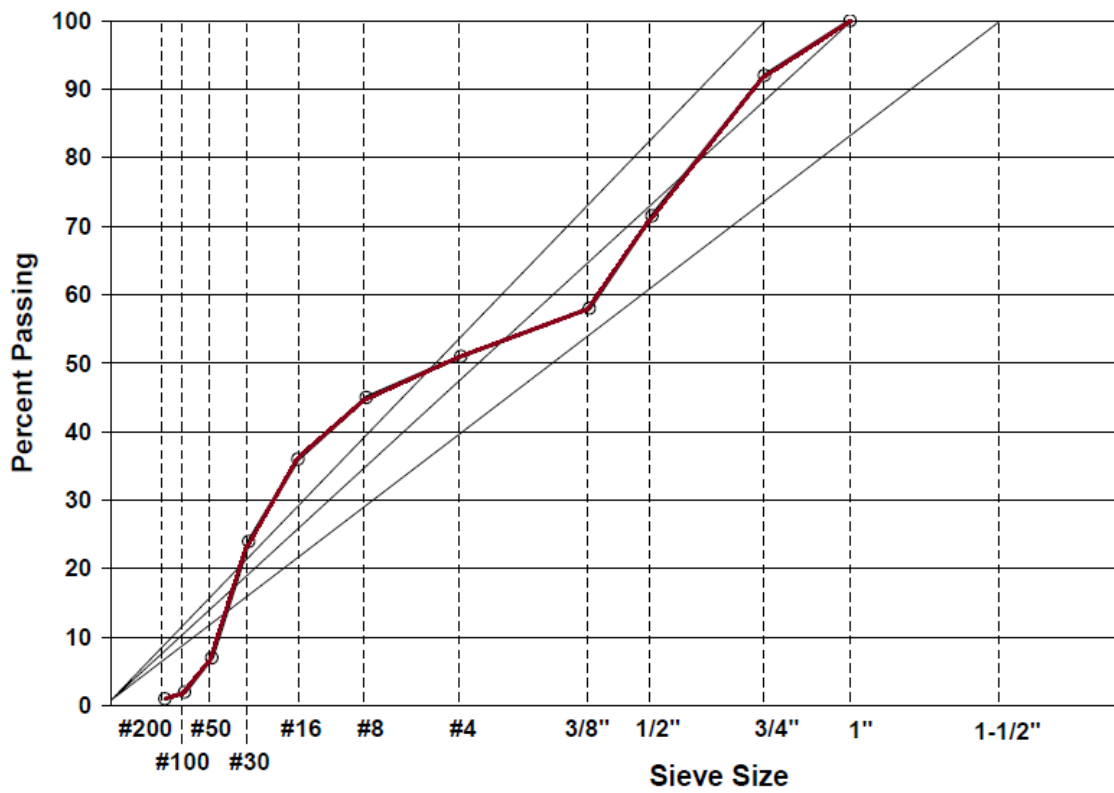


Figure 2-8. 0.45 power chart for a gap graded mix

## **2.2 Effect of Aggregate Gradation on Concrete Properties**

According to a recent study, optimized aggregate gradation concrete (OAG) provided 9% higher flexural strength than normal aggregate gradation concrete (NAG). There was a reduction in shrinkage and coefficient of thermal expansion when the aggregate gradation was optimized (Kim, et al. 2008).

In a report provided by the Innovative Pavement Research Foundation, the authors stated that the use of combined gradation for optimization plays a major role in the performance of concrete pavements at airports. Gap graded concrete mixtures are not acceptable according to the proposed specifications, as it may cause segregation and joint spalling, which might affect the long term performance of concrete pavements. Thus, use of combined gradation and innovative ways of optimizing the mixtures should be performed by the contractors and engineers (Tayabji, et al. 2007).

Study performed in Wisconsin showed that the use of optimized total aggregate gradation instead of near-gap-graded gradation in concrete pavement resulted in an increase in the compressive strength by 10 to 20%. Reduction in segregation, reduction in water demand by up to 15% to achieve desirable slump was observed. Desirable air content was achieved with 20 to 30% reduction in air entraining agent. In another study, optimized gradation was achieved by increasing the aggregate particles retained on #4 to #16 sieves and decreasing amount of fines on #50 to #200 sieves. A control mix with 60-40 blend of coarse/ fine aggregate and a nearly gap-graded aggregate was produced by removing the particles in #4 to #16 sieves. According to the study the optimized gradation mixes did not show consistent improvement in performance compared to the control mixes. The near gap-graded mixes showed reduced strength and increased shrinkage (Cramer, S.M. and Carpenter, A.J., 1999).

Figures 2-9 through 2-11 show the individual percentage retained chart, 0.45 power chart, and coarseness factor chart for optimized mixtures. This optimized mix resulted in reduction in cracking, increase in air entrainment, increase in strength, and decrease in placement time.

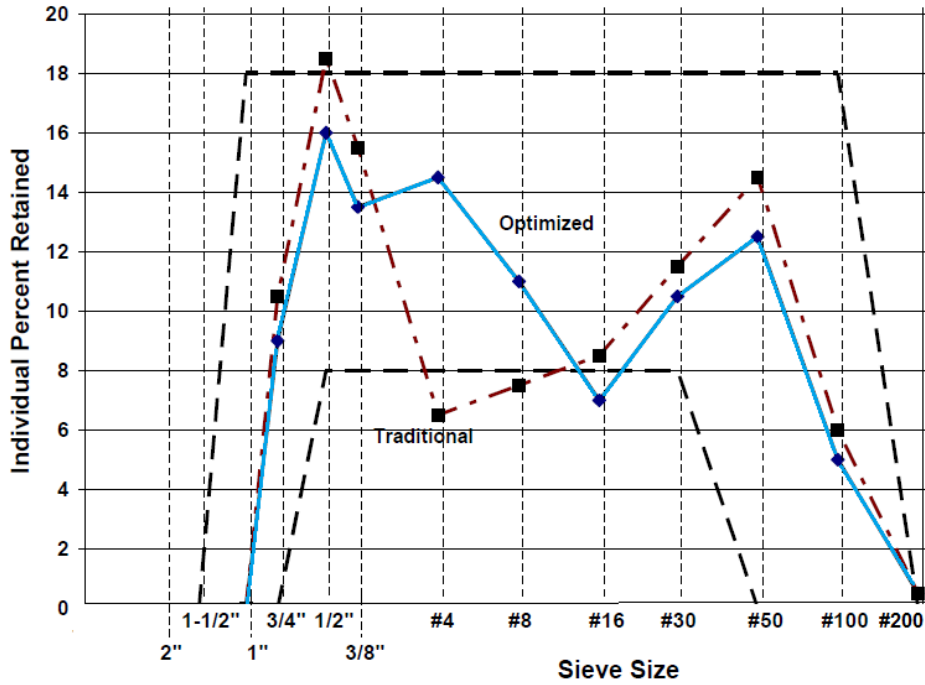


Figure 2-9. Individual percent retained for optimized mix

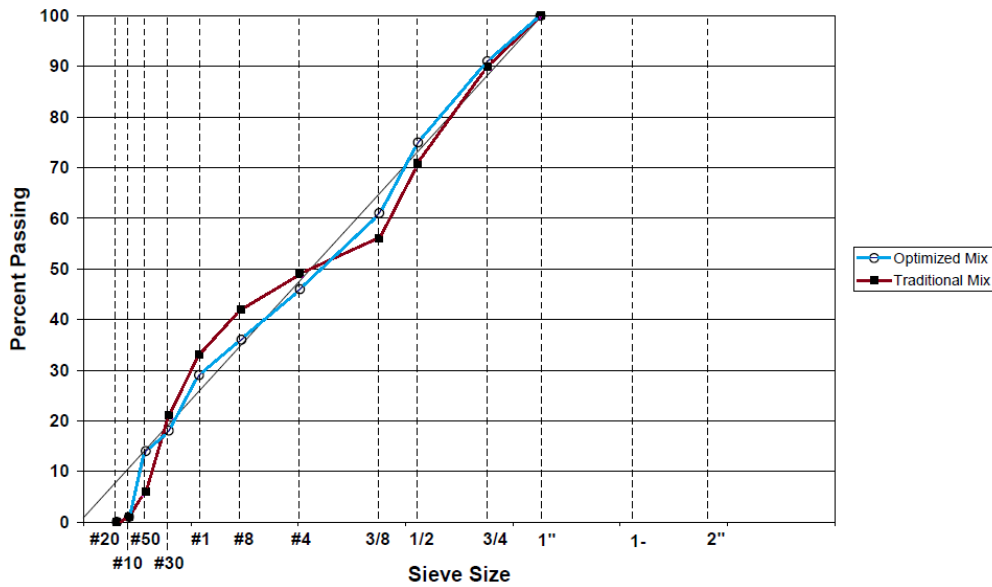


Figure 2-10. 0.45 power chart for optimized mix

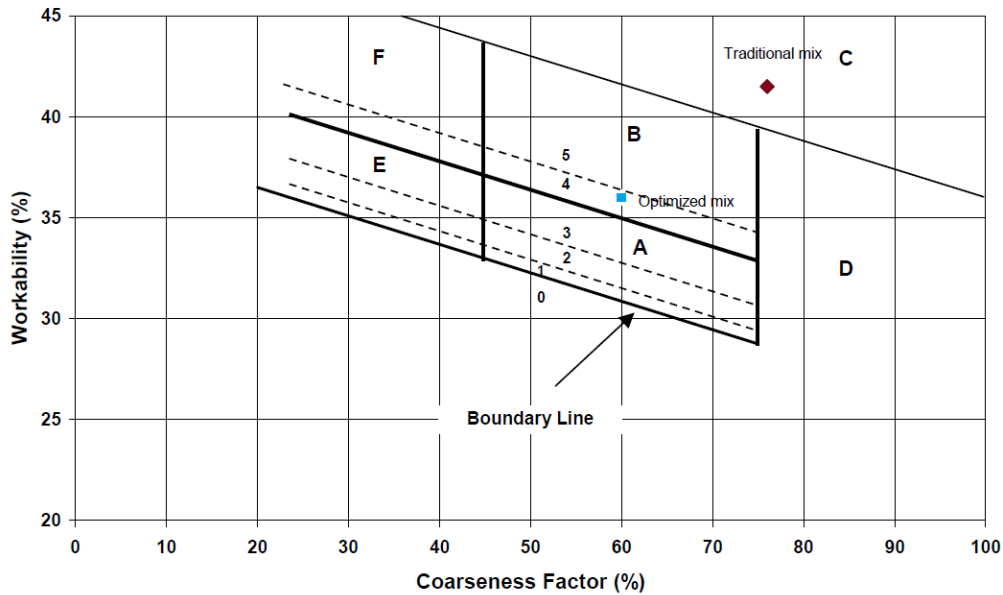


Figure 2-11. Coarseness factor chart for optimized mix

### 2.3 Properties of Recycled Asphalt Pavement

Reclaimed asphalt pavement (RAP) is bituminous concrete material removed and reprocessed from pavements which have to undergo resurfacing or reconstruction. The reclaiming process involves cold milling a portion of the existing pavement or full depth removal and crushing. The properties of RAP largely depend on the condition of pavement from where it is reclaimed. There can be significant variation in the material due to the type of mix, aggregate quality and size, asphalt mix consistency and asphalt content. RAP is usually finer than its original aggregate constituents, due to processing of the material. Typically, RAP is produced by crushing and screening the material to 1/4" to 1/2" in size (Griffiths and Krstulovich, 2002).

According to Kang, et al. 2011, addition of RAP to virgin aggregate increased the proportion of medium to coarse fractions in the mixtures. In the FA- aggregate- RAP mixtures, increase in the proportion of RAP increased the proportions of medium and coarse fraction as shown in the Figure 2-14. Results of the gradation from Huang's study showed that the fine RAP is much coarser than the virgin fine aggregate and coarse RAP is much finer than the virgin

coarse aggregate. The proportion of medium fractions in RAP aggregate is much higher, as shown in Figure 2-12. Similar trends were observed by Al-Oraimi, as shown in Figure 2-13.

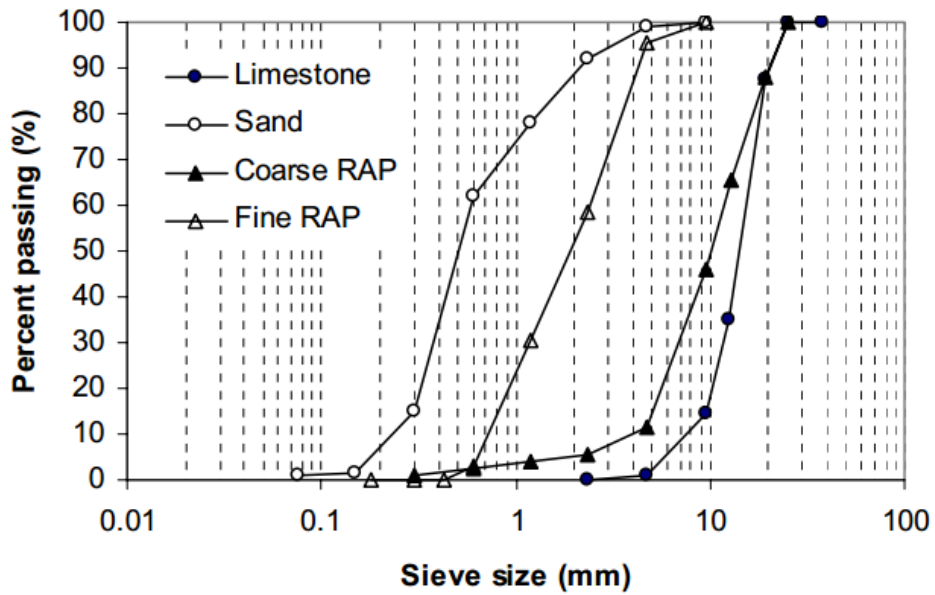


Figure 2-12. Gradation of aggregates and RAP (Huang, et al. 2006)

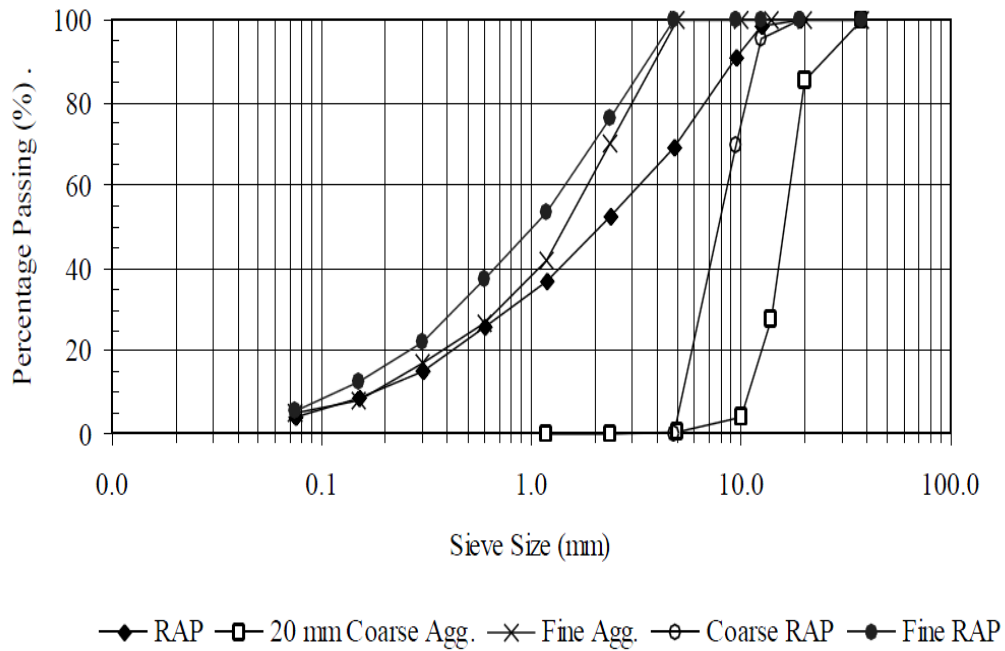


Figure 2-13. Grain size distribution for aggregate and RAP (Al-Oraimi, et al. 2007)

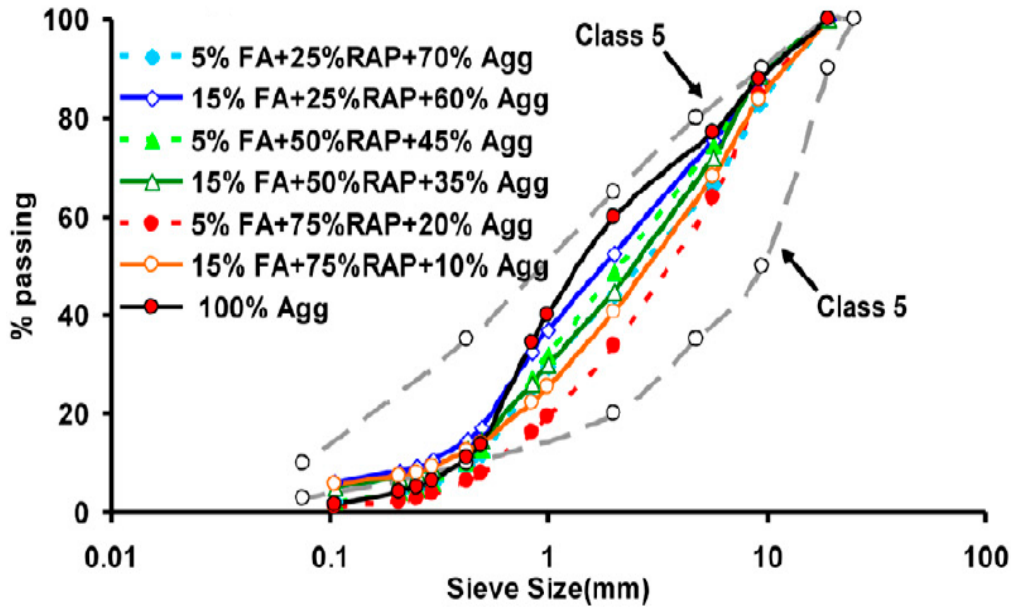


Figure 2-14. Particle size distribution of RAP and virgin aggregates (Kang, et al. 2011)

#### 2.4 Concrete Properties Containing Recycled Asphalt Pavement

In concrete incorporating RAP, the asphalt forms a thin film at the interface of cement mortar and aggregate. This asphalt film can be useful in resisting the crack propagation along this interface. Thus, crack develops along the aggregate rather than going through it, as shown in Figure 2-15, during which more energy can be dissipated (Huang, et al. 2006). Huang also showed that concrete made with only coarse RAP shows a better performance in toughness and has the least reduction in the concrete strength. For concrete with high percentage of RAP, aggregates do not separate after failure but sustain load even after initial failure. It has also been observed that with such a concrete with RAP, there is a systematic reduction in the strength of the concrete. Generally, the strength decreases with increase in the content of RAP (Huang, et al. 2005).

Hassan (Hassan, et al., 2000) showed that RAP aggregate reduced the compressive strength of the concrete and the reduction in the strength is proportional to the percentage of RAP used. The author also found that combination of fine RAP and coarse RAP cause more

reduction in strength than the combination of coarse RAP and sand. The performance properties of concrete containing RAP improved with the use of fly ash as indicated by the measurements of porosity and permeability. Concrete containing RAP enhances the ductility and strain capacity of the concrete. This improvement in property can be useful for applications such as rigid pavements, road bases and subbases.

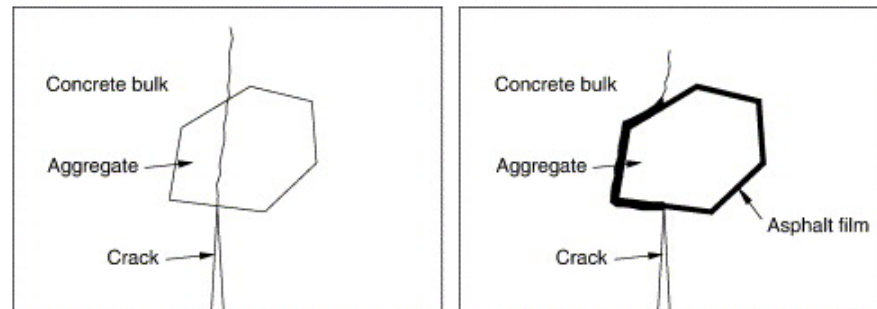


Figure 2-15. Propagation of crack through aggregate with and without asphalt film (Huang, et al. 2006)

Al-Oraimi (Al-Oraimi, et al. 2009), found that the general trend of strength development for RAP concrete and the relations between compressive strength, elastic modulus and flexural strength for concrete mixtures with RAP agreed well with the normal concrete. Reduction in slump with increasing RAP content was observed. According to the authors, RAP can be used as aggregate in non-structural applications but the percentage of RAP should be limited to achieve the required performance for the desired application. Figure 2-16 shows the reduction of compressive strength with increase in percentage of RAP, and Figure 2-17 shows the percent reduction in compressive strength for different percentage of RAP replacement.

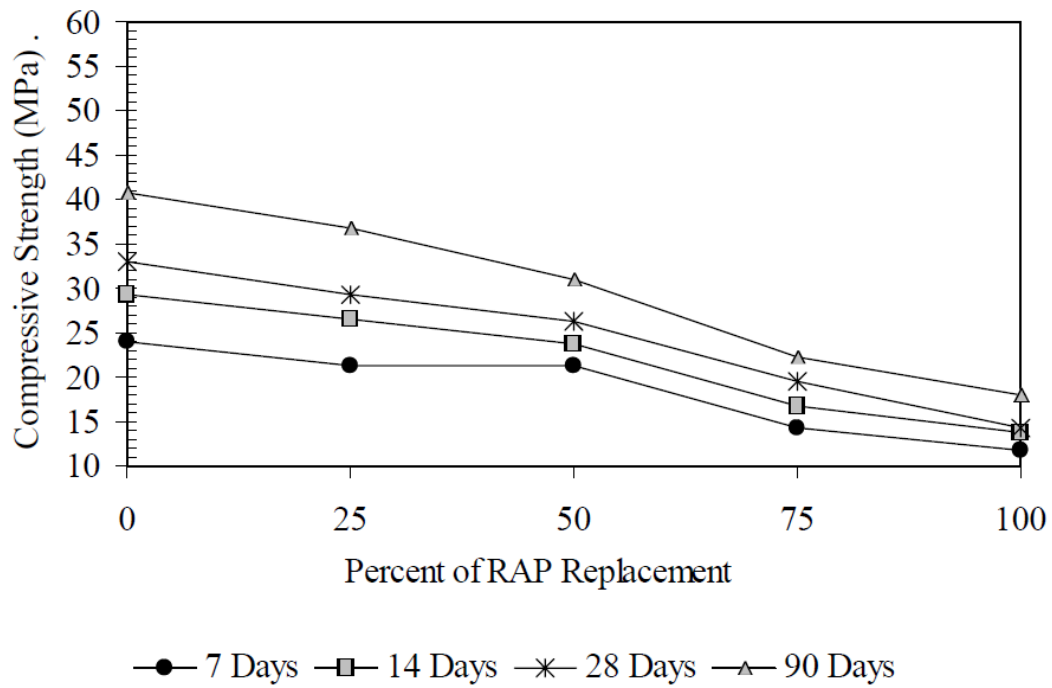


Figure 2-16. Compressive strength of concrete containing RAP (Al-Oraimi, et al. 2009)

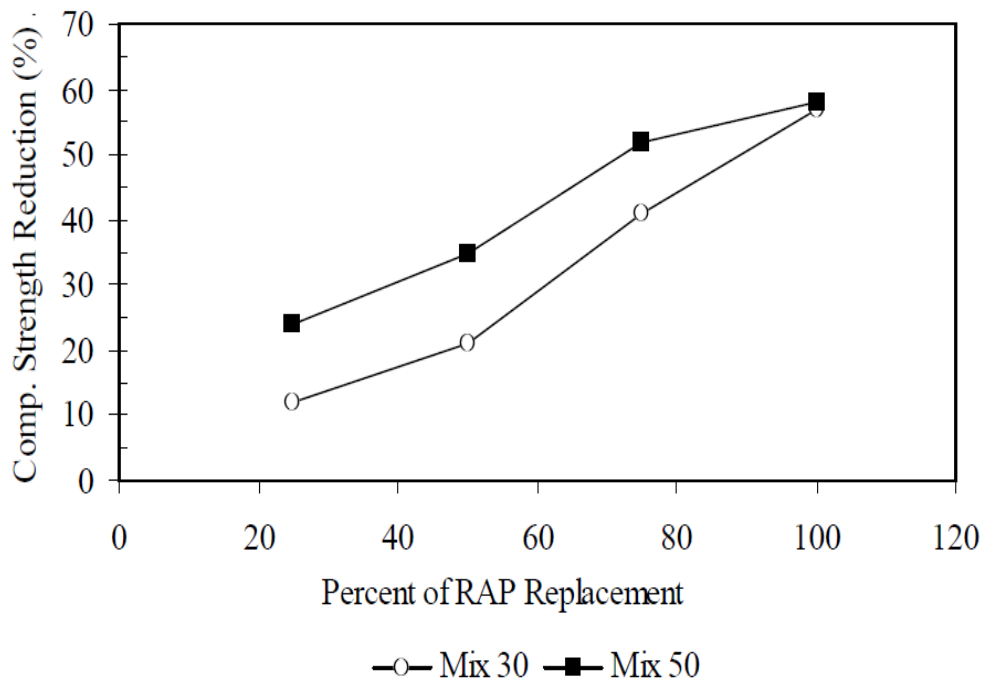


Figure 2-17. Reduction in compressive strength of concrete containing RAP (Al-Oraimi, et al. 2009)

Delwar (Delwar, et al. 1997) investigated varying percent of replacements for coarse and fine RAP (0, 25, 50, 75, and 100), with two different water to cement ratios (0.45 and 0.50). They concluded that in general concrete containing RAP increased the amount of entrapped air, decreased the unit weight and decreased the slump of the concrete. Reduction in modulus of elasticity and compressive strength was also observed with the increase in the percentage of RAP. Delwar concluded that concrete containing high percentage of RAP should be used for non- pavement applications like sidewalks, gutters and barriers.

Sommer (Sommer, 1994) performed a study with RAP replacement of 0, 25, 50, 75, and 100% in concrete. They found reduction in compressive strength, splitting tensile strength, flexural strength and elastic modulus with increasing percentage of RAP. They also stated that it would be acceptable to add 50% coarse RAP into the concrete mixtures and strength of RAP concrete could be improved by reducing the water to cement ratio.

Mathias (Mathias, et al. 2004) studied five different total RAP contents (0, 12.5, 26, 51, and 90%) for concrete mixtures. Compressive strength, splitting tensile strength and elastic modulus tests were performed at three different temperatures of 2, 20 and 40°C. Results showed that compressive strength, splitting tensile strength and elastic modulus decreased with increasing RAP and that as the amount of RAP in concrete increased, the concrete properties became more sensitive to temperature. They also performed fatigue testing and concluded that for concrete mixture with 90% RAP, the fatigue failure was approximately 10% lower to achieve at least one million cycles to fatigue failure.

Okafor (Okafor, 2010) found that RAP aggregate may be able to absorb more impact load than virgin aggregate after performing impact crushing test. His study also found that concrete mixtures with RAP had reduced slump but the mixtures were still workable. Reduction in the

strength of the concrete at different curing time and water cement ratio was also observed. He also stated that the failure in compression often resulted as the failure between RAP-mortar interface with little aggregate crushing, while the virgin aggregate often fail by crushing of the aggregate.

Katsakou (Katsakou and Koliass, 2007) replaced 10, 25, 50, 75, and 100% RAP for a cement treated mixture. They found the compressive strength decreased with increasing percentage of RAP content in the mix. For splitting tensile strength, the strength decreased with increase in RAP content. However, the flexural strength of the material was unchanged up to 50% RAP replacements. The rate of strength loss in tension was lower than in compression with increasing RAP content. They also found that the rate of decrease in the modulus of elasticity was greater than the rate at which the strength decreased.

Topcu (Topcu and Isikdag, 2009) studied the use of fine RAP as a replacement to natural fine aggregate in mortars with replacements of 0, 25, 50, 75, and 100%. They found the compressive strength, modulus of elasticity, flexural strength, and unit weight of concrete decreased as the percentage of RAP replacement increased. The amount of free shrinkage increased for the mixtures with RAP.

Researchers have also studied the use of RAP and aggregate freshly coated with asphalt in concrete for subbase applications. In general, they found reduction in compressive strength, modulus of elasticity, and flexural strength for concrete mixtures containing RAP and asphalt coated aggregates. They also found the drying shrinkage to increase for concrete mixtures containing RAP and asphalt coated aggregate. (Dumitru, et al. 1999, Patankar and Williams, 1970)

Li (Li, et al. 1998) studied the use of coarse aggregate coated with asphalt emulsion in cement mortar for the application of base layer as a lean concrete. They showed that cement-asphalt emulsion concrete had a more ductile fatigue failure with a longer period of crack propagation as compared with the control mixtures. It also resulted in a better fatigue performance at the same stress strength ratio relative to the control mixture. They studied the stress strain behavior and found that at higher temperatures, the stress peak is lower and the post-peak strain is significantly extended, enhancing the strain capability of the material. However, at lower temperatures, the stress-strain behavior was found to be similar to that of plain concrete.

In Austria, a section of concrete pavement was reconstructed using the crushed concrete from the existing highway and RAP from the preexisting asphalt overlay. The contractors also placed a 20 year guarantee for that pavement section subjected to skid resistance, joint seal performance, and other measures. Till today the roadway has not reported any problems. (Tompkins, et al. 2009)

**CHAPTER 3  
MATERIALS AND EXPERIMENTAL PROGRAM**

**3.1 Introduction**

This chapter presents the materials used for this research study and the concrete mix proportions used. It also presents the details of the material properties.

**3.2 Selection of Materials**

All the materials selected were approved by the FDOT materials office at Gainesville, Florida. Type I/II cement from Florida Rock Industries was selected for this research study. The fine aggregate used was a silica sand and the coarse aggregate used was a Florida limestone. Recycled asphalt pavement (RAP) was selected from four different districts in Florida, and was from FDOT-approved sources as shown in the Table 3-1. The various RAPs were selected such that there was a wide range of the recovered binder viscosity and recovered aggregate type. The details of the properties of the RAP's will be discussed in the section on material properties.

Table 3-1. Details of the RAP material selected for this research study

RAP Type	District Number	Location	Plant Name	Plant or Pit Number
1	2	Gainesville, Florida	V.E. Whitehurst and Sons, Inc.	A0212/A0213
2	3	Freeport, Florida	APAC-Florida, Inc. North Florida division	A0628
3	4	Vero beach, Florida	Community asphalt corporation	A0697
4	5	Ocala, Florida	Anderson Columbia company, Inc.	A0706

### 3.3 Material Properties

#### 3.3.1 Cement

Type I/II cement was used for all the concrete productions in this research study. The physical and chemical properties for the cement were provided by FDOT and are shown in Table 3-2. The results are compared with ASTM specifications.

Table 3-2. Physical and chemical properties of Portland cement

Test	Standard Specification	Cement Property	AASHTO M 85 For Type I/II
Loss of Ignition	ASTM C114	3.0%	<= 3.0
Cement Acid Insoluble	ASTM C114	0.57%	<= 0.75
Fineness of Portland Cement	ASTM C204	408.00 m <sup>2</sup> /Kg	>= 260.00 <= 430.00
Time of Setting (Initial)	ASTM C191	100.00 min	>= 45
Time of Setting (Final)	ASTM C191	300.00 min	<= 375.00
Autoclave Expansion	ASTM C151	0.04%	<= 0.80
3- Day Breaks for Compressive Strength of Cement	ASTM C109	3510.00 psi	>= 1450.00 psi
7- Day Breaks for Compressive Strength of Cement	ASTM C109	4580 psi	>= 2470.00 psi
Aluminum Oxide	ASTM C114	5.0%	<= 6.0%
Ferric Oxide	ASTM C114	4.0%	<= 6.0%
Magnesium Oxide	ASTM C114	1.3%	<= 6.0%
Sulfur Trioxide	ASTM C114	2.7%	<= 3.0%
Tricalcium Aluminate	ASTM C114	6%	<= 8.0%
Total Alkali as Na <sub>2</sub> O	ASTM C114	0.35%	<= 0.60%

### 3.3.2 Fine Aggregate

The fine aggregate is a silica sand, mined from the plant number #76-349. The properties of fine aggregate were provided by FDOT and are shown in Tables 3-3 through 3-5. Table 3-3 shows the specific gravity and water absorption of the fine aggregate. Table 3-4 shows the gradation of the first batch of fine aggregate and Table 3-5 shows the gradation of the second batch of fine aggregate. Both of the fine aggregates had the same specific gravities and only slight difference in water absorption. From the gradation results, it can be observed that fine aggregate #2 was much finer than the finer aggregate #1. For the gradation of fine aggregate #2, percent passing #30 sieve does not fit in the grading limits of ASTM specification. Figure 3-1 shows the gradation chart of the virgin fine aggregate. It can be seen that the fine aggregate gradation is very close to the maximum limits of the ASTM standards and is very fine.

Table 3-3. Specific gravity and water absorption of fine aggregate

Property	Unit	Fine Aggregate-1	Fine Aggregate-2
Bulk Specific Gravity (SSD)	/	2.63	2.63
Bulk Specific Gravity (Dry)	/	2.62	2.62
Apparent Specific Gravity (Dry)	/	2.65	2.65
Absorption	%	0.50	0.40

Table 3-4. Gradation of fine aggregate #1

US	Sieve Size		Cumulative Retained (%)	Passing (%)	Grading Limits	
	inch	mm			Min (%)	Max (%)
#4	0.187	4.75	0	100	95	100
#8	0.093	2.36	1	99	85	100
#16	0.046	1.18	9	91	65	97
#30	0.024	0.60	30	70	25	70
#50	0.012	0.30	68	32	5	35
#100	0.006	0.15	95	5	0	7
#200	0.003	0.075	100	0	0	2
Fineness modulus			2.03			

Table 3-5. Gradation of fine aggregate #2

US	Sieve Size		Cumulative Retained (%)	Passing (%)	Grading Limits	
	inch	mm			Min (%)	Max (%)
#4	0.187	4.75	0	100	95	100
#8	0.093	2.36	1	99	85	100
#16	0.046	1.18	7	93	65	97
#30	0.024	0.60	25	75	25	70
#50	0.012	0.30	69	31	5	35
#100	0.006	0.15	97	3	0	7
#200	0.003	0.075	100	0	0	2
Fineness modulus			1.99			

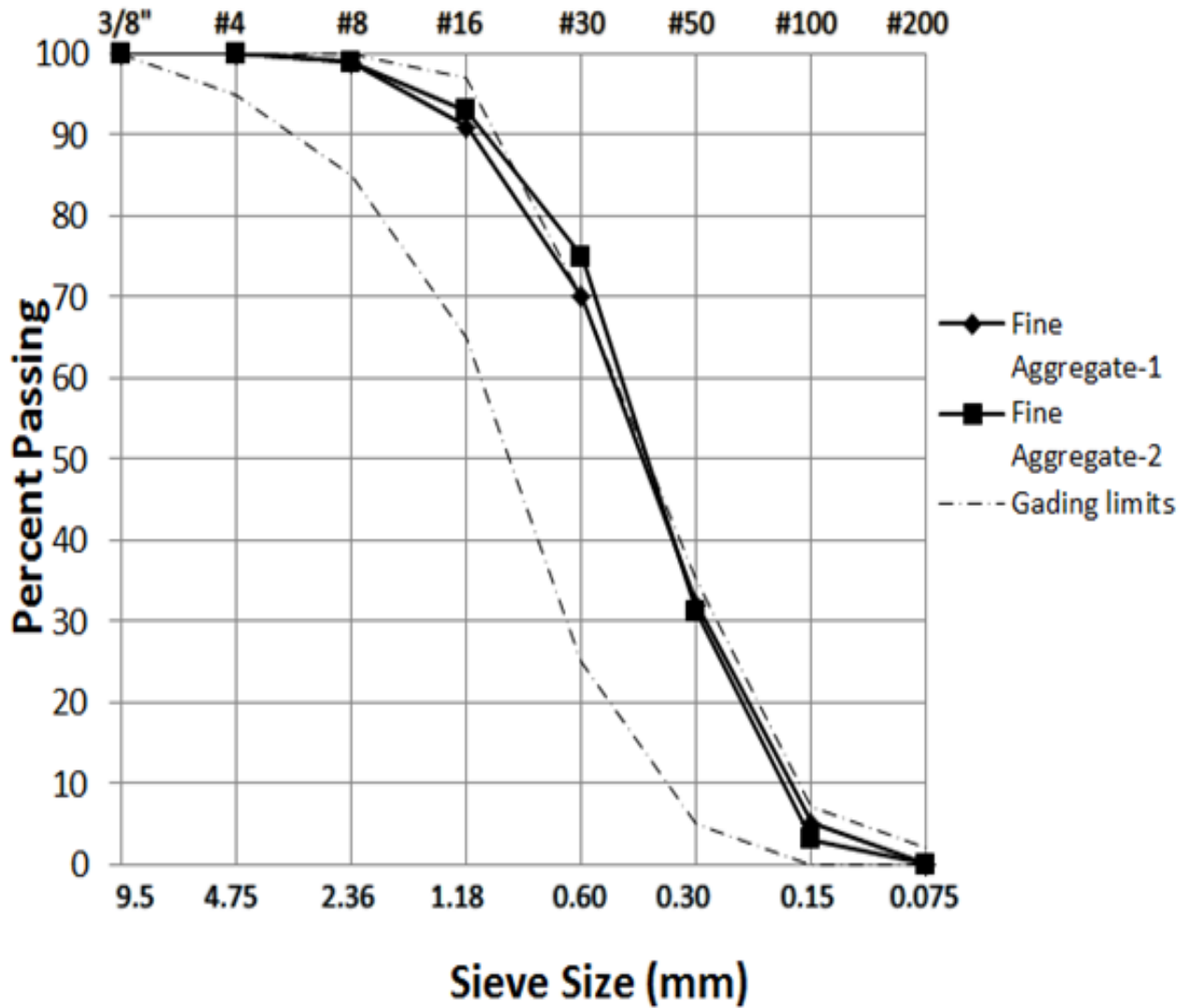


Figure 3-1. Gradation chart for virgin fine aggregate

### 3.3.3 Coarse Aggregate

The coarse aggregate used for this research study was Florida limestone, mined from the plant number #87-090. The properties of coarse aggregate were provided by FDOT and are shown in Tables 3-6 through 3-8. Table 3-6 shows the specific gravity and water absorption of the coarse aggregate. Table 3-7 shows the gradation of coarse aggregate #1 and Table 3-8 shows the gradation of coarse aggregate #2. Coarse aggregate #2 was coarser than coarse aggregate #1 and did not fit in the grading limits as shown in the Figure 3-2.

Table 3-6. Specific gravity and water absorption of coarse aggregate (Florida limestone)

Property	Unit	Coarse Aggregate-1	Coarse Aggregate-2
Bulk Specific Gravity (SSD)	/	2.43	2.41
Bulk Specific Gravity (Dry)	/	2.35	2.33
Apparent Specific Gravity (Dry)	/	2.55	2.53
Absorption	%	4.54	3.45

Table 3-7. Gradation of coarse aggregate #1 (Florida Limestone)

US	Sieve Size		Cumulative Retained (%)	Passing (%)	Grading Limits	
	inch	mm			Min (%)	Max (%)
11/2"	1.476	37.5	0	100	100	100
1"	0.984	25	0	100	95	100
1/2"	0.492	12.5	45	55	25	60
#4	0.187	4.75	94	6	0	10
#8	0.093	2.36	97	3	0	5

Table 3-8. Gradation of coarse aggregate #2 (Florida Limestone)

US	Sieve Size		Cumulative Retained (%)	Passing (%)	Grading Limits	
	inch	mm			Min (%)	Max (%)
11/2"	1.476	37.5	0	100	100	100
1"	0.984	25	1	99	95	100
1/2"	0.492	12.5	80	20	25	60
#4	0.187	4.75	98	2	0	10
#8	0.093	2.36	98	2	0	5

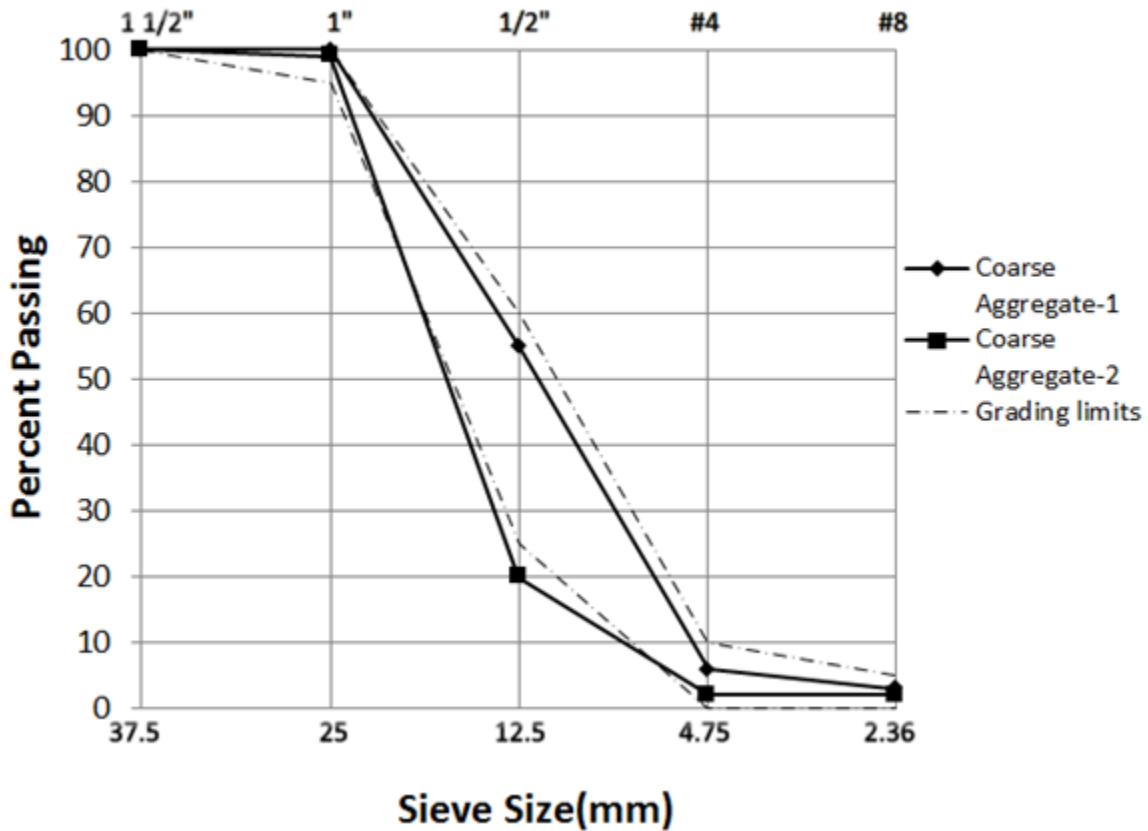


Figure 3-2. Gradation chart for virgin coarse aggregate

### 3.3.4 Recycled Asphalt Pavement (RAP)

The material that was retained on the number #4 sieve (4.75 mm) was considered as coarse RAP and the material passing number #4 sieve was considered as fine RAP. Both fine RAP and coarse RAP were tested for their physical properties by FDOT. The properties of RAP that were determined are gradation, recovered asphalt content, penetration and viscosity of the recovered asphalt binder.

Table 3-9 shows the properties of recovered asphalt binder from the various RAPs. The recovered asphalt binder viscosity is higher for the fine RAP than the coarse RAP. Fine RAP-1

has the highest asphalt binder viscosity among all other RAP's. For the coarse RAP's, not much difference in the recovered binder viscosity for different RAP types was observed.

Tables 3-10 and 3-11 show the specific gravity and water absorption of all the fine RAPs and coarse RAPs. The specific gravity and absorption for the fine RAP's are lower than those of the coarse RAP's.

Table 3-12 and Table 3-13 show the gradation of fine RAP and coarse RAP. The fineness modulus of the RAP's shows that fine RAP is much coarser than the virgin fine aggregate. The gradation curves for the fine RAP do not fit in the standard gradation limits of the virgin fine aggregate, as shown in the Figure 3-3.

The gradation of the coarse RAP shows it to be much finer than the virgin coarse aggregate and they do not fit in the standard gradation limits of virgin coarse aggregate as shown in the Figure 3-4.

Table 3-9. Properties of recovered asphalt binder from RAP

RAP Number	Recovered Aggregate Type	Recovered Viscosity (poises)		Asphalt Content (%)		Penetration of Recovered Asphalt (0.1 mm)	
		Fine RAP	Coarse RAP	Fine RAP	Coarse RAP	Fine RAP	Coarse RAP
1	Limestone and Granite	517963	202744	5.5	3.6	6	7
2	Calera Dense Limestone	434452	249890	5.5	4.3	13	17
3	Florida Limestone	422769	112847	4.9	3.9	8	15
4	Florida Limestone and Granite	308427	253709	5.9	4.4	/	/

Table 3-10. Specific gravity and water absorption of fine RAP

Property	Unit	Fine RAP-1	Fine RAP-2	Fine RAP-3	Fine RAP-4
Bulk Specific Gravity (SSD)	/	2.38	2.34	2.31	2.30
Bulk Specific Gravity (Dry)	/	2.33	2.32	2.30	2.26
Apparent Specific Gravity (Dry)	/	2.44	2.37	2.32	2.35
Absorption	%	1.92	1.00	0.51	1.80

Table 3-11. Specific gravity and water absorption of coarse RAP

Property	Unit	Coarse RAP-1	Coarse RAP-2	Coarse RAP-3	Coarse RAP-4
Bulk Specific Gravity (SSD)	/	2.43	2.38	2.33	2.35
Bulk Specific Gravity (Dry)	/	2.38	2.34	2.29	2.27
Apparent Specific Gravity (Dry)	/	2.50	2.43	2.38	2.47
Absorption	%	1.89	1.50	1.72	3.52

Table 3-12. Gradation of fine RAP

Sieve Size			Passing (%)			
US	inch	mm	RAP-1	RAP-2	RAP-3	RAP-4
3/8"	0.375	9.38	100	100	100	100
#4	0.187	4.75	75	94	85	80
#8	0.093	2.36	49	63	62	52
#16	0.046	1.18	33	40	47	32
#30	0.024	0.60	17	20	34	18
#50	0.012	0.30	5	6	16	6
#100	0.006	0.15	1	1	4	1
#200	0.003	0.075	0.15	0.2	0.5	0.3
Fineness modulus			4.2	3.76	3.52	4.11

Table 3-13. Gradation of coarse RAP

Sieve Size			Passing (%)			
US	inch	mm	RAP-1	RAP-2	RAP-3	RAP-4
1"	0.984	25	100	100	100	100
3/4"	0.75	19	99.6	99	100	100
1/2"	0.492	12.5	91	67	96	97
3/8"	0.375	9.5	63	46	64	82
#4	0.187	4.75	13	16	4	30
#8	0.093	2.36	0	0	1	0

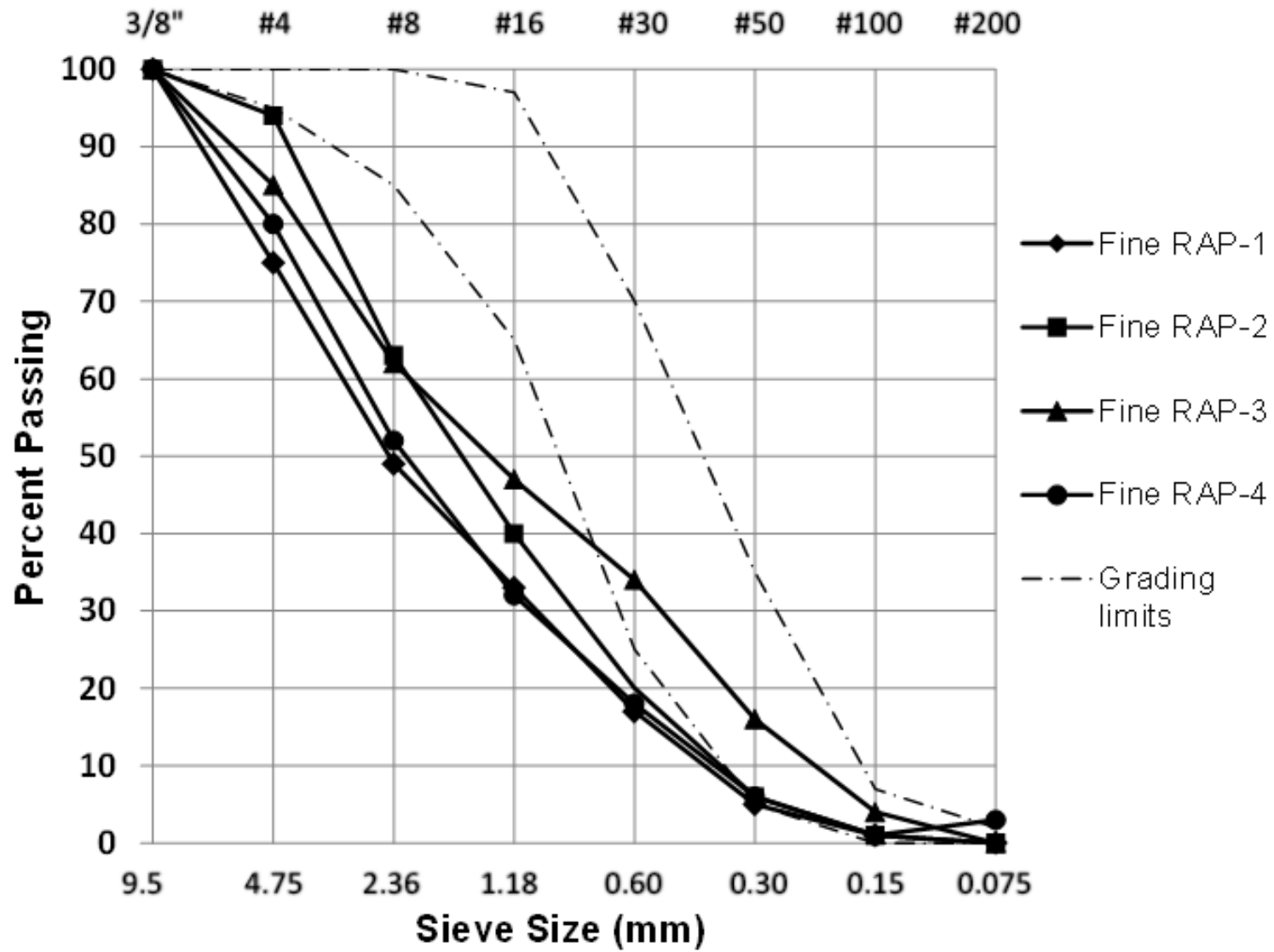


Figure 3-3. Gradation chart for fine RAP aggregate

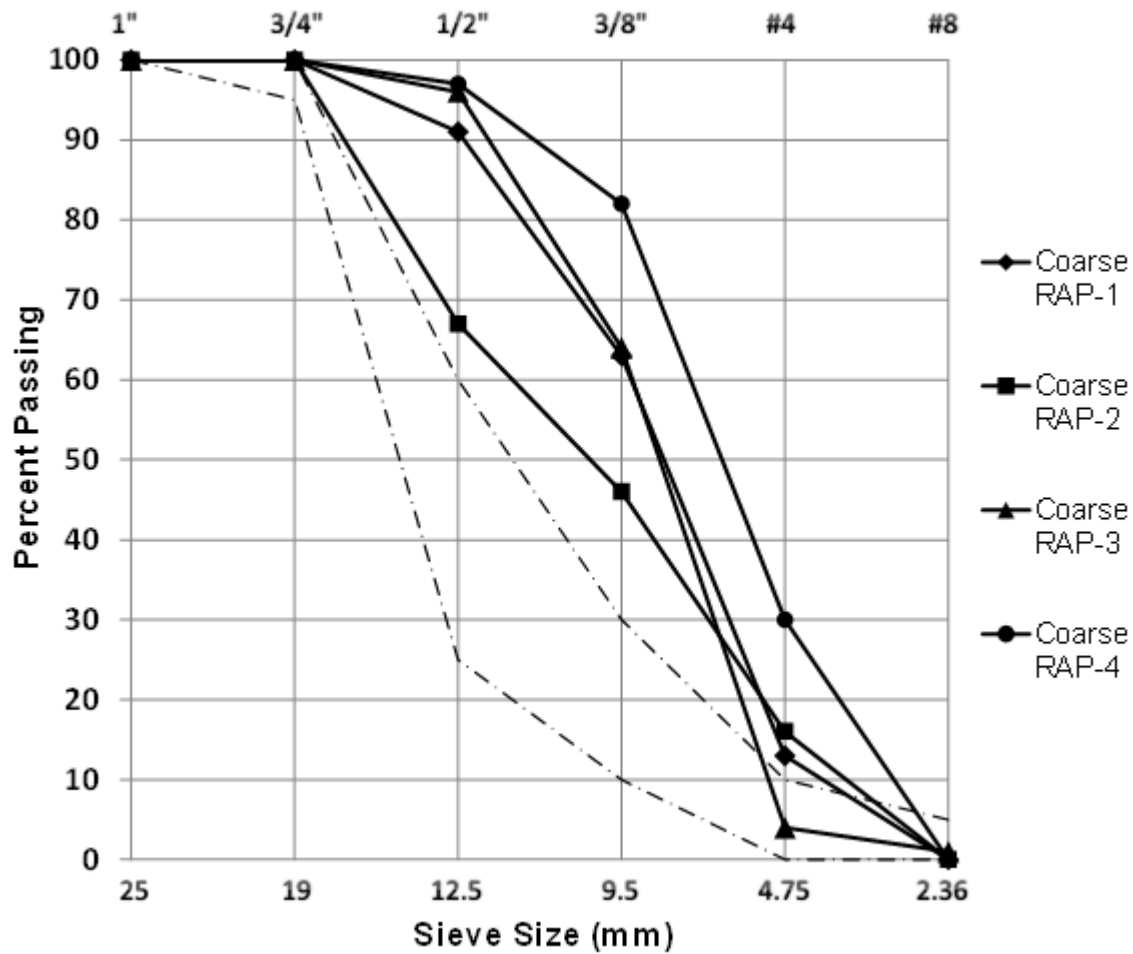


Figure 3-4. Gradation chart for coarse RAP aggregate

### 3.4 Concrete Mix Proportions

The concrete mix proportions with 0%, 20%, 40%, 70% and 100% RAP by volume of aggregate were designed for this research study. The control mixture with no RAP was designed based on a typical concrete pavement in Florida. The cement content was fixed between 490 lbs/yd<sup>3</sup> to 500 lbs/yd<sup>3</sup>, and the water cement ratio was fixed to 0.50. The percentage of total fine in mix was between 38% and 43% of the total aggregate in the mix, by volume. Trial mix was made before every production mix and the percentage fines were adjusted as needed depending on the workability of the trial batch. A water reducing admixture was added during trial batch to get the desired target slump. For all the mixtures, an air entraining admixture was added, as it is a

usual practice in Florida to improve the workability and durability of pavement concrete. The dosage of air entraining agent was kept constant and the slump of the concrete was achieved by adjusting the water reducing admixture.

A total of 19 mixtures were produced in the laboratory and evaluated in this research study. Three control mixtures using Florida limestone and fine silica sand aggregate with three different water cement ratios were produced. Concrete mixtures with four different RAP aggregates and with four different percent of aggregate replacements were evaluated in this research study.

For the concrete with 20% RAP, the virgin fine aggregate was replaced by 20% fine RAP by volume, and the virgin coarse aggregate was replaced by 20% coarse RAP by volume. For the concrete with 40% RAP, the virgin fine aggregate was replaced by 40% fine RAP by volume, and the virgin coarse aggregate was replaced by 40% coarse RAP by volume. For the concrete with 70% RAP, the virgin fine aggregate was replaced by 70% fine RAP by volume, and the virgin coarse aggregate was replaced by 70% coarse RAP by volume.

Table 3-14 shows all the concrete mixtures that were evaluated in this research study and Table 3-15 shows the mix proportions for these different concrete mixtures.

Table 3-14. Concrete mixtures containing RAP to be evaluated

Mix Type	Number	W/C	Cement (lbs/yd <sup>3</sup> )	Total Fine and Coarse Aggregate in Percentage by Volume				Total RAP (%)
				Virgin fine	Fine RAP	Virgin coarse	Coarse RAP	
Control	1	0.45	556	100	0	100	0	0
	2	0.50	500	100	0	100	0	0
	3	0.55	454	100	0	100	0	0
RAP-1	4	0.50	500	80	20	80	20	20
	5	0.50	500	60	40	60	40	40
	6	0.50	500	30	70	30	70	70
	7	0.50	500	0	100	0	100	100
RAP-2	4	0.50	500	80	20	80	20	20
	5	0.50	500	60	40	60	40	40
	6	0.50	500	30	70	30	70	70
	7	0.50	500	0	100	0	100	100
RAP-3	4	0.50	500	80	20	80	20	20
	5	0.50	500	60	40	60	40	40
	6	0.50	500	30	70	30	70	70
	7	0.50	500	0	100	0	100	100
RAP-4	4	0.50	500	80	20	80	20	20
	5	0.50	500	60	40	60	40	40
	6	0.50	500	30	70	30	70	70
	7	0.50	500	0	100	0	100	100

Table 3-15. Mix proportions of concrete mixtures used in this research study

Mix Type	Number	RAP (%)	W/C	Water (lbs/yd <sup>3</sup> )	Cement (lbs/yd <sup>3</sup> )	Coarse Aggregate (lbs/yd <sup>3</sup> )		Fine Aggregate (lbs/yd <sup>3</sup> )		AEA Daravair (oz)	WRDA 60 (oz)
						Virgin	RAP	Virgin	RAP		
Control	1	0	0.45	250	556	1816	0	1195	0	1	15
	2	0	0.50	250	500	1845	0	1212	0	1	12
	3	0	0.55	250	454	1865	0	1228	0	1	9
RAP-1	4	20	0.50	250	500	1460	368	1003	202	1	30
	5	40	0.50	250	500	1072	740	788	410	1	0
	6	70	0.50	250	500	485	1300	448	740	1	0
	7	100	0.50	250	500	0	1657	0	1265	1	46
RAP-2	4	20	0.50	248	493	1421	285	998	260	1	45
	5	40	0.50	248	495	1036	621	770	515	1	39
	6	70	0.50	250	499	528	1195	382	813	1	39
	7	100	0.50	248	495	0	1683	0	1167	1	62
RAP-3	4	20	0.50	246	491	1403	330	1049	226	1	30
	5	40	0.50	246	491	1047	660	821	441	1	30
	6	70	0.50	250	499	511	1137	415	804	1	30
	7	100	0.50	250	500	0	1562	0	1241	1	30
RAP-4	4	20	0.50	250	497	1338	346	1097	235	1	30
	5	40	0.50	250	497	959	702	853	470	1	15
	6	70	0.50	250	497	516	1166	412	800	1	18
	7	100	0.50	250	500	0	1525	0	1283	1	60

## **CHAPTER 4 EVALUATION OF AGGREGATE GRADATIONS OF CONCRETE CONTAINING RAP**

### **4.1 Combined Aggregate Gradation**

Table 4-1 and Table 4-2 show the combined gradations of fine and coarse aggregates with various percentages of aggregate replacements by RAP. Fineness modulus of the fine aggregate increased with the increase in the percentage of the RAP in the mixtures, due to the coarseness of the fine RAP.

The fine fraction of the aggregate and the coarse fraction of the aggregate were combined volumetrically to determine the individual percentage retained on each sieve. The “8-18” band was used as the reference for the minimum and maximum percent retained on the individual percentage retained chart.

From the individual percentage retained values, the coarseness factor and the workability of every mix were determined. The total material retained on the 3/8" sieve was considered as coarse particles. The total material retained on the #4 and #8 sieve was considered as intermediate particles. The ratio of particles retained on 3/8" sieve and the particles retained on 3/8", #4 and #8 sieve was the coarseness factor. The particles passing the #8 sieve was used to calculate the workability. This chart was developed for all the concrete mixtures to evaluate the effects of RAP on the workability of the concrete mix.

### **4.2 Evaluation of Aggregate Gradations**

Three major steps, as recommended by Shilstone were followed to evaluate the aggregate gradation of concrete mixtures containing RAP. First, the coarseness factor of the combined aggregate was determined to provide us an overview of the mixtures workability based on aggregate gradation.

Table 4-1. Combined gradation of fine aggregate with various percentages of RAP

Sieve Size	RAP-1			RAP-2			RAP-3			RAP-4		
	Percent Replacement			Percent Replacement			Percent Replacement			Percent Replacement		
	20	40	70	20	40	70	20	40	70	20	40	70
	Percent Passing			Percent Passing			Percent Passing			Percent Passing		
3/8	100	100	100	100	100	100	100	100	100	100	100	100
#4	96	91	85	99	97	95	97	94	90	97	93	88
#8	90	82	68	93	86	76	92	85	74	91	83	71
#16	75	67	53	80	71	59	79	73	61	83	73	57
#30	61	52	38	66	56	42	67	60	48	66	56	41
#50	28	23	16	27	23	16	28	25	21	28	23	17
#100	4	4	3	3	3	2	3	3	4	4	4	3
#200	0	0	0	0	0	0	0	0	0	0	0	0
Fineness Modulus	2.46	2.81	3.37	2.32	2.64	3.10	2.34	2.60	3.02	2.31	2.68	3.23

Table 4-2. Combined gradation of coarse aggregate with various percentages of RAP

Sieve Size	RAP-1			RAP-2			RAP-3			RAP-4		
	Percent Replacement			Percent Replacement			Percent Replacement			Percent Replacement		
	20	40	70	20	40	70	20	40	70	20	40	70
	Percent Passing			Percent Passing			Percent Passing			Percent Passing		
11/2"	100	100	100	100	100	100	100	100	100	100	100	100
1"	100	100	100	99	99	100	99	99	100	99	99	100
1/2"	62	70	81	29	39	54	34	48	72	36	53	79
#4	7	9	11	5	8	12	2	3	3	8	14	24
#8	2	2	1	2	1	1	2	1	1	2	1	0
Total Fineness Modulus	5.09	5.17	5.30	5.17	5.16	5.32	5.14	5.16	5.19	4.99	5.09	5.11

Second, the individual percentage retained chart was plotted to reveal the unwanted gaps in the particle sizes. Finally, the ideal 0.45 chart for aggregate gradation was plotted; deviation

from the ideal line will help us to differentiate between different concrete mixtures. Each of the above steps will be discussed separately in the following sections.

#### **4.2.1 Coarseness Factor of Combined Aggregate**

Figures 4-1 through 4-4 show the coarseness factor chart for concrete mixtures containing 0%, 20%, 40%, 70% and 100% RAP, respectively. The control mixture is plotted very close to the boundary line between zone II and zone IV, which shows that there is too much fines in the control mixtures making it prone to shrinkage and cracking. Figure 4-1 shows the coarseness factor chart for concrete mixtures containing 20% RAP. The mixtures with 20% RAP-1, 20% RAP-3 and 20% RAP-4 were located in zone II of the coarseness factor chart, which is the optimal zone on this chart. However, the mix with 20% RAP-2 was slightly off the optimal zone and located in zone I. Generally, the concrete mixtures with 20% RAP were very similar to the control mix, except for 20% RAP-1.

Figure 4-2 shows the coarseness factor chart for concrete mixtures containing 40% RAP. All the mixtures with 40% RAP were located in the optimal zone of the coarseness factor chart. The mixture with 40% RAP-1 was located on the trend bar, while the other mixtures were away from the trend bar. The coarseness factor decreased with addition of 40% RAP which shows the increase in the intermediate size particles in the mix. However, this causes a decrease in the workability for concrete mixtures with 40% RAP, but it is still a reasonable reduction since the mixtures are located in the optimum zone.

Figure 4-3 shows the coarseness factor chart for concrete mixtures containing 70% RAP. The mixtures with 70% RAP-2 and 70% RAP-3 were located on the trend bar and the mixtures with 70% RAP-1 and 70% RAP-4 were slightly below the trend bar, in zone V. This shows the coarseness of the mixture increases as the percentage of the RAP replacement increases, and the

workability decreases due to reduction in the fine particles in the mix. Similarly for all the mixtures with 100% RAP, the coarseness factor and the workability decreased, thus making the mix very coarse and unreasonable for any application. In general, the mixtures with 70% and 100% RAP need more fines to increase the workability of the mix. However, for the mixes with 20% RAP and 40% RAP, the workability and the coarseness factor are in the optimum zone for almost all the mixtures.

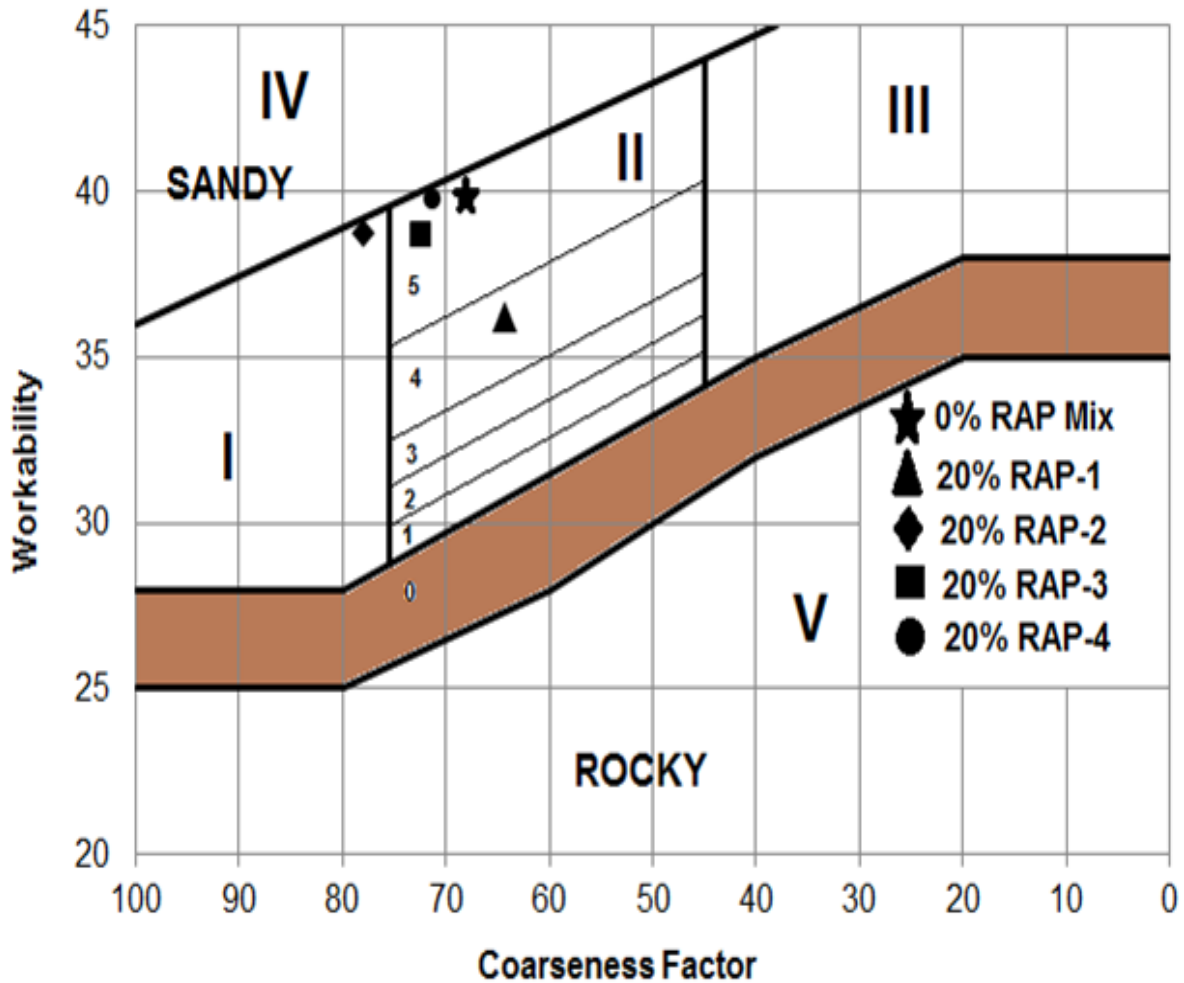


Figure 4-1. Coarseness factor chart for concrete mixtures containing 20% RAP

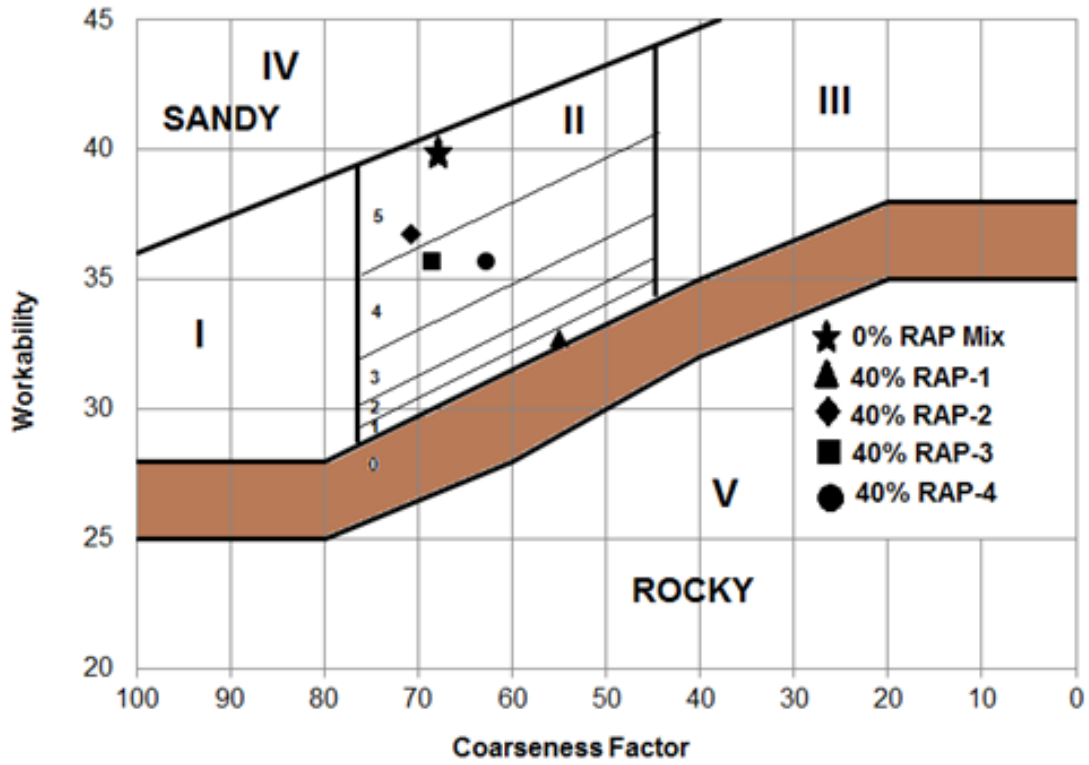


Figure 4-2. Coarseness factor chart for concrete mixtures containing 40% RAP

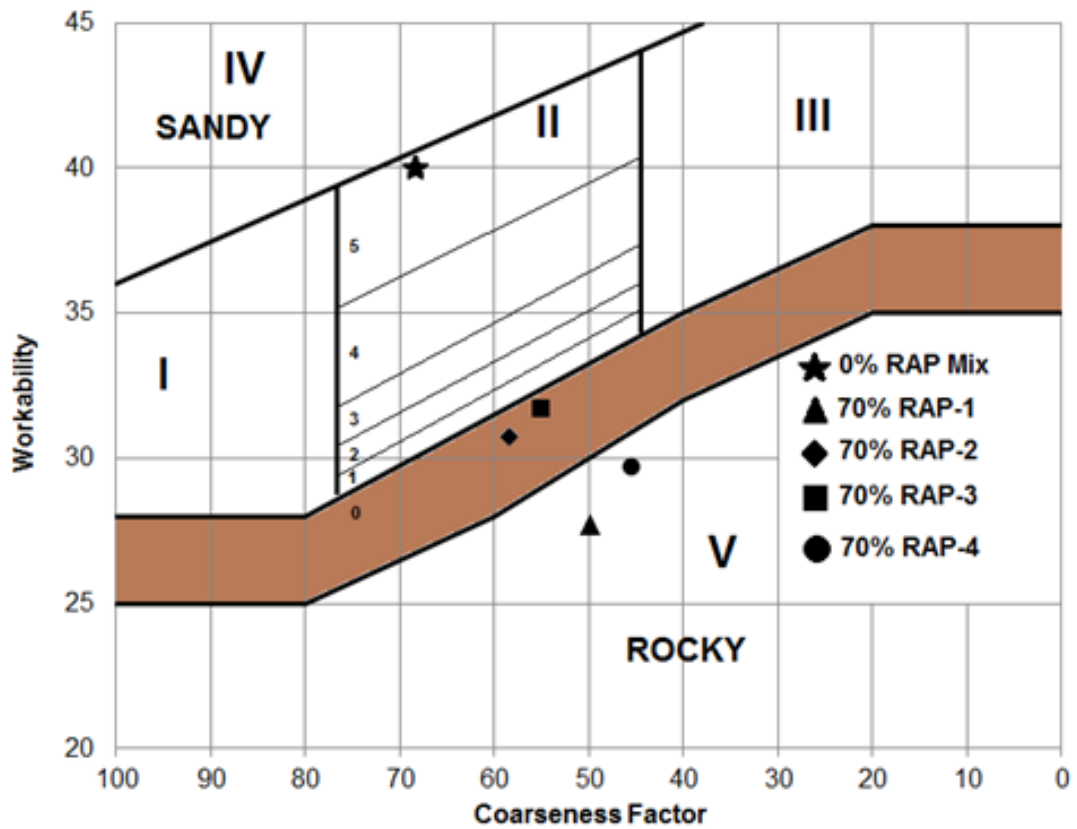


Figure 4-3. Coarseness factor chart for concrete mixtures containing 70% RAP

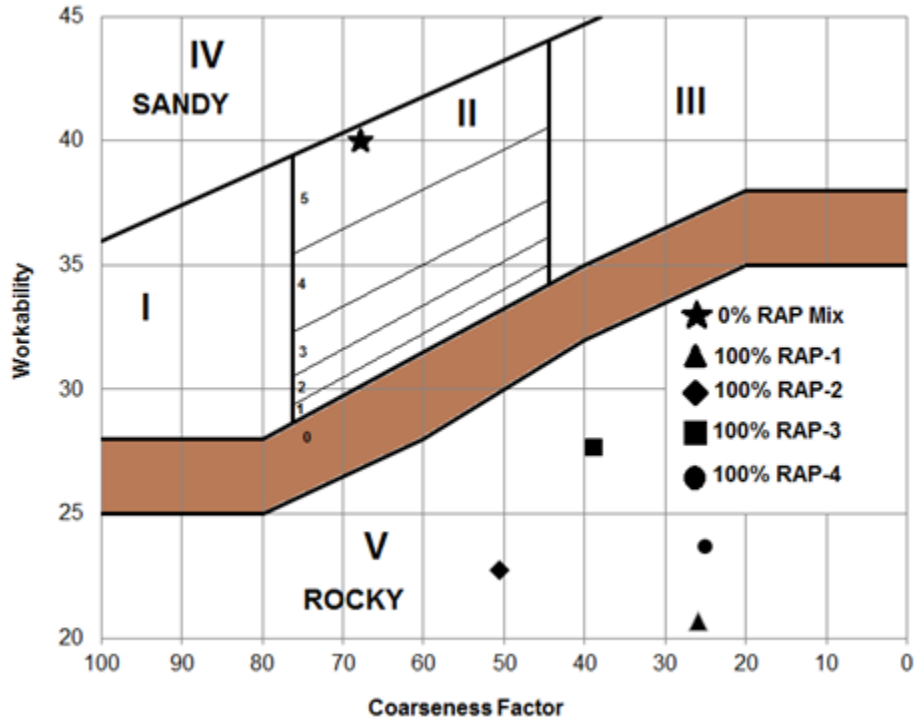


Figure 4-4. Coarseness factor chart for concrete mixtures containing 100% RAP

#### 4.2.2 Individual Percentage Retained of Combined Aggregate

The coarse aggregate and the fine aggregate were combined volumetrically for the specific mixture to determine the individual percentage retained chart. The individual percentage chart can help us to identify the excess or lack of aggregate particles on the specific sieves.

Figures 4-5 through 4-12 show the individual percentage retained charts for concrete mixtures with 0%, 20%, 40%, 70% and 100% RAP. For the mixtures with no RAP, there is a double hump behavior showing lack of intermediate sized particles retained on the #8 and #16 sieves and excessive particles retained on 3/8" and #30 sieves. For concrete mixtures with 20% RAP, there is too much material retained on the 3/8", #4 and #30 sieves. However, there is little increase in the intermediate size particles when compared with the mixture with no RAP.

For concrete mixtures with 40% RAP, there is much better improvement in intermediate size particles with increase in the material retained on the #8 and #16 sieves as compared with

the other mixtures. The concrete mixtures with 40% RAP also fitted better on the “8-18” band as compared with mixtures with other percentages of RAP replacements.

For concrete mixtures with 70% and 100% RAP, there are too much materials retained on 3/8", #4, #8 and #16 sieves, which shows that there is too much of intermediate sized particles with lack of very coarse and very fine aggregate. However, the mix with 70% RAP-2 did fit in the “8-18” band.

In general, the concrete mixtures with no RAP were gap graded with lack of intermediate sized particles. The addition of RAP increases the amount of intermediate size particles with concrete mixtures with 40% RAP fitting much better on the “8-18” band as compared with the mixes with other RAP replacements.

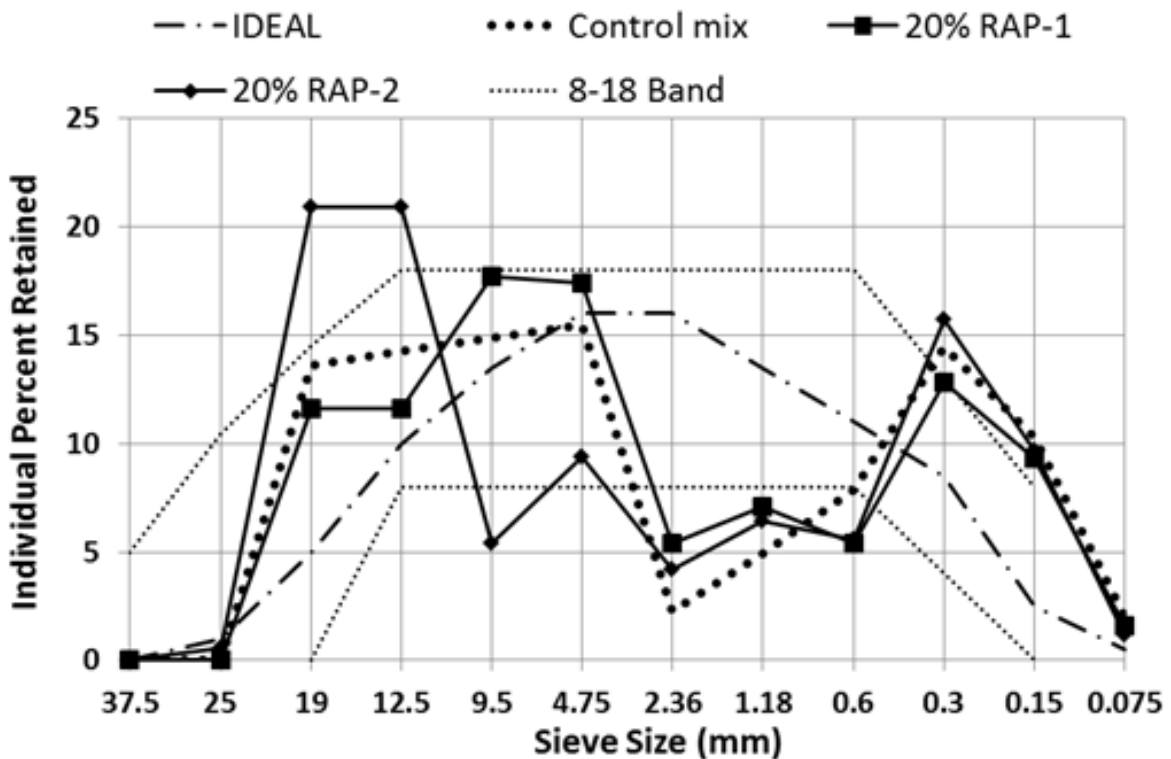


Figure 4-5. Individual percentage retained chart for concrete mixtures containing 20% RAP-1 and 20% RAP-2

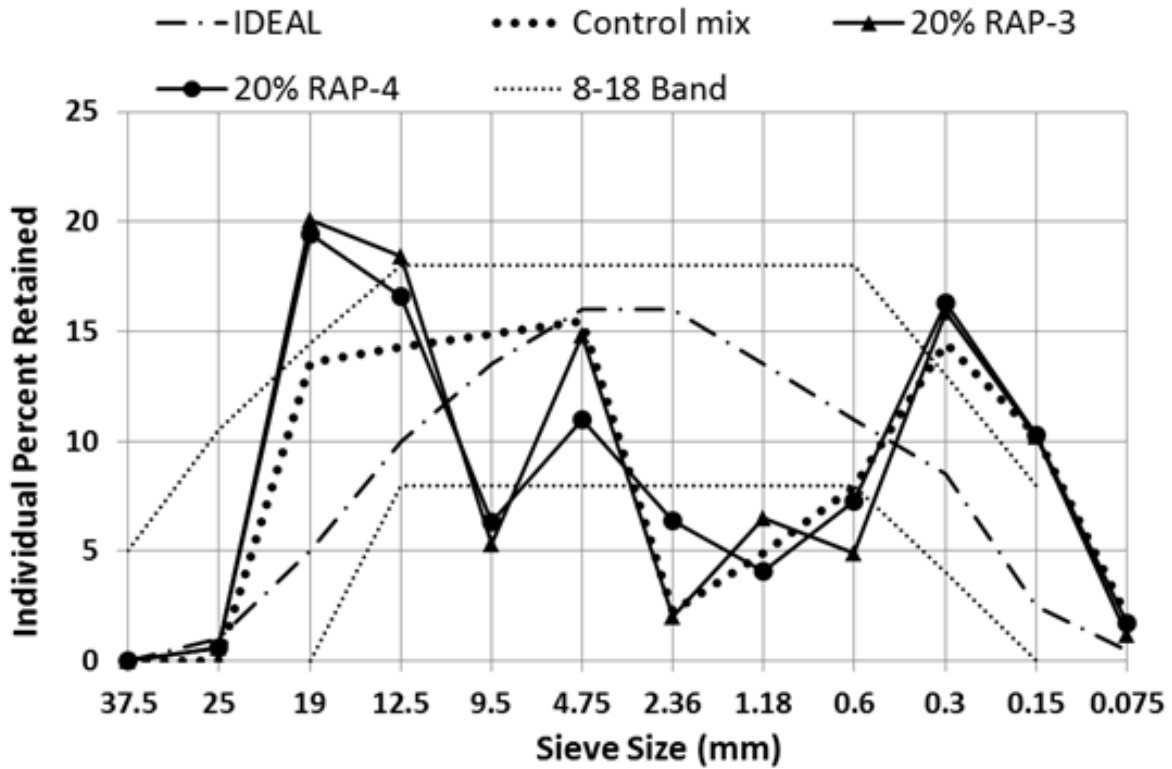


Figure 4-6. Individual percentage retained chart for concrete mixtures containing 20% RAP-3 and 20% RAP-4

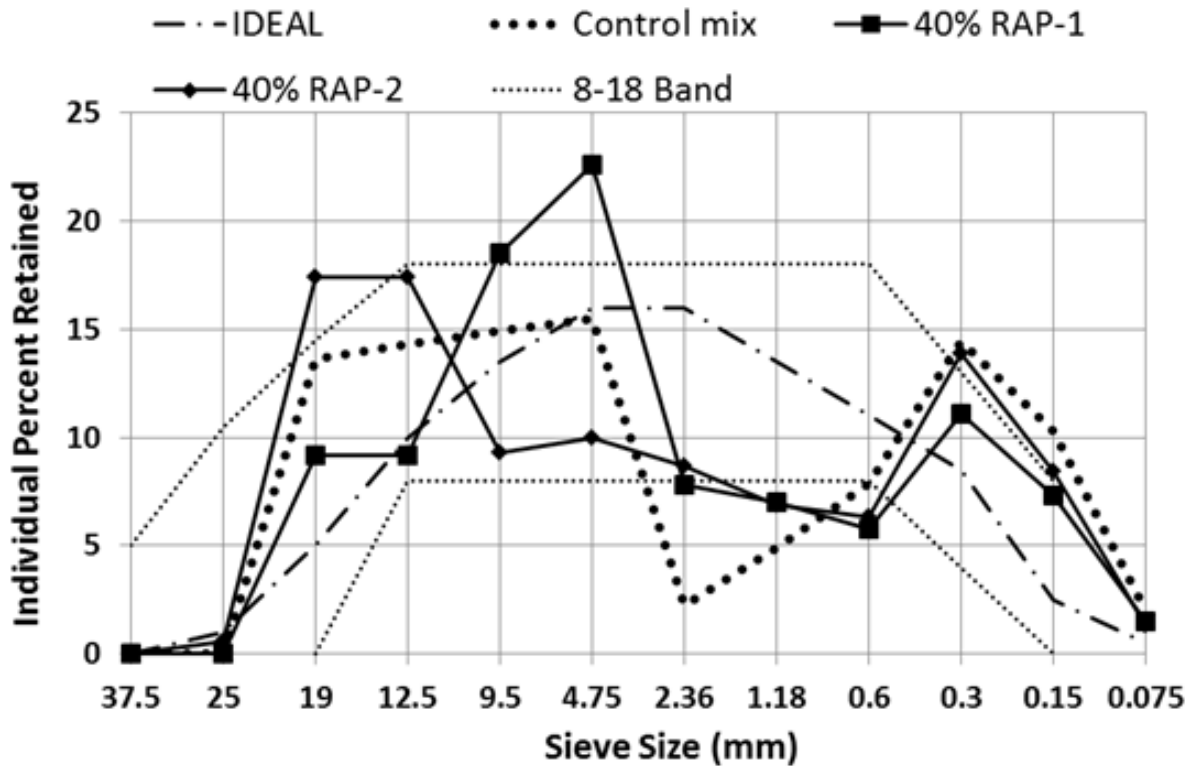


Figure 4-7. Individual percentage retained chart for concrete mixtures containing 40% RAP-1 and 40% RAP-2

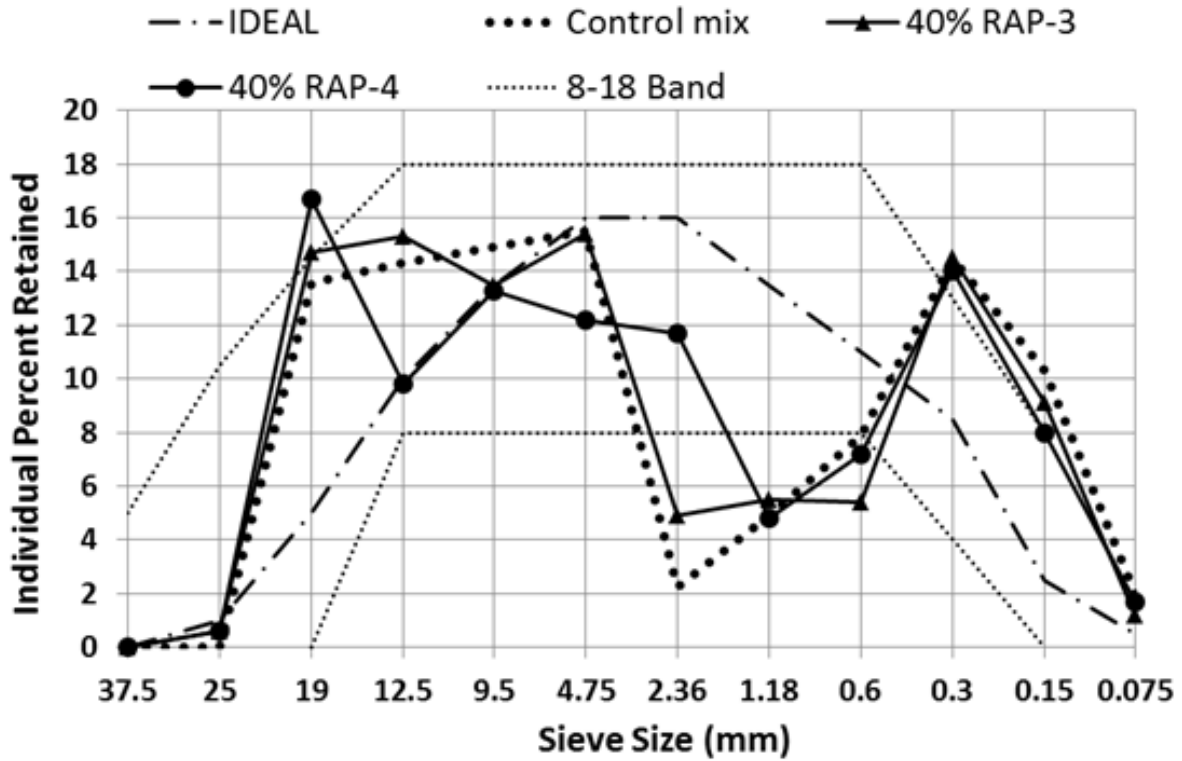


Figure 4-8. Individual percentage retained chart for concrete mixtures containing 40% RAP-3 and 40% RAP-4

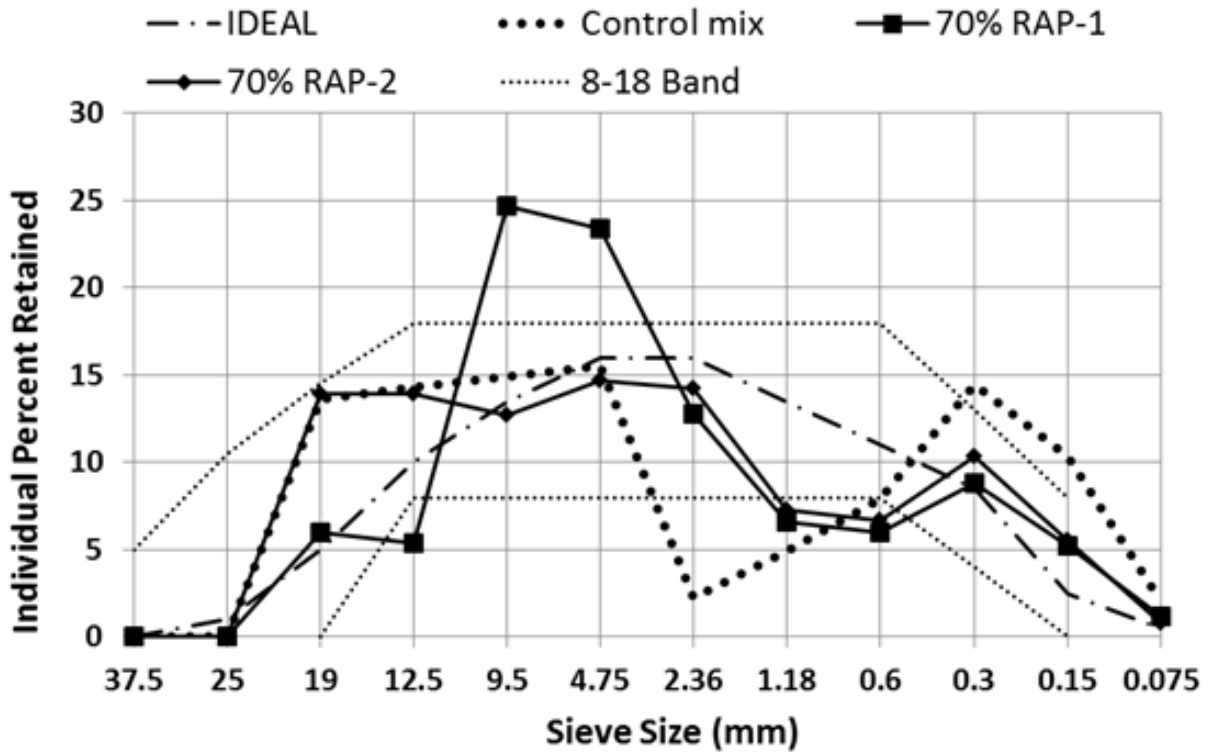


Figure 4-9. Individual percentage retained chart for concrete mixtures containing 70% RAP-1 and 70% RAP-2

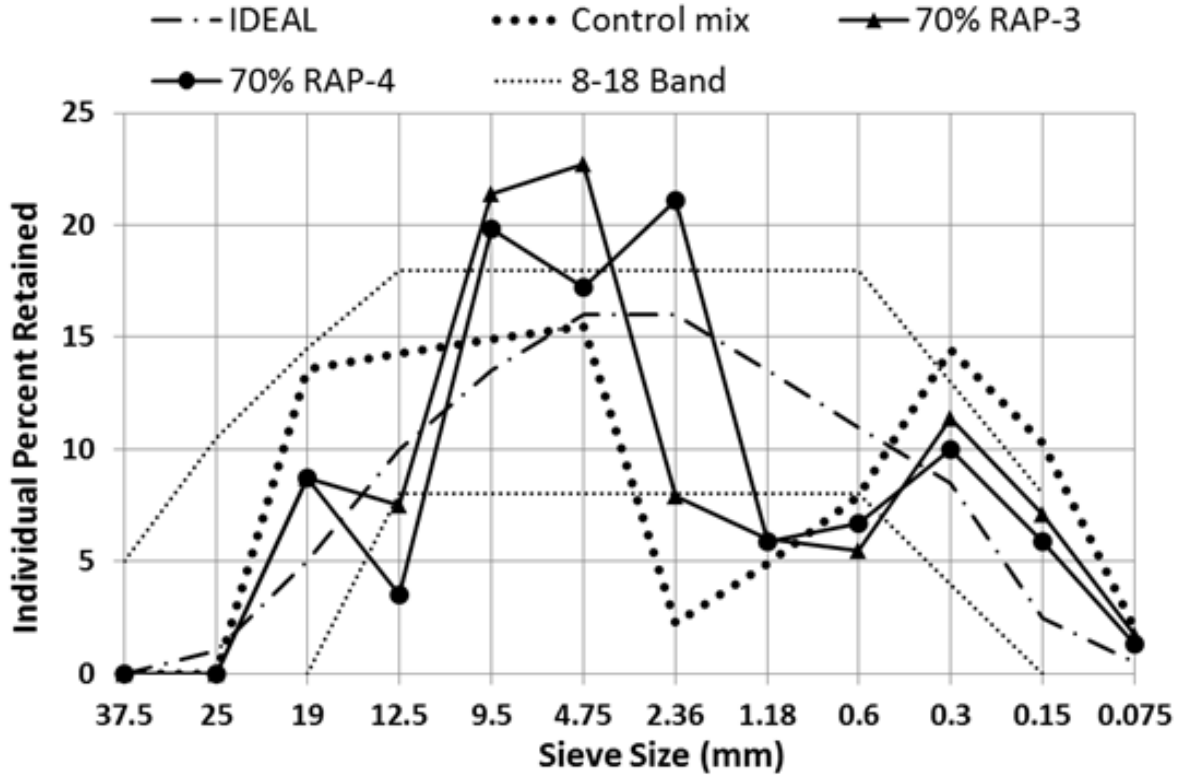


Figure 4-10. Individual percentage retained chart for concrete mixtures containing 70% RAP-3 and 70% RAP-4

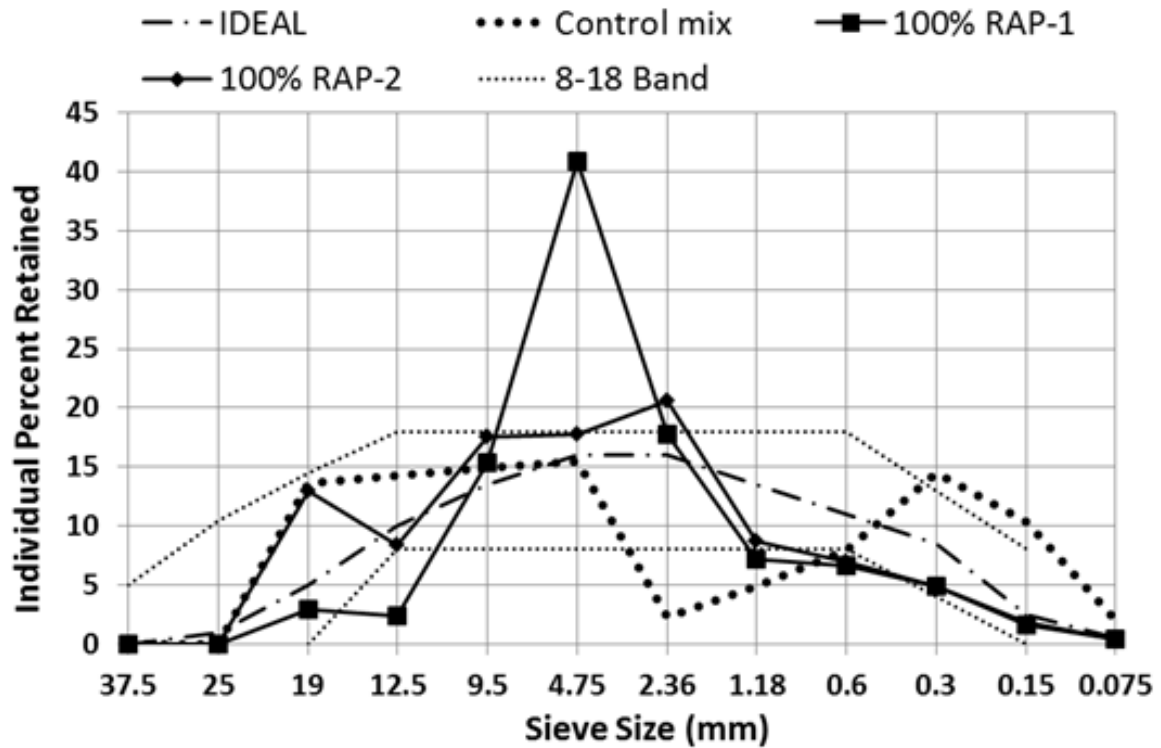


Figure 4-11. Individual percentage retained chart for concrete mixtures containing 100% RAP-1 and 100% RAP-2

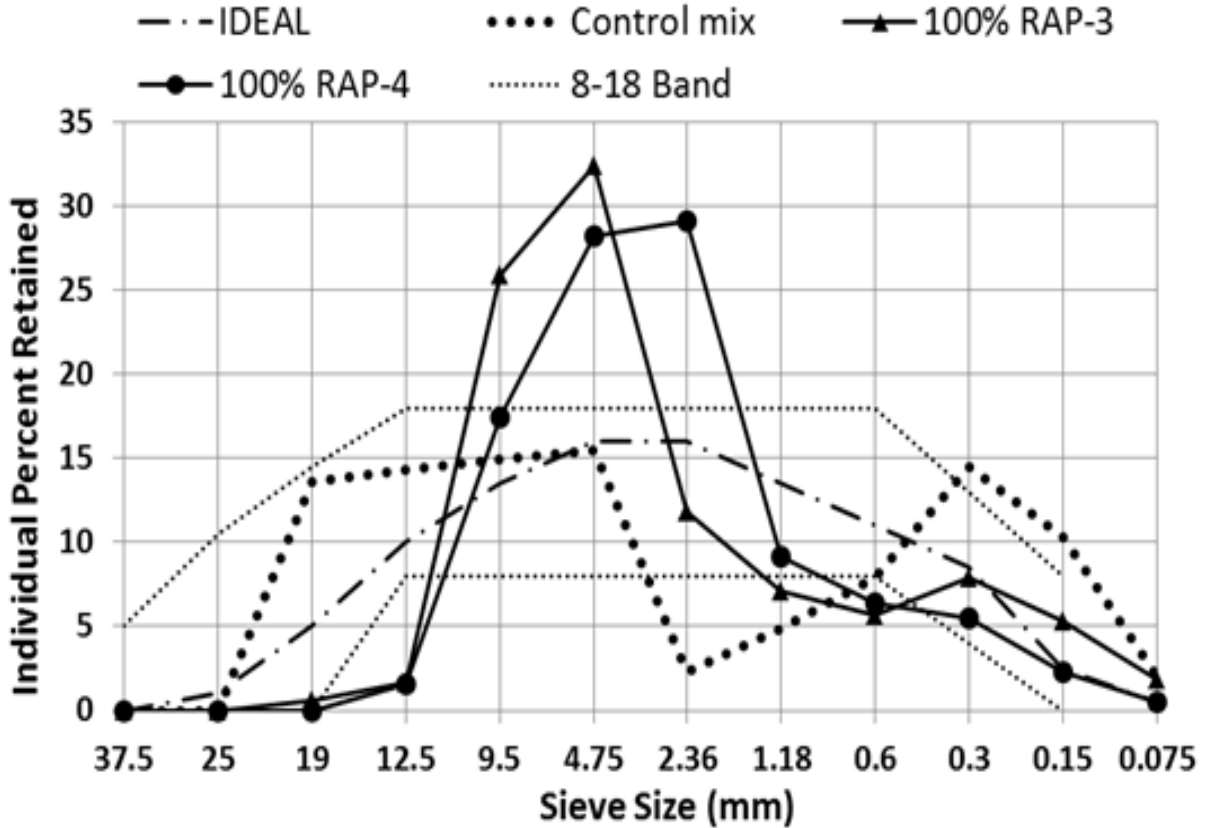


Figure 4-12. Individual percentage retained chart for concrete mixtures containing 100% RAP-3 and 100% RAP-4

#### 4.2.3 0.45 Power Chart of Combined Aggregate

The 0.45 power chart was plotted for all the aggregate gradations with different RAP replacements as shown in Figures 4-13 to 4-16. The 0.45 power chart shows that the coarse RAP is much finer than the virgin coarse aggregate with too much RAP passing 3/4", 1/2" and 3/8", while the fine RAP is much coarser than the virgin fine aggregate with very little passing the #30 and #50 sieves. The concrete mixtures without RAP are gap graded with little material between #8 and #30 sieves. In general, the 0.45 power chart for 40% RAP replacement mixtures was closer to the optimum line than the other mixtures.

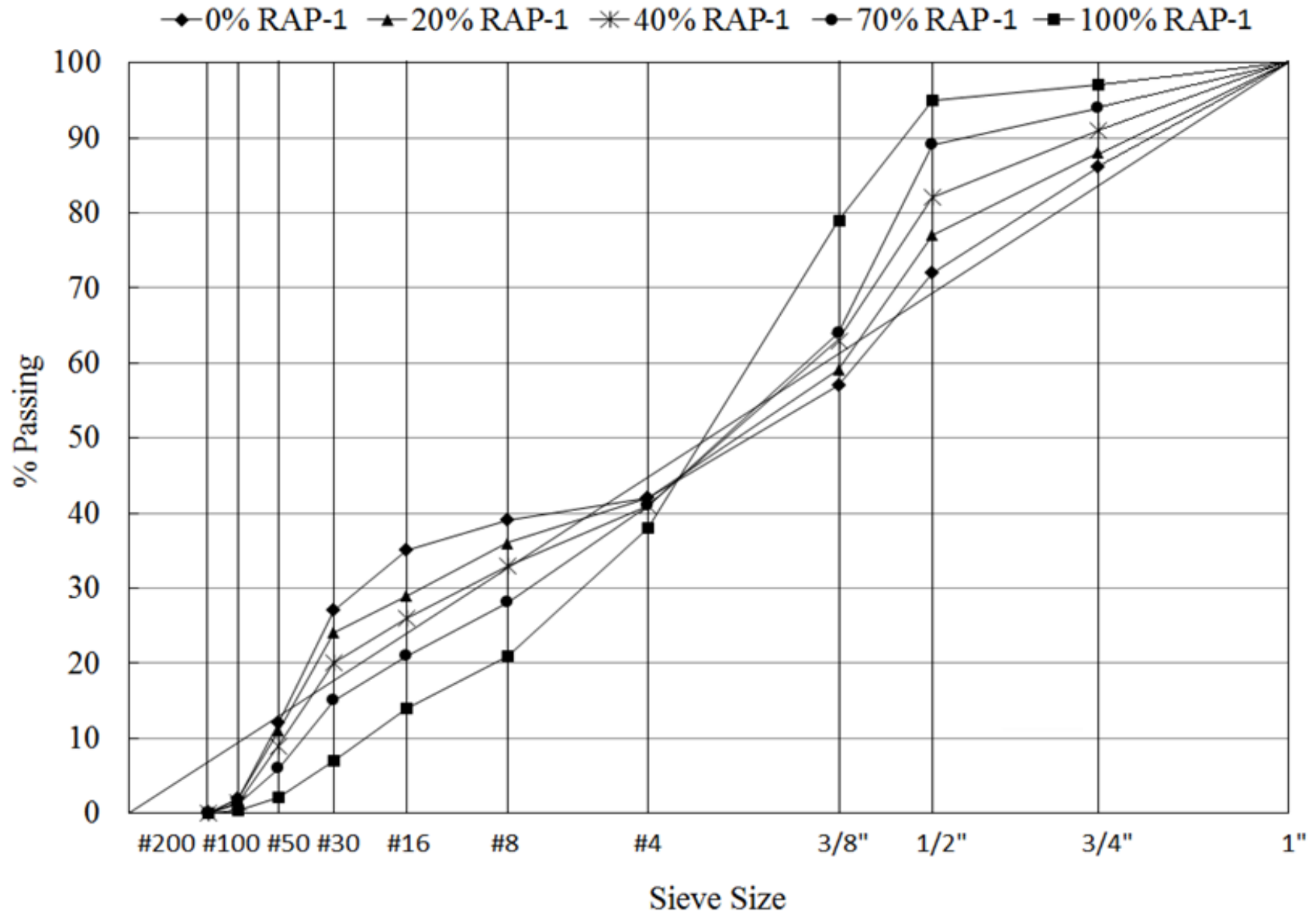


Figure 4-13. 0.45 power chart for gradation of concrete mixtures containing RAP-1

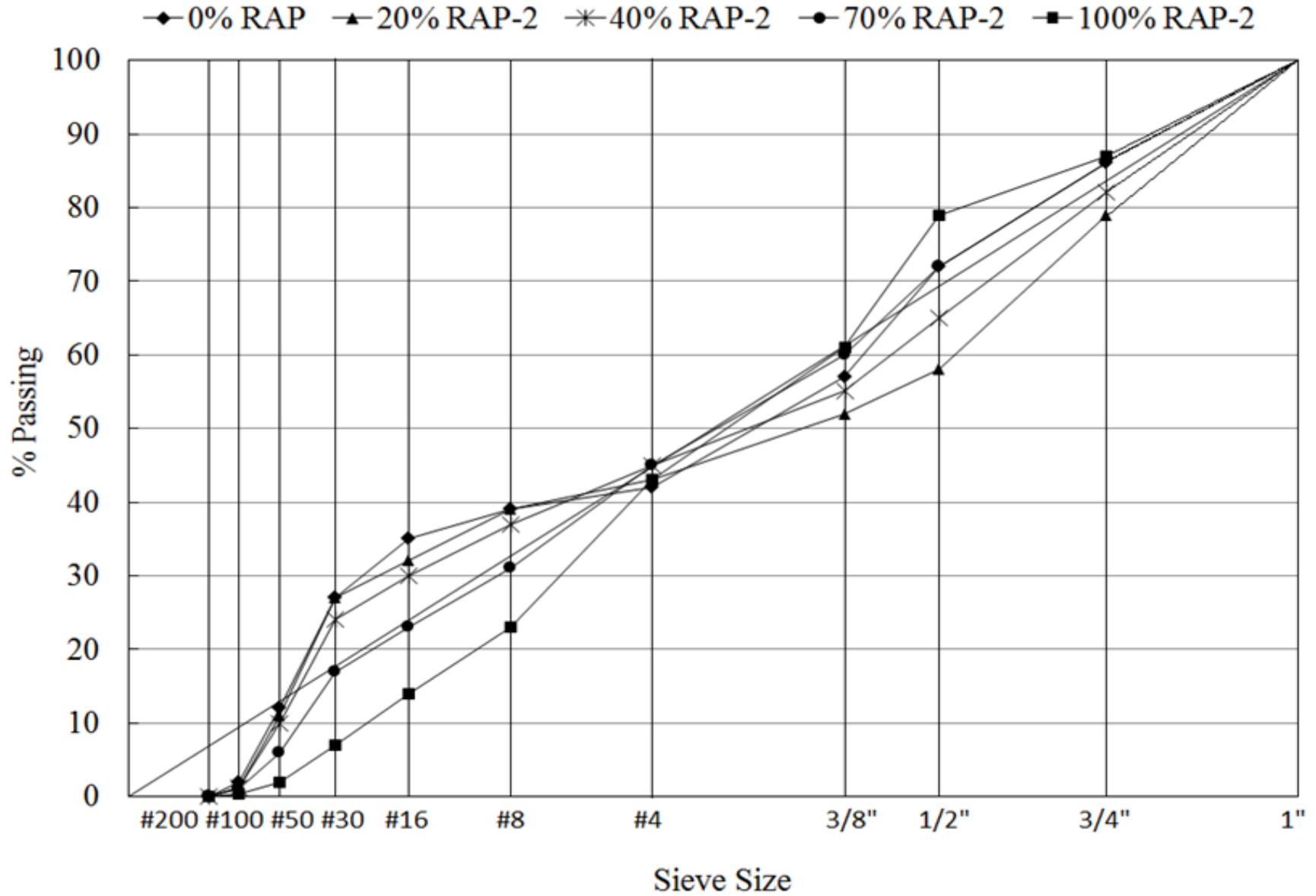


Figure 4-14. 0.45 power chart for gradation of concrete mixtures containing RAP-2

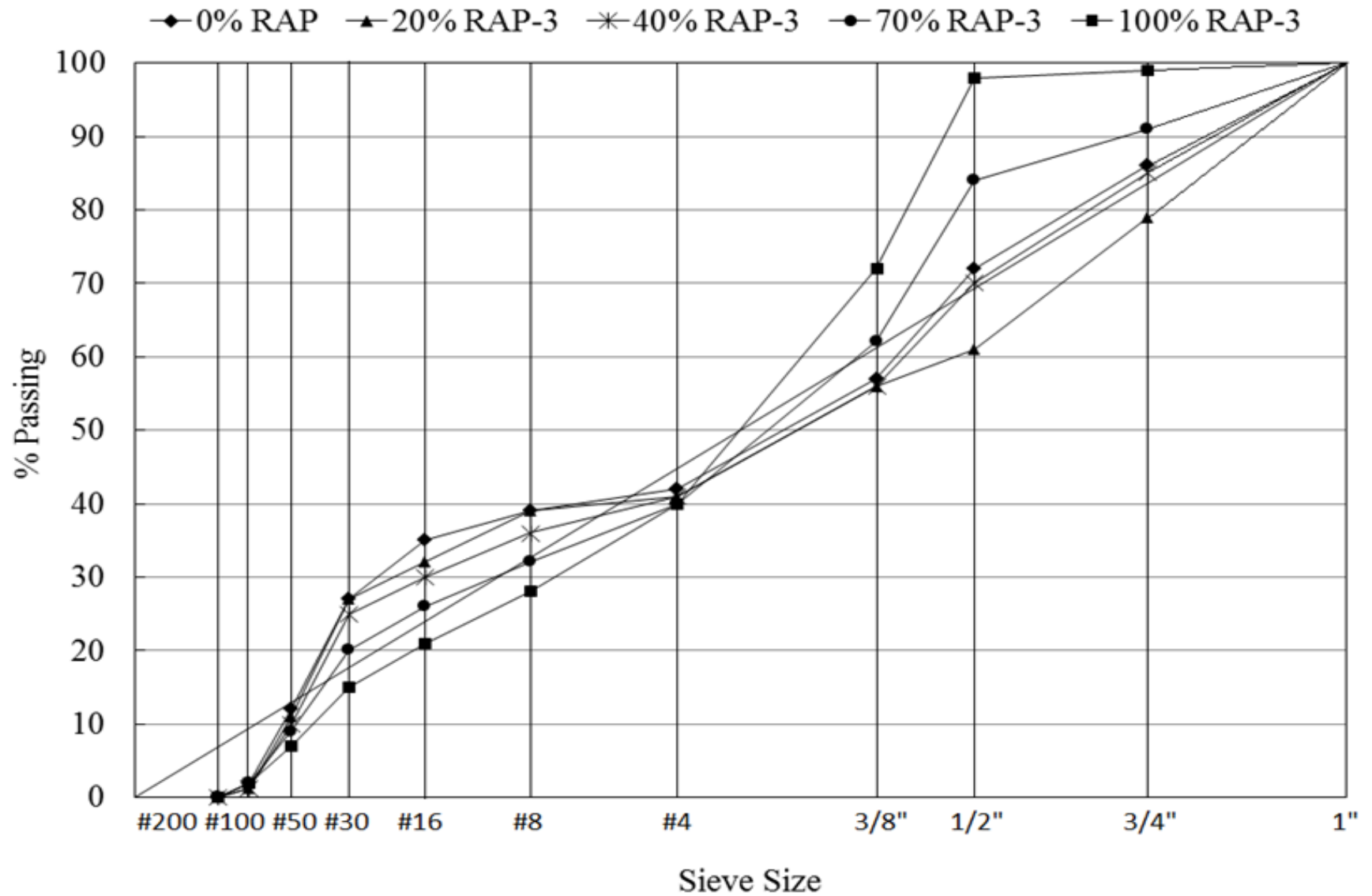


Figure 4-15. 0.45 power chart for gradation of concrete mixtures containing RAP-3

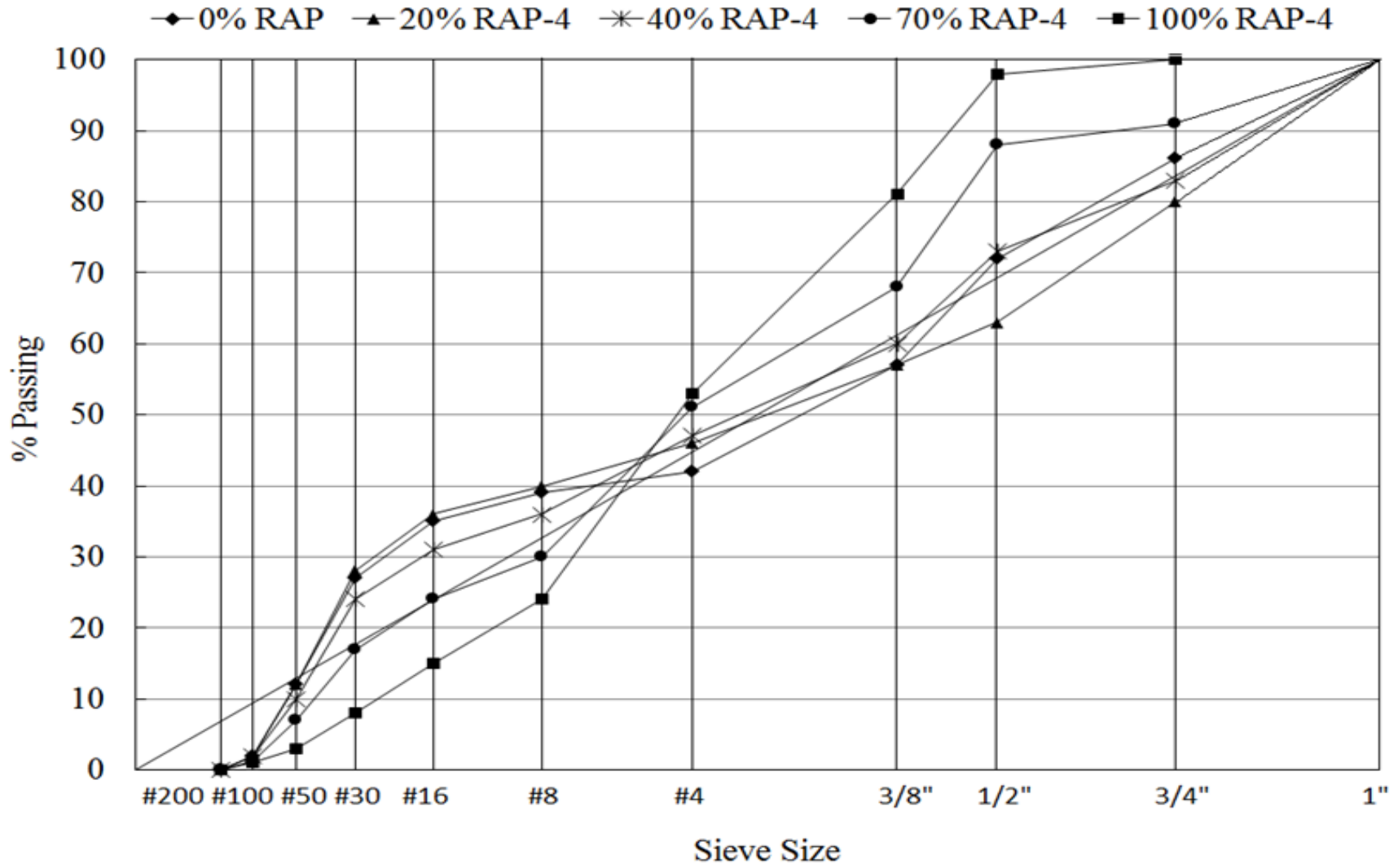


Figure 4-16. 0.45 power chart for gradation of concrete mixtures containing RAP-4

### **4.3 Summary of Findings**

- The addition of RAP to virgin aggregate improves the combined gradation of the aggregate.
- The fineness modulus of the fine aggregate increased as the percentage of fine RAP increased in the mix.
- The individual percent retained on the #8 and #16 sieves increased as the percentage of RAP increased in the mix.
- The concrete mixtures with 40% RAP showed the best gradation in terms of the coarseness factor, individual percent retained on #8 and #16 sieves, and 0.45 power chart.

## CHAPTER 5 CONCRETE PRODUCTION AND TEST METHODS

### 5.1 Introduction

This chapter presents the details of the methods for the preparation of concrete in laboratory, specimen preparation and curing procedure. Table 5-1 shows all the standard tests performed on the fresh and hardened concrete. The details of these tests are also presented in this chapter.

Table 5-1. Standard tests on fresh and hardened concrete

Concrete Test	Standard
Slump	ASTM C143
Unit Weight	ASTM C138
Air Content	ASTM C173
Fresh Concrete Temperature	ASTM C1064
Compressive Strength	ASTM C39
Young's Modulus	ASTM C 469
Flexural Strength	ASTM C 78
Splitting Tensile Strength	ASTM C 496
Poisson's Ratio	ASTM C 469
Coefficient of Thermal Expansion	AASHTO T 336-09
Drying Shrinkage	ASTM C157

### 5.2 Fabrication and Curing of Concrete Specimens

Concrete mixtures were produced at the FDOT materials concrete laboratory in Gainesville, Florida. Drum mixer with a capacity of 9.5 cubic feet was used to produce concrete. Trial batches were produced before every production batch in order to ensure the slump and workability of the concrete mixtures. Table 5-1 shows the number of specimens and volume of the concrete produced per batch.

#### 5.2.1 Concrete Preparation

The following steps were performed to produce concrete in the laboratory:

- Fill the cloth bags with the coarse and fine aggregates required for mix.
- Dry the fine aggregate for at least 24 hours in the oven at 230°F, and then let it cool for another 24 hours inside the lab.



Figure 5-1. Scale used for weighing materials



Figure 5-2. Drum mixer used for mixing concrete

- Soak the coarse aggregate for 48 hours and let it sit outside the tank for 30 minutes before weighing.
- Store all the RAP material inside the lab in cloth bags and weigh it as-is for mixing, except for RAP-1, which was soaked before mixing.
- Use the weighing scale to weigh all the materials for mixing as shown in Figure 5-1.
- Place all the aggregate in the drum mixer as shown in Figure 5-2.
- Mix it for 30 seconds.
- Add all of the air entraining agent to half of the mixing water
- Add half of the mixing water with air entraining agent into the drum mixer and mix it for 1 minute.
- Add the required water reducer into the remaining half of the mixing water.
- Place cement into the mixer and add the remaining half of the mixing water with the water reducer, mix it for 3 minutes, followed by a 2 minute rest, followed by 3 minute mixing.
- Perform fresh concrete property test to ensure the workability.
- If workability is not achieved, add more water reducer to the mix

### **5.2.2 Specimen Preparation**

After the concrete was produced, some portion was immediately used to perform tests to determine fresh concrete properties. The remaining concrete was used to fabricate different concrete specimens as follows:

- Cylinders, beams and prisms were casted.
- Molds were filled by concrete into three layers and each layer was vibrated for almost 45 seconds. If the concrete is not workable, vibrate it for additional time in order to ensure proper consolidation.
- A vibrating table was used to consolidate all the specimens.
- The concrete specimens were covered with polyethylene sheets to avoid loss of moisture as shown in Figure 5-3.
- Specimens were removed from the molds after 24 hours and placed in the moist curing room as shown in Figure 5-4.

- Figure 5-5 shows the hardened concrete surface of concrete mixtures containing different percentages of RAP



Figure 5-3. Specimens covered with polyethylene sheets



Figure 5-4. Moisture room used for curing specimens



Figure 5-5. Hardened surface of concrete containing RAP

### 5.3 Tests on Fresh Concrete

The slump test was immediately performed after the concrete was produced in order to ensure the workability of the mix. If the right workability was not achieved, then some water reducing admixture was added to make the concrete more workable. As the target slump was achieved, the remaining tests on the fresh concrete were performed in accordance to the ASTM standards as mentioned below. The results of the fresh concrete tests are discussed in chapter 6.

The following fresh concrete tests were performed:

- Slump: - The slump test measures the workability of the fresh concrete. The slump test was performed in accordance with ASTM C143 standard. The slump value was used to evaluate the consistency of fresh concrete.
- Air content test: - The volumetric method was used to determine the air content in accordance with ASTM C173 standard.
- Unit weight test: - The density of the fresh concrete can be determined by weighing a known volume of concrete. This test was used to verify the density of concrete mixture for quality control in accordance with the ASTM C 138 standard.
- Temperature test: - This test was used to ensure the temperature of fresh concrete was within the normal range, and that there was no unexpected condition in the fresh concrete. Temperature of the fresh concrete was determined in accordance with ASTM C1064.

Table 5-2. Fresh and hardened concrete tests run per batch of concrete

Test Name	Sample Size	Sample Volume (ft <sup>3</sup> )	Curing Age (days)	Number of Samples Per Mix	Volume of Samples Per Mix (ft <sup>3</sup> )	Total Volume Per Mix (ft <sup>3</sup> )
Compressive Strength	4" × 8"	0.0587	7, 14, 28, 90	12	0.7044	
Flexural Strength	4" × 4" × 14"	0.129	7, 14, 28, 90	20	2.58	
Modulus of Elasticity	4" × 8"	0.0587	7, 14, 28, 90	12	0.7044	
Splitting Tensile Strength	4" × 8"	0.0587	7, 14, 28, 90	12	0.7044	9.0
Coefficient of Thermal Expansion	4" × 8"	0.0587	7, 14, 28, 90	12	0.7044	
Free Shrinkage	3" × 3" × 11.25"	0.05859	7, 14, 28, 90	6	0.70308	
Air content of Fresh Concrete	-	0.071	-	-	0.071	
Slump of Fresh Concrete*	-	-	-	-	-	-
Unit Weight of Fresh Concrete*	-	-	-	-	-	-
Total	-	-	-	-	6.17	-

Note: \* The fresh concrete used in the slump and unit weight tests were re-used

## 5.4 Tests on Hardened Concrete

### 5.4.1 Compressive Strength Test

The compressive strength was performed on 4" × 8" concrete cylinder specimens in accordance with ASTM C39 standard test method. Three replicate specimens were tested at each of the different curing times of 7, 14, 28 and 90 days. Prior to the test, both the ends of the specimen were ground in order to ensure uniform load during testing. The load was applied continuously without stopping or shocking at the stress rate of  $35 \pm 7$  psi/s. Since the ends of the specimen had been ground, no capping compound or rubber pads were applied as shown in Figure 5-6.

The compressive strength of the specimen is calculated by dividing the maximum load carried by the specimen during the test by the average cross-sectional area determined as shown in the following equation

$$\sigma = \frac{P}{A} \quad (5-1)$$

Where,

$\sigma$  = Ultimate compressive strength of cylinder in psi,

P = Ultimate compressive axial load applied to cylinder in lbs,

A = cross-sectional area ( $A = \pi r^2$ ) of the cylinder in inches

There are five types of fracture in concrete cylinder according to the ASTM standard. These fractures are cone fracture, cone and split fracture, cone and shear fracture, shear fracture and columnar fracture. Majority of the specimens encountered shear fracture in this research study.



Figure 5-6. Compressive strength test equipment

#### 5.4.2 Young's Modulus and Poisson's Ratio Test

The Young's modulus or modulus of elasticity and Poisson's ratio test was performed on 4" × 8" concrete cylinder specimens in accordance with ASTM C469 standard test method as shown in Figure 5-7. Three replicate specimens were tested at each of the different curing times of 7, 14, 28 and 90 days. Compressive load was applied to the concrete cylinder in the longitudinal direction. The test was carried out on a compressive testing machine which had connections to the load cell and the LVDT (linear variable differential transformer). Prior to the Young's modulus test, the compressive strength test was performed on three specimens in accordance with ASTM C39 standard. The 40% of the ultimate compressive strength was determined from three samples and averaged. Then 40% of the average ultimate compressive strength was applied on the specimens to perform the elastic modulus test. For each specimen four repetitions were performed and the average of last three was recorded as the elastic modulus of that specimen. The equation used to measure the elastic modulus is as follows.

$$E = \frac{\sigma_2 - \sigma_1}{\varepsilon_2 - \varepsilon_1} \quad (5-2)$$

$$E = \frac{\sigma_2 - \sigma_1}{\varepsilon_2 - 0.000050} \quad (5-3)$$

Where,

E = Chord modulus of elasticity.

$\sigma_1$  = Stress corresponding to a longitudinal strain of 50 millionths.

$\sigma_2$  = Stress corresponding to 40% of ultimate load.

$\varepsilon_1$  = 50 millionths.

$\varepsilon_2$  = Longitudinal strain generated by stress  $\sigma_2$

Poisson's ratio was measured using the horizontal LVDT that measures twice the horizontal strain in the front while the whole setup rotates about a pivot point in the backside.

The Poisson's ratio was calculated using the following equation,

$$\mu = \frac{\varepsilon t_2 - \varepsilon t_1}{\varepsilon_2 - 0.000050} \quad (5-4)$$

Where,

$\mu$  = Poisson's ratio

$\varepsilon t_1$  = transverse strain at specimen mid height due to stress of  $\sigma_1$

$\varepsilon t_2$  = transverse strain at specimen mid height due to stress of  $\sigma_2$

$\varepsilon_1$  = 50 millionths

$\varepsilon_2$  = longitudinal strain due to the stress of  $\sigma_2$

Young's modulus and Poisson's ratio test were nondestructive with maximum applied load of 40% of the average ultimate compressive strength. The loading rate was adjusted to 35±7 psi/s.

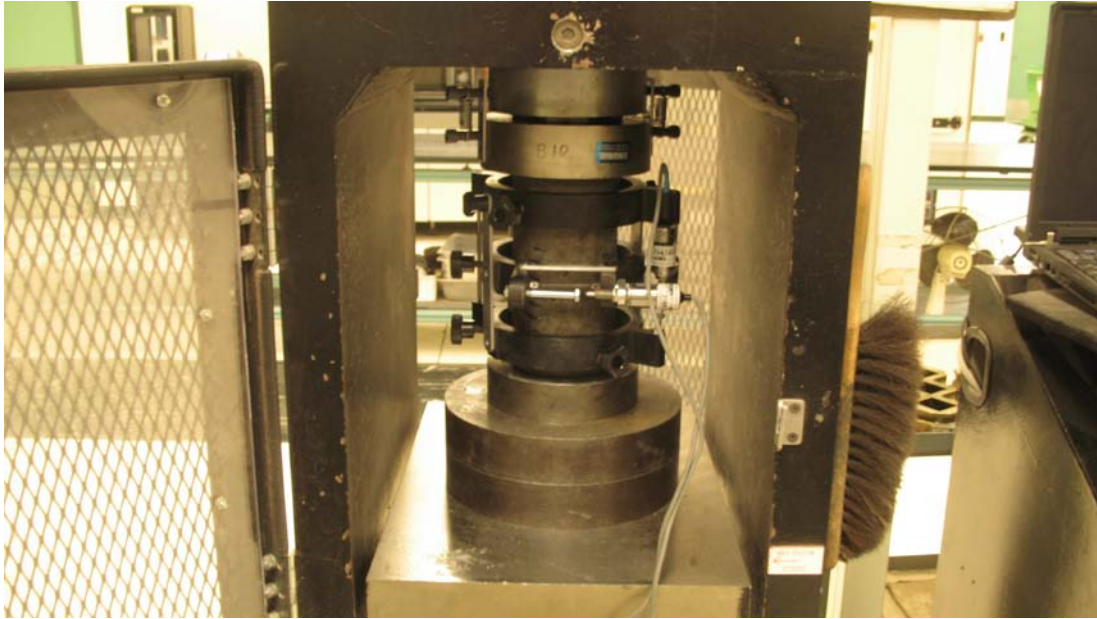


Figure 5-7. Modulus of elasticity and Poisson's ratio test apparatus

### 5.4.3 Flexural Strength Test

The flexural strength test was performed on 4" × 4" × 14" concrete beam specimens in accordance with the ASTM C78 standard test method. Three replicate specimens were tested at each of the different curing times of 7, 14, 28 and 90 days. Before testing, the loading surface and the edges of the beams were ground evenly by using a hand grinding stone. The grinding ensured that the applied load was uniform. The flexural strength was determined according to the type of failure or fracture in the beam.

If the fracture initiates in the tension surface within the middle third of the span length, calculate the modulus of rupture using the following equation,

$$R = \frac{PL}{bd^2} \quad (5-5)$$

Where,

R = modulus of rupture of the specimen in psi.

P = maximum applied load on the specimen as indicated by the machine in lbf

L = span length in inches.

b = average depth of the specimen measured near the fracture in inches

d = average depth of the specimen measured near the fracture in inches.

If the fracture occurs in the tension surface outside of the middle third of the span length by not more than 5% of the span length, calculate the modulus of rupture as follows,

$$R = \frac{3Pa}{bd^2} \quad (5-6)$$

Where,

a = average distance between line of fracture and the nearest support measured on the tension surface of the beam in inches.

If the fracture occurs in the tension surface outside of the middle third of the span length by more than 5% of the span length, discard the results of the tests.

The following steps were followed to determine the stress-strain values from the flexural strength test:

- The test was run using an Instron 3384 testing machine as shown in Figure 5-9.
- The tension surface which is the bottom side of the beam was smoothed with sand paper and cleaned with acetone.
- Mark the center point, one third point and support point of the beam with a permanent marker.
- One strain gauge (PL-60-11-3L) was glued on the smoothed surface at center of the beam using the special Loctite 454 glue.
- Allow the glue to dry to get a perfect bond between strain gauge and the beam (approximately 45 minutes was sufficient for the glue to dry for this test)
- Secure the wire in the area where it connects to the strain gauge using regular tape.
- Place the beams properly centered on the loading frame such that the one-third mark accurately aligns with the loading platens.
- Attach the strain gauge to the data acquisition system to acquire the voltage readings

- Run the testing machine at a rate of 13.33 lbs/s, while acquiring both voltage data and the load cell data.
- The Labview program on the computer was programmed to calculate the strain from the voltage data from the strain gauge and the stress was calculated from the load determined from the Instron machine.
- Load the beam to failure.
- Figure 5-8 shows the failure of beams containing RAP

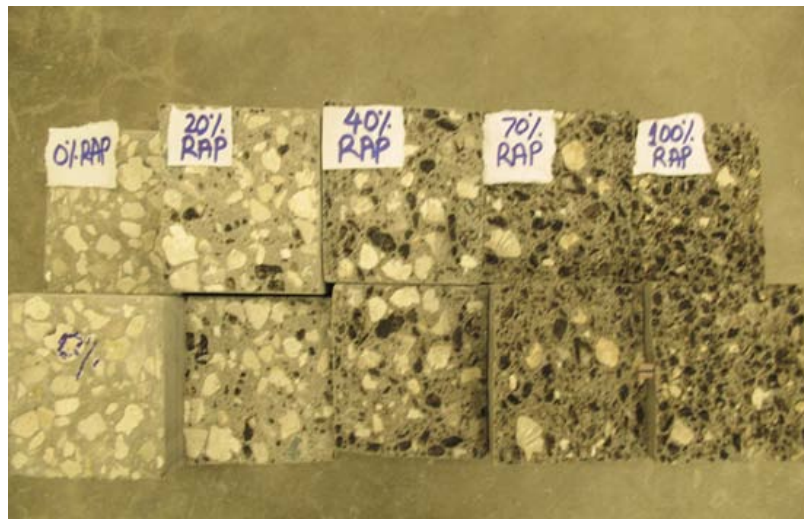


Figure 5-8. Concrete specimens tested in flexural strength



Figure 5-9. Flexural strength test apparatus

#### 5.4.4 Splitting Tensile Strength Test

The splitting tensile strength test was performed on 4" × 8" concrete cylinder specimen in accordance with ASTM C496 standard test method as shown in Figure 5-10. Three replicate specimens were tested at each of the different curing times of 7, 14, 28 and 90 days. The specimens were marked along the center line using a permanent marker prior to the test. The specimen was placed in a jig which helps it to be clamped and aligned properly during the test. Load is applied to the specimen through thin strips of plywood placed on the top and bottom sides of the specimen. The load is increased until failure occurs by indirect tension in the form of splitting along vertical diameter as shown in Figure 5-11. The splitting tensile strength is calculated using the following equation,

$$T_i = \frac{2P_i}{\pi LD} \quad (5-7)$$

Where,

$T_i$  = splitting tensile strength of cylinder in psi,

$P_i$  = maximum applied load to break the cylinder in psi

$L$  = length of cylinder in inches

$D$  = diameter of cylinder in inches



Figure 5-10. Splitting tensile strength test apparatus



Figure 5-11. Concrete specimens before and after splitting tensile strength test

#### 5.4.5 Drying Shrinkage Test

Drying shrinkage test was performed on  $3'' \times 3'' \times 11.25''$  concrete prism specimens in accordance with ASTM C157 standard test method. Steel end plates with a hole at their center were used to install gage studs at both ends of the specimen. The specimens were removed from the moulds after 24 hours of concrete mixing and specimen preparation. An initial reading was immediately taken with a length comparator as shown in Figure 5-12. Three specimens were then allowed to dry at ambient condition in the laboratory and three specimens placed in the

moisture room. Length measurement on the specimen was taken at 7, 14, 28 and 90 days of curing time. The length change of a specimen at any age after the initial comparator reading was calculated as follows,

$$\Delta L_x = \frac{\text{Initial CRD} - \text{Final CRD}}{G} \quad (5-8)$$

Where,

$\Delta L_x$  = length change of specimen at any age,

CRD = difference between the comparator reading of the specimen and the reference bar,

G = gauge length.



Figure 5-12. Drying shrinkage test extensometer

#### 5.4.6 Coefficient of Thermal Expansion Test

The coefficient of thermal expansion was performed on 4" × 8" concrete cylinder specimens in accordance with AASHTO TP-60-00 standard test method. Three replicate specimens were tested at each of the different curing times of 7, 14, 28 and 90 days. This test measures the coefficient of thermal expansion of concrete specimen, maintained in a saturated

condition, by measuring the length change of the specimen due to specified temperature changes. The measured length change is corrected for any change in length of the measuring apparatus, and the coefficient of thermal expansion is then calculated by dividing the corrected length change by the temperature change and then the specimen length. The coefficient of thermal expansion of one expansion or contraction test segment of a concrete specimen is calculated as follows:

$$CTE = \left( \frac{\Delta L_a}{L_o} \right) \Delta T \quad (5-9)$$

Where,

CTE= Coefficient of thermal expansion

$\Delta L_a$  = actual length change of specimen during temperature change, mm or in.

$L_o$  = measured length of specimen at room temperature, mm or in.

$\Delta T$  = measured temperature change in °C.

$$\Delta L_a = \Delta L_m + \Delta L_f \quad (5-10)$$

Where,

$\Delta L_m$  = measured length change of specimen during temperature change, mm or in.

$\Delta L_f$  = length change of the measuring apparatus during temperature change, mm or in.

$$\Delta L_f = C_f \times L_o \times \Delta T \quad (5-11)$$

Where,

$C_f$  = correction factor accounting for the change in length of the measurement apparatus with temperature, in<sup>-6</sup>/in/°C.

The test result is the average of the expansion reading and the contraction reading

$$CTE = \frac{CTE \text{ expansion} + CTE \text{ contraction}}{2} \quad (5-12)$$



Figure 5-13. Grinding machine used to grind concrete specimens



Figure 5-14. Coefficient of thermal expansion test equipment

The cylinders were sawed and ground as shown in Figure 5-13 to the length of  $7.0 \pm 0.1$  in and then lengths were measured to the nearest 0.004 in. After measuring the length, specimens were submersed in the controlled temperature bath. The lower end of the specimen is firmly seated against the support button, and the LVDT tip is seated against the upper end of the

specimen. The initial temperature of the bath was set to  $10 \pm 1^\circ\text{C}$ . After reaching the temperature, the bath was allowed to remain at this temperature until thermal equilibrium of the specimen has been reached, as measured by the LVDT to the nearest 0.00001in. Then temperature of the bath was changed to  $50 \pm 1^\circ\text{C}$  to get the second reading of the LVDT. The temperature was again changed to  $10 \pm 1^\circ\text{C}$  to get the final reading of the LVDT. The average value from the three specimens was used to measure the coefficient of the thermal expansion of the concrete mix. The test setup for the coefficient of thermal expansion test is shown in Figure 5-14.

## **CHAPTER 6 CONCRETE TEST RESULTS AND ANALYSIS**

### **6.1 Introduction**

This chapter presents the results and analysis of fresh and hardened concrete properties. Using the data evaluated from the concrete mixtures containing RAP in this study, the relationships among the compressive strength, flexural strength, modulus of elasticity and splitting tensile strength were developed and presented in this chapter.

### **6.2 Results of Fresh Concrete Properties**

The results of fresh concrete properties evaluated for all the concrete mixtures are shown in Table 6-1. For the concrete mixtures without RAP, the slump was slightly higher and ranged between 3 to 5 inches (target slump was 1 to 3 inches), and for the concrete mixtures with RAP, the slump was lower and ranged between 0 to 3 inches. The slump of concrete mixtures with RAP decreased as the percentage of RAP replacement increased in the mix. For all the concrete mixtures with 70% and 100% RAP, the workability of the mix was poor compared with concrete mixtures with 20% and 40% RAP. The percentage air of the mix increased as the RAP content increased. However, for most of the concrete mixtures with RAP, the percentage air was within the targeted range of 2 to 5%. The unit weight of the concrete mixtures decreased as the percentage of RAP replacement increased. The unit weight of concrete mixtures without RAP was 140 lbs/ft<sup>3</sup>. For concrete mixtures with 20%, 40%, and 70% RAP the unit weight was between 135 lbs/ft<sup>3</sup> and 140 lbs/ft<sup>3</sup>. For mixtures with 100% RAP, it was between 130 lbs/ft<sup>3</sup> and 135 lbs/ft<sup>3</sup>. The temperature of concrete for all the mixtures was between 70 and 78°F, with RAP mixtures having slightly higher temperature compared to the normal mix.

Table 6-1. Fresh concrete properties of the mixtures evaluated in this research study

Mix Type	Number	RAP (%)	W/C	Slump (in)	Air Content (%)	Unit Weight (lbs/ft <sup>3</sup> )	Temperature (°F)
Control	1	0	0.45	3.50	4.50	140	73
	2	0	0.50	4.25	3.20	140	70
	3	0	0.55	5.00	3.30	140	74
RAP-1	4	20	0.50	4.25	4.50	139	77
	5	40	0.50	3.25	3.70	139	72
	6	70	0.50	3.00	3.75	135	75
	7	100	0.50	1.50	6.80	130	77
RAP-2	4	20	0.50	1.25	5.50	139	73
	5	40	0.50	1.00	5.00	137	73
	6	70	0.50	0.75	4.50	136	73
	7	100	0.50	0.25	4.00	135	75
RAP-3	4	20	0.50	1.25	4.25	139	75
	5	40	0.50	1.75	4.25	138	75
	6	70	0.50	1.00	3.50	137	75
	7	100	0.50	0.50	3.50	132	77
RAP-4	4	20	0.50	1.25	4.50	138	77
	5	40	0.50	1.25	4.50	138	77
	6	70	0.50	0.25	4.70	137	77
	7	100	0.50	0.25	5.00	132	77

## 6.3 Analysis of Strength Test Results

### 6.3.1 Compressive Strength Test Results

Table 6-2 summarizes the average compressive strength of all the concrete mixtures evaluated in this research study. For all the concrete mixtures, there is a reduction in compressive strength with increase in the percentage of RAP in the concrete mix as shown in Figure 6-1.

Figure 6-2 shows the development of compressive strength at different curing times with respect to the strength at 28 day curing time. In general, the concrete mixtures with RAP exhibited strength gain with respect to curing time. For mixtures with RAP-1, RAP-2, and RAP-3, the strength development was almost similar to the control mix. For concrete mixtures with RAP-4, the development of strength was much higher than any other mix, especially for 100% RAP-4 mix. For the mix with 70% RAP-3, there was no strength gain observed at 90 days of curing time.

Figure 6-3 shows the reduction in compressive strength of concrete mixtures containing RAP at 90 days of curing time, relative to the strength of the control mix. For concrete mixtures with 100% RAP, there is almost 70% reduction in compressive strength, when compared with the control mix. For concrete mixtures with 70% RAP, there is almost 60% reduction in compressive strength, when compared with the control mix. For concrete mixtures with 40% RAP, there is almost 40% reduction in compressive strength, when compared with the control mix. For concrete mixtures with 20% RAP, there is almost 20% reduction in compressive strength, when compared with the control mix. There was slightly higher reduction observed for concrete mixture with 20% RAP-1 and the concrete mixtures with RAP-4 showed the least reduction in compressive strength when compared with all other concrete containing RAP.

The standard deviation was determined from six concrete specimens for each concrete mix at different curing times. The standard deviation for concrete mixtures with RAP-1 and RAP-2

was lower than the concrete mixtures with RAP-3 and RAP-4. The minimum standard deviation of 17 psi was observed for concrete mixture with 100% RAP-2 at 28 days of curing time, and the maximum standard deviation of 316 psi was observed for concrete mixture with 70% RAP-3 at 90 days of curing time. In general, the concrete mixtures with RAP exhibited lower standard deviation values for compressive strength.

Table 6-2. Compressive strength of concrete mixtures evaluated

Mix Type	Number	RAP (%)	W/C	Average Compressive Strength of RAP Concrete (psi)			
				Curing Time (days)			
				7	14	28	90
Control	1	0	0.45	5600	6165	6621	7031
	2	0	0.50	4284	4654	5376	5793
	3	0	0.55	3380	3823	4532	4982
RAP-1	4	20	0.50	2808	3356	3542	3944
	5	40	0.50	2357	2727	2950	3330
	6	70	0.50	1582	1794	2030	2205
	7	100	0.50	1060	1316	1438	1460
RAP-2	4	20	0.50	3450	3902	4167	4539
	5	40	0.50	2378	2637	2920	3080
	6	70	0.50	1557	1607	1874	1959
	7	100	0.50	1289	1450	1501	1568
RAP-3	4	20	0.50	3536	3797	4250	4455
	5	40	0.50	2580	2785	3095	3211
	6	70	0.50	1962	2125	2364	1915
	7	100	0.50	1401	1527	1589	1818
RAP-4	4	20	0.50	3348	3825	3892	4564
	5	40	0.50	2518	2740	2855	3343
	6	70	0.50	2000	2051	2232	2509
	7	100	0.50	1432	1379	1479	1793

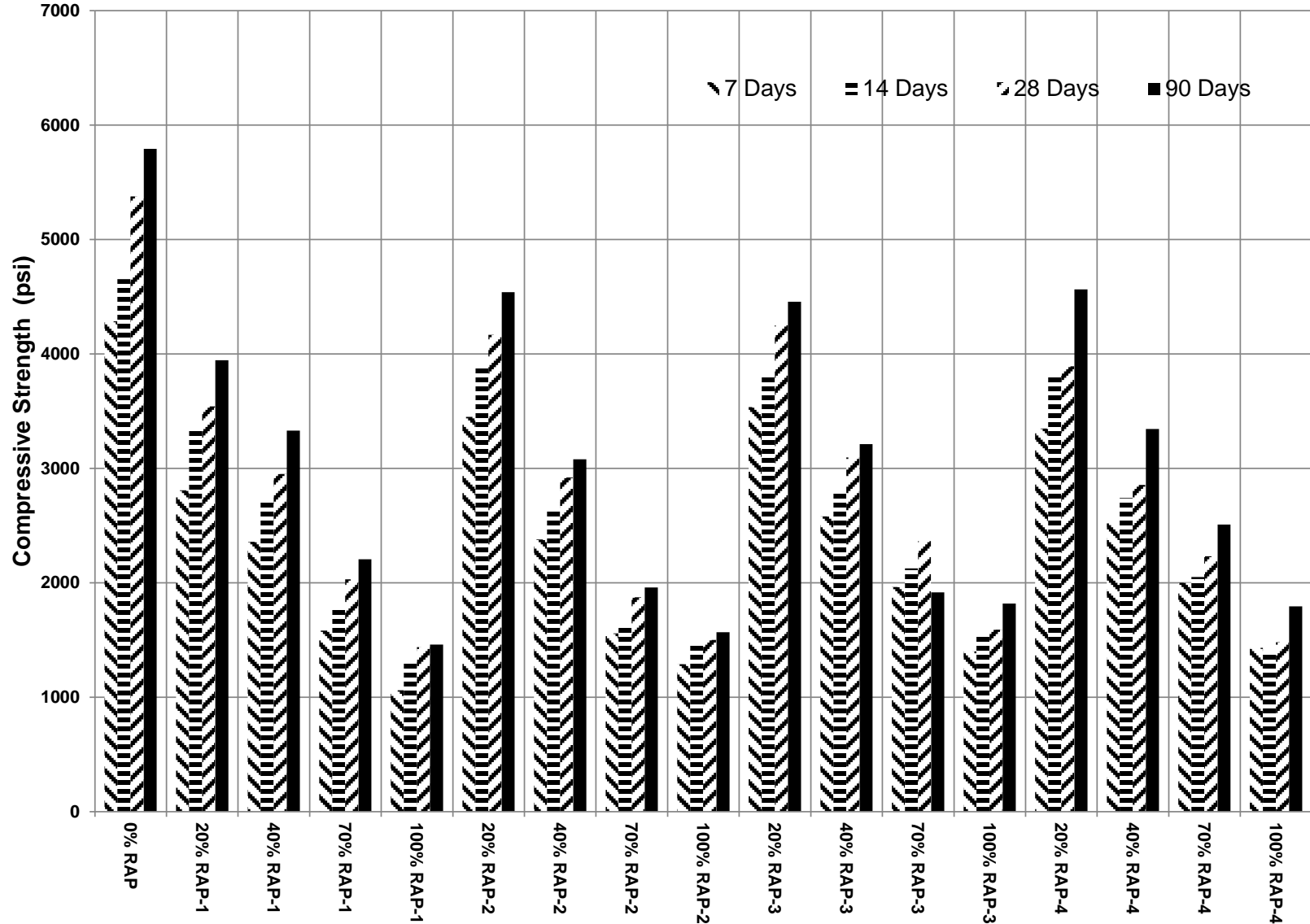


Figure 6-1. Compressive strength of concrete mixtures containing RAP

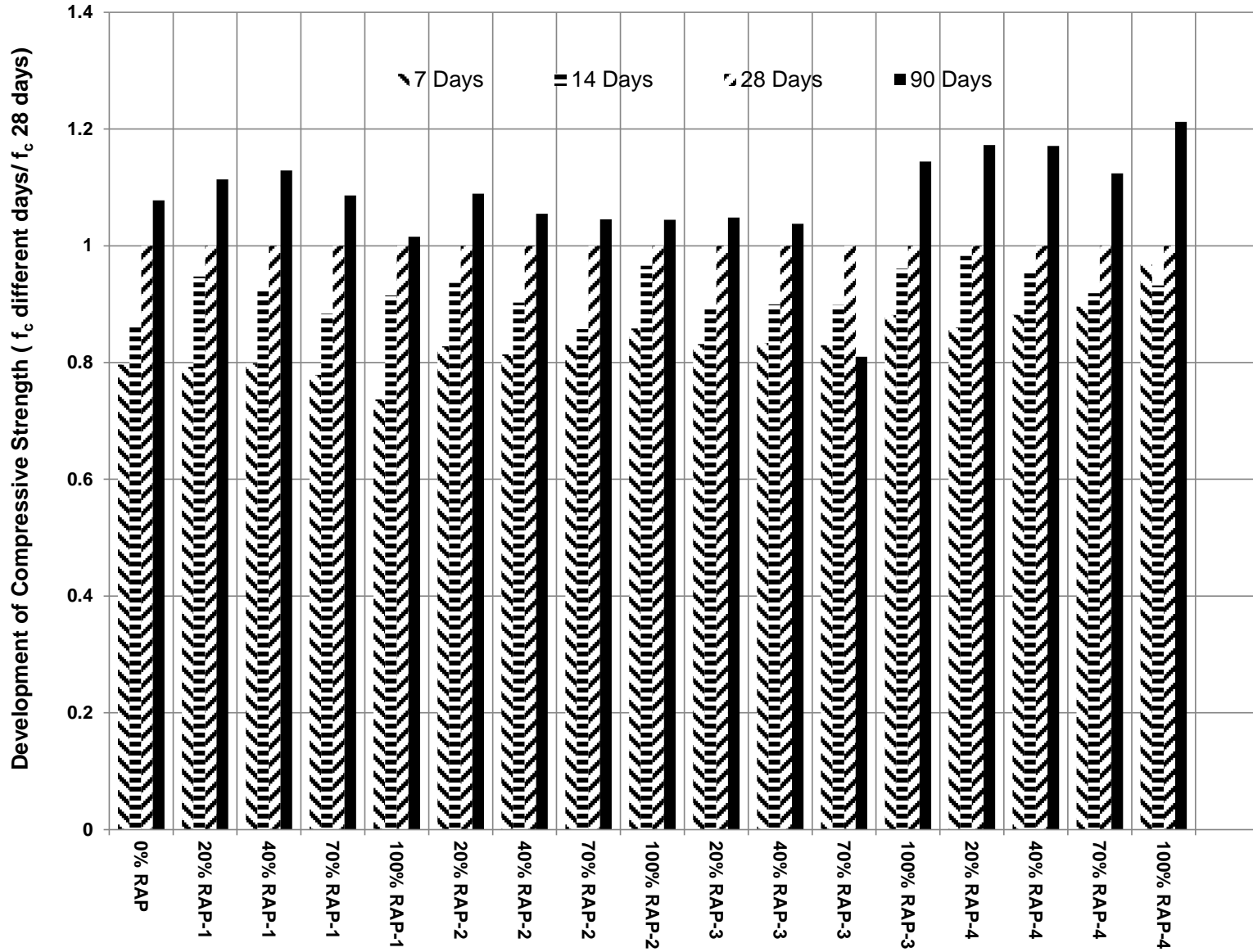


Figure 6-2. Development of compressive strength at different curing times relative to the strength at 28 days curing time

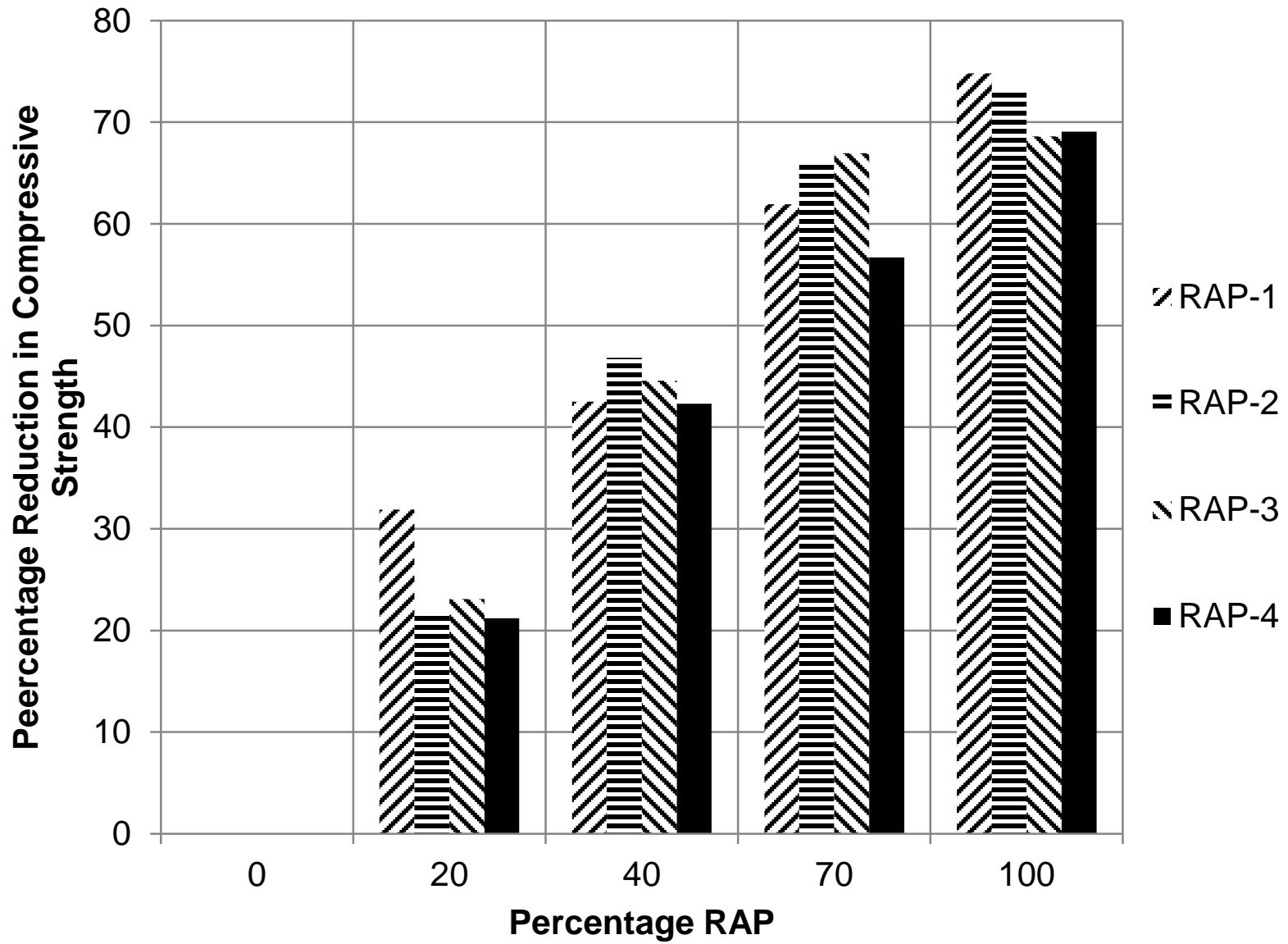


Figure 6-3. Percentage reduction in compressive strength of concrete containing RAP

### **6.3.2 Modulus of Elasticity Test Results**

Table 6-3 summarizes the average modulus of elasticity of all the concrete mixtures evaluated in this research study. For all the concrete mixtures, there is a reduction in elastic modulus with increase in the percentage of RAP as shown in Figure 6-4.

Figure 6-5 shows the development of modulus of elasticity of concrete mixtures at different curing times relative to the elastic modulus at 28 days curing time. The concrete mixtures with RAP showed development in modulus of elasticity with respect to time. The development of modulus of elasticity with time was much higher for 70% and 100% RAP mixtures, when compared with 20% and 40% RAP mixtures. In general, concrete mixtures with RAP show development in modulus of elasticity with respect to time.

Figure 6-6 shows the reduction in modulus of elasticity of concrete mixtures containing RAP at 90 days of curing time, with respect to normal concrete. The reduction in modulus of elasticity for concrete mixtures with RAP was almost similar to that of the compressive strength reductions. There was not much difference in the reduction of modulus of elasticity between different RAP types.

The standard deviation of the elastic modulus was determined from three concrete specimens for each concrete mix at different curing times. For the concrete mixtures without RAP the maximum standard deviation for modulus of elasticity was 172,498 psi. For concrete mixtures with RAP-1, RAP-2, RAP-3 and RAP-4 the maximum standard deviation for modulus of elasticity was 303 ksi, 120 ksi, 266 ksi and 196 ksi, respectively.

Table 6-3. Modulus of elasticity of concrete mixtures evaluated

Mixture Type	Number	RAP (%)	W/C	Average Modulus of Elasticity of RAP Concrete ( $\times 10^6$ psi)			
				Curing Time (days)			
				7	14	28	90
Control	1	0	0.45	4.42	4.41	4.57	4.70
	2	0	0.50	3.97	4.22	4.43	4.44
	3	0	0.55	3.88	4.09	4.22	4.24
RAP-1	4	20	0.50	3.15	3.35	3.45	3.67
	5	40	0.50	2.53	2.80	2.99	3.00
	6	70	0.50	1.70	1.77	1.82	2.00
	7	100	0.50	1.12	1.25	1.26	1.26
RAP-2	4	20	0.50	3.24	3.46	3.69	3.88
	5	40	0.50	2.54	2.71	2.77	2.87
	6	70	0.50	1.65	1.75	1.84	1.97
	7	100	0.50	1.25	1.23	1.37	1.38
RAP-3	4	20	0.50	3.42	3.50	3.61	3.78
	5	40	0.50	2.62	2.67	2.80	2.80
	6	70	0.50	1.77	1.89	1.89	2.11
	7	100	0.50	1.16	1.28	1.24	1.23
RAP-4	4	20	0.50	3.54	3.33	3.62	3.67
	5	40	0.50	2.52	2.62	2.72	2.83
	6	70	0.50	1.75	1.77	1.78	2.01
	7	100	0.50	1.16	1.25	1.19	1.33

### 6.3.3 Poisson's Ratio Test Results

Table 6-4 summarizes the average Poisson's ratios of all the concrete mixtures evaluated in this research study. For all the concrete mixtures, the numerical value of Poisson's ratio was between 0.20 and 0.30. The concrete mixtures without RAP exhibited low values of Poisson's ratio. The Poisson's ratio increased as the percentage of the RAP increased in the concrete mixtures. Figure 6-7 shows the Poisson's ratio at various curing time, with different types of RAP in the concrete mixtures. The Poisson's ratio value was slightly higher for the mixtures containing RAP-1, as compared with all other mixtures with RAP.

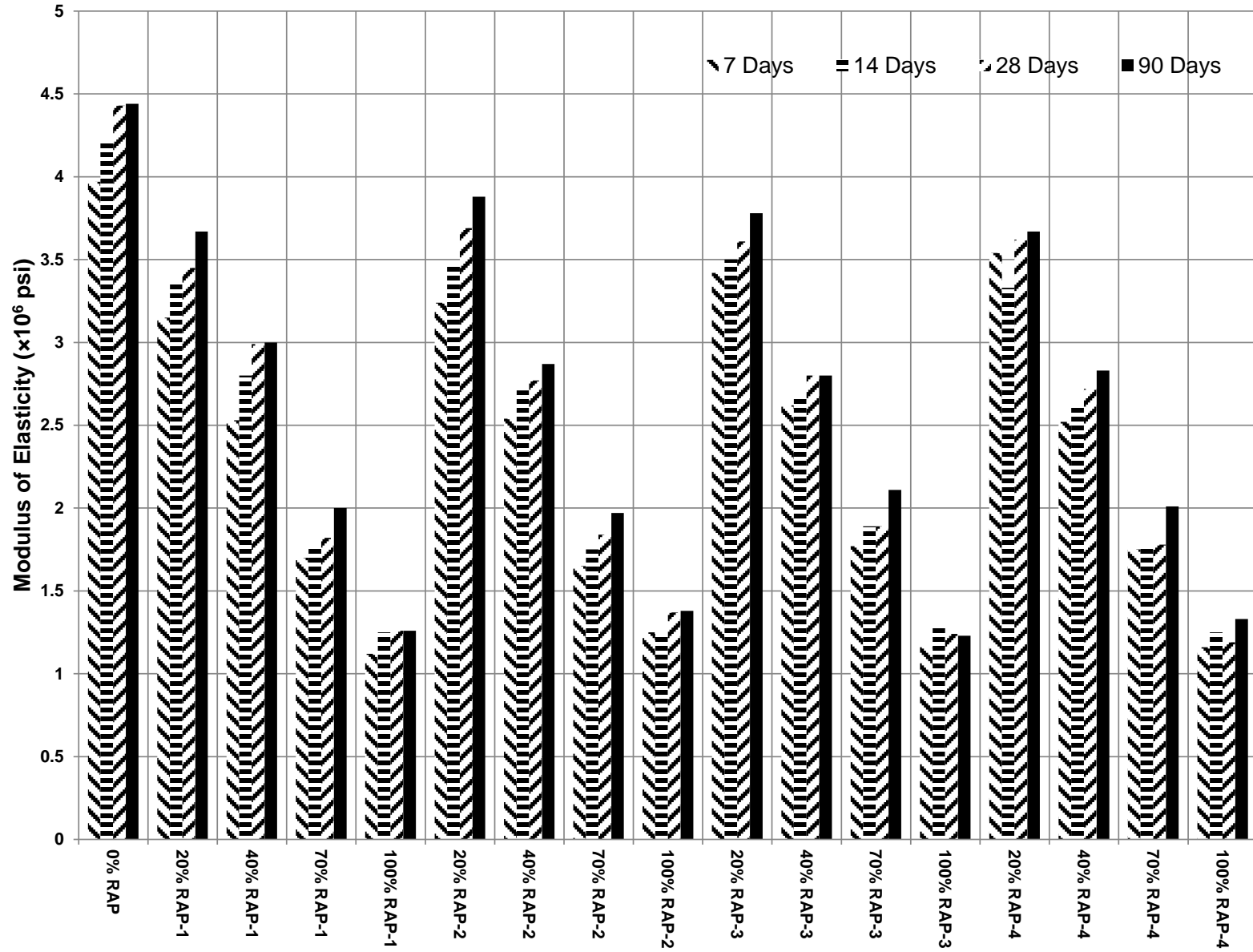


Figure 6-4. Modulus of elasticity of concrete mixtures containing RAP

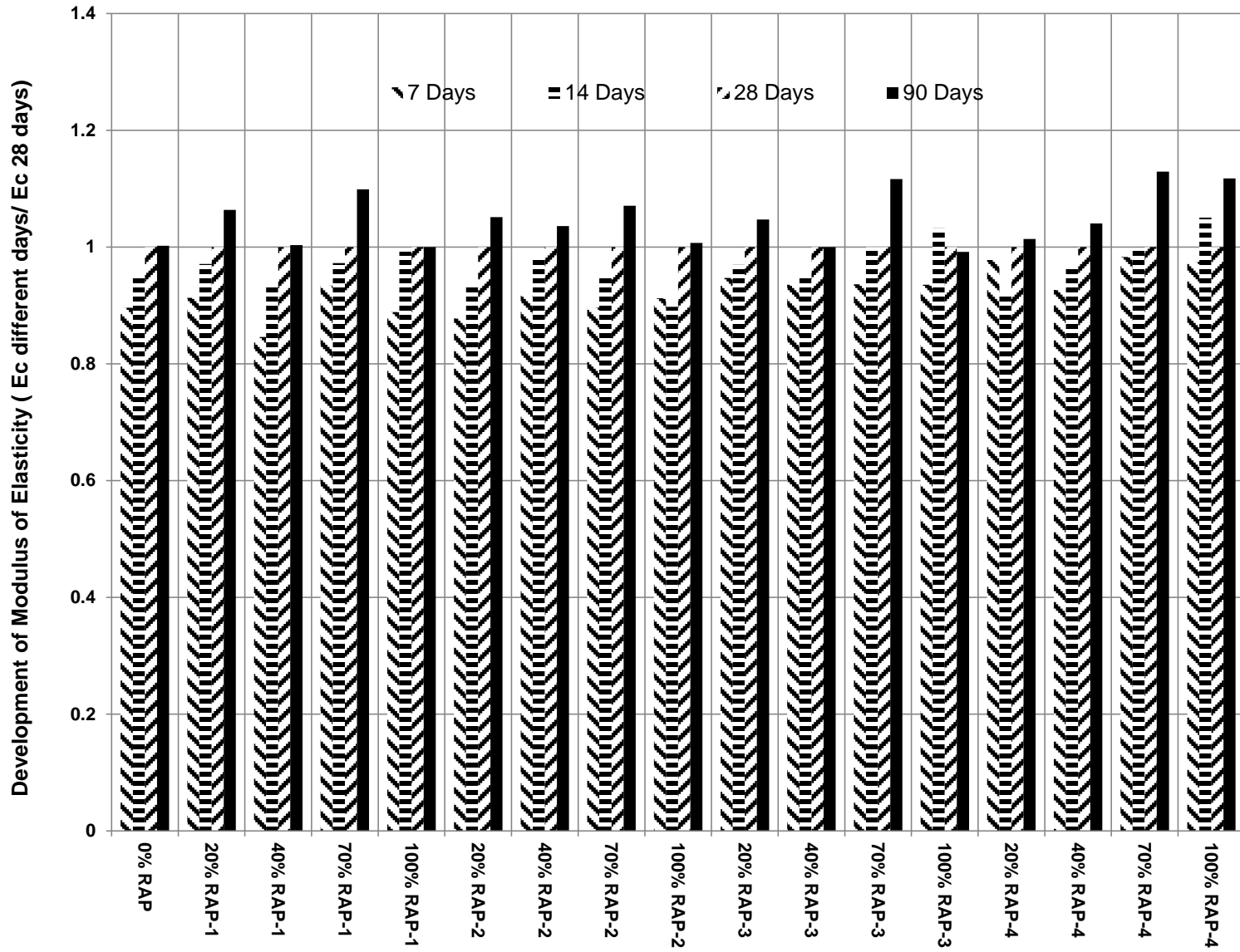


Figure 6-5. Development of modulus of elasticity at different curing times relative to the elastic modulus at 28 days curing time

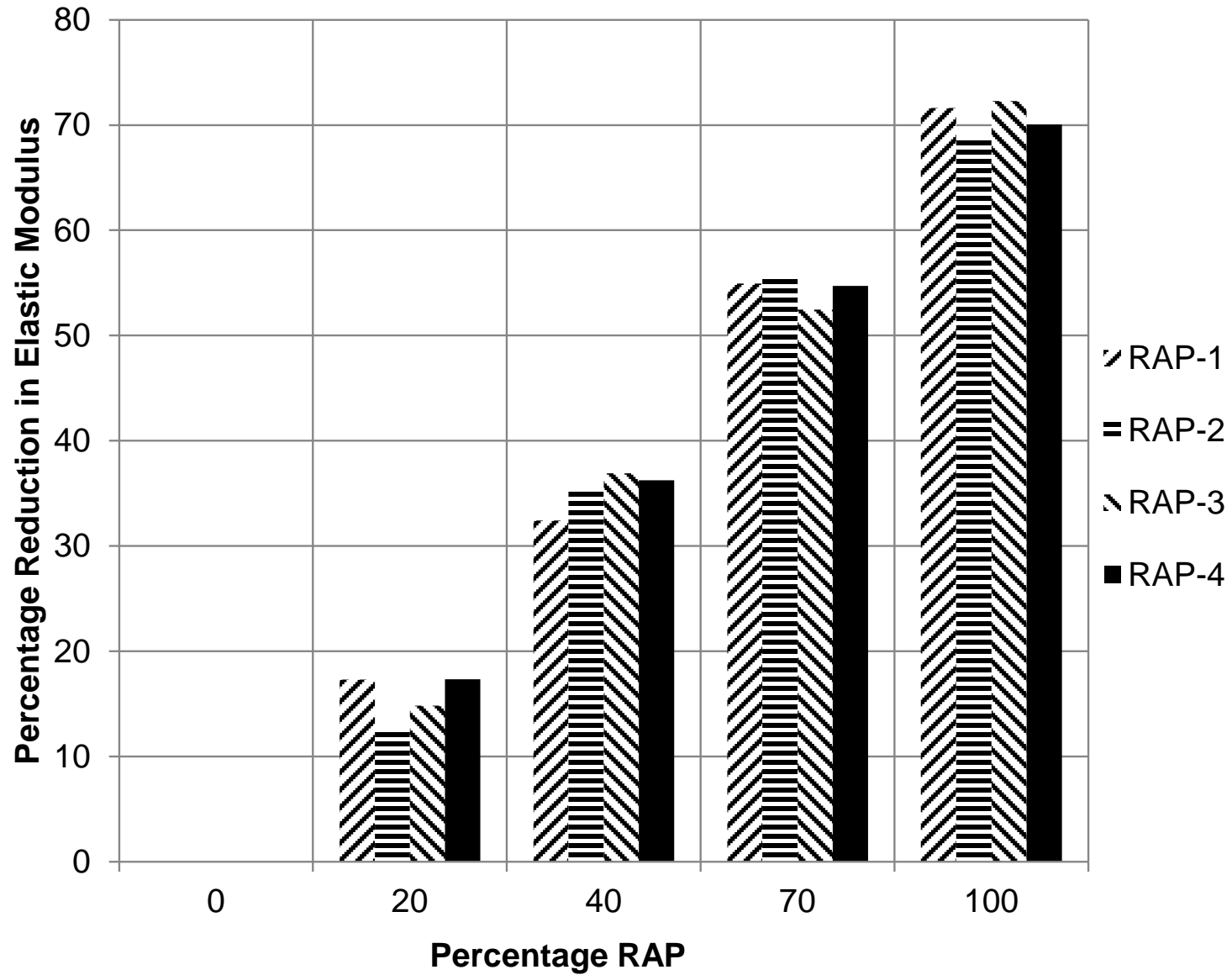


Figure 6-6. Percentage reduction in modulus of elasticity of concrete mixtures containing RAP

Most of the concrete mixtures with RAP evaluated in this study exhibited increase in Poisson's ratio at the initial curing time, and very minimal change or increase was observed after the 28 days of curing. For concrete mixtures with no RAP, the value of Poisson's ratio was between 0.20 and 0.25. For concrete mixtures with 20%, 40% and 70% RAP, the Poisson's ratio was close to 0.25, and for mixtures with 100% RAP the Poisson's ratio was slightly higher and was between 0.25 and 0.30.

Table 6-4. Poisson's ratio of concrete mixtures evaluated

Mixture Type	Number	RAP (%)	W/C	Average Poisson's Ratio of RAP Concrete			
				Curing Time (days)			
				7	14	28	90
Control	1	0	0.45	0.25	0.24	0.24	0.25
	2	0	0.50	0.21	0.22	0.24	0.23
	3	0	0.55	0.22	0.23	0.24	0.23
RAP-1	4	20	0.50	0.23	0.25	0.25	0.24
	5	40	0.50	0.25	0.26	0.25	0.27
	6	70	0.50	0.27	0.28	0.27	0.28
	7	100	0.50	0.25	0.29	0.31	0.29
RAP-2	4	20	0.50	0.23	0.25	0.26	0.24
	5	40	0.50	0.25	0.24	0.25	0.25
	6	70	0.50	0.26	0.25	0.25	0.25
	7	100	0.50	0.26	0.27	0.28	0.27
RAP-3	4	20	0.50	0.23	0.24	0.24	0.23
	5	40	0.50	0.23	0.23	0.24	0.24
	6	70	0.50	0.25	0.23	0.25	0.26
	7	100	0.50	0.25	0.27	0.25	0.23
RAP-4	4	20	0.50	0.25	0.24	0.24	0.24
	5	40	0.50	0.26	0.26	0.25	0.26
	6	70	0.50	0.28	0.25	0.25	0.26
	7	100	0.50	0.25	0.26	0.26	0.28

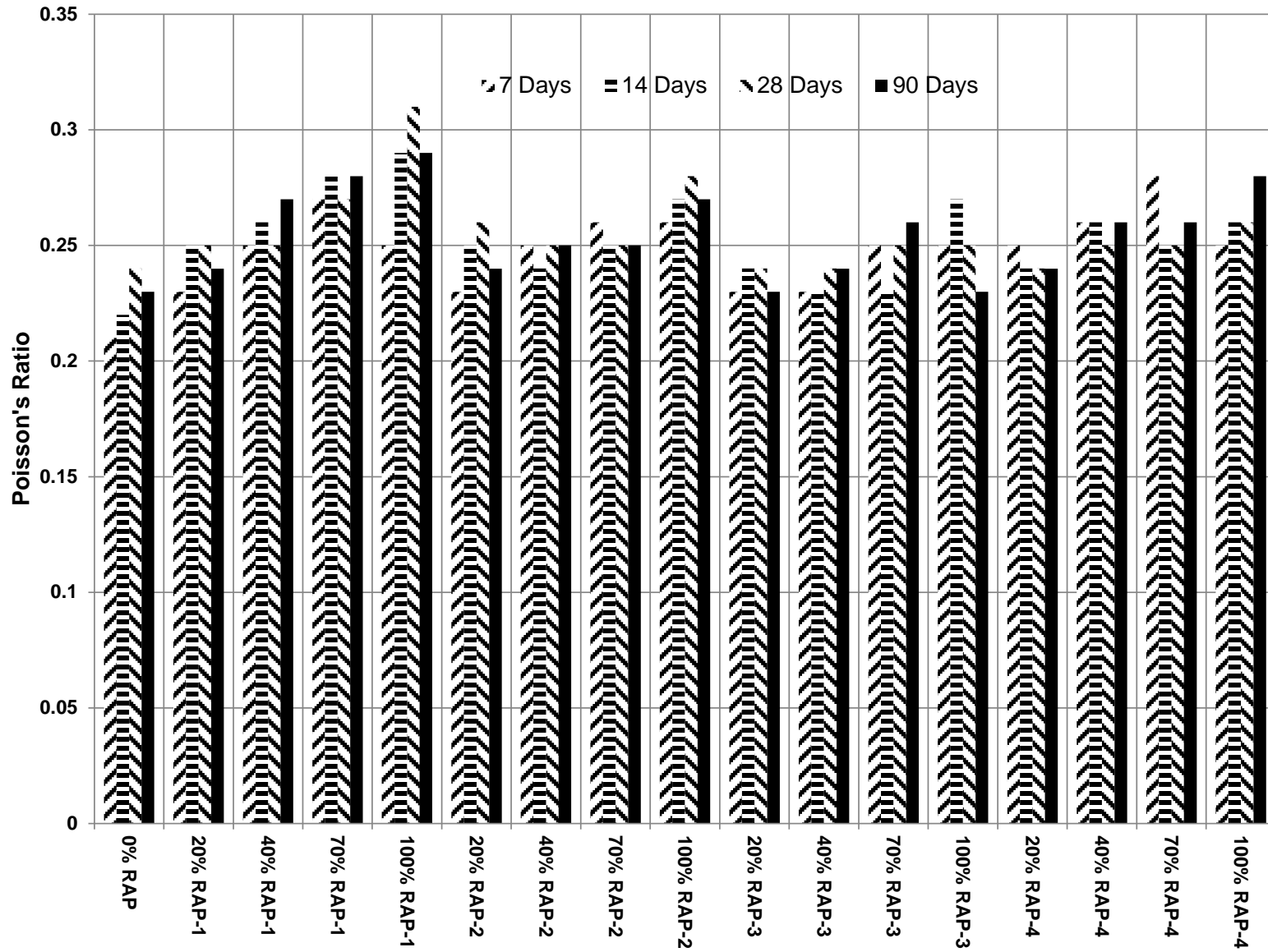


Figure 6-7. Poisson's ratio of concrete mixtures containing RAP

### 6.3.4 Flexural Strength Test Results

Table 6-5 summarizes the average flexural strength of all the concrete mixtures evaluated in this research study. For all the concrete mixtures, there is a reduction in flexural strength with increase in the percentage of RAP in the mix as shown in Figure 6-8.

Figure 6-9 shows the development of flexural strength of concrete mixtures at different curing times relative to the flexural strength at 28 days curing time. The concrete mixtures with RAP showed development in flexural strength with respect to time, as compared with the control mix. The development of flexural strength with time was much higher for the 70% and 100% RAP mixtures, as compared with the 20% and 40% RAP mixtures. In general, concrete mixtures with RAP show development in flexural strength with respect to time.

Figure 6-10 shows the reduction of flexural strength of concrete mixtures containing RAP at 90 days of curing time, relative to the flexural strength at the normal concrete. The reductions in flexural strength of concrete mixtures with RAP-1 and RAP-4 were much lower than that of RAP-2 and RAP-3, except for 20% RAP-1. In general, the maximum reduction in flexural strength was 50%, 40%, 30%, and 20% for the concrete mixtures with 100%, 70%, 40%, and 20% RAP, respectively. These reductions in the flexural strength is lower than the corresponding reduction in compressive strength and splitting tensile strength, which exhibited maximum reductions of almost 70% and 60%, respectively. Thus concrete mixtures containing RAP show 10% to 20% lower reduction in flexural strength, when compared with the corresponding reduction in compressive strength and splitting tensile strength.

The standard deviation was determined from three concrete specimens for each concrete mix at different curing times. For the concrete mixtures without RAP, the maximum standard deviation for flexural strength was 73 psi. For concrete mixtures with RAP-1, RAP-2, RAP-3 and RAP-4 the maximum standard deviation for flexural strength was 48 psi, 38 psi, 40 psi and

42 psi, respectively. In general, the standard deviations of flexural strength for all the concrete mixtures were low.

Table 6-5. Flexural Strength of concrete mixtures evaluated

Mixture Type	Number	RAP (%)	W/C	Average Flexural Strength of RAP Concrete (psi)			
				Curing Time (days)			
				7	14	28	90
Control	1	0	0.45	665	745	750	753
	2	0	0.50	630	666	686	694
	3	0	0.55	592	630	664	680
RAP-1	4	20	0.50	490	540	563	520
	5	40	0.50	471	513	575	586
	6	70	0.50	382	420	453	489
	7	100	0.50	301	343	394	405
RAP-2	4	20	0.50	517	598	583	633
	5	40	0.50	465	482	517	520
	6	70	0.50	380	385	410	414
	7	100	0.50	334	362	370	370
RAP-3	4	20	0.50	525	533	570	594
	5	40	0.50	471	475	479	516
	6	70	0.50	409	389	386	441
	7	100	0.50	332	324	342	360
RAP-4	4	20	0.50	564	551	597	620
	5	40	0.50	460	464	514	552
	6	70	0.50	368	404	428	473
	7	100	0.50	356	354	358	415

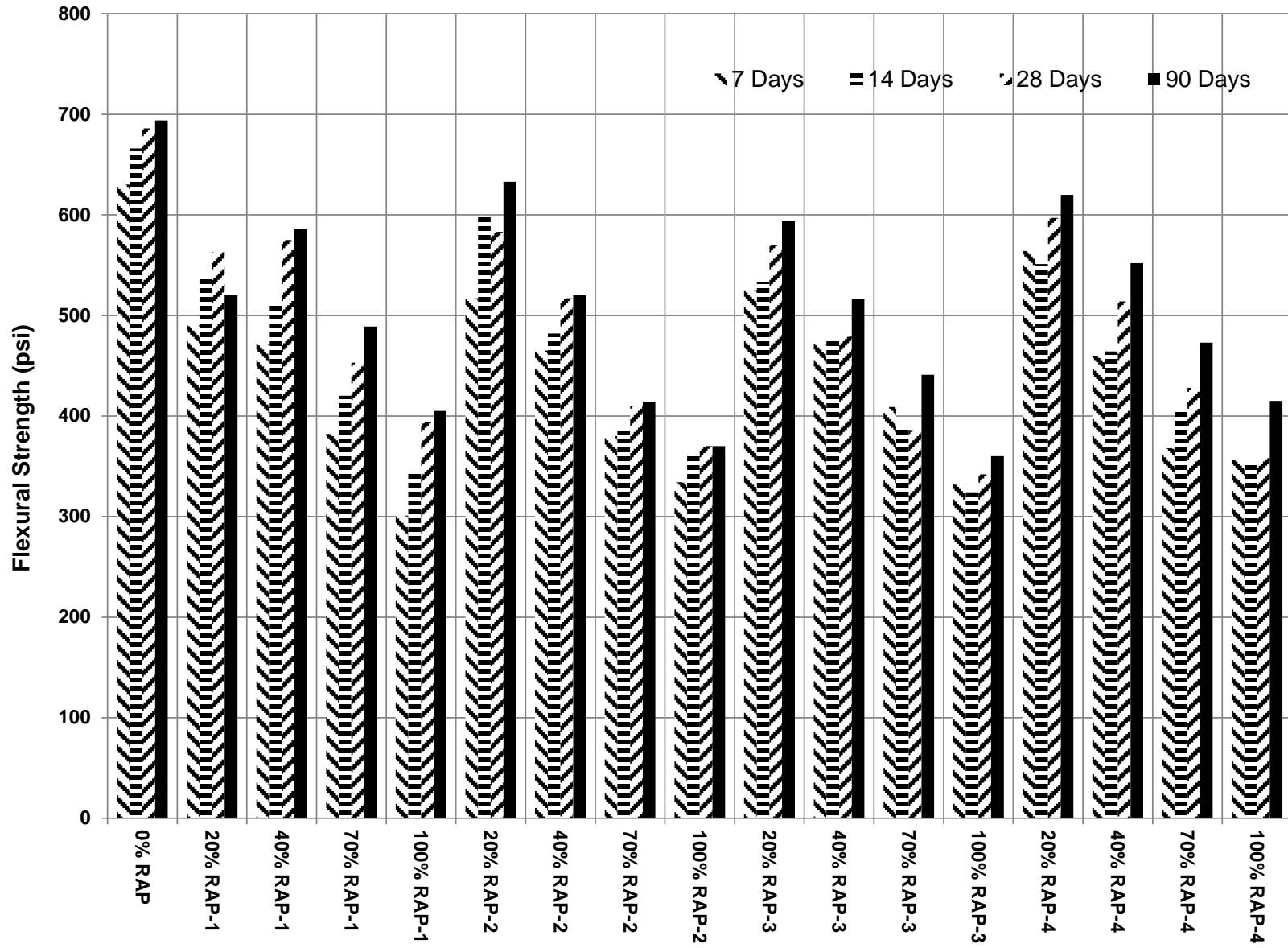


Figure 6-8. Flexural strength of concrete mixtures containing RAP

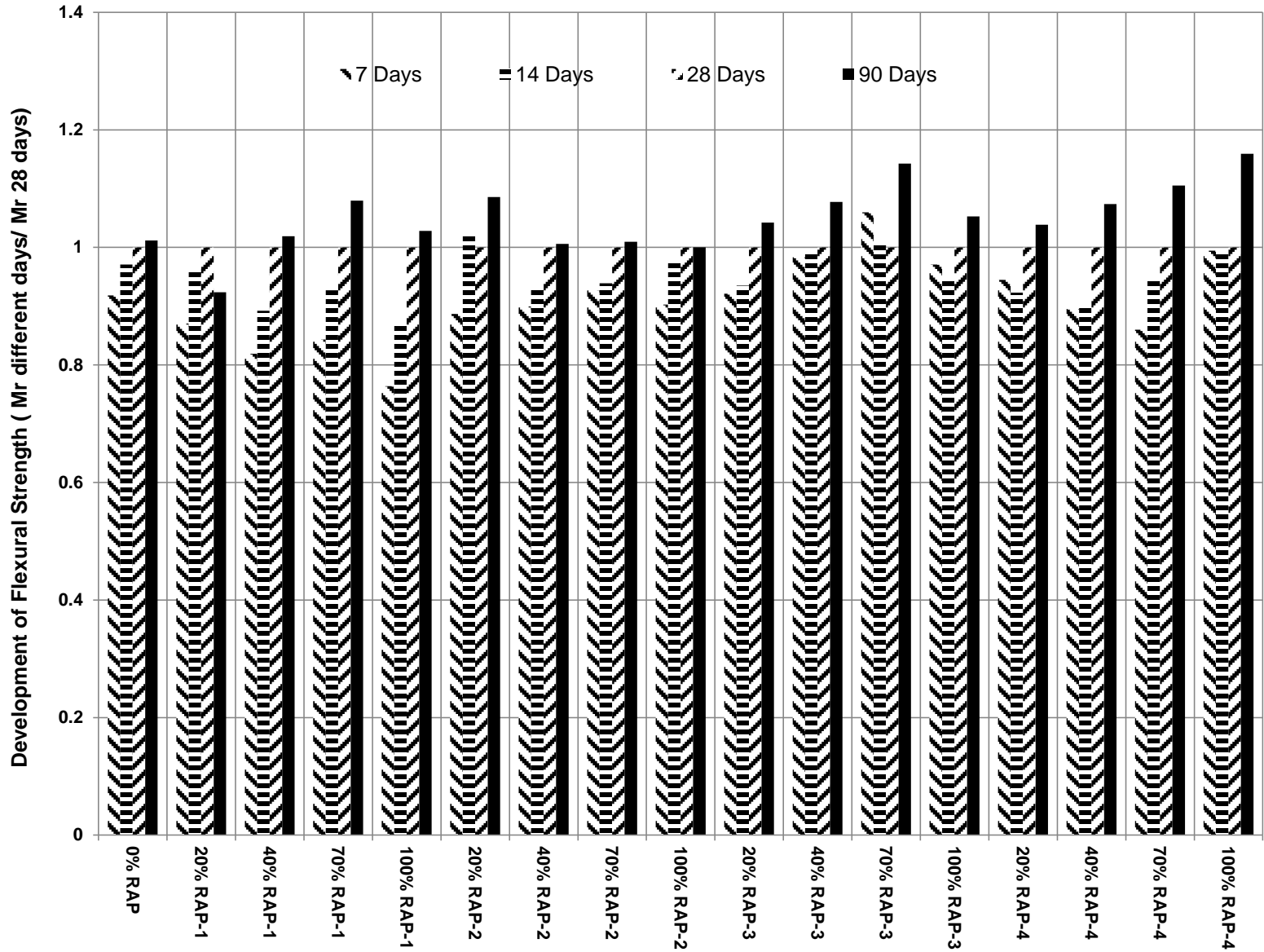


Figure 6-9. Development of flexural strength at different curing times relative to the flexural strength at 28 days curing time

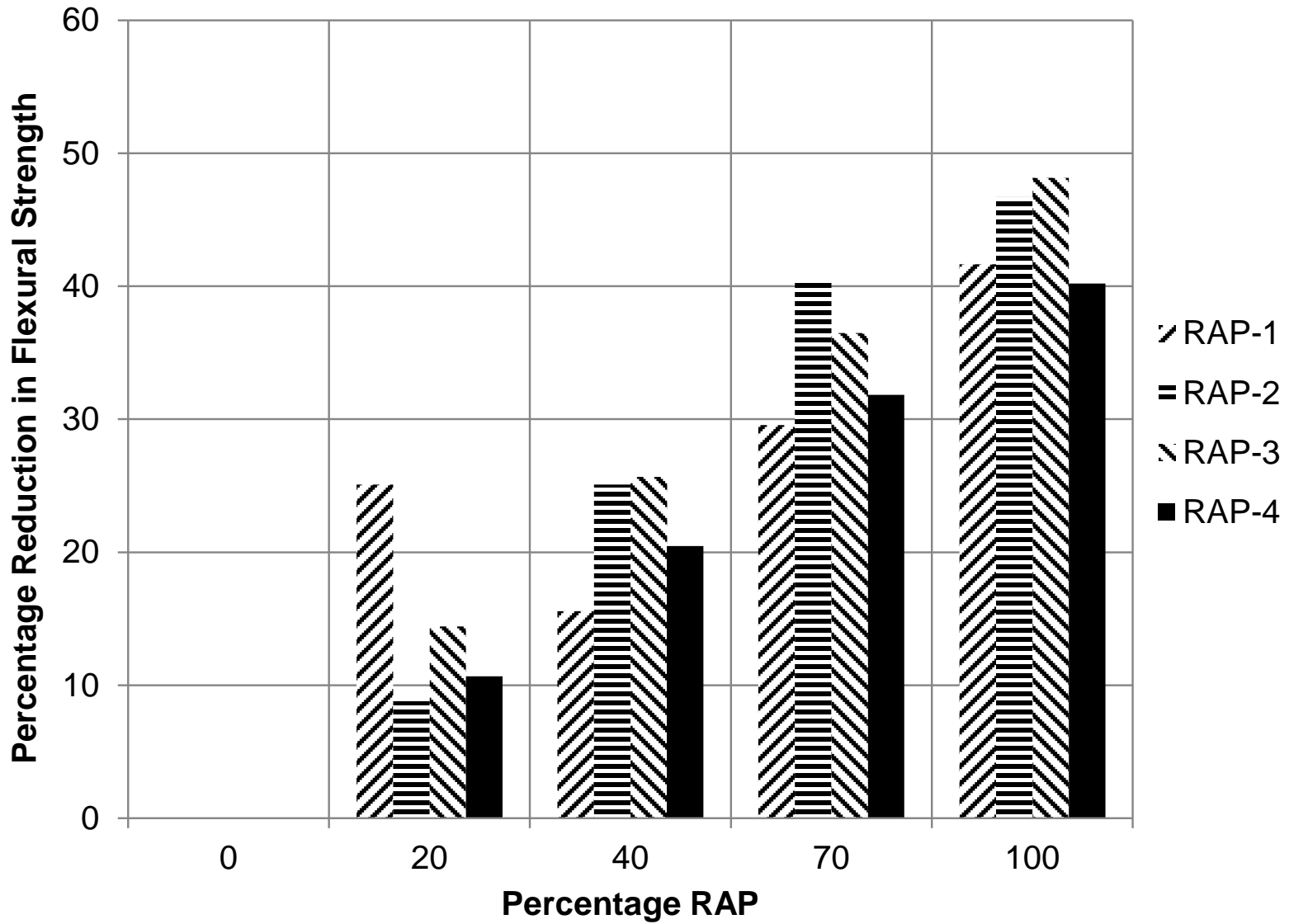


Figure 6-10. Percentage reduction in flexural strength of concrete mixtures containing RAP

### 6.3.5 Modulus of Toughness Test Results

Table 6-6 summarizes the average toughness of all the concrete mixtures evaluated in this research study. The toughness was calculated by determining the area under the stress-strain curve. These stress and strain values were determined from the beam or flexural strength test. Figures 6-11 through 6-14 show the stress-strain plots for different concrete mixtures containing RAP at different curing times. The concrete mixtures without RAP fail at a much higher stress, but the strain at failure is much lower due to brittle behavior of the concrete material. In case of concrete mixtures with RAP, the failure stress decreases as the percentage of RAP increases, but the failure strain increases as the percentage of RAP increases. Figure 6-15 shows the relative toughness of concrete mixtures with different types of RAP, as compared to that of the control mixture with no RAP. In general, the toughness of the concrete increased as the percentage of RAP in the mix increased. This also indicates that the concrete mixtures with RAP perform better in bending, which may benefit the performance of the concrete pavements.

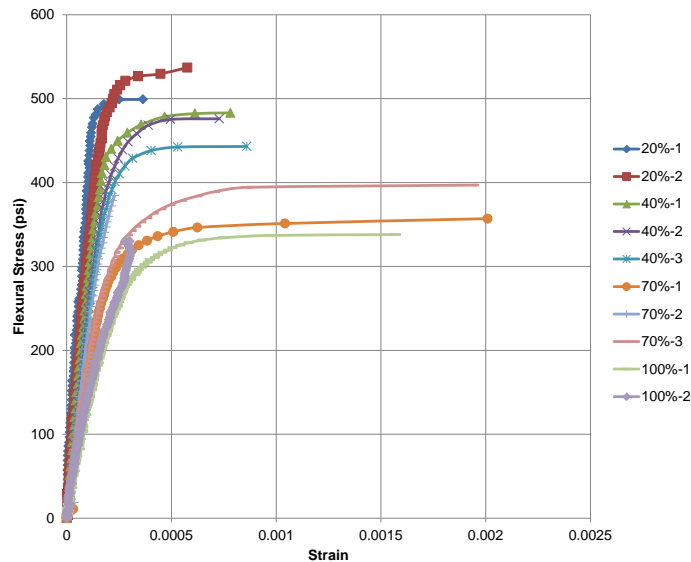


Figure 6-11. Stress strain plots for concrete containing RAP-2 at 7 days of curing time

Table 6-6. Flexural toughness of concrete containing RAP

Mixture Type	Number	RAP (%)	W/C	Average Flexural Toughness of RAP Concrete (lb-in/in <sup>3</sup> )			
				Curing Time (days)			
				7	14	28	90
Control	1	0	0.45	/	/	0.13	0.08
	2	0	0.50	/	/	0.18	0.12
	3	0	0.55	/	/	0.19	0.06
RAP-1	4	20	0.50	/	/	/	0.27
	5	40	0.50	/	/	/	0.42
	6	70	0.50	/	/	/	0.55
	7	100	0.50	/	/	/	0.76
RAP-2	4	20	0.50	0.21	0.26	0.18	0.27
	5	40	0.50	0.23	0.30	0.33	0.33
	6	70	0.50	0.68	0.58	0.42	0.42
	7	100	0.50	0.47	0.75	0.74	0.67
RAP-3	4	20	0.50	0.26	0.21	0.26	0.32
	5	40	0.50	0.42	0.40	0.26	0.45
	6	70	0.50	0.57	0.43	0.33	0.48
	7	100	0.50	1.03	0.51	0.69	0.48
RAP-4	4	20	0.50	0.18	0.29	0.31	0.26
	5	40	0.50	0.26	0.21	0.43	0.40
	6	70	0.50	0.45	0.45	0.50	0.37
	7	100	0.50	0.42	0.42	0.73	0.61

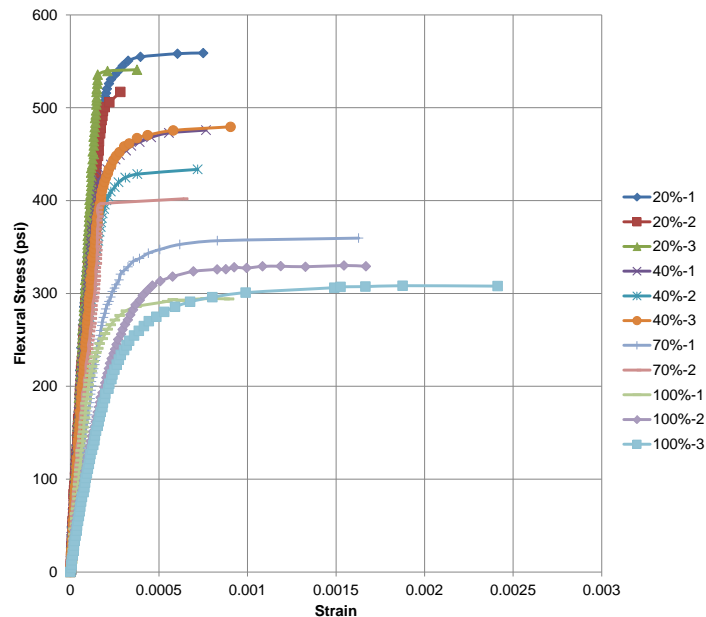


Figure 6-12. Stress strain plots for concrete containing RAP-3 at 14 days of curing time

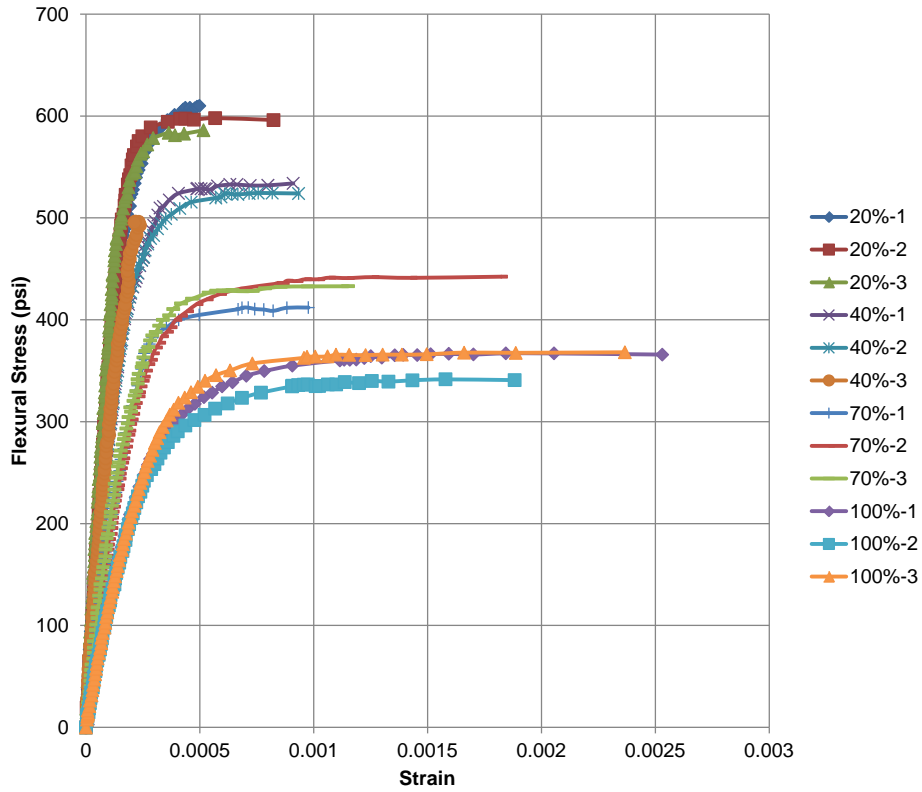


Figure 6-13. Stress strain plots for concrete containing RAP-4 at 28 days of curing time

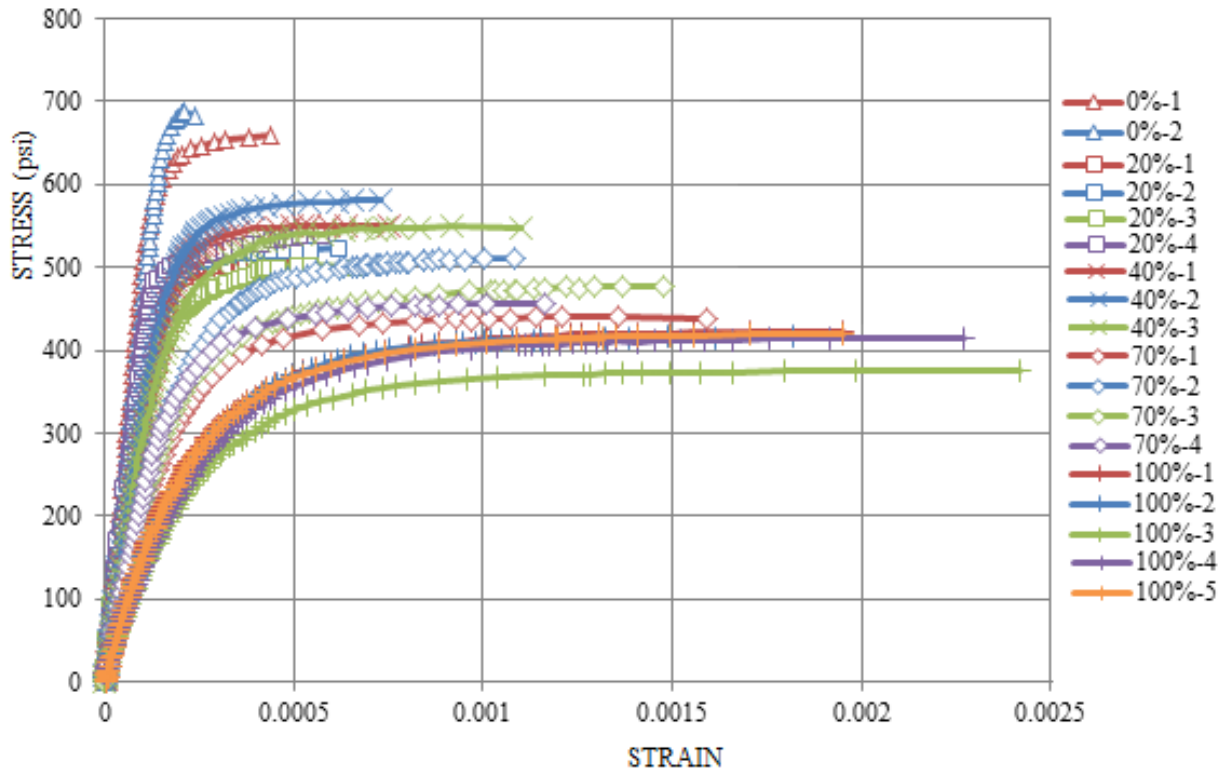


Figure 6-14. Stress strain plots for concrete containing RAP-1 at 90 days of curing time

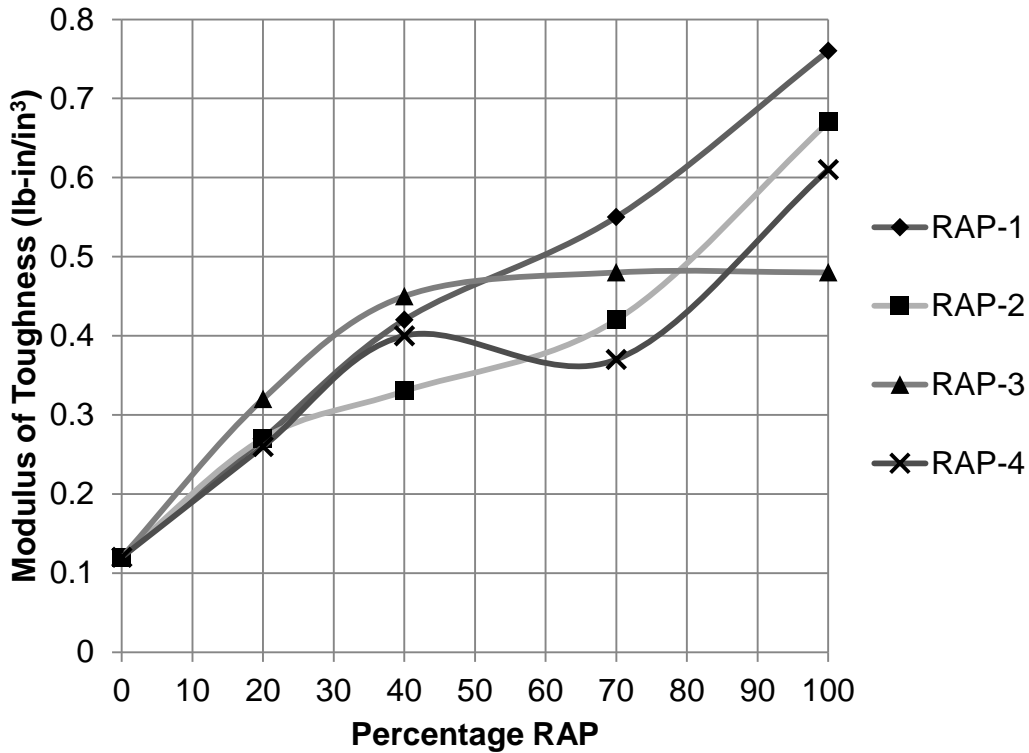


Figure 6-15. Modulus of toughness for concrete mixtures containing different RAP's at 90 days of curing time

### 6.3.6 Splitting Tensile Strength Test Results

Table 6-7 summarizes the average splitting tensile strength of all the concrete mixtures evaluated in this research study. For all the concrete mixtures, there is a reduction in the splitting tensile strength with increase in the percentage of RAP in the mix, as shown in Figure 6-16.

Figure 6-17 shows the development of splitting tensile strength at different curing times relative to that at 28 day curing time. For concrete mixtures with RAP-4, there was no development in splitting tensile strength at different curing times. In general, the other mixtures did show development in splitting tensile strength with curing time.

Figure 6-18 shows the percentage reduction in the splitting tensile strength of concrete mixtures containing RAP at 90 days of curing, relative to that of the normal concrete. The maximum reduction in splitting tensile strength was around 60% for concrete mixtures with

100% RAP. The trends in the reduction of splitting tensile strength were very similar for the concrete mixtures with different types of RAP.

The standard deviation was determined from three concrete specimens for each concrete mix at different curing times. For the concrete mixtures without RAP, the maximum standard deviation for splitting tensile strength was 80 psi. For concrete mixtures with RAP-1, RAP-2, RAP-3 and RAP-4 the maximum standard deviation for splitting tensile strength was 37 psi, 46 psi, 34 psi and 54 psi, respectively. In general, the standard deviations of splitting tensile strength for all the concrete mixtures were low.

Table 6-7. Splitting tensile strength of concrete containing RAP

Mixture Type	Number	RAP (%)	W/C	Average Splitting Tensile Strength of RAP Concrete (psi)			
				Curing Time (days)			
				7	14	28	90
Control	1	0	0.45	490	592	664	658
	2	0	0.50	473	525	517	562
	3	0	0.55	418	438	510	537
RAP-1	4	20	0.50	380	400	452	455
	5	40	0.50	333	368	370	396
	6	70	0.50	249	270	303	265
	7	100	0.50	188	202	190	244
RAP-2	4	20	0.50	427	428	442	476
	5	40	0.50	314	352	370	413
	6	70	0.50	232	262	258	253
	7	100	0.50	198	227	218	217
RAP-3	4	20	0.50	390	432	400	445
	5	40	0.50	334	322	351	369
	6	70	0.50	257	282	273	291
	7	100	0.50	204	206	202	241
RAP-4	4	20	0.50	369	390	451	433
	5	40	0.50	308	355	371	348
	6	70	0.50	248	305	336	280
	7	100	0.50	224	230	220	209

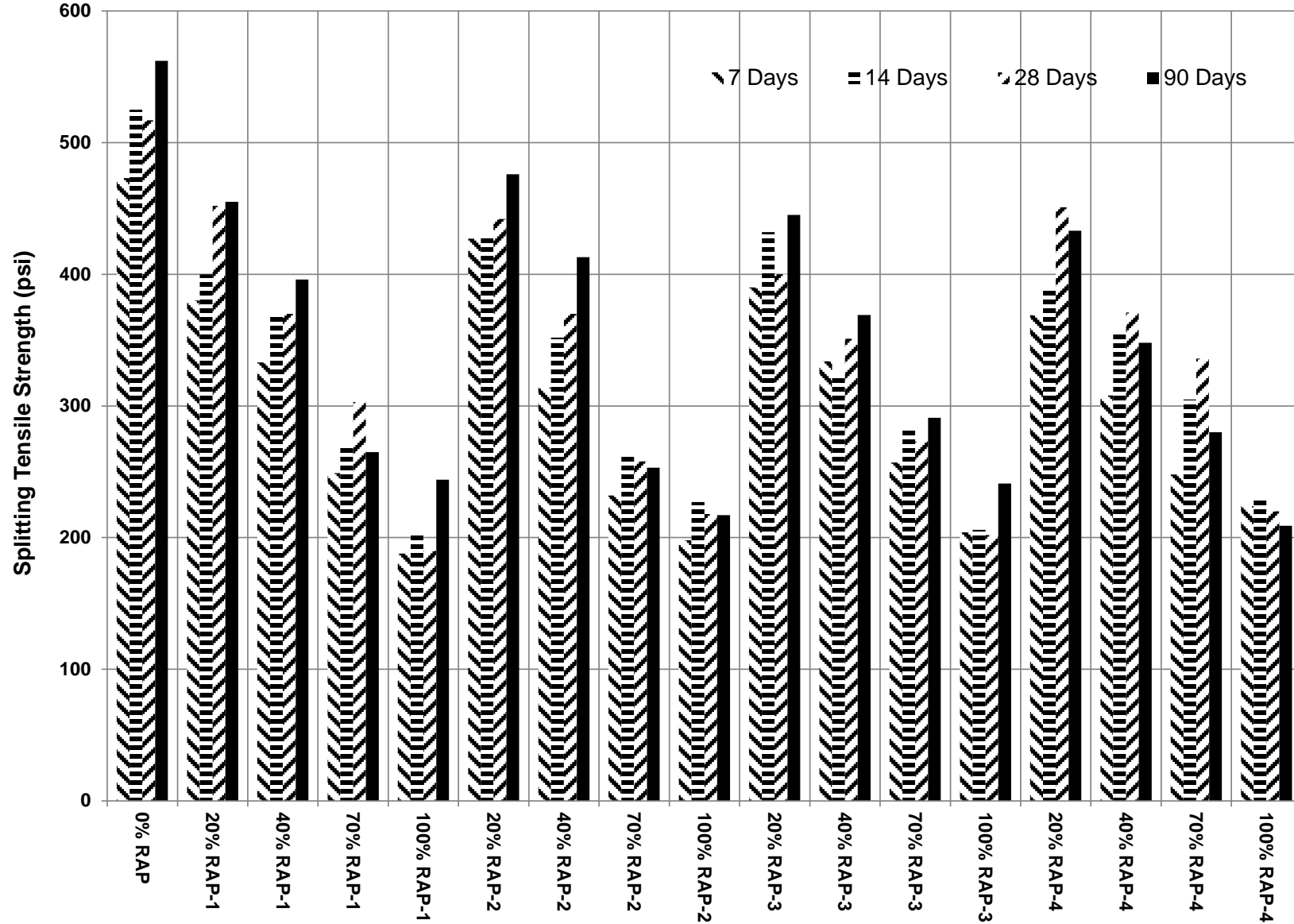


Figure 6-16. Splitting tensile strength of concrete mixtures containing RAP

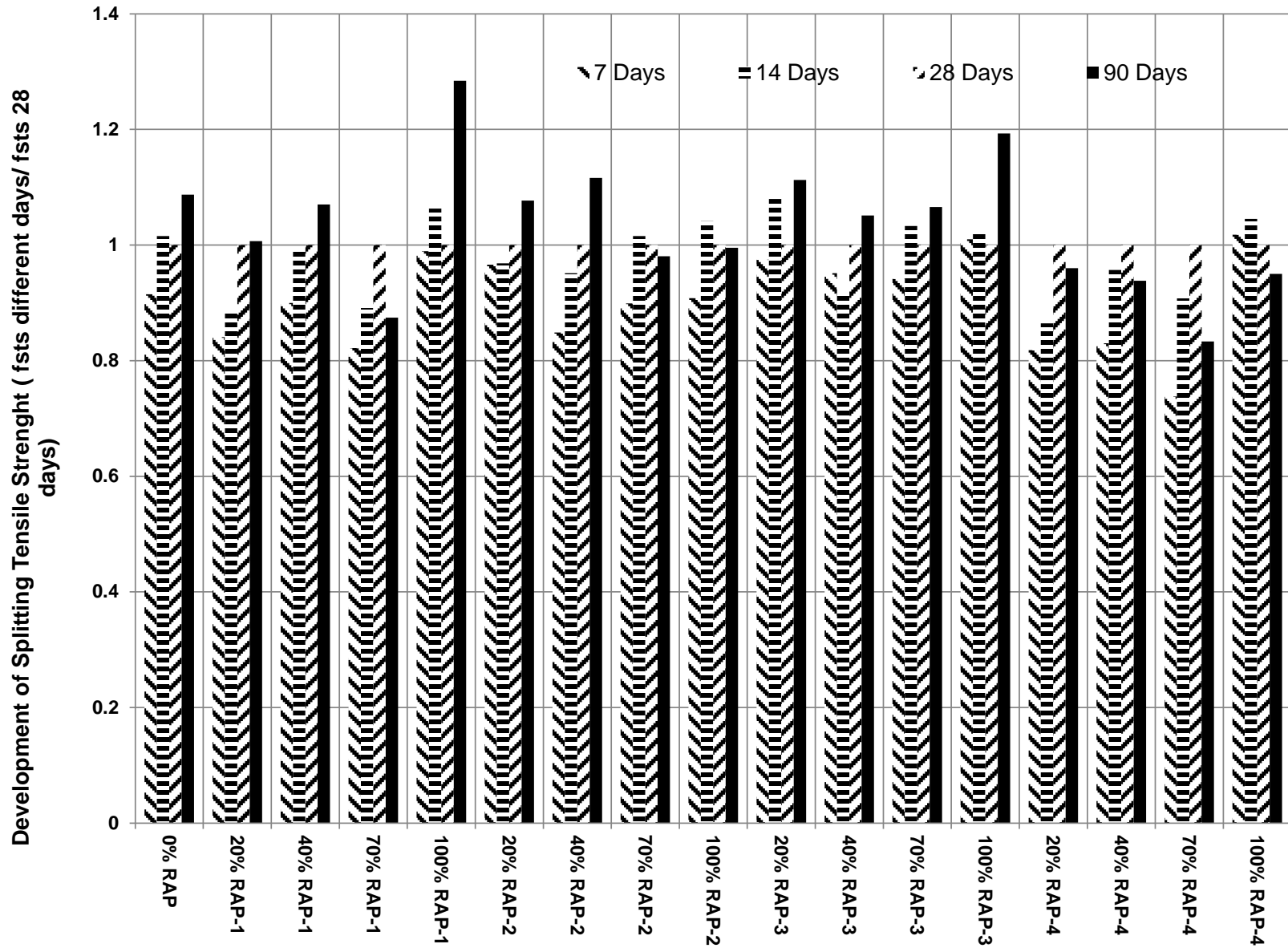


Figure 6-17. Development of splitting tensile strength at different curing times compared to that of 28 days curing time

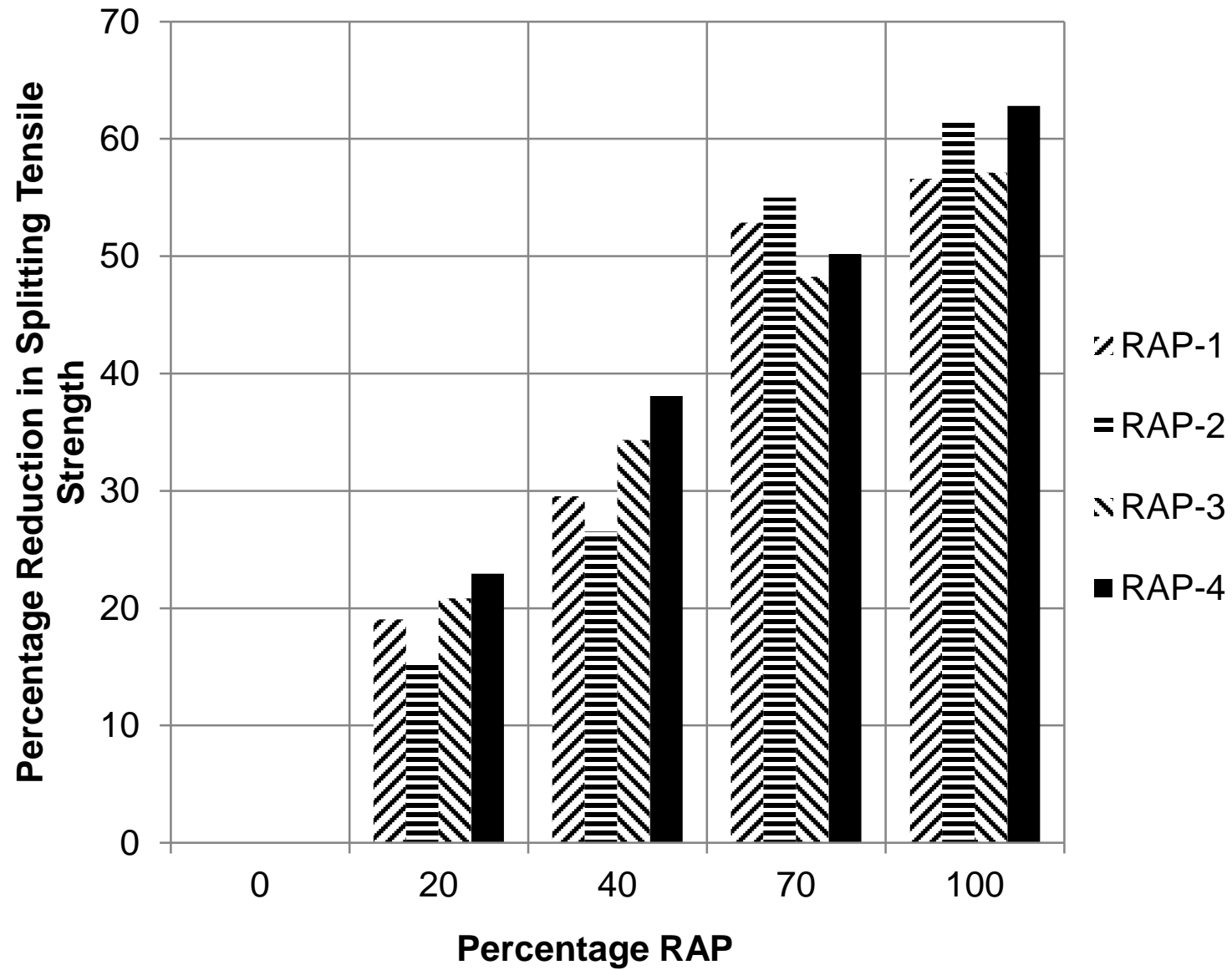


Figure 6-18. Percentage reduction in splitting tensile strength at 90 days of curing relative to the control mix

### 6.3.7 Coefficient of Thermal Expansion Test Results

Table 6-8 summarizes the average coefficient of thermal expansion of all the concrete mixtures evaluated in this research study. The coefficient of thermal expansion increased as the percentage of RAP increased in the concrete mixtures. Due to some apparent outliers in the data, the outlier data were removed and replaced with corrected values based on interpolation from the more reliable data. Table 6-9 shows the adjusted coefficient of thermal expansion. For concrete mixtures without RAP the coefficient of thermal expansion was very low at 14 days curing time, compared with those at 7 days, 28 days, and 90 days. Therefore the 14 days coefficient of thermal expansion was adjusted by using the average value between 7 days and 28 days. For concrete mixtures with RAP, the coefficient of thermal expansion increases as the percentage RAP increases. Therefore, the coefficient of thermal expansion was adjusted by using the average value between two mixtures with different RAP replacement, such that the coefficient of thermal expansion increased with the increasing percentage of RAP. Figure 6-19 shows the adjusted coefficient of thermal expansion for concrete mixtures with RAP-1. The coefficient of thermal expansion for 20% RAP-1 was higher than the 40% RAP-1 mix. Therefore, the coefficient of thermal expansion for 20% RAP-1 was adjusted by using the average value between 0% RAP and 40% RAP-1. Similar procedure was followed for all other RAP mixtures as shown in Figure 6-20, Figure 6- 21, and Figure 6-22.

Figures 6-23 through 6-26 show the adjusted coefficient of thermal expansion for concrete mixtures containing different RAP's at different curing times. The coefficient of thermal expansion for concrete mixtures with RAP-4 was low, as compared with that of the other mixtures. This adjusted coefficient of thermal expansion values were used for stress analysis as presented in Chapter 7.

Table 6-8. Actual Coefficient of thermal expansion of concrete containing RAP

Mixture Type	Number	RAP (%)	W/C	Average Coefficient of Thermal Expansion of RAP Concrete ( $\times 10^{-6}/^{\circ}\text{F}$ )			
				Curing Time (days)			
				7	14	28	90
Control	1	0	0.45	4.56	4.86	4.84	3.62
	2	0	0.50	4.64	3.68	4.35	4.04
	3	0	0.55	/	4.49	3.97	3.47
RAP-1	4	20	0.50	4.88	5.00	4.89	4.88
	5	40	0.50	4.87	4.85	4.85	4.80
	6	70	0.50	5.27	4.93	5.45	5.15
	7	100	0.50	5.49	5.92	6.26	5.87
RAP-2	4	20	0.50	4.58	4.69	4.63	4.76
	5	40	0.50	4.87	4.86	4.93	5.35
	6	70	0.50	5.46	4.73	4.83	4.76
	7	100	0.50	5.32	5.37	5.61	5.31
RAP-3	4	20	0.50	4.80	4.41	4.70	/
	5	40	0.50	4.35	4.41	4.57	/
	6	70	0.50	4.73	4.35	4.83	/
	7	100	0.50	4.81	5.13	5.05	4.13
RAP-4	4	20	0.50	4.45	4.87	4.33	5.00
	5	40	0.50	4.61	4.32	4.36	4.52
	6	70	0.50	4.79	4.08	/	4.30
	7	100	0.50	4.84	4.88	4.50	4.72

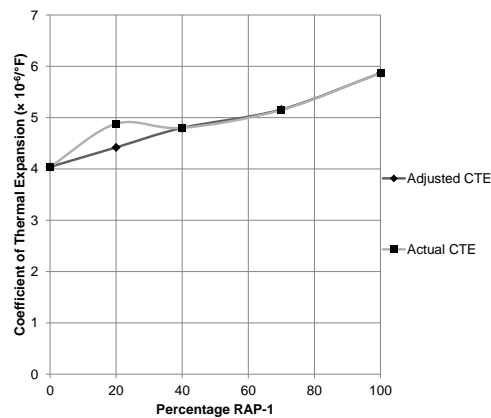


Figure 6-19. Adjusted coefficient of thermal expansion for RAP-1 at 90 days of curing time

Table 6-9. Adjusted coefficient of thermal expansion of concrete containing RAP

Mixture Type	Number	RAP (%)	W/C	Average Coefficient of Thermal Expansion of RAP Concrete ( $\times 10^{-6}/^{\circ}\text{F}$ )			
				Curing Time (days)			
				7	14	28	90
Control	1	0	0.45	4.56	4.86	4.84	3.62
	2	0	0.50	4.64	4.50	4.35	4.04
	3	0	0.55	/	4.49	3.97	3.47
RAP-1	4	20	0.50	4.76	4.75	4.6	4.42
	5	40	0.50	4.87	4.85	4.85	4.8
	6	70	0.50	5.27	4.93	5.46	5.16
	7	100	0.50	5.49	5.92	6.26	5.87
RAP-2	4	20	0.50	4.75	4.69	4.63	4.4
	5	40	0.50	4.87	4.86	4.93	4.58
	6	70	0.50	5.1	5.12	5.27	4.76
	7	100	0.50	5.32	5.37	5.61	5.31
RAP-3	4	20	0.50	4.8	4.89	4.46	4.3
	5	40	0.50	4.76	5.01	4.57	4.57
	6	70	0.50	4.73	5.07	4.83	4.83
	7	100	0.50	4.79	5.13	5.07	4.6
RAP-4	4	20	0.50	4.71	4.87	4.57	4.52
	5	40	0.50	4.75	4.87	4.54	4.52
	6	70	0.50	4.79	4.88	4.53	4.62
	7	100	0.50	4.84	4.88	4.51	4.72

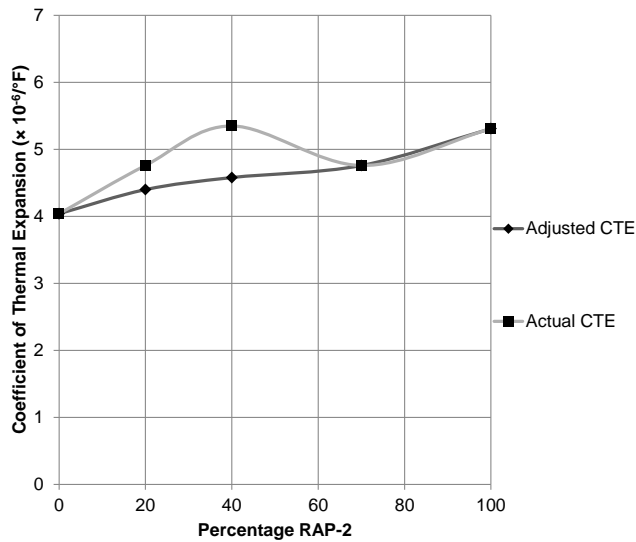


Figure 6-20. Adjusted coefficient of thermal expansion for RAP-2 at 90 days of curing time

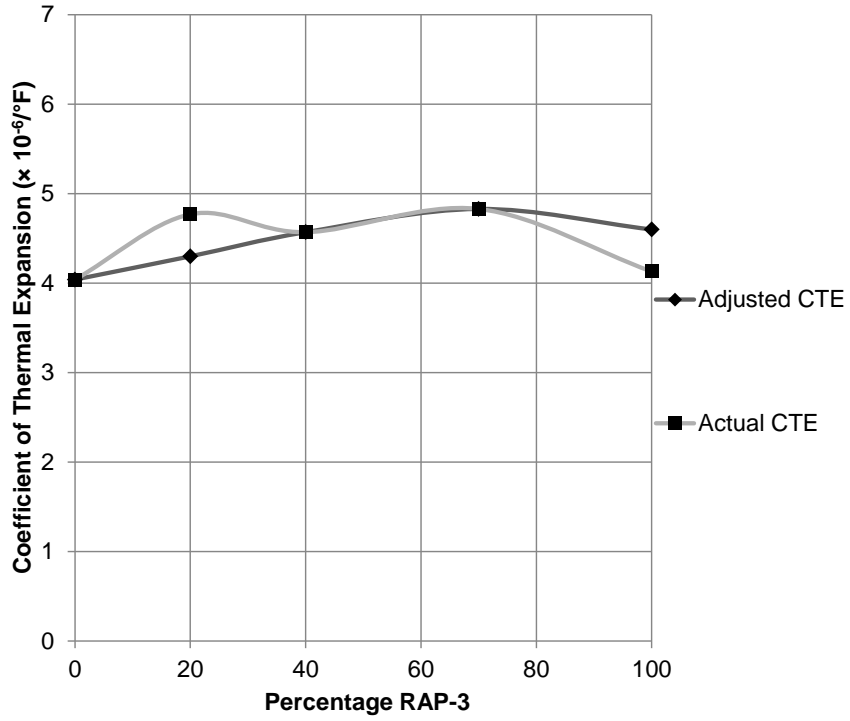


Figure 6-21. Adjusted coefficient of thermal expansion for RAP-3 at 90 days of curing time

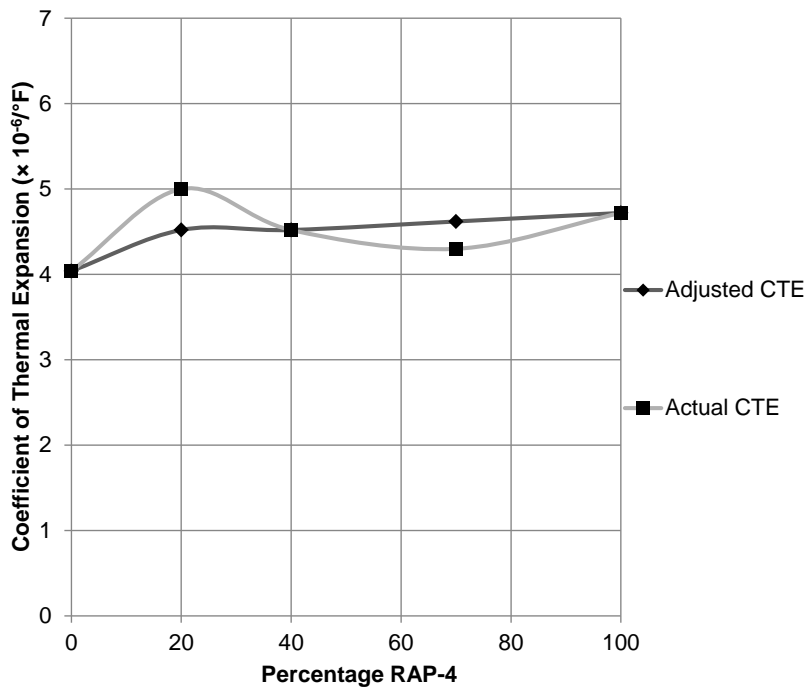


Figure 6-22. Adjusted coefficient of thermal expansion for RAP-4 at 90 days of curing time

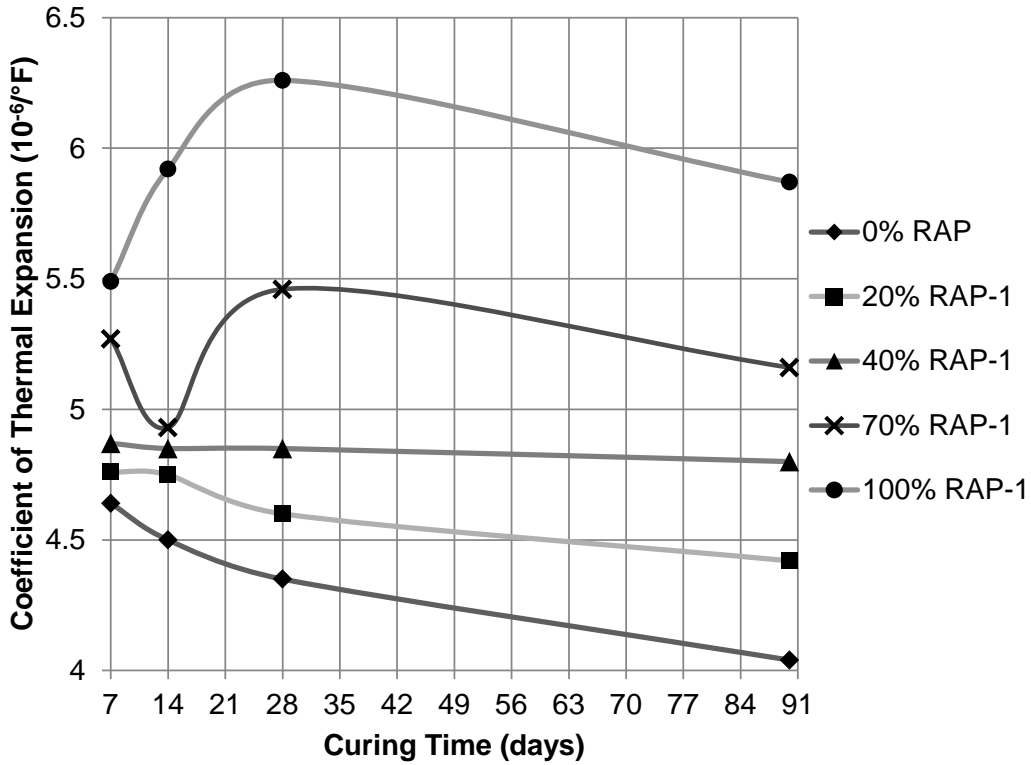


Figure 6-23. Coefficient of thermal expansion of concrete mixtures containing RAP-1

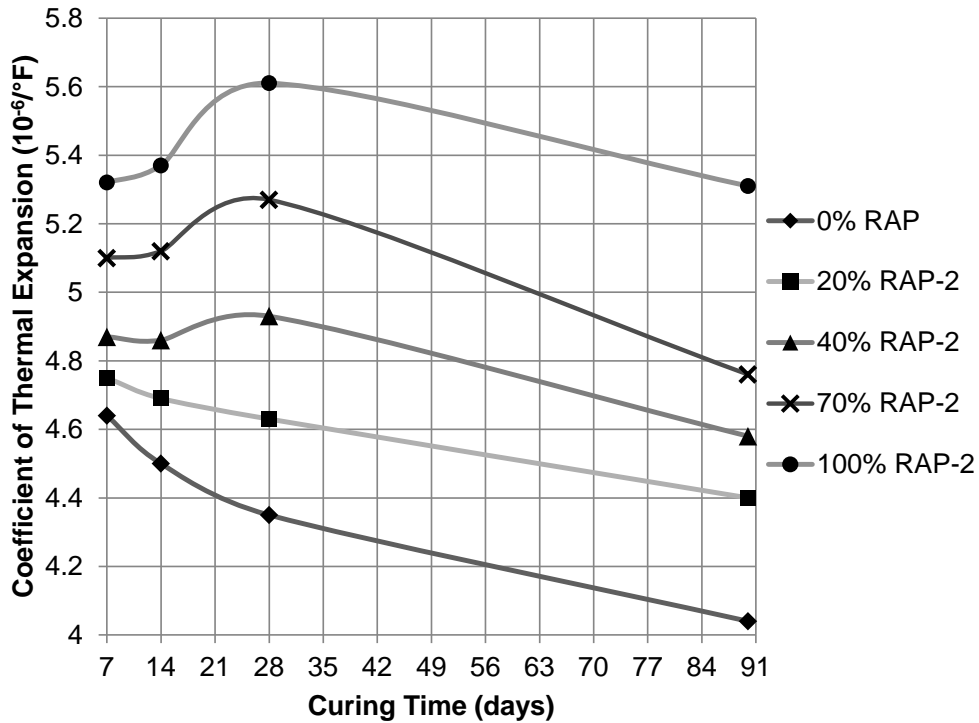


Figure 6-24. Coefficient of thermal expansion of concrete mixtures containing RAP-2

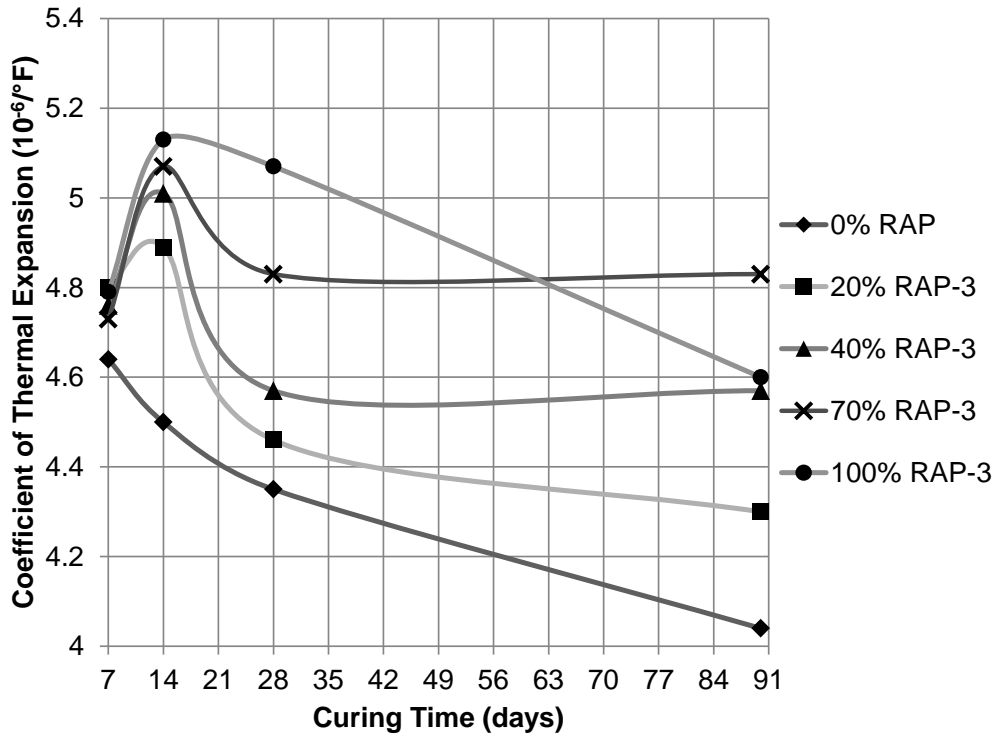


Figure 6-25. Coefficient of thermal expansion of concrete mixtures containing RAP-3

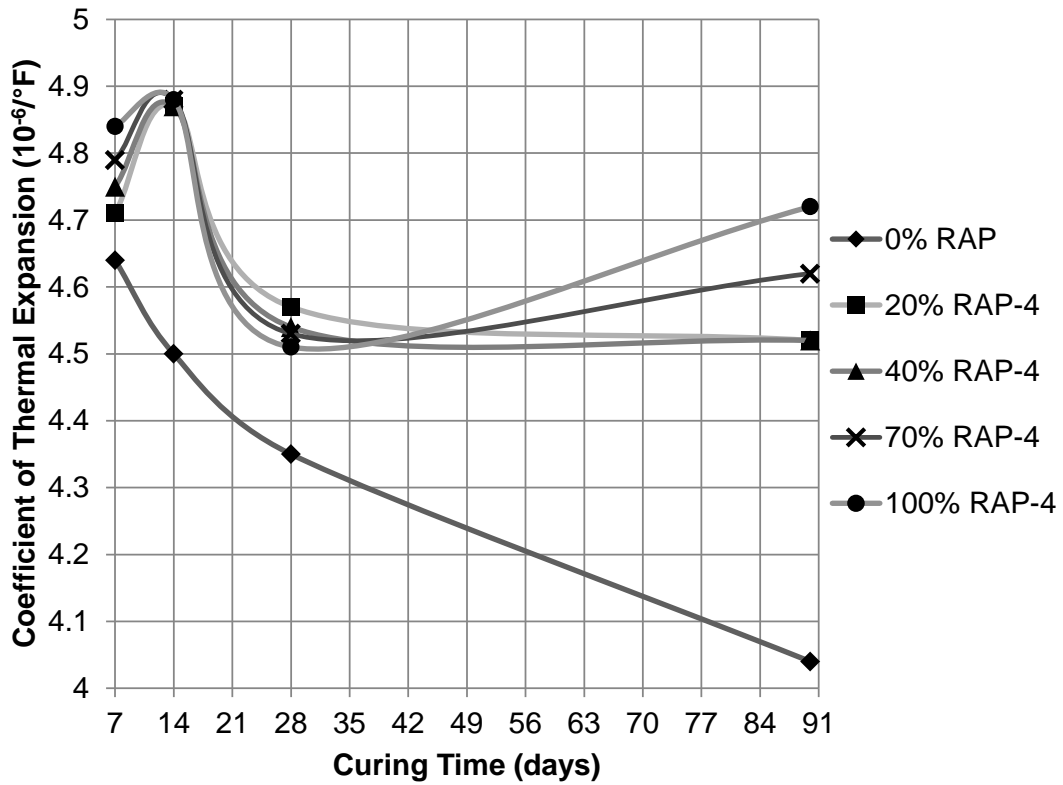


Figure 6-26. Coefficient of thermal expansion of concrete mixtures containing RAP-4

### **6.3.8 Drying Shrinkage Test Results**

Table 6-10 summarizes the average shrinkage strain values for all the concrete mixtures evaluated in this research study. Figures 6-27 through 6-34 show the percent length change for concrete containing different RAP types at different curing times. The percent length was determined by multiplying the actual shrinkage strain reading by 100. The positive value for length change indicates that the concrete specimen has shrunk, and the negative value indicates that the concrete specimen has expanded.

Figures 6-27 through 6-30 show the percent length change for the concrete specimens when air cured. For concrete mixtures with no RAP, the shrinkage rate was very high at the initial curing time, but the rate was reduced in the later stages of curing time. In general, the shrinkage of concrete mixtures increased as the percentage of RAP in the mix increased, and for concrete mixtures with 100% RAP, the drying shrinkage was very high compared with all other mixtures

Table 6-11 shows the shrinkage strain of concrete mixtures after they were moist cured. For concrete mixtures with no RAP, there was shrinkage in the concrete specimens at the initial stage of curing time, but at the later stage, it underwent some expansion.

For mixtures with RAP-1, the concrete specimens underwent expansion in the initial curing time. After 28 days, the specimens did not undergo much length change as shown in Figure 6-31. For mixtures with RAP-2, 20% RAP mix and 40% RAP mix specimens underwent shrinkage till 14 days of curing time. After 14 days, the specimens underwent some expansion as shown in Figure 6-32. For mixtures with RAP-3, all the mixtures underwent some expansion as shown in Figure 6-33. For mixtures with RAP-4, all the mixtures underwent very little expansion as shown in Figure 6-34.

In general, the concrete specimens with RAP when moist cured undergo shrinkage or expansion rapidly till 28 days of curing time, and then the specimens undergo very little length change.

Table 6-10. Drying shrinkage strain of concrete containing RAP after air curing

Mixture Type	Number	RAP (%)	W/C	Average Drying Shrinkage Strain ( $10^{-6}$ )			
				Curing Time (days)			
				7	14	28	90
Control	1	0	0.45	55	240	260	430
	2	0	0.50	130	243	250	265
	3	0	0.55	85	90	100	240
RAP-1	4	20	0.50	100	170	235	500
	5	40	0.50	75	145	250	450
	6	70	0.50	75	125	230	490
	7	100	0.50	185	300	520	905
RAP-2	4	20	0.50	115	290	250	390
	5	40	0.50	200	290	200	370
	6	70	0.50	140	180	235	460
	7	100	0.50	190	190	350	680
RAP-3	4	20	0.50	123	220	340	480
	5	40	0.50	170	280	395	510
	6	70	0.50	210	360	510	710
	7	100	0.50	280	450	660	870
RAP-4	4	20	0.50	130	265	360	430
	5	40	0.50	170	310	470	600
	6	70	0.50	175	325	450	640
	7	100	0.50	360	590	840	1160

Note- Positive value is shrinkage and negative value is shrinkage

Table 6-11. Drying shrinkage strain of concrete containing RAP after moisture curing

Mixture Type	Number	RAP (%)	W/C	Average Drying Shrinkage Strain ( $\times 10^{-6}$ )			
				Curing Time (days)			
				7	14	28	90
Control	1	0	0.45	15	150	-50	-40
	2	0	0.50	90	30	-57	-60
	3	0	0.55	100	-140	-195	-140
RAP-1	4	20	0.50	-50	-55	-75	45
	5	40	0.50	-97	-120	-85	-70
	6	70	0.50	-255	-245	-305	-225
	7	100	0.50	-135	-195	-205	-240
RAP-2	4	20	0.50	135	210	-45	-25
	5	40	0.50	45	70	-140	-180
	6	70	0.50	-30	-250	-260	-260
	7	100	0.50	-310	-290	-320	-320
RAP-3	4	20	0.50	-50	-45	-60	-25
	5	40	0.50	-50	-40	-45	-70
	6	70	0.50	-90	-110	-100	-90
	7	100	0.50	-20	-30	-35	-30
RAP-4	4	20	0.50	-60	-35	-30	-50
	5	40	0.50	-120	-85	-45	-70
	6	70	0.50	-75	-45	-55	-70
	7	100	0.50	35	0	-20	-30

Note- Positive value is shrinkage and negative value is expansion

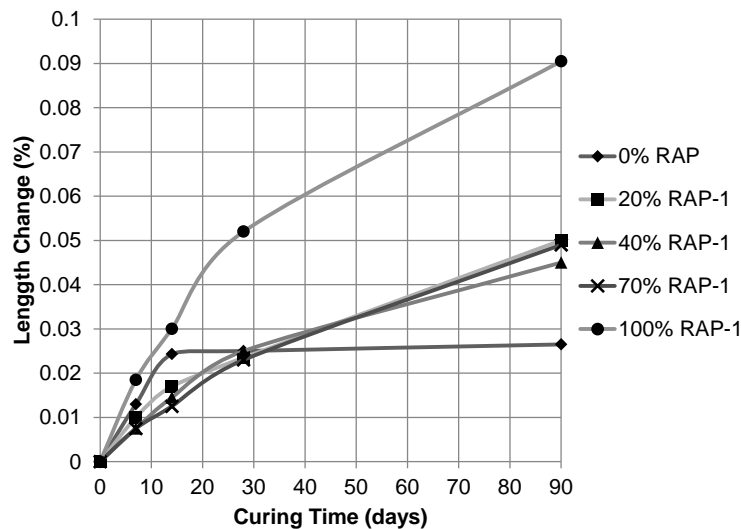


Figure 6-27. Drying shrinkage of concrete mixtures with RAP-1 after air curing

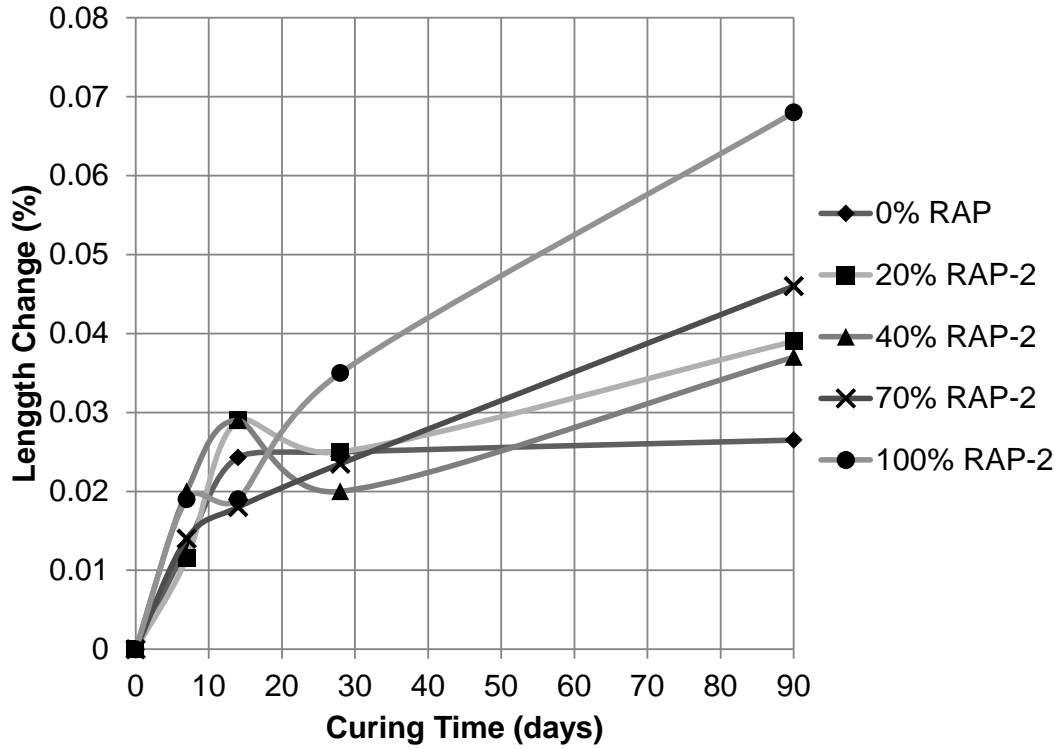


Figure 6-28. Drying shrinkage of concrete mixtures with RAP-2 after air curing

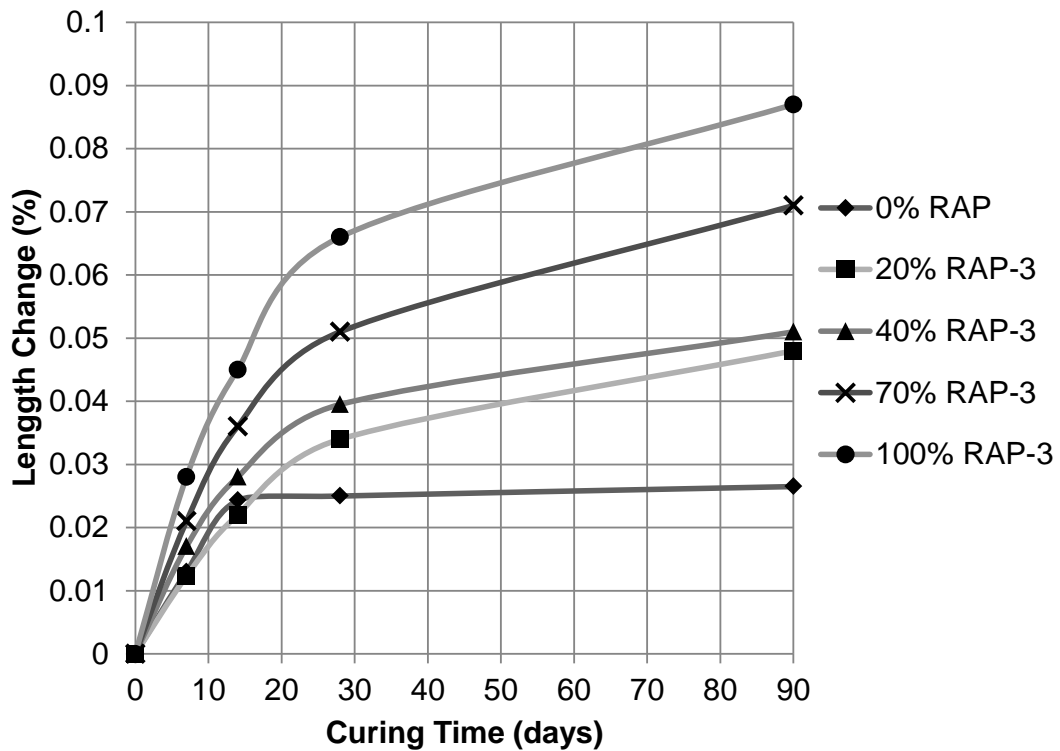


Figure 6-29. Drying shrinkage of concrete mixtures with RAP-3 after air curing

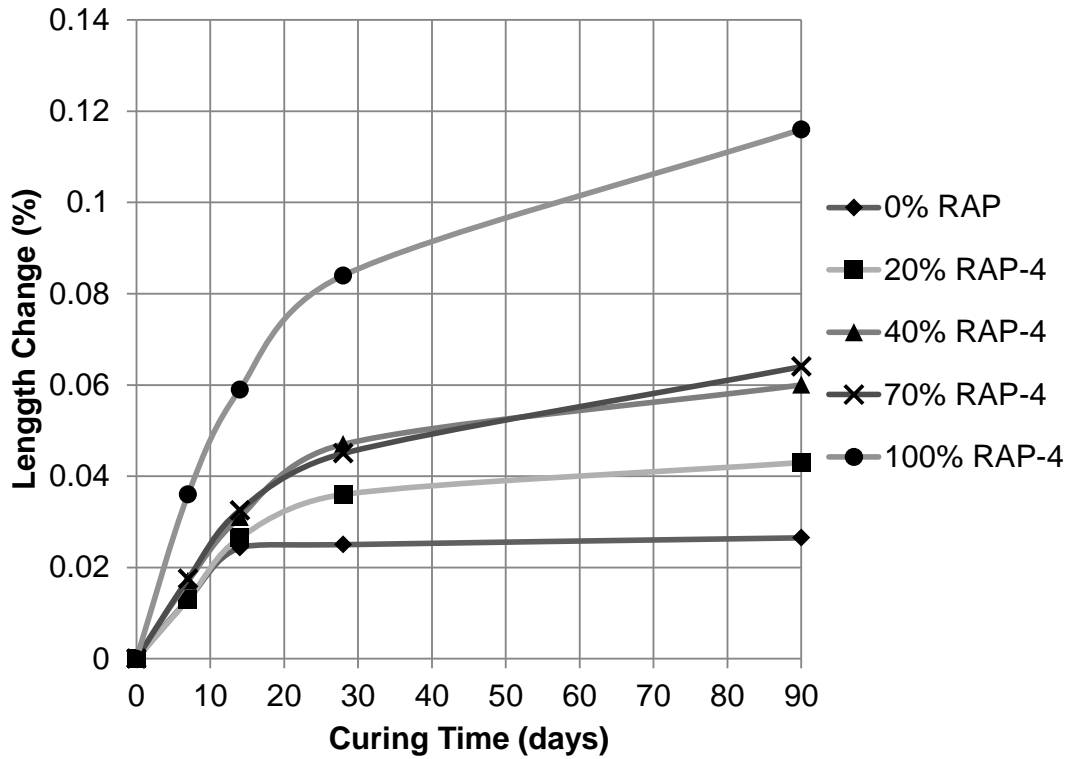


Figure 6-30. Drying shrinkage of concrete mixtures with RAP-4 after air curing

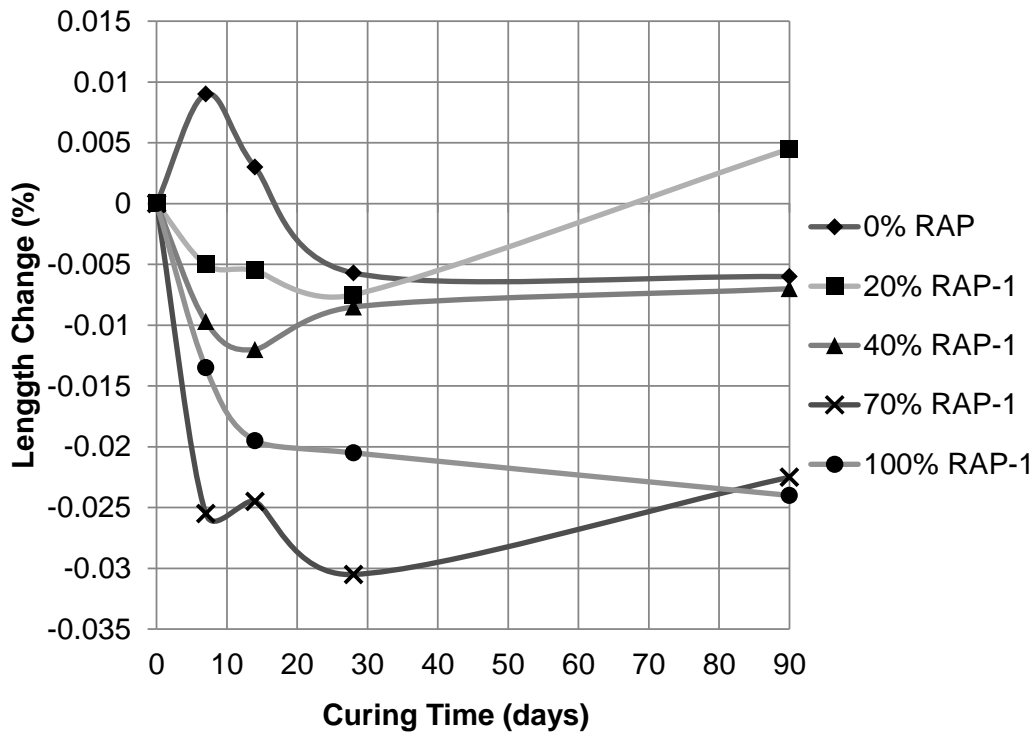


Figure 6-31. Drying shrinkage of concrete mixtures with RAP-1 after moisture curing

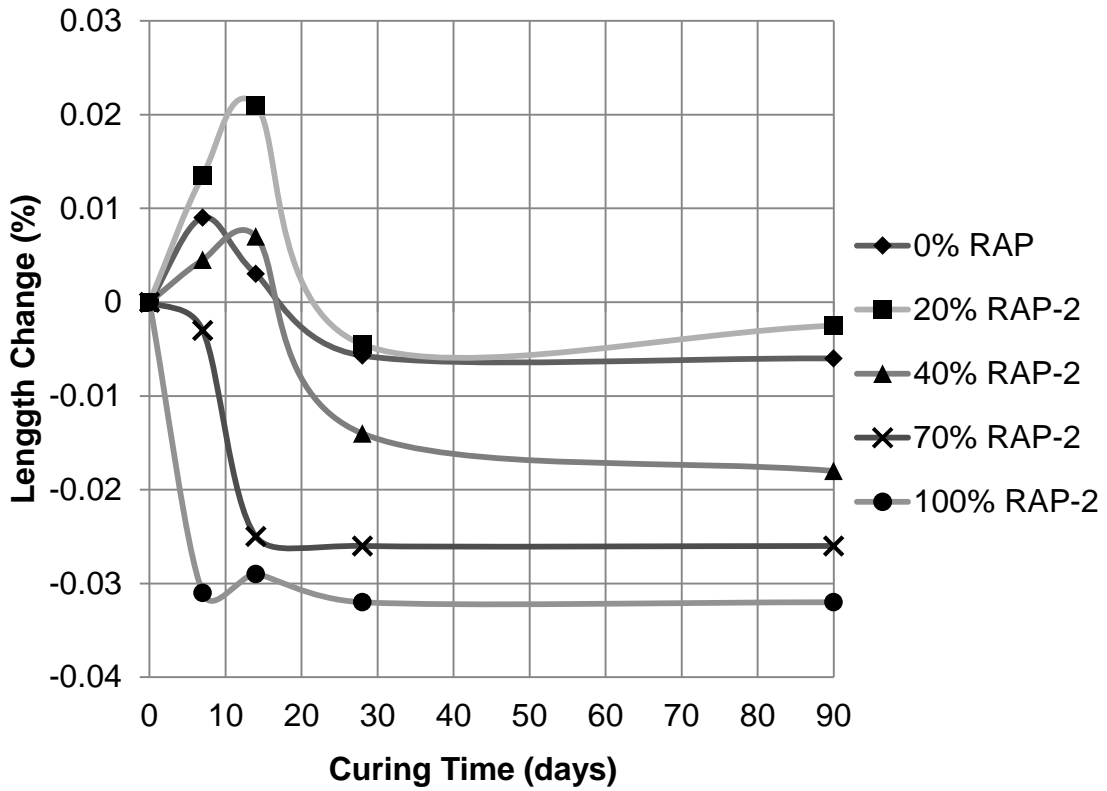


Figure 6-32. Drying shrinkage of concrete mixtures with RAP-2 after moisture curing

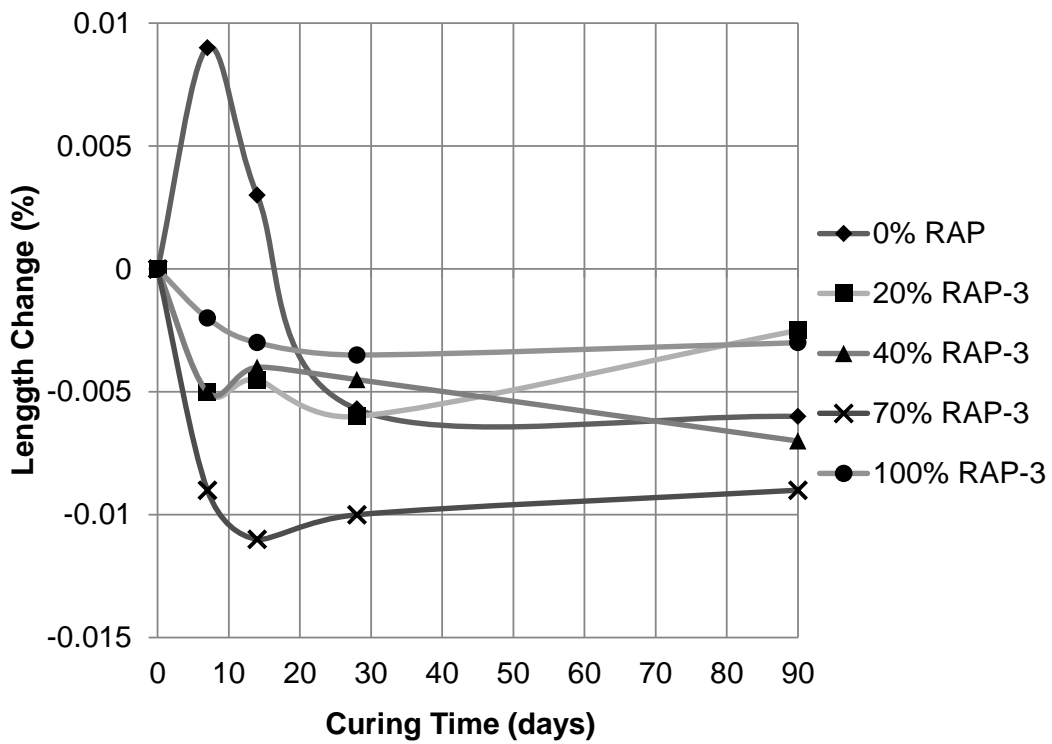


Figure 6-33. Drying shrinkage of concrete mixtures with RAP-3 after moisture curing

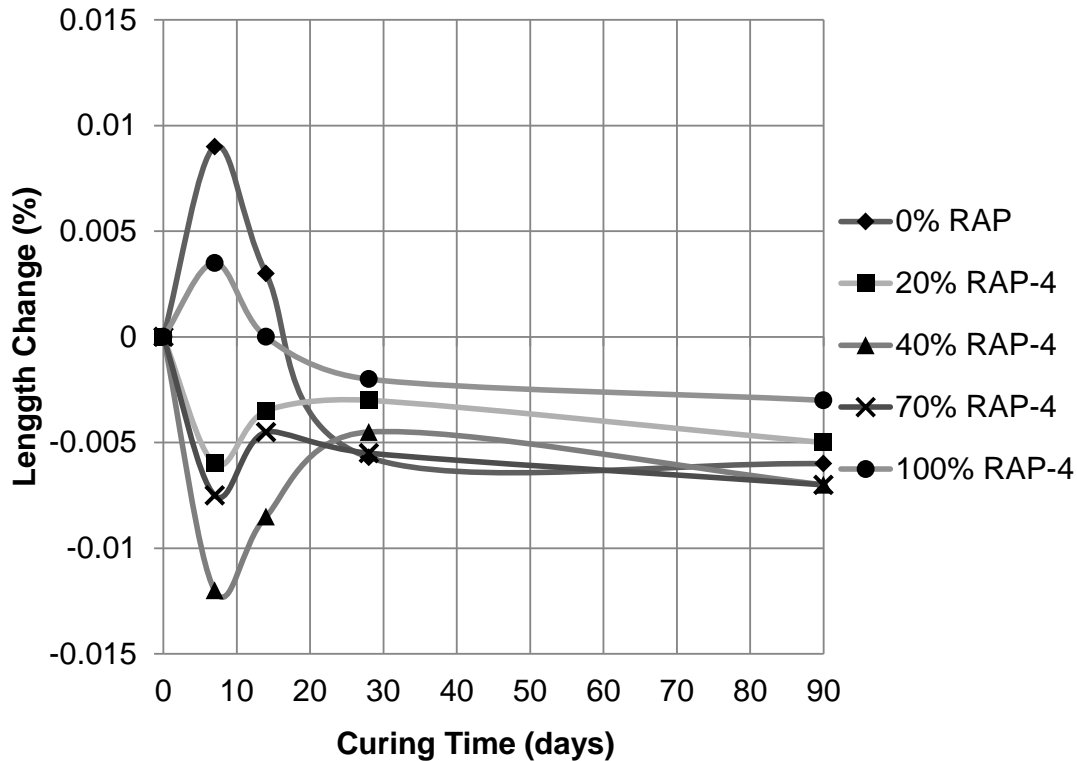


Figure 6-34. Drying shrinkage of concrete mixtures with RAP-4 after moist curing

## 6.4 Relationship among the Concrete Properties

### 6.4.1 Relationship between Compressive Strength and Flexural Strength

Compressive strength of the concrete is one of the important properties used in concrete mix design. The relationship between compressive strength and flexural strength is very important for concrete pavements, since the performance of concrete pavement is highly dependent on the flexural strength of the concrete. The relationship between compressive strength and flexural strength was developed and plotted as shown in Figure 6-35. Regression equation was developed to best fit the relationship between compressive strength ( $f_c$ ) and flexural strength ( $R$ ). The ACI equation is also used for comparison as shown on the plot. From the plot, it can be seen that the coefficient of the ACI equation is slightly lower for regular concrete as compared with the one predicted for RAP concrete based on the experimental data in this study.

Therefore, based on the experimental data of this research study, the ACI equation will underestimate the flexural strength of RAP concrete.

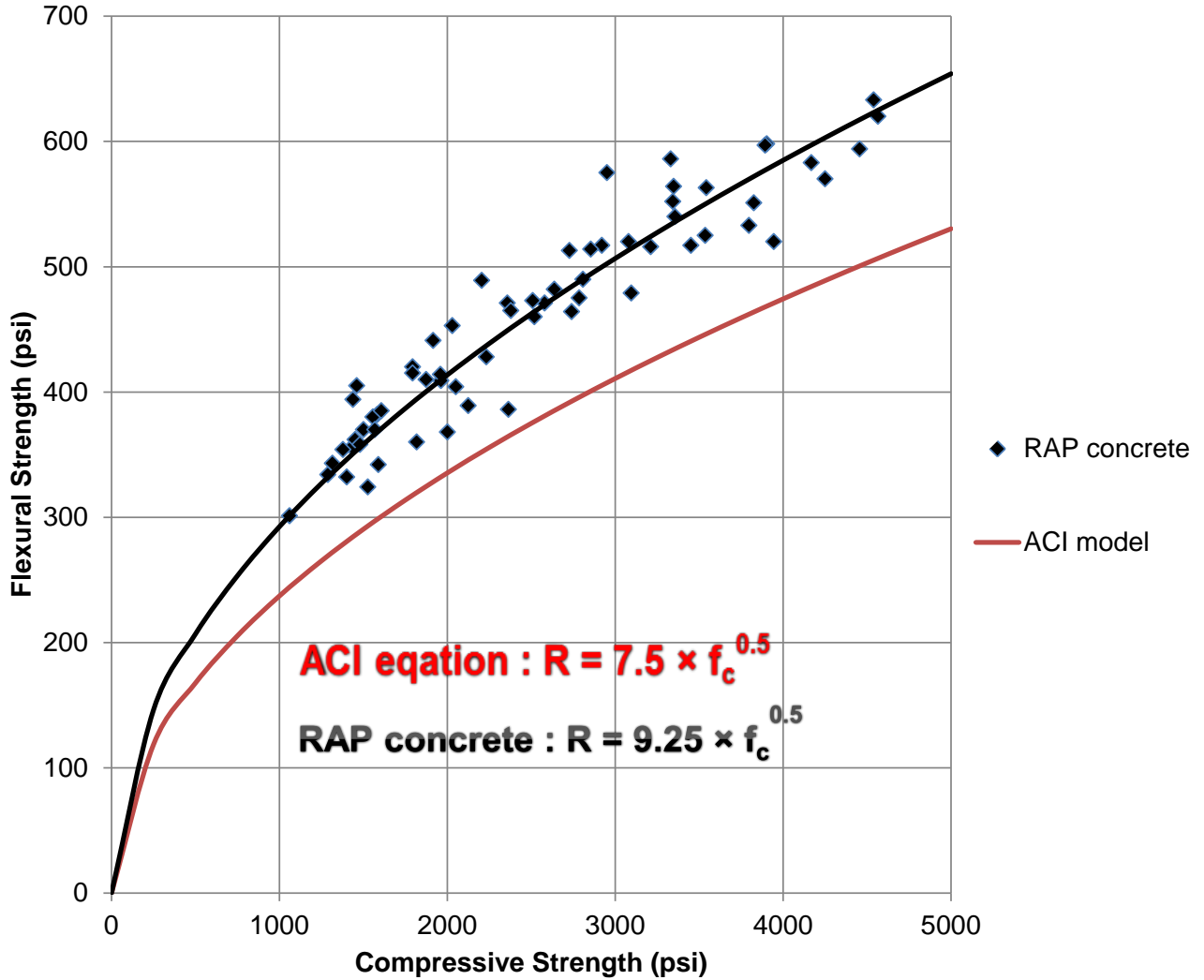


Figure 6-35. Relationship between compressive strength and flexural strength

#### 6.4.2 Relationship between Compressive Strength and Modulus of Elasticity

The modulus of elasticity is an important material property that affects the stress/strain behavior of concrete slab, and also an important input to programs for concrete pavement analysis, such as FEACONS and MEPDG.

The relationship between compressive strength and modulus of elasticity based on the experimental data in this research study is plotted and compared to the ACI equation as shown in the Figure 6-36. It shows that as the compressive strength of the concrete containing RAP decreases, the rate of decrease in the modulus of elasticity is even higher, when compared with the normal concrete. Therefore, the ACI equation will overestimate the elastic modulus and will not be suitable to predict the modulus of elasticity of concrete containing RAP, especially for concrete mixtures containing higher percentage of RAP.

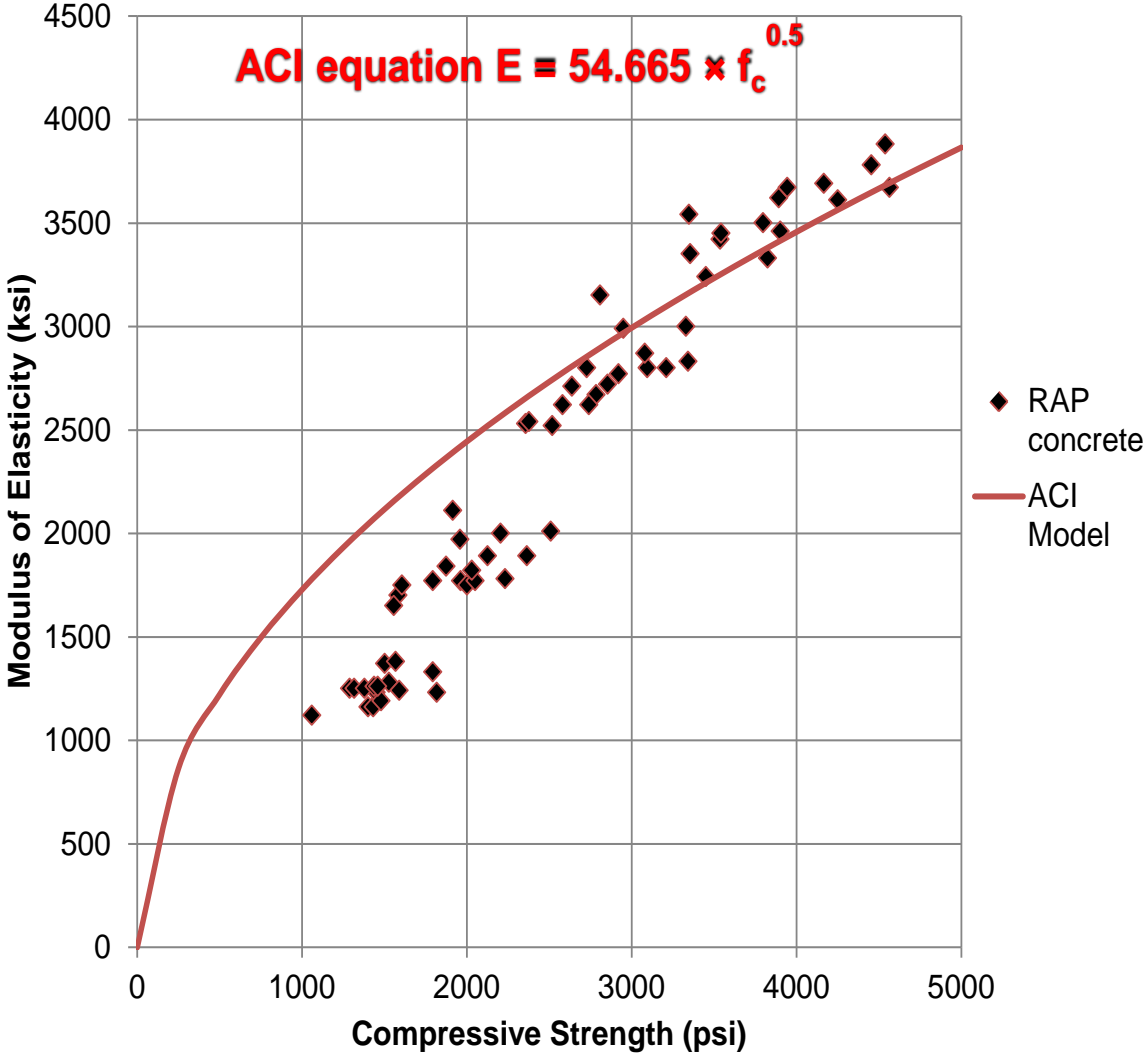


Figure 6-36. Relationship between compressive strength and elastic modulus

### 6.4.3 Relationship between Compressive Strength and Splitting Tensile Strength

The relationship between compressive strength and splitting tensile strength was plotted as shown in Figure 6-37. The regression equation was developed to best fit the experimental data for this study, and to establish relationship between compressive strength ( $f_c$ ) and splitting tensile strength ( $f_{ct}$ ) of concrete containing RAP.

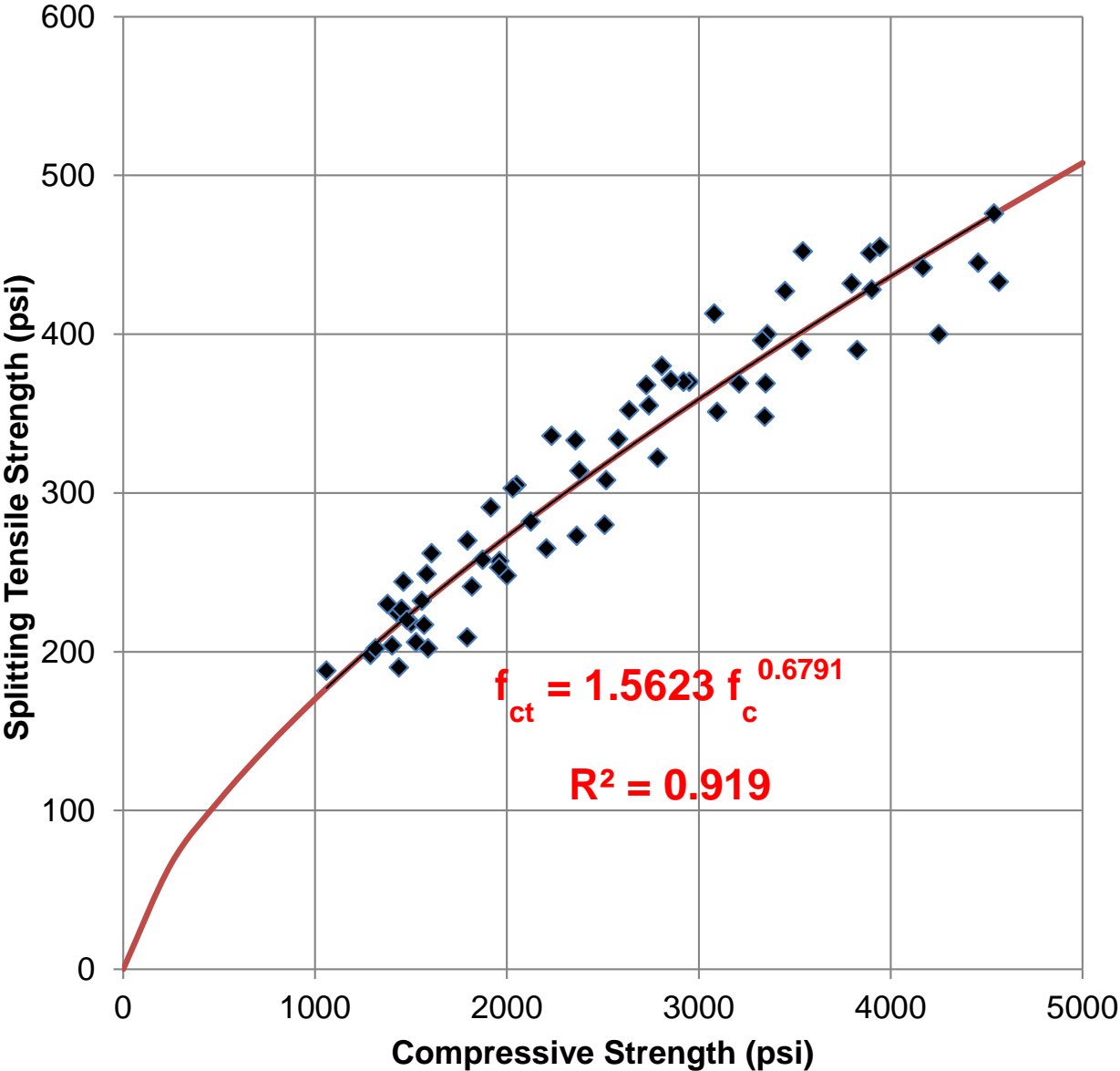


Figure 6-37. Relationship between compressive strength and splitting tensile strength

### 6.4.4 Relationship between Splitting Tensile Strength and Flexural Strength

The relationship between splitting tensile strength and flexural strength was plotted as shown in Figure 6-38. The regression equation was developed to best fit the experimental data for this study, and to establish relationship between splitting tensile strength ( $f_{ct}$ ) and flexural strength (R) of concrete containing RAP.

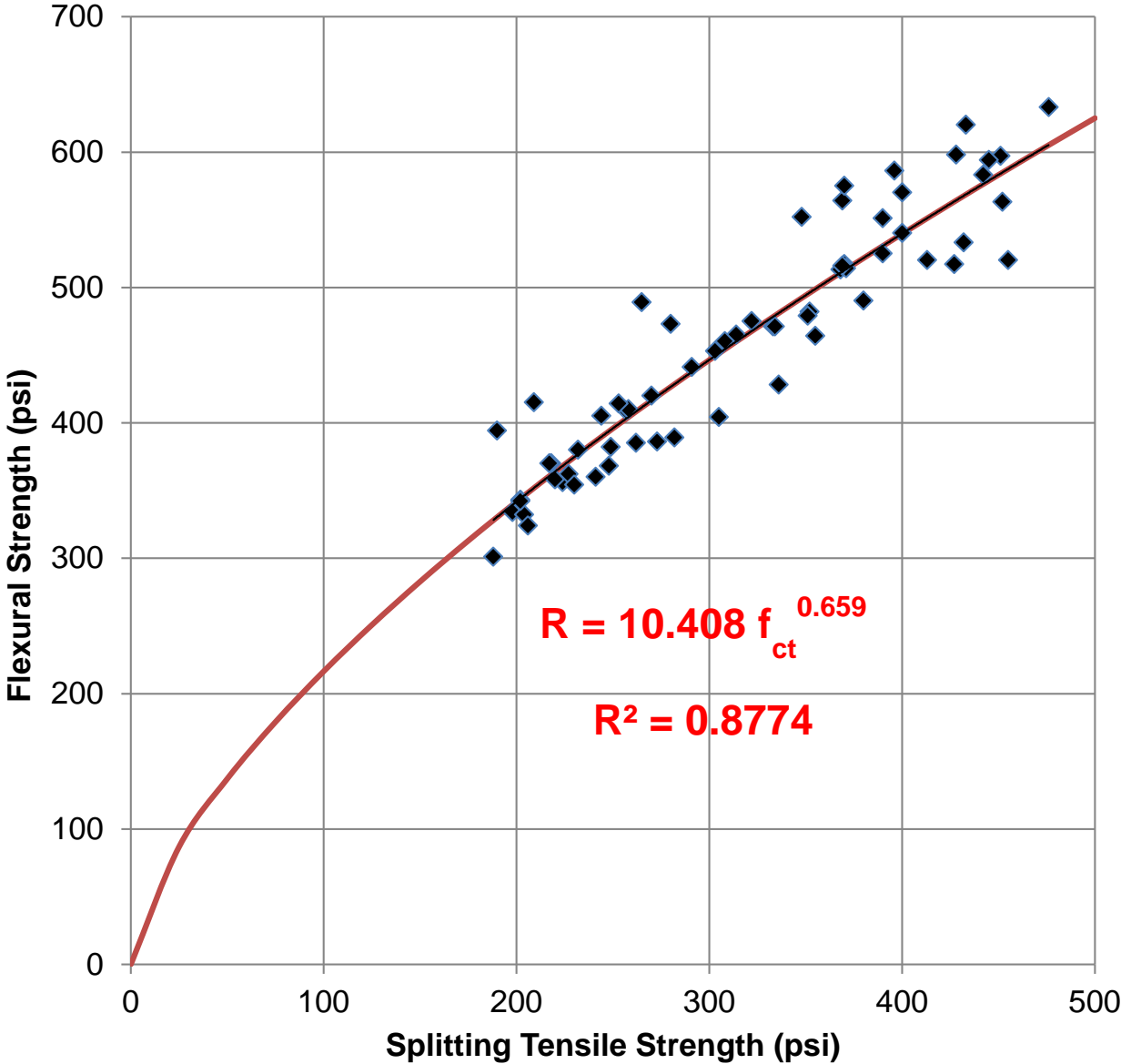


Figure 6-38. Relationship between splitting tensile strength and flexural strength

## 6.5 Summary of Findings

- The compressive strength, modulus of elasticity, flexural strength, and splitting tensile strength decreased as the percentage of RAP increased in the concrete mix.
- The reduction in flexural strength in the concrete containing RAP was 10% to 20% lower than the corresponding reduction in compressive strength and splitting tensile strength of the concrete containing RAP.
- The rate of reduction in modulus of elasticity in the concrete containing RAP was much higher than the corresponding reduction in compressive strength of the concrete containing RAP.
- The drying shrinkage, coefficient of thermal expansion, and Poisson's ratio increased as the percentage of RAP in the concrete increased.
- RAP-4 which consisted of limestone, granite, and polymer modified binder produced concrete mixtures with lower coefficient of thermal expansion and much higher flexural strength, when compared to concrete mixtures containing other RAP's.
- The failure strain and toughness of concrete increased as the percentage of RAP increased in the mix.
- The ACI equation underestimates the flexural strength of concrete mixtures containing RAP, based on the results of concrete mixtures evaluated in this research study.
- The ACI equation will tend to overestimate the modulus of elasticity and cannot be used to estimate the modulus of elasticity of concrete mixtures containing RAP, based on the results of concrete mixtures evaluated in this research study.

## **CHAPTER 7**

### **EVALUATION OF POTENTIAL PERFORMANCE IN CONCRETE PAVEMENT SLABS**

#### **7.1 Introduction**

Using the measured properties of concrete containing RAP, analysis was performed using FEACONS IV program and the mechanistic empirical design guide program (MEPDG) to determine how each of the concrete mixtures containing different percentages of RAP, and different type of RAP, would perform if it were used in a typical concrete pavement in Florida. This chapter presents the results of these analyses.

#### **7.2 Critical Stress Analysis Using FEACONS IV Program**

Using the measured elastic modulus and the coefficient of thermal expansion to model the concrete, analysis was performed to determine the maximum stresses in a typical concrete pavement slab if it were under a critical combination of load and temperature condition. Prior study has shown that a 22-kip axle load applied at the middle of the slab edge, when there was a temperature differential of +20° F in the concrete slab, represents a critical loading condition in Florida. Thus, this loading condition was used in the analysis.

The FEACONS IV (Finite Element Analysis of Concrete Slabs, version IV) program was used to perform the stress analysis. The FEACONS program was previously developed at the University of Florida for FDOT for the analysis of PCC pavements subjected to load and thermal effects, and has demonstrated to be a fairly effective and reliable tool for this type of analysis.

The following parameters were used to model the concrete pavement: Slab thickness = 12"; slab length = 15'; slab width = 12'; Modulus of subgrade reaction,  $k_s = 0.4$  kci; edge stiffness,  $k_e = 30$  ksi; Joint linear stiffness,  $k_l = 500$  ksi; joint torsion stiffness  $k_t = 1000$  k-in/in.

Critical stress analyses were performed using the properties of the concrete containing different percentages of RAP at different curing times. The maximum stress in the concrete slab

under the critical condition was first computed. The maximum computed stress was divided by the flexural strength of the concrete to obtain the stress to flexural strength ratio, which can indicate the potential performance of the concrete in service. According to fatigue theory, a low stress to strength ratio would indicate a higher number of load repetitions to failure and potentially better performance for concrete pavements in the field.

The results of the stress analysis for all the concrete mixtures evaluated in this research study are summarized in Tables 7-2 through 7-5 for different curing times. For the concrete mixtures with RAP, there was no reduction in stress to strength ratio at initial curing time of 7 days and 14 days. However, at 28 days and 90 days the stress to strength ratio for concrete mixtures with RAP was comparable to that of conventional mix, and some even lower. For concrete mixtures with RAP, the stress-strength ratio decreased as the percentage of RAP increased in the mix. In general, concrete mixtures with RAP-1 and RAP-4 had lower stress-strength ratio, when compared with RAP-2 and RAP-3 concrete mixtures at 28 days and 90 days of curing time. Figure 7-1 and Figure 7-2 show the computed stress to strength ratios for concretes at 28 days and 90 days of curing time. For the concrete mixtures with stress-strength ratio less than 0.5, it would take infinite number of load cycles for concrete to fail. At 28 days of curing time, concrete mixtures with 40%, 70%, and 100% RAP-1 and RAP-4 had lower stress-strength ratio, as compared with other mixtures with RAP. At 90 days of curing time, concrete mixtures with 40%, 70%, and 100% RAP-1 and RAP-4 had stress-strength ratio equal to 0.5 and even lower. This shows that concrete containing RAP has the potential to perform well in service.

### **7.3 Analysis Using Mechanistic Empirical Pavement Design Guide**

The mechanistic empirical pavement design guide (MEPDG) was used to assess the potential performance of concrete pavements, if concrete containing RAP were to be used in a

typical concrete pavement in Florida. A jointed plain concrete pavement (JPCP) with a design life of 25 years was used in the analysis. Table 7-1 shows the performance criteria used in the MEPDG model.

Table 7-1. Performance criteria used in the MEPDG model

Criteria	Limit	Reliability
Initial IRI (in/mile)	58	-
Terminal IRI (in/mile)	160	90
Transverse cracking (% slabs cracked)	10	90
Mean joint faulting (in)	0.12	90

Hierarchy level 1 was used for the input parameters for the analysis. Default values were used for traffic volume adjustment and vehicle class distribution. Traffic growth factor function was considered linear with a growth rate of 2%. Table 7-5 shows the traffic information used in the model. The climate data was acquired from the program for the conditions in Gainesville, Florida.

The pavement structure to be analyzed consisted of four layers with a 10 inch thick concrete slab as layer 1. Layer 2 was 4 inch thick asphalt concrete. Layer 3 was a 12 inch compacted subgrade (A-3), and layer 4 was modeled as a semi-infinite natural subgrade (A-2-4). All the details of the input files used are provided in the appendix C. (Ping, W.V. and Kampmann, R., 2008)

Table 7-2. Results of critical stress analysis using concrete properties at 7 days curing

Mixture Type	Number	Percentage RAP	W/C	Modulus of Elasticity (ksi)	Coefficient of Thermal Expansion ( $\times 10^{-6}/^{\circ}\text{F}$ )	Unit Weight (lbs/ft <sup>3</sup> )	Computed Maximum Stress (psi)	Measured Ultimate Flexural Strength (psi)	Computed Stress to Flexural Strength ratio
Control	2	0	0.50	3970	4.64	140	331	630	0.53
	4	20	0.50	3150	4.76	139	296	496	0.60
RAP-1	5	40	0.50	2530	4.87	139	266	471	0.56
	6	70	0.50	1700	5.27	135	219	382	0.57
	7	100	0.50	1120	5.49	130	174	301	0.58
RAP-2	4	20	0.50	3240	4.75	139	300	517	0.58
	5	40	0.50	2540	4.87	137	267	465	0.57
	6	70	0.50	1650	5.10	136	211	380	0.55
	7	100	0.50	1250	5.32	135	183	334	0.55
RAP-3	4	20	0.50	3420	4.80	139	311	525	0.59
	5	40	0.50	2620	4.76	138	267	471	0.57
	6	70	0.50	1770	4.73	137	213	409	0.52
	7	100	0.50	1160	4.79	132	169	332	0.51
RAP-4	4	20	0.50	3540	4.71	139	315	564	0.56
	5	40	0.50	2520	4.75	138	262	460	0.57
	6	70	0.50	1750	4.79	136	214	368	0.58
	7	100	0.50	1160	4.84	132	169	356	0.47

Table 7-3. Results of critical stress analysis using concrete properties at 14 days curing

Mixture Type	Number	Percentage RAP	W/C	Modulus of Elasticity (ksi)	Coefficient of Thermal Expansion ( $\times 10^{-6}/^{\circ}\text{F}$ )	Unit Weight (lbs/ft <sup>3</sup> )	Computed Maximum Stress (psi)	Measured Ultimate Flexural Strength (psi)	Computed Stress to Flexural Strength ratio
Control	2	0	0.50	4220	4.50	140	343	666	0.52
RAP-1	4	20	0.50	3350	4.75	139	307	540	0.57
	5	40	0.50	2800	4.85	139	281	513	0.55
	6	70	0.50	1770	4.93	135	218	420	0.52
	7	100	0.50	1250	5.92	130	197	343	0.57
	4	20	0.50	3460	4.69	139	311	598	0.52
RAP-2	5	40	0.50	2710	4.86	137	275	482	0.57
	6	70	0.50	1750	5.12	136	219	385	0.57
	7	100	0.50	1230	5.37	135	183	362	0.51
	4	20	0.50	3500	4.89	139	319	533	0.60
RAP-3	5	40	0.50	2670	5.01	138	277	475	0.58
	6	70	0.50	1890	5.07	137	227	389	0.58
	7	100	0.50	1280	5.13	132	184	324	0.57
	4	20	0.50	3330	4.87	139	309	551	0.56
RAP-4	5	40	0.50	2620	4.87	138	272	464	0.57
	6	70	0.50	1770	4.88	136	215	409	0.53
	7	100	0.50	1250	4.88	132	177	354	0.50

Table 7-4. Results of critical stress analysis using concrete properties at 28 days curing

Mixture Type	Number	Percentage RAP	W/C	Modulus of Elasticity (ksi)	Coefficient of Thermal Expansion ( $\times 10^{-6}/^{\circ}\text{F}$ )	Unit Weight (lbs/ft <sup>3</sup> )	Computed Maximum Stress (psi)	Measured Ultimate Flexural Strength (psi)	Computed Stress to Flexural Strength ratio
Control	2	0	0.50	4430	4.35	140	341	686	0.50
	4	20	0.50	3450	4.60	139	307	563	0.54
RAP-1	5	40	0.50	2990	4.85	139	292	575	0.51
	6	70	0.50	1820	5.46	135	232	453	0.51
	7	100	0.50	1260	6.26	130	206	394	0.52
	4	20	0.50	3690	4.63	139	320	583	0.55
RAP-2	5	40	0.50	2770	4.93	137	281	517	0.54
	6	70	0.50	1840	5.27	136	228	410	0.55
	7	100	0.50	1370	5.61	135	198	370	0.53
	4	20	0.50	3610	4.46	139	310	570	0.54
RAP-3	5	40	0.50	2800	4.57	138	272	479	0.57
	6	70	0.50	1890	4.83	137	223	386	0.57
	7	100	0.50	1240	5.07	132	179	342	0.52
	4	20	0.50	3620	4.57	139	314	597	0.53
RAP-4	5	40	0.50	2720	4.54	138	268	514	0.52
	6	70	0.50	1780	4.53	136	210	428	0.49
	7	100	0.50	1190	4.51	132	168	358	0.47

Table 7-5. Results of critical stress analysis using concrete properties at 90 days curing

Mixture Type	Number	Percentage RAP	W/C	Modulus of Elasticity (ksi)	Coefficient of Thermal Expansion ( $\times 10^{-6}/^{\circ}\text{F}$ )	Unit Weight (lbs/ft <sup>3</sup> )	Computed Maximum Stress (psi)	Measured Ultimate Flexural Strength (psi)	Computed Stress to Flexural Strength ratio
Control	2	0	0.50	4440	4.04	140	333	694	0.48
RAP-1	4	20	0.50	3670	4.42	139	311	520	0.60
	5	40	0.50	3000	4.80	139	292	586	0.50
	6	70	0.50	2000	5.16	135	239	491	0.48
	7	100	0.50	1260	5.87	130	196	405	0.48
RAP-2	4	20	0.50	3880	4.40	139	320	633	0.50
	5	40	0.50	2870	4.58	137	277	520	0.53
	6	70	0.50	1970	4.76	136	227	414	0.55
	7	100	0.50	1380	5.31	135	194	370	0.52
RAP-3	4	20	0.50	3780	4.30	139	311	594	0.52
	5	40	0.50	2800	4.57	138	272	516	0.53
	6	70	0.50	2110	4.83	137	238	441	0.54
	7	100	0.50	1230	4.60	132	171	360	0.48
RAP-4	4	20	0.50	3670	4.52	139	314	620	0.51
	5	40	0.50	2830	4.52	138	274	552	0.50
	6	70	0.50	2010	4.62	136	227	473	0.48
	7	100	0.50	1330	4.72	132	181	415	0.44

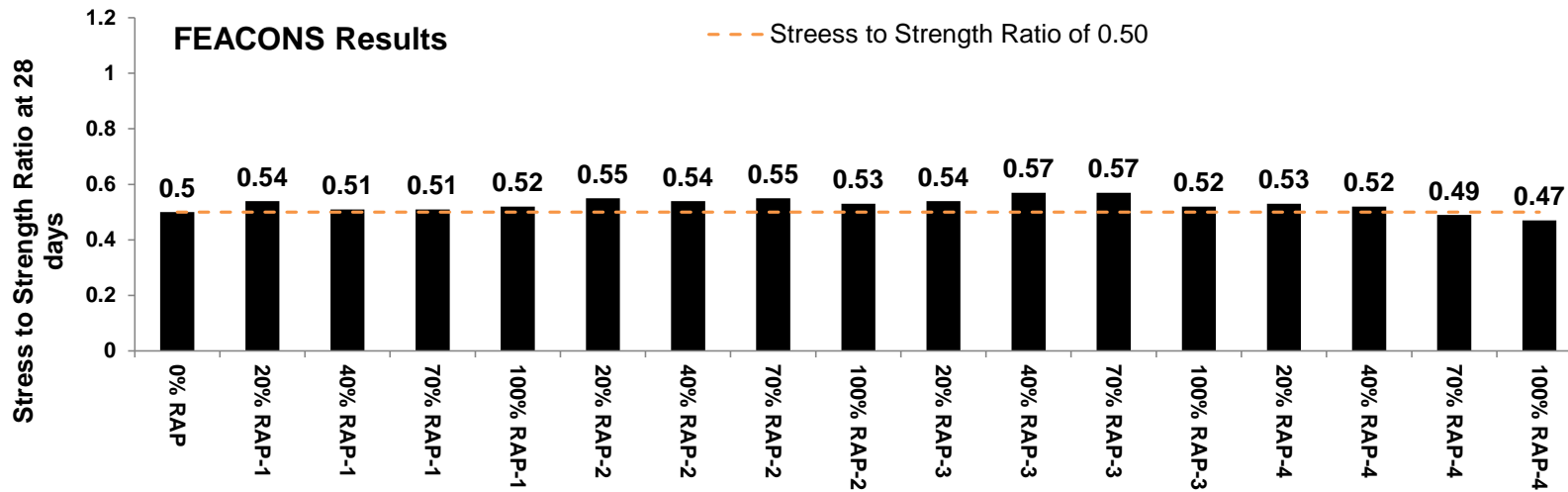


Figure 7-1. Stress-strength ratio of concrete mixtures containing RAP at 28 days of curing time

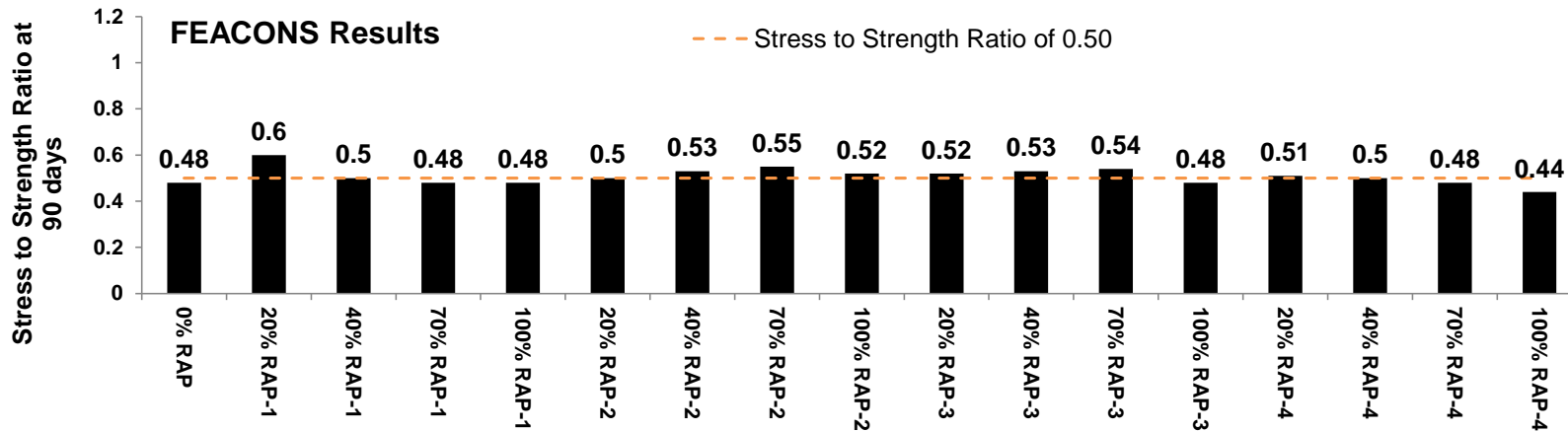


Figure 7-2. Stress-strength ratio of concrete mixtures containing RAP at 90 days of curing time

Table 7-6. Traffic information used in the MEPDG model

Initial two way AADT	7000
Number of lanes in design direction	2
Percent of trucks in design direction (%)	50
Percent of trucks in design lane (%)	95
Operational speed (mph)	70

Table 7-7. Predicted terminal IRI from MEPDG analysis of pavements using concrete containing RAP

Mix Type	No	RAP (%)	Distress Target	Reliability Target	Distress Predicted	Reliability Predicted	Acceptable
Control	2	0	160	90	67.5	99.99	Pass
RAP-1	4	20	160	90	94	97.53	Pass
	5	40	160	90	69.6	99.99	Pass
RAP-2	4	20	160	90	64.2	99.99	Pass
	5	40	160	90	79.2	99.74	Pass
RAP-3	4	20	160	90	74.3	99.93	Pass
	5	40	160	90	75.7	99.90	Pass
RAP-4	4	20	160	90	89.3	99.50	Pass
	5	40	160	90	83.3	99.86	Pass

Table 7-8. Predicted mean terminal joint faulting from MEPDG analysis of pavements using concrete containing RAP

Mix Type	No	RAP (%)	Distress Target	Reliability Target	Distress Predicted	Reliability Predicted	Acceptable
Control	2	0	0.12	90	0.018	99.99	Pass
RAP-1	4	20	0.12	90	0.033	99.83	Pass
	5	40	0.12	90	0.021	99.99	Pass
RAP-2	4	20	0.12	90	0.01	99.99	Pass
	5	40	0.12	90	0.032	99.87	Pass
RAP-3	4	20	0.12	90	0.025	99.97	Pass
	5	40	0.12	90	0.025	99.97	Pass
RAP-4	4	20	0.12	90	0.04	99.48	Pass
	5	40	0.12	90	0.03	99.92	Pass

It is to be pointed out that the MEPDG model is semi-empirical in nature. The predicted pavement performance is based in part on the performance data of past pavements of similar characteristic. Since there have not been performance data on pavements made with concrete

containing RAP, the reliability of the predicted performance is questionable. The analysis was run just to see what the MEPDG model would predict based on the input concrete properties.

Tables 7-7 and 7-8 show the predicted international roughness index (IRI) and mean joint faulting at the end of 25-year life. The IRI defines the characteristic of the longitudinal profile of a traveled wheel track and provides a measure of roughness of the pavement. All the concrete pavements evaluated, which uses concrete with different amounts of RAP pass the IRI criterion with a high level of reliability and a very low level of distress. All the concrete pavements evaluated pass the performance criteria for mean joint faulting. The prediction on transverse cracking is highly sensitive to the coefficient of thermal expansion and concrete strength. For almost all the pavements using concrete mixtures with RAP, the predicted transverse cracking was very high, except for the concrete mixtures with 40% RAP-1 and 40% RAP-4 as shown in Table 7-9. For concrete mixtures with 70% and 100% RAP the measured strength was lower than the minimum strength recommended by the MEPFG program. Therefore, for concrete mixtures with 70% and 100% RAP, the MEPDG analysis was not performed.

Table 7-9. Predicted terminal transverse cracking from MEPDG analysis of pavement using concrete containing RAP

Mix Type	No	RAP (%)	Distress Target	Reliability Target	Distress Predicted	Reliability Predicted	Acceptable
Control	2	0	10	90	0.7	97.7	Pass
	4	20	10	90	49.9	0.04	Fail
RAP-1	5	40	10	90	0.8	97.23	Pass
	4	20	10	90	14.2	31.04	Fail
RAP-2	5	40	10	90	27.6	3.89	Fail
	4	20	10	90	18.6	17.03	Fail
RAP-3	5	40	10	90	32.8	1.49	Fail
	4	20	10	90	14.3	53.32	Fail
RAP-4	5	40	10	90	5.3	92.77	Pass

## 7.4 Analysis of Ultimate Load to Cause Failure of Pavement Slab

The concrete containing RAP has been shown to have much higher failure strain and toughness than the control concrete with no RAP. However, the behavior of the concrete beyond its elastic limit was not considered in the analysis using the FEACONS model, which analyzes the behavior of the concrete only within its elastic range. How does the increased failure strain of these more ductile concrete affect the maximum load the concrete pavement slab can take before failure? The analysis described in this section addresses this question.

### 7.4.1 Finite Element Model

A 15-ft. long by 12-ft. wide by 12-in. thick concrete slab was modeled using the ADINA software. The slab is supported by the springs which represent the Winkler foundation beneath the slab as shown in Figure 7-3.

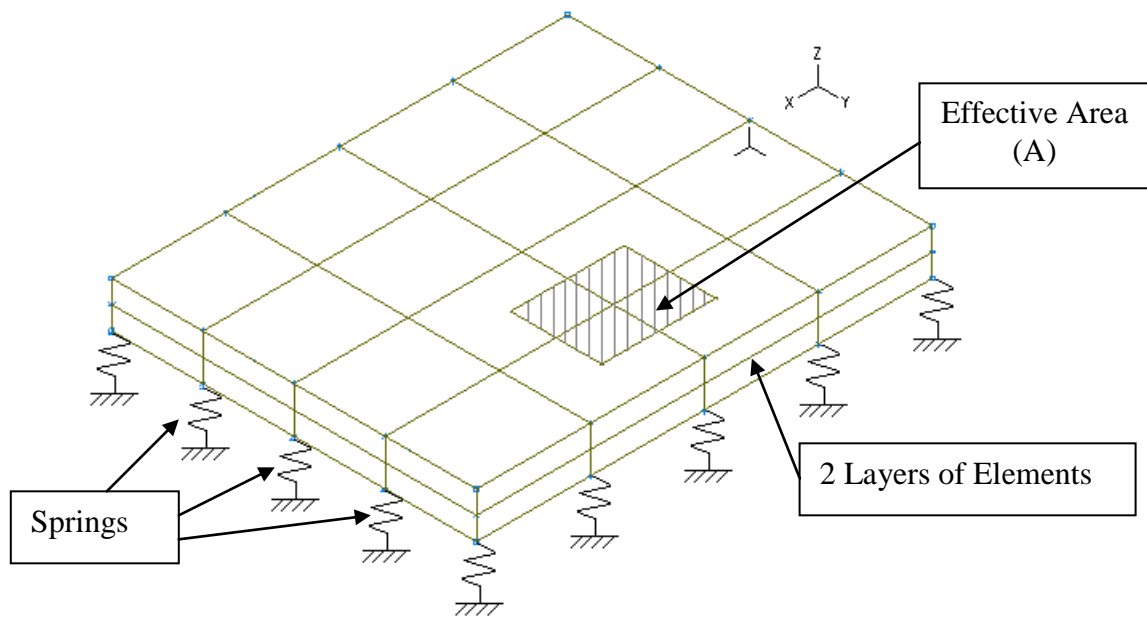


Figure 7-3. Modeling of slab on spring foundation

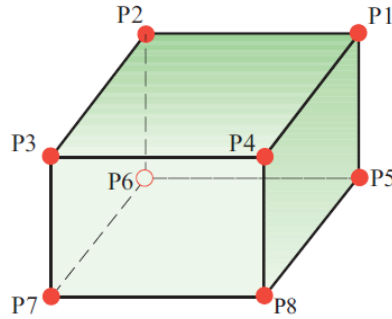


Figure 7-4. Eight-node isoparametric brick element

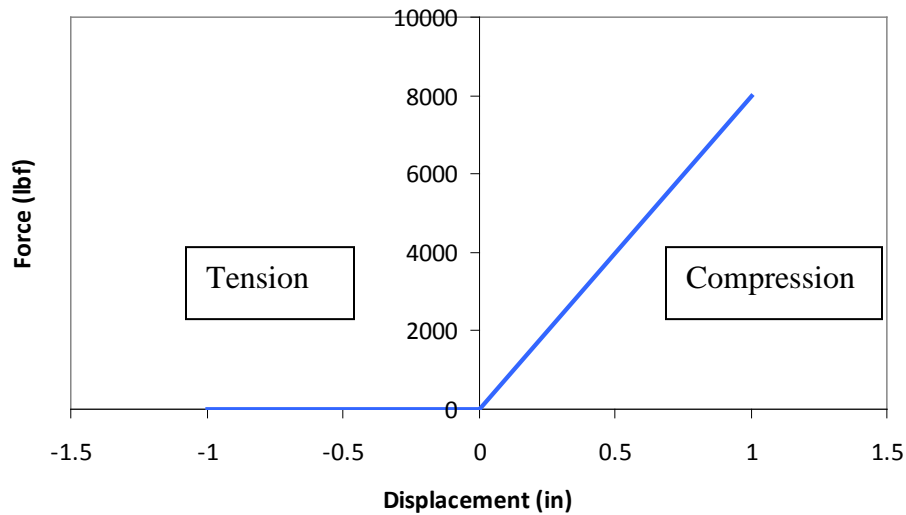


Figure 7-5. Force-displacement relationship of the springs

The concrete slab was modeled using 3-dimensional eight-node isoparametric brick elements that have 3 degrees of freedom (x-translation, y-translation and z-translation) as illustrated in Figure 7-4. The finite element mesh consists of 36 divisions in slab length, 36 divisions in slab width, and 2 divisions in slab thickness. The springs were modeled as nonlinear springs that simulate the contact between the slab and the foundation (to ensure the slab is out of contact with the springs when it is lifted). The force-displacement relationship of the springs is illustrated in Figure 7-5. The compressive stiffness of each spring is 8,000 lbf/in, which was

calculated from the modulus of subgrade reaction ( $k_s$ ) and the effective area ( $A$ ) supported by each spring as given by the following equation:

$$K = k_s \times A \quad (7-1)$$

where:  $K$  = spring compressive stiffness, lbf/in,

$$k_s = 0.4 \text{ kci},$$

$$A = 5 \times 4 = 20 \text{ in}^2.$$

### 7.4.2 Modeling of Critical Loading Condition

The critical loading condition considered in this analysis consisted of slab weight, a positive temperature differential of 20 °F and a single axle load of different weights placed at mid-edge of the slab as shown in Figure 7-6. The single axle load consisted of two equal-weight tires which were 6 feet apart from each other. Additionally, each tire had a tire contact area of 80 in<sup>2</sup> (10 in. x 8 in.).

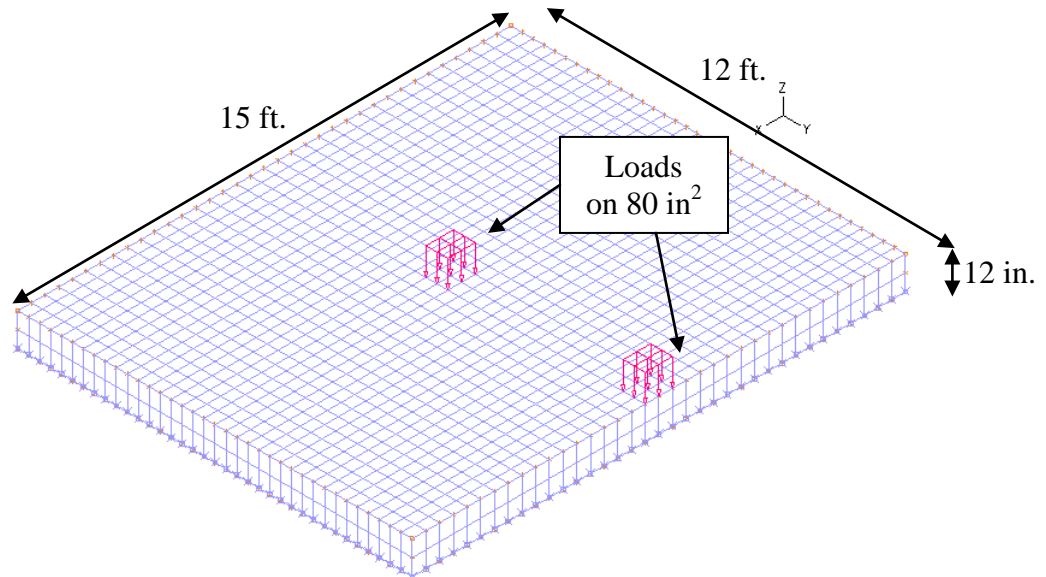


Figure 7-6. Single axle load of equal-weight tires placed at the mid-edge of slab

### 7.4.3 Modeling of Stress-Strain Behavior of Concrete Material

To evaluate the more realistic behavior of concrete slabs containing RAP, a concrete model was developed in ADINA using the stress-strain relationship of the concrete. The stress-strain diagrams were obtained from the Flexural Strength Test on the concrete specimens containing RAP. These stress-strain diagrams have been presented in Section 6.35 of Chapter 6. A few examples of such stress-strain diagrams are shown in Figure 7-7.

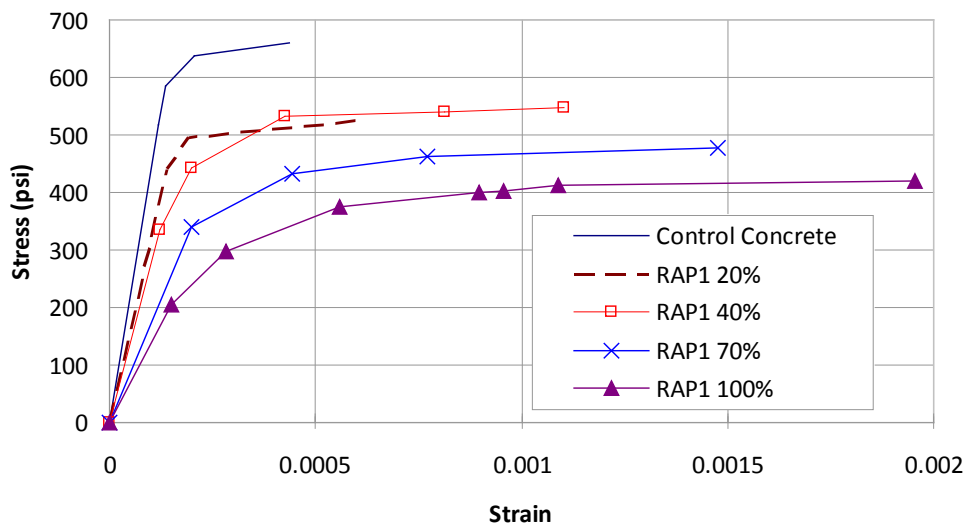


Figure 7-7. Examples of stress-strain diagrams of concrete containing RAP

### 7.4.4 Analysis to Determine Failure Load of Pavement Slab Containing RAP

Using the developed ADINA model, analysis was performed to determine the maximum axle load the modeled slab can take before failure would occur. For each of the concrete considered, the load contact area was kept constant during the analysis process while the applied load was increased incrementally in magnitude until concrete failure.

Table 7-10. Failure Loading Pressure and Toughness of Concrete Containing RAP

Type	% RAP	Specimen	Failure Loading Pressure (psi)	Failure Axle Load (kip)	Toughness (lbf/in <sup>2</sup> )
Control			412.7	66.0	0.232608
RAP-1	20%		340	54.4	0.270587
	40%		490	78.4	0.526082
	70%		520	83.2	0.60596
	100%		510	81.6	0.71039
RAP-2	20%	1	498	79.7	0.295282
		2	409	65.4	0.241027
		3	390	62.4	0.307008
	40%	1	360	57.6	0.310192
		2	460	73.6	0.437577
		3	382	61.1	0.379371
	70%	1	382	61.1	0.379371
		2	432	69.1	0.588726
		3	330	52.8	0.289279
	100%	1	441	70.6	0.644196
2		-	-	-	
3		-	-	-	
RAP-3	20%	1	448	71.7	0.338919
		2	-	-	-
		3	437	69.9	0.287694
	40%	1	387	61.9	0.339771
		2	434	69.4	0.492375
		3	413	66.1	0.267685
	70%	1	425	68.0	0.452963
		2	398	63.7	0.412595
		3	391	62.6	0.567601
	100%	1	437	69.9	0.556885
2		400	64.0	0.395378	
3		-	-	-	
RAP-4	20%	1	420	67.2	0.242803
		2	416	66.6	0.170548
		3	-	-	-
	40%	1	383	61.3	0.266251
		2	-	-	-
		3	460	73.6	0.348185
	70%	1	393	62.9	0.304576
		2	430	68.8	0.448006
		3	383	61.3	0.296464
	100%	1	408	65.3	0.52535
2		450	72.0	0.634419	
3		520	83.2	0.61745	

Table 7-10 shows the failure loading pressures and axle loads for the concrete slab using various different concrete containing RAP. The corresponding toughnesses of the concrete are also shown in the table. The numbers in red indicate the cases where the slab using the RAP concrete can carry more load than the slab using the control concrete. Among the 33 RAP concretes evaluated, 19 of them gave higher failure load while 14 of them gave lower failure load than the control concrete.

Figure 7-8 shows the plot of failure axle load vs. toughness of the concrete containing RAP. It can be seen that there is a positive correlation between the failure load and the toughness of the concrete. Using a concrete with a higher toughness will tend to give a higher loading capacity to the concrete slab.

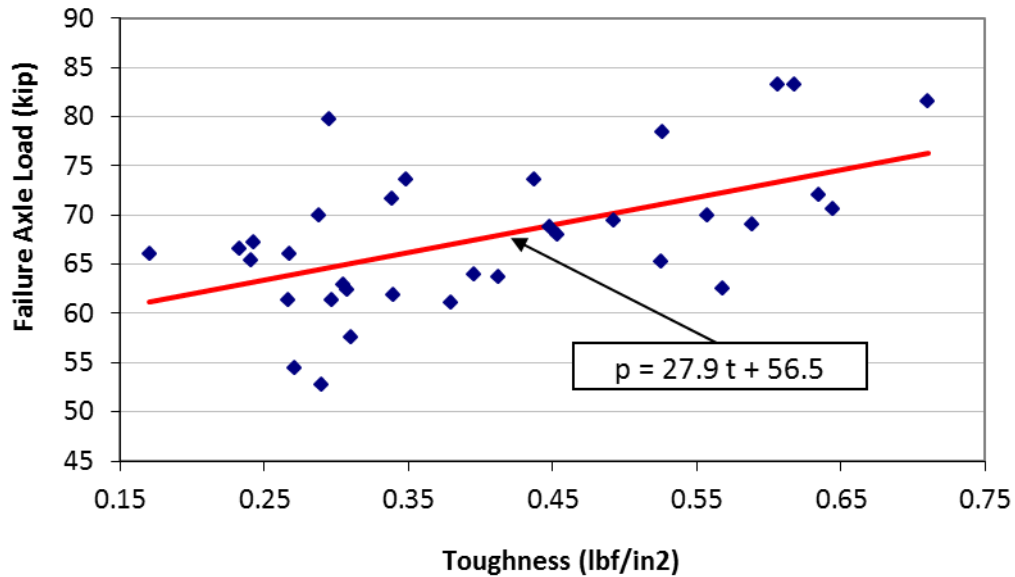


Figure 7-8. Failure loading pressure vs. toughness

## 7.5 Summary of Findings

The results of critical stress analysis using FEACONS show that the maximum stress in a typical concrete pavement slab decreases as the percentage of RAP increases in the mix, due to decrease in the elastic modulus of the concrete. Although the flexural strength of the concrete containing RAP was lower than that of the conventional concrete. The maximum stress to flexural strength ratio for concrete mixtures containing RAP was generally comparable to that of the conventional mix. This indicates that concrete containing RAP will potentially have comparable performance as that of a conventional concrete when used in pavement slabs.

The results of MEPDG analysis on the potential performance of typical concrete pavements in Florida using concrete containing RAP indicate that these type of pavement will have acceptable IRI and joint faulting, but relatively high predicted transverse cracking. Since the MEPDG is a semi-empirical model which is based on the historical performance data, the predicted performance of concrete containing RAP is questionable, due to the lack of past performance data on these special concrete pavement.

The results of analysis of failure load of concrete pavement slab using ADINA show that, on the average, the pavement slabs using RAP concrete have higher failure load than the slab using the control concrete. Using a concrete with a higher toughness will tend to give a higher loading capacity to the concrete slab.

## CHAPTER 8 DEVELOPMENT OF CRITERIA FOR RAP CONCRETE

### 8.1 Development of Stress-Strength Ratio Charts

The modulus of elasticity, flexural strength, and coefficient of thermal expansion for concrete mixtures containing RAP ranged from  $1 \times 10^6$  psi to  $4 \times 10^6$  psi, 300 psi to 650 psi, and  $4.5 \times 10^{-6}/^{\circ}\text{F}$  to  $6.5 \times 10^{-6}/^{\circ}\text{F}$ , respectively. Critical stress analysis was performed on typical concrete pavement slabs using concrete with different combinations of coefficient of thermal expansion, modulus of elasticity, and flexural strength within these ranges.

The maximum stress in concrete caused by a 22-kip axial load applied to the center edge of a 12-inch slab with a temperature differential of  $20^{\circ}\text{F}$  was calculated using the FEACONS program. The maximum stress to flexural strength ratios were calculated and presented in Tables 8-1 through 8-4. Using these values, the stress-strength ratio charts were developed as shown in Figures 8-1 through 8-4. Two lines showing the combination of flexural strength and elastic modulus of concrete that would produce a stress to strength ratio of 0.5 and 0.6 are plotted on these figures for different values of coefficient of thermal expansion.

Figures 8-1 through 8-4 can be used for concrete mixtures with CTE ranging from  $4.25 \times 10^{-6}/^{\circ}\text{F}$  to  $4.75 \times 10^{-6}/^{\circ}\text{F}$ ,  $4.75 \times 10^{-6}/^{\circ}\text{F}$  to  $5.25 \times 10^{-6}/^{\circ}\text{F}$ ,  $5.25 \times 10^{-6}/^{\circ}\text{F}$  to  $5.75 \times 10^{-6}/^{\circ}\text{F}$ , and  $5.75 \times 10^{-6}/^{\circ}\text{F}$  to  $6.25 \times 10^{-6}/^{\circ}\text{F}$ , respectively. The results of critical stress analysis for all the concrete mixtures evaluated at 90 days curing time are plotted on these charts. This chart can be used to predict the performance of concrete mixtures containing RAP by knowing the flexural strength, elastic modulus and coefficient of thermal expansion of concrete.

Figure 8-1 shows the stress-strength chart for concrete mixtures with a coefficient of thermal expansion of  $4.5 \times 10^{-6}/^{\circ}\text{F}$ . According to the chart, concrete mixtures with 40%, 70%, and 100% RAP gave a lower stress-strength ratio than the conventional mix. Though the

coefficient of thermal expansion increases as the percentage of RAP increases, the stress-strength ratio for concrete containing RAP is still lower due to the reduction in elastic modulus of the concrete as shown in Figures 8-2 through 8-4. This shows that there is a potential for the improvement in the performance of concrete pavement containing RAP. According to this analysis, the optimal concrete mixture for concrete pavement is not necessarily a concrete with a high flexural strength but a concrete with a proper combination of low modulus of elasticity, low coefficient of thermal expansion, and adequate flexural strength. The following steps must be followed to use the stress-strength ratio charts to determine an optimum concrete mix containing RAP for concrete pavement slabs:

- Determine the modulus of elasticity, flexural strength, and coefficient of thermal expansion of concrete mixtures containing RAP using the ASTM and AASHTO standards.
- Using the measured coefficient of thermal expansion, determine the appropriate stress-strength ratio chart or table to use. For example, for the concrete mixtures with CTE ranging from  $4.25 \times 10^{-6}/^{\circ}\text{F}$  to  $4.75 \times 10^{-6}/^{\circ}\text{F}$ , use the stress-strength ratio chart or the table with a CTE of  $4.5 \times 10^{-6}/^{\circ}\text{F}$ .
- From the appropriate stress-strength ratio chart or table, determine the stress-strength ratio for the particular concrete mix by interpolation using its measured modulus of elasticity, flexural strength, and coefficient of thermal expansion.
- The concrete mix with the lowest stress-strength ratio should give the best potential performance as a pavement concrete.

Table 8-1. Stress analysis for concrete mixtures with a coefficient of thermal expansion of  $4.5 \times 10^{-6}/^{\circ}\text{F}$

MR (psi)	300	400	500	600	700
E (ksi)	Coefficient of Thermal Expansion= $4.5 \times 10^{-6}/^{\circ}\text{F}$				
	Stress to Strength Ratio				
1000	0.51	0.38	0.30	0.25	0.22
2000	0.75	0.56	0.45	0.37	0.32
3000	0.94	0.71	0.56	0.47	0.40
4000	1.10	0.82	0.66	0.55	0.47
5000	1.23	0.92	0.74	0.62	0.53

Table 8-2. Stress analysis for concrete mixtures with a coefficient of thermal expansion of  $5.0 \times 10^{-6}/^{\circ}\text{F}$

MR (psi)	300	400	500	600	700
E (ksi)	Coefficient of Thermal Expansion= $5.0 \times 10^{-6}/^{\circ}\text{F}$				
	Stress to Strength Ratio				
1000	0.53	0.40	0.32	0.26	0.23
2000	0.78	0.59	0.47	0.39	0.33
3000	0.99	0.74	0.59	0.50	0.42
4000	1.16	0.87	0.69	0.58	0.50
5000	1.30	0.98	0.78	0.65	0.56

Table 8-3. Stress analysis for concrete mixtures with a coefficient of thermal expansion of  $5.5 \times 10^{-6}/^{\circ}\text{F}$

MR (psi)	300	400	500	600	700
E (ksi)	Coefficient of Thermal Expansion= $5.5 \times 10^{-6}/^{\circ}\text{F}$				
	Stress to Strength Ratio				
1000	0.54	0.40	0.32	0.27	0.23
2000	0.81	0.61	0.49	0.40	0.35
3000	1.03	0.77	0.62	0.51	0.44
4000	1.21	0.91	0.73	0.60	0.52
5000	1.37	1.03	0.82	0.68	0.58

Table 8-4. Stress analysis for concrete mixtures with a coefficient of thermal expansion of  $6.0 \times 10^{-6}/^{\circ}\text{F}$

MR (psi)	300	400	500	600	700
E (ksi)	Coefficient of Thermal Expansion= $6.0 \times 10^{-6}/^{\circ}\text{F}$				
	Stress to Strength Ratio				
1000	0.56	0.42	0.34	0.28	0.24
2000	0.85	0.64	0.51	0.43	0.37
3000	1.08	0.81	0.65	0.54	0.46
4000	1.28	0.96	0.77	0.64	0.55
5000	1.44	1.08	0.87	0.72	0.62

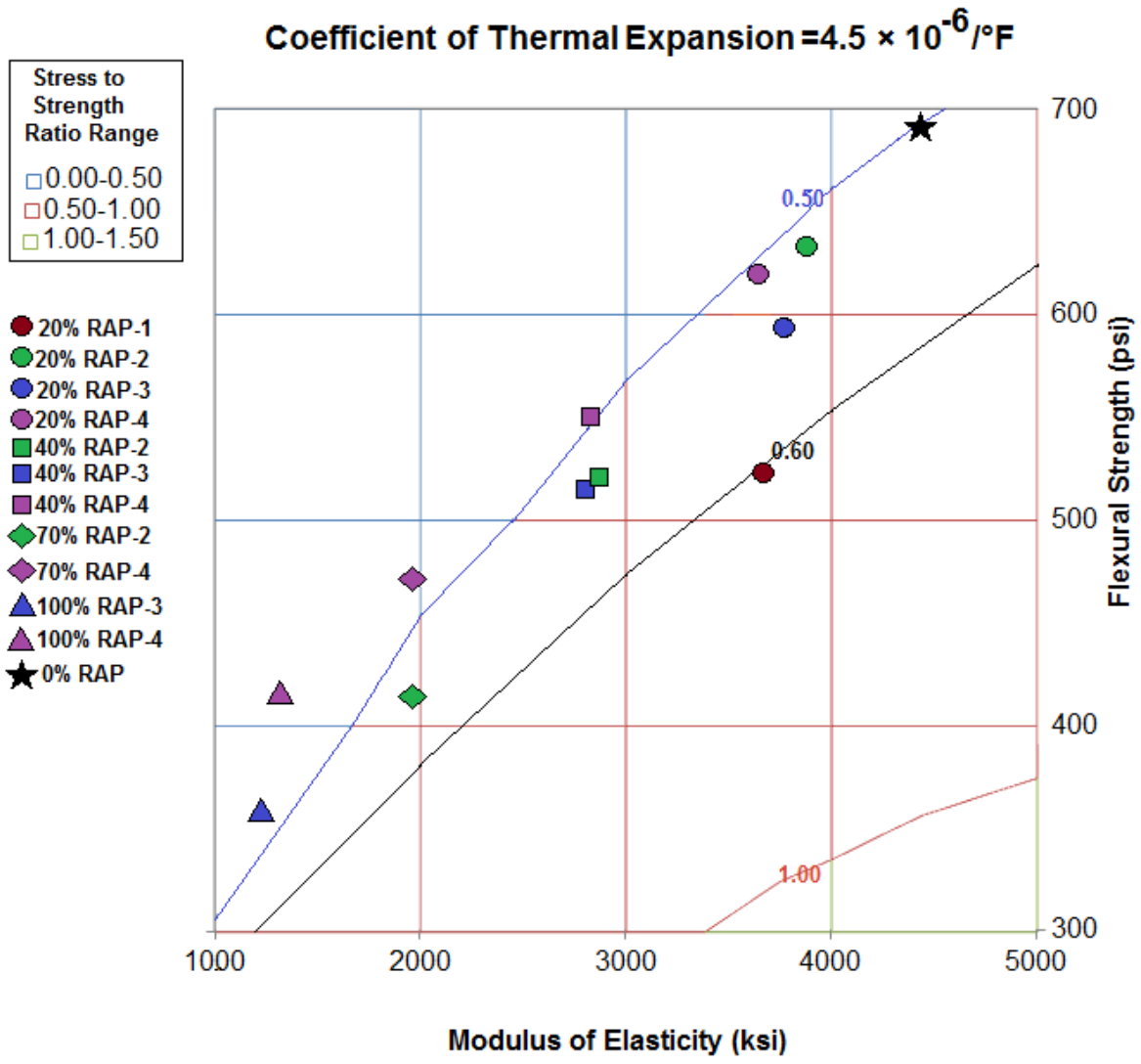


Figure 8-1. Stress-strength ratio chart for concrete with a CTE of  $4.5 \times 10^{-6}/^{\circ}\text{F}$

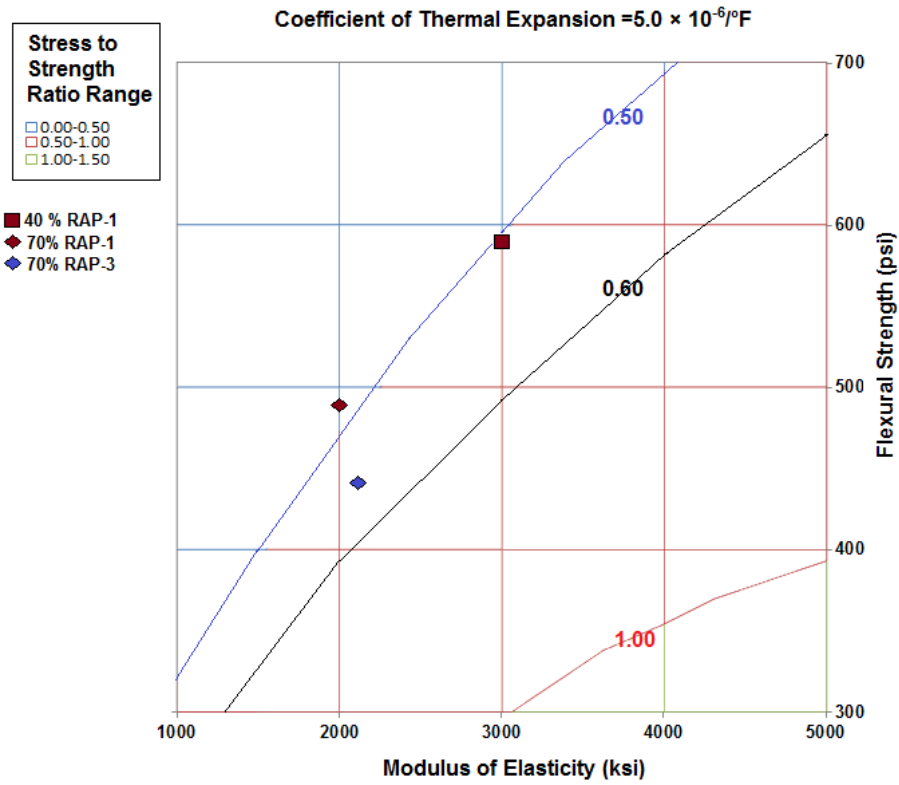


Figure 8-2. Stress-strength ratio chart for concrete with a CTE of  $5.0 \times 10^{-6}/^{\circ}\text{F}$

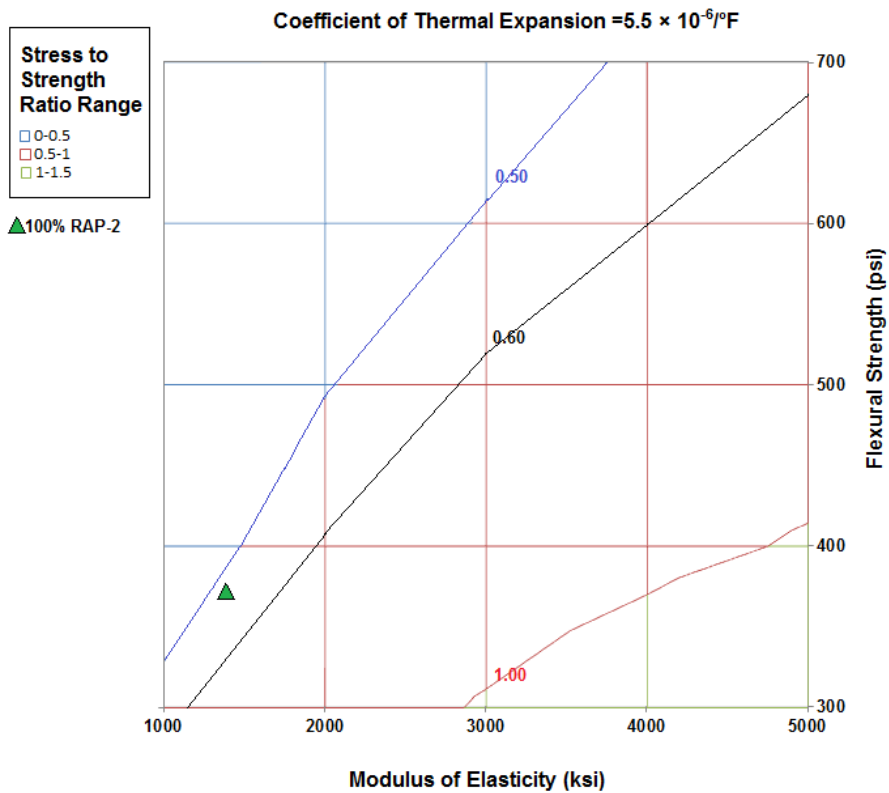


Figure 8-3. Stress-strength ratio chart for concrete with a CTE of  $5.5 \times 10^{-6}/^{\circ}\text{F}$

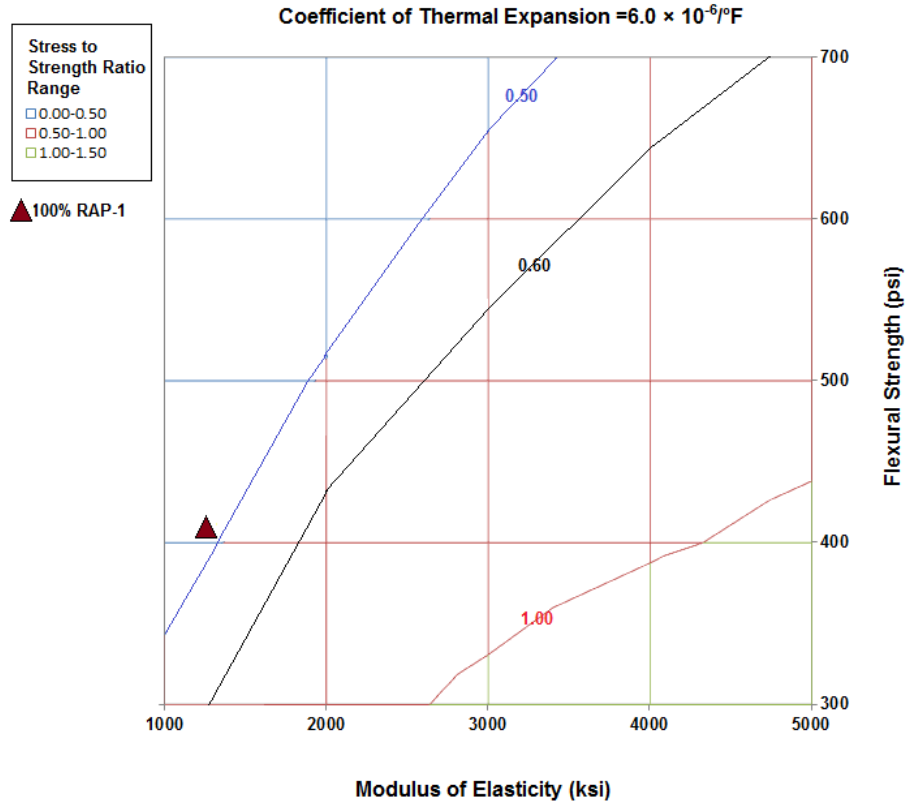


Figure 8-4. Stress-strength ratio chart for concrete with a CTE of  $6.0 \times 10^{-6}/^{\circ}\text{F}$

## **CHAPTER 9 SUMMARY OF FINDINGS, CONCLUSIONS AND RECOMMENDATIONS**

### **9.1 Findings from This Study**

#### **9.1.1 Mechanical and Thermal Properties of Concrete Containing RAP**

From the results of the laboratory testing program in this study, the compressive strength, modulus of elasticity, splitting tensile strength and flexural strength of the concrete containing RAP were observed to decrease as the percentage of RAP increased in the mix. With the incorporation of RAP in concrete, the reduction in flexural strength was 10% to 20% lower than the corresponding reduction in compressive strength. The percent reduction in modulus of elasticity of the concrete with the incorporation of RAP was much higher than the corresponding reduction in compressive strength. The failure strain and toughness of concrete increased as the percentage of RAP increased in the mix. The Poisson's ratio, drying shrinkage, and coefficient of thermal expansion increased slightly as the percentage of RAP increased in the mix. The commonly used ACI equations which relate compressive strength to the flexural strength and modulus of elasticity of concrete would underestimate the flexural strength and overestimate the elastic modulus of the concrete containing RAP. Based on the data obtained in this study, regression equations relating compressive strength to flexural strength and elastic modulus of concrete containing RAP were developed.

#### **9.1.2 Combined Aggregate Gradation of Concrete Containing RAP**

The addition of RAP to concrete mixture can improve the combined aggregate gradation of the mix. The intermediate size particles increased as the percentage of RAP increased in the mix. The control mix used in this study, which was a typical pavement concrete used in Florida and used a #57 stone and a fine silica sand, had a lack of particles retained on the #8 and #16 sieves. The mixtures with 40% RAP replacement showed improvement in gradation towards a well-

graded aggregate blend. For the concrete mixtures with 70% and 100% RAP, the amount of intermediate size particles increased, but there was a lack of very fine aggregate making the concrete mixtures difficult to mix.

### **9.1.3 Stress Analysis of Concrete Containing RAP**

The results of critical stress analysis show that the maximum stresses in pavement decreases as the RAP content of the mix increases, due to decrease in the elastic modulus of the concrete. Though the flexural strength of the concrete with RAP was lower than that of the conventional concrete, the computed stress to strength ratio for some of the RAP concrete was lower than that for the conventional concrete. The results of analysis of ultimate failure load of concrete pavement slab show that, on the average, the pavement slabs using RAP concrete have higher failure load than the slab using the control concrete. This indicates that RAP concrete can have potentially better performance than a conventional concrete when used in concrete pavement slabs.

Stress-strength ratio tables and charts were developed for convenient determination of stress-strength ratios for different RAP concrete mixes with different combinations of flexural strength, elastic modulus and coefficient of thermal expansion. The optimum concrete mix to be adopted for concrete pavement application is the mix with lowest stress-strength ratio.

## **9.2 Conclusions and Recommendations**

The results of the laboratory testing program and finite element analysis indicate that the use of RAP as aggregate replacement in pavement concrete appears to be not only feasible but also offers the possibility of improving the performance of concrete pavement.

Recommended mix design procedure for concrete containing RAP is as follows:

- Proportion the RAP and virgin aggregates to be used to achieve the maximum density for the combined aggregate gradation of the concrete mixtures.

- Evaluate the flexural strength, modulus of elasticity, and coefficient of thermal expansion for concrete mixtures using the ASTM and AASHTO standards.
- Perform critical stress analysis as discussed in the Section 7-2 of Chapter 7. Determine the maximum critical stress and the stress to strength ratio for each concrete mix. In absence of the critical stress analysis, use the charts or tables as presented in Chapter 8 for estimation of stress-strength ratio. Optimum mix is the one with the lowest stress to strength ratio.

Since the findings from this research have been based mainly on the results of laboratory study and theoretical finite element analysis, the actual performance of concrete containing RAP needs to be validated by field testing. It is recommended that the following field testing program be conducted:

(1) Construct a concrete pavement test section with a minimum length of 180 feet within an existing highway with medium traffic. This test section will have a minimum of twelve 15-ft slabs.

(2) Use a minimum of four different concrete mixes containing different %RAP. The recommended percentages of RAP to be used are 0, 20, 40 and 70%. These four concrete mixes are to be designed to achieve the optimum stress to strength ratio from critical stress analysis using the material properties measured from the trial mixes.

(3) Construct three replicate slabs for each mix design. There will be a minimum of 12 test slabs for the four mix designs to be used.

(4) Install temperature data loggers at different depths in the concrete slabs to monitor the temperature variation within the slabs. The temperature differentials within the test slabs as measured by these temperature data loggers can be used to perform critical stress analysis to determine the maximum temperature-load induced stresses in these test slabs.

(5) Install weigh-in motion equipment on the test road to monitor traffic.

(6) Conduct periodic condition survey on these test slabs to evaluate their performance.

## REFERENCES

- Abrams, D.A., 1918, "Design of Concrete Mixtures," Structural Materials Research Laboratory, Bulletin No.1, pp. 1-22.
- ACI 302.1R-04, Guide for Concrete Floor and Slab Construction.
- Al-Oraimi, S., Hassan, H.F. and Hago, A., 2009, "Recycling of Reclaimed Asphalt Pavement in Portland Cement Concrete," The Journal of Engineering Research, Vol. 6(1), pp. 37-45.
- Bermel, B.N., 2011, "Feasibility of Reclaimed Asphalt Pavement as Aggregate in Portland Cement Concrete Pavement," Master of Science Thesis, Montana State University, Bozeman, Montana, pp. 195.
- Collins, R.J. and Ciesielski, S.K., 1994, "Recycling and Use of Waste Materials and By-Products in Highway Construction, NCHRP Synthesis of Highway Practice, No.199, Transportation Research Board, Washington, DC, USA, pp. 92.
- Crammer, S.M., Hall, M. and Parry, J., 1995, "Effect of Optimized Total Aggregate Gradation on Portland Cement Concrete for Wisconsin Pavements," Transportation Research Board, Record No.1478, pp. 100-106.
- Crammer, S.M., and Carpenter, A.J., 1999, "Influence of Total Aggregate Gradation on Freeze-Thaw and Other Performance Measures of Paving Concrete, Transportation Research Board, Record No. 1668, pp. 1-8.
- Delwar, M., Fahmy, M. and Taha, R., 1997, "Use of Reclaimed Asphalt Pavement as an Aggregate in Portland Cement Concrete," ACI Materials Journal, Vol. 94(3), pp. 251-256.
- Dumitru, I., Smorchevsky, G. and Caprar, V., 1999, "Trends in the Utilization of Recycled Materials and By-Products in Concrete Industry in Australia," Concrete 99, Our Concrete Environment, Sydney, Australia, pp. 289-301.
- Edwards, L., 1918, "Proportioning of Mortars and Concretes by Surface Area of Aggregate," ASTM Proceedings, Vol. 18(2), pp. 235.
- Fuller, W.B. and Thompson, S.E., 1907, "The Laws of Proportioning Concrete" ASCE Journal, Vol. LVII (2), pp. 67-113.
- Griffiths, C.T. and Krstulovich, J.M., 2002, "Utilization of Recycled Materials in Illinois Highway Construction, Research Report No.142, Illinois Department of Transportation.
- Hassan, K.E., Brooks, J.J. and Erdman, M., 2000, "The Use of Reclaimed Asphalt Pavement (RAP) Aggregates in Concrete," Waste Materials in Construction, Waste Management Series, Elsevier Science, Oxford, Vol. 1, pp. 121-128.

- Huang, B., Shu, X. and Li, G., 2005, "Laboratory Investigation of Portland Cement Concrete Containing Recycled Asphalt Pavements," *Cement and Concrete Research*, Vol. 35(10), pp. 2008-2013.
- Huang, B., Shu, X. and Burdette, E.G., 2006, "Mechanical Properties of Concrete Containing Recycled Asphalt Pavements," *Magazine of Concrete Research*, Vol. 58(5), pp. 313-320.
- Iowa Department of Transportation, 2005, "Aggregate Proportioning Guide for Plain Cement Concrete Pavement.
- Kang, D.H., Gupta, S.C., Ranaivoson, A.Z., 2011, "Recycled Materials as Substitutes for Virgin Aggregates in Road Construction: I – Hydraulic and Mechanical Characteristics, *Soil Science Society of America*, Vol. 75(4), pp. 1265-1275.
- Katsakou, M. and Koliass, S., 2007, "Mechanical Properties of Cement-Bound Recycled Pavements," *Proceeding of the Institution of Civil Engineers-Construction Materials*, Vol. 160(4), pp. 171-179.
- Kim, D.H. and Won, M., 2008, "Pilot Implementation of Optimized Aggregate Gradation for Concrete Paving," Report No. FHWA/TX-09/5-9026-01-1, Texas Department of Transportation, Texas.
- Koehler, E.P. and Fowler, D.W., 2007, "Aggregate in Self-Consolidating Concrete," International Center for Aggregate, Research Report No. 108-2F, Austin, Texas.
- Koehler, E.P. and Fowler, D.W., 2007, "Selecting Aggregates for Self-Consolidating Concrete," The University of Texas at Austin, Austin, Texas, USA.
- Koliass, S., 1996, "Mechanical Properties of Cement-Treated Mixtures of Milled Bituminous Concrete and Crushed Aggregates," *Materials and Structures*, Vol. 29. pp. 411-417.
- Koliass, S., 1996, "The Influence of the Type of Loading and Temperature on the Modulus of Elasticity of Cement-Bound Mixes of Milled Bituminous Concrete and Crushed Aggregate," *Materials and Structures*, Vol. 29, pp. 543-551.
- Lafrenz, J.L., "Aggregate Gradation Control for Plain Cement Concrete Pavements," U.S., Air Force, HQ Air Force Civil Engineering, Support Agency, Tyndall AFB, Florida, USA.
- Li, G., Zhao, Y., Pang, S.S. and Huang, W., 1998, "Experimental Study of Cement-Asphalt Emulsion Composite," *Cement and Concrete Research*, Vol. 28(5), pp. 635-641.
- Mathias, V., Sedran, T. and De Larrard, F., 2004, "Recycling Reclaimed Asphalt Pavement in Concrete Roads," International RILEM Conference on the Use of Recycled Materials in Buildings and Structures, Barcelona, Spain, pp. 10.
- Mathias, V., Sedran, T. and De Larrard, F., 2009, "Modeling of Mechanical Properties of Cement Concrete Incorporating Reclaimed Asphalt Pavement," *Road Materials and Pavement Design*, Vol. 10(1), pp. 63-82.

- Okafor, F.O., 2010, "Performance of Recycled Asphalt Pavement as Coarse Aggregate in Concrete," Leonardo Electronic Journal of Practices and Technologies, 17, pp. 47-58.
- Patankar, V.D. and Williams, R.I.T., 1970, "Bitumen in Dry Lean Concrete," Highways and Traffic Engineering, Vol. 38(1721), pp. 32-35.
- Ping, W.V. and Kampmann, R., 2008, "Engineering Properties of Florida Concrete Mixes for Implementing the AASHTO Recommended Mechanistic-Empirical Rigid Pavement Design Guide," FDOT Research Report No. BD-543-14, Tallahassee, Florida, USA.
- Richardson, D.N., 2005. "Aggregate Gradation Optimization-Literature Research," Report No. RDT 05-001, University of Missouri-Rolla, Missouri, USA.
- Shilstone, J.H., 1990, "Concrete Mixture Optimization, ACI Concrete International, Vol. 12(6), pp. 33-39
- Shilstone, J.M., "The Aggregate: The Most Important Value-Adding Component in Concrete," The Shilstone Companies Inc., Dallas, Texas.
- Sommer, H., 1994, "Recycling of Concrete for the Reconstruction of the Concrete Pavement of the Motorway Vienna-Salzburg," 7<sup>th</sup> International Concrete Roads Symposium, Vienna, Austria, pp. 5.
- Tailbot, A.N. and Richart, F.E., 1923, "The Strength of Concrete," Bulletin No.137, Engineering Experiment Station, University of Illinois, Urbana.
- Tayabji, S. and Anderson, J., 2007, "Supplemental Report for Proposed Specification for Construction of Concrete Airfield Pavements," Innovative Pavement Research Foundation, Report IPRF-01-6-002-04-1a, pp. 92.
- Tia, M., Wu, C.L., Ruth, B.E., Bloomquist, D. and Choubane, B., 1989, "Field Evaluation of Rigid Pavement Design System-Phase IV, Research Report No. 4910450424912, Department of Civil Engineering, University of Florida, Gainesville, Florida, USA.
- Tia, M., Bloomquist, D., Alungbe, G.D. and Richardson, D., 1991, "Coefficient of Thermal Expansion of Concrete Used in Florida," Research Report No. 4910450422912, Department of Civil Engineering, University of Florida, Gainesville, Florida, USA.
- Tompkins, D., Khazanovich, L., Darter, M.I. and Walter, F., 2009, "Design and Construction of Sustainable Pavements," Transportation Research Board, Record No. 2098, pp. 75-85.
- Topcu, I.B. and Isikdag, B., 2009, "Effects of Crushed RAP on Free and Restrained Shrinkage of Mortars," International Journal of Concrete Structures and Materials, Vol. 3(2), pp. 91-95.
- Weymouth, C.A.G., 1933, "Effect of Particle Interface in Mortars and Concrete, Rock Products, pp. 26.

Weymouth, C.A.G., 1938, "A Study of Fine Aggregate in Freshly Mixed Mortars and Concretes," ASTM Proceedings, Vol. 38(2), pp. 354.

Young, R.B., 1919, "Some Theoretical Studies on Proportioning Concrete by the Method of Surface Area of Aggregate," ASTM Proceedings, Vol. 19(2), pp. 444.

**APPENDIX A**  
**STRENGTH TEST DATA**

Table A-1. Compressive strength test results for concrete containing no RAP

Specimen Number	W/C	RAP (%)	Curing Period (days)	Average Length (in)	Average Diameter (in)	Failure Load (lbs)	Compressive Strength (psi)
1	0.45	0	7	7.6630	4.0080	71660	5680
2	0.45	0	7	7.6538	4.0155	71130	5617
3	0.45	0	7	7.8473	4.0125	69650	5508
4	0.45	0	7	7.6026	4.0111	74240	5875
5	0.45	0	7	7.8166	4.0108	71560	5664
6	0.45	0	7	7.7812	4.0231	69300	5452
1	0.45	0	14	7.6422	4.0086	81360	6447
2	0.45	0	14	7.7405	3.9846	76730	6153
3	0.45	0	14	7.8096	4.0240	74990	5897
4	0.45	0	14	7.6963	4.0115	78590	6218
5	0.45	0	14	7.7783	4.0150	73630	5816
6	0.45	0	14	7.7297	4.0135	75890	5999
1	0.45	0	28	7.6057	4.0045	84510	6710
2	0.45	0	28	7.6756	4.0115	84100	6654
3	0.45	0	28	7.7182	4.0173	82400	6501
4	0.45	0	28	7.6830	4.0068	77900	6178
5	0.45	0	28	7.7606	4.0108	83600	6617
6	0.45	0	28	7.6452	4.0275	80650	6331
1	0.45	0	90	7.6885	4.0183	85910	6774
2	0.45	0	90	7.7500	4.0135	92020	7274
3	0.45	0	90	7.6964	4.0172	89380	7052
4	0.45	0	90	7.6870	4.0120	88940	7035
5	0.45	0	90	7.7560	4.0075	91480	7253
6	0.45	0	90	7.6975	4.0265	88030	6913
1	0.50	0	7	7.6492	3.9933	55940	4467
2	0.50	0	7	7.6597	3.9932	54350	4340
3	0.50	0	7	7.6573	4.0073	51010	4044
4	0.50	0	7	7.6393	4.0015	55320	4399
5	0.50	0	7	7.6648	4.0228	51410	4045
6	0.50	0	7	7.7130	4.0130	53320	4216
1	0.50	0	14	7.6335	4.0100	56650	4486
2	0.50	0	14	7.8773	4.0155	63470	5012
3	0.50	0	14	7.6757	4.0162	56570	4465

Table A-1. (Continued)

Specimen Number	W/C	RAP (%)	Curing Period (days)	Average Length (in)	Average Diameter (in)	Failure Load (lbs)	Compressive Strength (psi)
4	0.50	0	14	7.6428	4.0117	63070	4990
1	0.50	0	28	7.5880	4.0120	67540	5343
2	0.50	0	28	7.5770	4.0026	66470	5283
3	0.50	0	28	7.5925	4.0203	69810	5499
4	0.50	0	28	7.5505	4.000	67100	5340
5	0.50	0	28	7.5642	4.0152	58640	4631
6	0.50	0	28	7.6168	4.0012	66650	5301
1	0.50	0	90	7.6915	4.0125	73060	5778
2	0.50	0	90	7.6305	4.0195	74230	5850
3	0.50	0	90	7.6538	4.0208	72960	5746
4	0.50	0	90	7.6690	3.9985	70840	5641
5	0.50	0	90	7.7050	4.0123	71770	5676
6	0.50	0	90	7.6870	4.0125	76110	6019
1	0.55	0	7	7.6275	4.0178	43140	3403
2	0.55	0	7	7.6585	4.0173	44890	3542
3	0.55	0	7	7.5850	4.0147	40480	3198
4	0.55	0	7	7.6377	4.0053	43270	3435
5	0.55	0	7	7.6358	4.0115	42590	3370
6	0.55	0	7	7.7165	3.9965	46470	3705
1	0.55	0	14	7.6975	4.0183	45520	3590
2	0.55	0	14	7.5708	4.0148	46830	3700
3	0.55	0	14	7.6547	4.0053	52670	4181
4	0.55	0	14	7.7012	4.0000	44210	3519
5	0.55	0	14	7.4673	4.0038	52470	4168
6	0.55	0	14	7.5933	4.0257	48600	3819
1	0.55	0	28	7.6247	4.0115	57240	4530
2	0.55	0	28	7.5697	3.9782	52930	4259
3	0.55	0	28	7.4713	4.0137	60750	4802
4	0.55	0	28	7.6156	3.9973	58500	4662
5	0.55	0	28	7.6055	3.9985	61620	4908
6	0.55	0	28	7.5830	4.0133	56150	4439
1	0.55	0	90	7.5625	4.0347	58510	4577
2	0.55	0	90	7.6063	4.0112	64120	5075

Table A-1. (Continued)

Specimen Number	W/C	RAP (%)	Curing Period (days)	Average Length (in)	Average Diameter (in)	Failure Load (lbs)	Compressive Strength (psi)
3	0.55	0	90	7.6493	4.0068	66770	5296
4	0.55	0	90	7.5625	4.0415	57200	4459
5	0.55	0	90	7.6063	4.0085	62150	4925
6	0.55	0	90	7.6493	4.0123	57710	4565

Table A-2. Compressive strength test results for concrete containing RAP-1

Specimen Number	W/C	RAP-1 (%)	Curing Period (days)	Average Length (in)	Average Diameter (in)	Failure Load (lbs)	Compressive Strength (psi)
1	0.50	20	7	7.6328	4.0030	34610	2750
2	0.50	20	7	7.6972	4.0400	36080	2815
3	0.50	20	7	7.9818	4.0450	36700	2856
4	0.50	20	7	7.6858	4.0098	37290	2953
5	0.50	20	7	7.7090	4.0075	36530	2896
6	0.50	20	7	7.6992	4.0255	37280	2929
1	0.50	20	14	7.6566	4.0068	41370	3281
2	0.50	20	14	7.6627	4.0162	43360	3423
3	0.50	20	14	7.6785	4.0070	42080	3337
4	0.50	20	14	7.6200	4.0117	42080	3329
5	0.50	20	14	7.7130	4.0342	40730	3186
6	0.50	20	14	7.6636	4.0310	40500	3174
1	0.50	20	28	7.6727	4.0145	43980	3475
2	0.50	20	28	7.7355	3.9800	44570	3583
3	0.50	20	28	7.6503	4.0220	45150	3554
4	0.50	20	28	7.6460	4.0172	47160	3721
5	0.50	20	28	7.6750	3.9927	44990	3593
6	0.50	20	28	7.6582	3.9872	48880	3915
1	0.50	20	90	7.6075	4.0320	52800	4135
2	0.50	20	90	7.6832	4.0220	49230	3875
3	0.50	20	90	7.6857	4.0015	48070	3822
4	0.50	20	90	7.6408	4.0015	54040	4297
5	0.50	20	90	7.6335	4.0155	49960	3945
6	0.50	20	90	7.6590	4.0095	51230	4057
1	0.50	40	7	7.6598	4.0282	30520	2395
2	0.50	40	7	7.6230	4.0473	29530	2295

Table A-2. Continued

Specimen Number	W/C	RAP-1 (%)	Curing Period (days)	Average Length (in)	Average Diameter (in)	Failure Load (lbs)	Compressive Strength (psi)
3	0.50	40	7	7.6172	4.0182	30180	2380
4	0.50	40	7	7.5580	4.0177	32710	2580
5	0.50	40	7	7.6342	4.0135	31290	2473
6	0.50	40	7	7.5010	4.0190	31160	2456
1	0.50	40	14	7.5482	4.0075	34300	2719
2	0.50	40	14	7.7132	4.0210	35800	2819
3	0.50	40	14	7.5852	4.0170	33480	2642
4	0.50	40	14	7.6308	4.0272	35920	2820
5	0.50	40	14	7.6318	3.9957	35980	2869
6	0.50	40	14	7.5980	4.0195	32910	2594
1	0.50	40	28	7.6067	4.0108	35630	2820
2	0.50	40	28	7.5890	4.0240	37690	2964
3	0.50	40	28	7.5108	4.0085	38250	3031
4	0.50	40	28	7.5502	4.0038	38410	3051
5	0.50	40	28	7.5295	4.0247	39000	3066
6	0.50	40	28	7.5445	4.0157	38970	3077
1	0.50	40	90	7.5583	4.0125	41020	3244
2	0.50	40	90	7.6700	4.0063	42220	3349
3	0.50	40	90	7.6848	4.0083	42900	3400
4	0.50	40	90	7.7235	4.0225	42140	3316
5	0.50	40	90	7.5675	4.0225	43450	3419
6	0.50	40	90	7.7418	4.0200	42630	3359
1	0.50	70	7	7.6363	4.0166	20250	1598
2	0.50	70	7	7.6357	4.0020	19130	1521
3	0.50	70	7	7.5167	4.0140	20610	1629
4	0.50	70	7	7.6423	4.0105	21340	1689
5	0.50	70	7	7.6348	4.0128	21700	1716
6	0.50	70	7	7.6103	4.0153	20680	1633
1	0.50	70	14	7.5482	3.9996	22240	1770
2	0.50	70	14	7.5505	4.0121	22950	1815

Table A-2. Continued

Specimen Number	W/C	RAP-1 (%)	Curing Period (days)	Average Length (in)	Average Diameter (in)	Failure Load (lbs)	Compressive Strength (psi)
3	0.50	70	14	7.5482	4.0190	22760	1794
4	0.50	70	14	7.6613	4.0103	23260	1841
5	0.50	70	14	7.6675	4.0093	22540	1785
6	0.50	70	14	7.6420	3.9860	23360	1872
1	0.50	70	28	7.5047	4.0035	25320	2011
2	0.50	70	28	7.6618	4.0023	23960	1904
3	0.50	70	28	7.6810	3.9905	27180	2173
4	0.50	70	28	7.6287	3.9910	23530	1881
5	0.50	70	28	7.5850	4.0158	27110	2140
6	0.50	70	28	7.7023	4.0057	24620	1954
1	0.50	70	90	7.6615	4.0025	28380	2256
2	0.50	70	90	7.6667	4.0093	28270	2239
3	0.50	70	90	7.6350	4.0075	26580	2107
4	0.50	70	90	7.6580	3.9948	26350	2102
5	0.50	70	90	7.6620	4.0087	26240	2079
6	0.50	70	90	7.6780	4.0050	27410	2176
1	0.50	100	7	7.6025	3.9942	13580	1084
2	0.50	100	7	7.5552	4.0032	14150	1124
3	0.50	100	7	7.5840	3.9990	12210	972
4	0.50	100	7	7.4283	4.0168	12910	1019
5	0.50	100	7	7.5387	4.0043	14560	1156
6	0.50	100	7	7.6642	4.0092	9220	730
1	0.50	100	14	7.5238	3.9695	16840	1361
2	0.50	100	14	7.5117	4.0076	16720	1325
3	0.50	100	14	7.6540	3.9976	15880	1265
4	0.50	100	14	7.5333	3.9992	14900	1186
5	0.50	100	14	7.6660	4.0108	16320	1292
6	0.50	100	14	7.6012	4.0168	16420	1296
1	0.50	100	28	7.4962	3.9900	18780	1502
2	0.50	100	28	7.6075	3.9972	17520	1396
3	0.50	100	28	7.7040	3.9912	17730	1417
4	0.50	100	28	7.6023	3.9973	17660	1407

Table A-2. Continued

Specimen Number	W/C	RAP-1 (%)	Curing Period (days)	Average Length (in)	Average Diameter (in)	Failure Load (lbs)	Compressive Strength (psi)
5	0.50	100	28	7.4960	4.0168	18240	1439
6	0.50	100	28	7.5745	4.0185	16660	1314
1	0.50	100	90	7.6040	4.0210	18950	1492
2	0.50	100	90	7.6485	4.0062	17880	1418
3	0.50	100	90	7.6648	4.0248	18700	1470
4	0.50	100	90	7.6790	4.0058	18000	1428
5	0.50	100	90	7.5220	4.0318	19600	1535
6	0.50	100	90	7.5840	4.0190	17950	1415

Table A-3. Compressive strength test results for concrete containing RAP-2

Sample Number	W/C	RAP-2 (%)	Curing Period (days)	Average Length (in)	Average Diameter (in)	Failure Load (lbs)	Compressive Strength (psi)
1	0.50	20	7	7.6802	4.0220	43110	3393
2	0.50	20	7	7.7202	4.0150	43990	3475
3	0.50	20	7	7.7278	4.0238	43700	3437
4	0.50	20	7	7.6690	4.0098	42300	3350
5	0.50	20	7	7.7725	4.0235	41000	3225
6	0.50	20	7	7.6838	4.0168	43560	3438
1	0.50	20	14	7.7270	4.0225	47950	3773
2	0.50	20	14	7.6888	4.0108	49620	3927
3	0.50	20	14	7.6153	4.0085	50030	3964
4	0.50	20	14	7.7763	4.0305	49380	3870
5	0.50	20	14	7.7013	4.0020	50010	3976
6	0.50	20	14	7.6098	4.0345	51010	3990
1	0.50	20	28	7.6878	4.0103	50180	3973
2	0.50	20	28	7.7178	4.0268	54940	4314
3	0.50	20	28	7.6613	3.9993	52460	4176
4	0.50	20	28	7.6348	4.0148	52840	4174
5	0.50	20	28	7.6752	4.0120	52510	4154
6	0.50	20	28	7.6633	4.0175	53190	4196
1	0.50	20	90	7.6790	4.0200	57230	4509
2	0.50	20	90	7.7415	4.0497	57200	4441
3	0.50	20	90	7.6993	3.9993	57640	4588
4	0.50	20	90	7.7405	4.0147	58090	4589

Table A-3. Continued

Specimen Number	W/C	RAP-2 (%)	Curing Period (days)	Average Length (in)	Average Diameter (in)	Failure Load (lbs)	Compressive Strength (psi)
5	0.50	20	90	7.6748	4.0338	59480	4654
6	0.50	20	90	7.7918	4.0302	59060	4630
1	0.50	40	7	7.6983	4.0110	31440	2488
2	0.50	40	7	7.7303	4.0216	29210	2300
3	0.50	40	7	7.7093	4.0150	29370	2320
4	0.50	40	7	7.7625	4.0300	31280	2452
5	0.50	40	7	7.7878	4.0328	29580	2316
6	0.50	40	7	7.8383	4.0273	30640	2405
1	0.50	40	14	7.6150	3.9978	33900	2701
2	0.50	40	14	7.7365	4.0141	32690	2583
3	0.50	40	14	7.7655	4.0256	33120	2602
4	0.50	40	14	7.6458	4.0082	33640	2666
5	0.50	40	14	7.7420	4.0197	34140	2690
6	0.50	40	14	7.6755	4.0148	35120	2774
1	0.50	40	28	7.6760	4.0182	36590	2885
2	0.50	40	28	7.7133	4.0163	37220	2938
3	0.50	40	28	7.7223	4.0143	36720	2901
4	0.50	40	28	7.7083	4.0138	35550	2810
5	0.50	40	28	7.6448	4.0202	38220	3011
6	0.50	40	28	7.7408	4.0100	37100	2938
1	0.50	40	90	7.8140	4.0268	39520	3103
2	0.50	40	90	7.6960	4.0185	40100	3162
3	0.50	40	90	7.8335	4.0067	37000	2935
4	0.50	40	90	7.8170	4.0128	32160	2543
5	0.50	40	90	7.6843	3.9997	39110	3113
6	0.50	40	90	7.7945	4.0203	39030	3075
1	0.50	70	7	7.6290	4.0200	19450	1532
2	0.50	70	7	7.7188	4.0242	19310	1518
3	0.50	70	7	7.7460	4.0326	20330	1592
4	0.50	70	7	7.6208	4.0480	19780	1537
5	0.50	70	7	7.6808	4.0005	20860	1660
6	0.50	70	7	7.6180	4.0108	20500	1623
1	0.50	70	14	7.6893	4.0106	19790	1567
2	0.50	70	14	7.7727	4.0153	19360	1529

Table A-3. Continued

Specimen Number	W/C	RAP-2 (%)	Curing Period (days)	Average Length (in)	Average Diameter (in)	Failure Load (lbs)	Compressive Strength (psi)
3	0.50	70	14	7.6927	4.0070	21600	1713
4	0.50	70	14	7.7305	4.0068	21490	1704
5	0.50	70	14	7.7198	4.0058	21470	1704
6	0.50	70	14	7.6193	4.0303	21670	1699
1	0.50	70	28	7.5977	4.0035	24890	1977
2	0.50	70	28	7.6837	4.0025	22630	1799
3	0.50	70	28	7.6713	4.0210	23280	1833
4	0.50	70	28	7.8000	4.0325	22540	1765
5	0.50	70	28	7.7863	4.0198	23260	1833
6	0.50	70	28	7.6690	4.0158	23780	1878
1	0.50	70	90	7.6770	4.0576	25470	1970
2	0.50	70	90	7.6545	4.0362	24930	1948
3	0.50	70	90	7.6808	4.0118	24100	1907
4	0.50	70	90	7.6353	4.0273	26610	2089
5	0.50	70	90	7.7143	4.0278	23130	1815
6	0.50	70	90	7.6160	4.0378	21230	1658
1	0.50	100	7	7.6768	4.0180	16270	1283
2	0.50	100	7	7.6680	4.0180	16110	1271
3	0.50	100	7	7.6960	4.0253	16430	1291
4	0.50	100	7	7.6143	4.0140	16890	1335
5	0.50	100	7	7.7448	4.0055	16210	1286
6	0.50	100	7	7.7500	4.0110	16370	1296
1	0.50	100	14	7.7628	4.0305	17100	1340
2	0.50	100	14	7.7323	4.0140	19050	1505
3	0.50	100	14	7.7098	4.0106	18750	1484
4	0.50	100	14	7.6572	4.0292	17670	1386
5	0.50	100	14	7.6633	4.0295	15560	1220
6	0.50	100	14	7.7425	4.0163	17970	1418
1	0.50	100	28	7.6158	4.0018	18660	1484
2	0.50	100	28	7.7703	4.0071	18730	1485
3	0.50	100	28	7.7395	4.0280	19360	1519
4	0.50	100	28	7.6555	4.0113	19010	1504
5	0.50	100	28	7.8645	4.0200	18610	1466
6	0.50	100	28	7.6775	4.0278	19030	1494

Table A-3. Continued

Specimen Number	W/C	RAP-2 (%)	Curing Period (days)	Average Length (in)	Average Diameter (in)	Failure Load (lbs)	Compressive Strength (psi)
1	0.50	100	90	7.5708	4.0260	15670	1231
2	0.50	100	90	7.7308	4.0167	19530	1541
3	0.50	100	90	7.6648	4.0182	20050	1581
4	0.50	100	90	7.9748	3.9843	21260	1705
5	0.50	100	90	7.7065	4.0168	15940	1258
6	0.50	100	90	7.6868	4.0272	20380	1600

Table A-4. Compressive strength test results for concrete containing RAP-3

Specimen Number	W/C	RAP-3 (%)	Curing Period (days)	Average Length (in)	Average Diameter (in)	Failure Load (lbs)	Compressive Strength (psi)
1	0.50	20	7	7.7765	4.0169	44750	3531
2	0.50	20	7	7.7175	4.0103	43640	3455
3	0.50	20	7	7.7133	4.0230	45490	3579
4	0.50	20	7	7.7120	4.0175	45300	3574
5	0.50	20	7	7.7288	4.0248	45010	3538
6	0.50	20	7	7.6768	4.0098	39950	3164
1	0.50	20	14	7.8073	4.0160	47580	3756
2	0.50	20	14	7.7740	4.0165	48220	3806
3	0.50	20	14	7.6463	4.0163	47930	3783
4	0.50	20	14	7.7620	4.0220	50590	3982
5	0.50	20	14	7.7740	4.0233	50140	3944
6	0.50	20	14	7.7365	4.0225	48390	3808
1	0.50	20	28	7.7447	4.0070	51330	4070
2	0.50	20	28	7.8278	4.0135	54930	4342
3	0.50	20	28	7.7893	4.0052	54280	4308
4	0.50	20	28	7.6748	4.0233	51300	4035
5	0.50	20	28	7.7378	4.0263	47130	3702
6	0.50	20	28	7.7855	4.0230	48380	3806
1	0.50	20	90	7.6905	4.0113	57060	4515
2	0.50	20	90	7.7235	4.0270	52330	4109
3	0.50	20	90	7.7005	4.0247	59430	4671
4	0.50	20	90	7.6765	4.0207	56320	4436
5	0.50	20	90	7.6413	4.0093	56490	4475
6	0.50	20	90	7.6783	4.0162	60040	4739

Table A-4. Continued

Specimen Number	W/C	RAP-3 (%)	Curing Period (days)	Average Length (in)	Average Diameter (in)	Failure Load (lbs)	Compressive Strength (psi)
1	0.50	40	7	7.7298	4.0210	33810	2662
2	0.50	40	7	7.6555	4.0370	34060	2661
3	0.50	40	7	7.7533	4.0275	34790	2731
4	0.50	40	7	7.7365	4.0233	34380	2704
5	0.50	40	7	7.7498	4.0110	35100	2778
1	0.50	40	14	7.8125	4.0122	36760	2908
2	0.50	40	14	7.8070	4.0006	34870	2774
3	0.50	40	14	7.7753	4.0157	33620	2655
4	0.50	40	14	7.7315	4.0058	35430	2811
5	0.50	40	14	7.6585	4.0240	37000	2909
6	0.50	40	14	7.6405	4.0120	36000	2848
1	0.50	40	28	7.6815	4.0323	42400	3320
2	0.50	40	28	7.6373	4.0305	38810	3042
3	0.50	40	28	7.6360	4.0195	36260	2858
4	0.50	40	28	7.7275	4.0283	42340	3322
5	0.50	40	28	7.6803	4.0352	40830	3193
6	0.50	40	28	7.7590	4.0205	42000	3308
1	0.50	40	90	7.7580	4.0150	35680	2818
2	0.50	40	90	7.6645	4.0180	42850	3379
3	0.50	40	90	7.6445	4.0173	43030	3395
4	0.50	40	90	7.5965	4.0170	40290	3179
5	0.50	40	90	7.6845	4.0080	43430	3442
6	0.50	40	90	7.5885	4.0212	39890	3141
1	0.50	70	7	7.7942	4.0163	26360	2081
2	0.50	70	7	7.8555	4.0143	23800	1880
3	0.50	70	7	7.6368	4.0118	24090	1906
4	0.50	70	7	7.8115	4.0243	25490	2004
5	0.50	70	7	7.6578	3.9983	23570	1877
6	0.50	70	7	7.7595	4.0203	27500	2166
1	0.50	70	14	7.7805	4.0151	27390	2163
2	0.50	70	14	7.7225	4.0422	24670	1922
3	0.50	70	14	7.6610	4.0243	28570	2246
4	0.50	70	14	7.6868	4.0168	25520	2014
5	0.50	70	14	7.7563	4.0158	21440	1693
6	0.50	70	14	7.7305	4.0198	24610	1939

Table A-4. Continued

Specimen Number	W/C	RAP-3 (%)	Curing Period (days)	Average Length (in)	Average Diameter (in)	Failure Load (lbs)	Compressive Strength (psi)
1	0.50	70	28	7.6263	4.0172	29320	2312
2	0.50	70	28	7.7718	4.0238	29310	2305
3	0.50	70	28	7.7840	4.0150	30910	2441
4	0.50	70	28	7.8208	4.0085	27130	2150
5	0.50	70	28	7.8105	3.9977	27130	2161
6	0.50	70	28	7.8173	4.0182	28420	2241
1	0.50	70	90	7.5535	4.0253	23120	1817
2	0.50	70	90	7.5630	4.0165	23020	1817
3	0.50	70	90	7.8123	4.0238	26440	2079
4	0.50	70	90	7.6743	4.0268	32440	2547
5	0.50	70	90	7.7395	4.0200	26960	2124
6	0.50	70	90	7.8203	4.0357	33430	2613
1	0.50	100	7	7.7748	4.0240	17820	1401
2	0.50	100	7	7.7183	4.0180	17720	1398
3	0.50	100	7	7.7968	4.0395	17620	1375
4	0.50	100	7	7.6653	3.9855	15100	1210
5	0.50	100	7	7.7010	4.0228	15130	1190
6	0.50	100	7	7.6023	4.0155	14460	1142
1	0.50	100	14	7.6738	4.0153	20260	1600
2	0.50	100	14	7.6355	4.0123	16810	1330
3	0.50	100	14	7.6283	4.0437	20840	1623
4	0.50	100	14	7.6508	4.0213	20950	1650
5	0.50	100	14	7.6930	4.0220	14000	1102
6	0.50	100	14	7.6283	4.0215	16360	1288
1	0.50	100	28	7.8440	4.0220	17370	1367
2	0.50	100	28	7.5528	4.0192	22440	1769
3	0.50	100	28	7.7383	4.0255	20290	1594
4	0.50	100	28	7.8098	4.0295	16590	1301
5	0.50	100	28	7.8553	4.0112	18310	1449
6	0.50	100	28	7.5835	3.9997	18560	1477
1	0.50	100	90	7.5740	4.0175	22900	1806
2	0.50	100	90	7.6968	4.0218	24000	1889
3	0.50	100	90	7.5560	4.0160	21940	1732
4	0.50	100	90	7.6003	4.0053	22670	1799
5	0.50	100	90	7.7828	4.0307	21720	1702

Table A-5. Compressive strength test results for concrete containing RAP-4

Specimen Number	W/C	RAP-4 (%)	Curing Period (days)	Average Length (in)	Average Diameter (in)	Failure Load (lbs)	Compressive Strength (psi)
1	0.50	20	7	7.7025	4.0230	43210	3399
2	0.50	20	7	7.7900	4.0245	43460	3416
3	0.50	20	7	7.6878	4.0155	40220	3176
4	0.50	20	7	7.7560	4.0180	45540	3592
5	0.50	20	7	7.7700	4.0203	44610	3514
6	0.50	20	7	7.6813	4.0030	45010	3576
1	0.50	20	14	7.6995	4.0125	50570	3999
2	0.50	20	14	7.6395	4.0198	47830	3769
3	0.50	20	14	7.6338	4.0452	46730	3636
4	0.50	20	14	7.7198	4.0118	49320	3902
5	0.50	20	14	7.6925	4.0128	49570	3920
6	0.50	20	14	7.7768	4.0085	46540	3688
1	0.50	20	28	7.6345	4.0172	51560	4068
2	0.50	20	28	7.6765	4.0147	45170	3568
3	0.50	20	28	7.6975	3.9977	50360	4012
4	0.50	20	28	7.6933	4.0088	54790	4341
5	0.50	20	28	7.5450	3.9805	51050	4102
6	0.50	20	28	7.6108	4.0212	50380	3967
1	0.50	20	90	7.6305	4.0135	59410	4696
2	0.50	20	90	7.7145	4.0113	56650	4483
3	0.50	20	90	7.7245	3.9977	56310	4486
4	0.50	20	90	7.6540	4.0155	54770	4325
5	0.50	20	90	7.6935	4.0095	54310	4301
6	0.50	20	90	7.7253	4.0050	50780	4031
1	0.50	40	7	7.6055	4.0332	31040	2430
2	0.50	40	7	7.6145	4.0193	31340	2470
3	0.50	40	7	7.5965	4.0210	33140	2610
4	0.50	40	7	7.6950	4.0173	28540	2252
5	0.50	40	7	7.6448	4.0322	26500	2075
6	0.50	40	7	7.6800	4.0255	32080	2521
1	0.50	40	14	7.6285	4.0217	36220	2851
2	0.50	40	14	7.8065	4.0270	31860	2501
3	0.50	40	14	7.6803	4.0030	35650	2833
4	0.50	40	14	7.6283	4.0080	31000	2457
5	0.50	40	14	7.7240	4.0168	30410	2400

Table A-5. Continued

Specimen Number	W/C	RAP-4 (%)	Curing Period (days)	Average Length (in)	Average Diameter (in)	Failure Load (lbs)	Compressive Strength (psi)
1	0.50	40	28	7.6505	4.0125	38850	3072
2	0.50	40	28	7.6225	4.0127	34190	2704
3	0.50	40	28	7.7313	4.0183	34990	2759
4	0.50	40	28	7.6278	4.0252	39280	3087
5	0.50	40	28	7.6215	4.0143	35680	2819
6	0.50	40	28	7.5740	4.0383	39550	3088
1	0.50	40	90	7.5360	3.9930	43640	3485
2	0.50	40	90	7.6723	3.9943	40740	3251
3	0.50	40	90	7.5718	4.0175	41700	3290
4	0.50	40	90	7.7020	3.9892	41400	3312
5	0.50	40	90	7.7103	4.0262	37620	2955
6	0.50	40	90	7.5668	3.9962	37410	2983
1	0.50	70	7	7.7190	4.0090	25050	1984
2	0.50	70	7	7.6835	4.0292	23830	1869
3	0.50	70	7	7.6205	4.0183	26860	2118
4	0.50	70	7	7.6053	3.9937	24020	1917
5	0.50	70	7	7.6828	4.0097	24940	1975
6	0.50	70	7	7.6645	4.0137	20660	1633
1	0.50	70	14	7.6213	3.9928	26930	2151
2	0.50	70	14	7.5988	4.0120	23410	1852
3	0.50	70	14	7.5948	4.0073	27060	2146
4	0.50	70	14	7.6180	4.0030	20620	1638
5	0.50	70	14	7.6125	4.0203	22390	1764
6	0.50	70	14	7.6930	4.0250	23290	1830
1	0.50	70	28	7.7913	4.0263	27610	2169
2	0.50	70	28	7.7865	3.9928	29100	2324
3	0.50	70	28	7.7630	4.0035	27600	2192
4	0.50	70	28	7.7028	4.0230	29040	2285
5	0.50	70	28	7.6375	4.0203	29750	2344
6	0.50	70	28	7.7130	4.0050	28350	2250
1	0.50	70	90	7.6683	4.0220	32460	2555
2	0.50	70	90	7.6573	4.0113	30990	2452
3	0.50	70	90	7.6310	3.9962	31370	2501
4	0.50	70	90	7.6660	3.9977	31130	2480

Table A-5. Continued

Specimen Number	W/C	RAP-4 (%)	Curing Period (days)	Average Length (in)	Average Diameter (in)	Failure Load (lbs)	Compressive Strength (psi)
5	0.50	70	90	7.5580	3.9938	31270	2496
6	0.50	70	90	7.6705	3.9865	33610	2693
1	0.50	100	7	7.6960	4.0247	18820	1479
2	0.50	100	7	7.6215	4.0293	17010	1334
3	0.50	100	7	7.5553	4.0220	18510	1457
4	0.50	100	7	7.6515	4.0095	16530	1309
5	0.50	100	7	7.7155	4.0210	15600	1228
6	0.50	100	7	7.6475	4.0200	15460	1218
1	0.50	100	14	7.6168	4.0140	16400	1296
2	0.50	100	14	7.5883	4.0055	19610	1556
3	0.50	100	14	7.6833	4.0185	16120	1271
4	0.50	100	14	7.6320	4.0087	20900	1656
5	0.50	100	14	7.6238	3.9977	21050	1677
6	0.50	100	14	7.6678	4.0118	21060	1666
1	0.50	100	28	7.8455	4.0102	16450	1302
2	0.50	100	28	7.8310	4.0192	22000	1734
3	0.50	100	28	7.6283	4.0173	17530	1383
4	0.50	100	28	7.5380	4.0208	20660	1627
5	0.50	100	28	7.5968	4.0208	20430	1609
6	0.50	100	28	7.6303	4.0050	20920	1661
1	0.50	100	90	7.6473	4.0050	22450	1782
2	0.50	100	90	7.5960	4.0083	22670	1797
3	0.50	100	90	7.6840	4.0158	22640	1787
4	0.50	100	90	7.5783	4.0280	23010	1806
5	0.50	100	90	7.7695	3.9935	23380	1867
6	0.50	100	90	7.6370	4.0075	18880	1497

Table A-6. Modulus of elasticity and poison's ratio test results for concrete containing no RAP

Specimen Number	W/C	RAP (%)	Curing Period (days)	Average Length (in)	Average Diameter (in)	Modulus of Elasticity ( $10^6$ psi)	Poison's Ratio
1	0.45	0	7	7.6026	4.0111	4.47	0.24
2	0.45	0	7	7.8166	4.0108	4.37	0.26
3	0.45	0	7	7.7812	4.0231	4.43	0.25

Table A-6. Continued

Specimen Number	W/C	RAP (%)	Curing Period (days)	Average Length (in)	Average Diameter (in)	Modulus of Elasticity ( $10^6$ psi)	Poisson's Ratio
1	0.45	0	14	7.6963	4.0115	4.37	0.25
2	0.45	0	14	7.7783	4.0150	4.35	0.23
3	0.45	0	14	7.7297	4.0135	4.50	0.24
1	0.45	0	28	7.6830	4.0068	4.62	0.25
2	0.45	0	28	7.7606	4.0108	4.52	0.24
3	0.45	0	28	7.6452	4.0275	4.57	0.24
1	0.45	0	90	7.6870	4.0120	4.62	0.27
2	0.45	0	90	7.7560	4.0075	4.67	0.23
3	0.45	0	90	7.6975	4.0265	4.77	0.24
1	0.50	0	7	7.6393	4.0015	3.92	0.20
2	0.50	0	7	7.6648	4.0228	3.95	0.21
3	0.50	0	7	7.7130	4.0130	4.05	0.23
1	0.50	0	14	7.6202	4.0231	4.32	/
2	0.50	0	14	7.6258	4.0018	4.20	0.22
3	0.50	0	14	7.6428	4.0117	4.15	0.22
1	0.50	0	28	7.5505	4.000	4.58	0.22
2	0.50	0	28	7.5642	4.0152	4.38	0.25
3	0.50	0	28	7.6168	4.0012	4.32	0.26
1	0.50	0	90	7.6690	3.9985	4.33	0.25
2	0.50	0	90	7.7050	4.0123	4.35	0.23
3	0.50	0	90	7.6870	4.0125	4.52	0.22
1	0.55	0	7	7.6377	4.0053	4.00	0.22
2	0.55	0	7	7.6358	4.0115	3.81	0.21
3	0.55	0	7	7.7165	3.9965	3.83	0.23
1	0.55	0	14	7.7012	4.0000	3.95	0.22
2	0.55	0	14	7.4673	4.0038	4.32	0.24
3	0.55	0	14	7.5933	4.0257	4.01	0.22
1	0.55	0	28	7.6156	3.9973	4.00	0.25
2	0.55	0	28	7.6055	3.9985	4.42	0.22
3	0.55	0	28	7.5830	4.0133	4.25	0.24
1	0.55	0	90	7.5625	4.0415	4.15	0.22
2	0.55	0	90	7.6063	4.0085	4.32	0.23
3	0.55	0	90	7.6493	4.0123	4.25	0.24

Table A-7. Modulus of elasticity and poison's ratio test results for concrete containing RAP-1

Specimen Number	W/C	RAP-1 (%)	Curing Period (days)	Average Length (in)	Average Diameter (in)	Modulus of Elasticity ( $10^6$ psi)	Poison's Ratio
1	0.50	20	7	7.6858	4.0098	3.20	0.24
2	0.50	20	7	7.7090	4.0075	3.28	0.23
3	0.50	20	7	7.6992	4.0255	2.98	0.22
1	0.50	20	14	7.6200	4.0117	3.33	0.24
2	0.50	20	14	7.7130	4.0342	3.28	0.26
3	0.50	20	14	7.6636	4.0310	3.45	0.25
1	0.50	20	28	7.6460	4.0172	3.53	0.26
2	0.50	20	28	7.6750	3.9927	3.38	0.26
3	0.50	20	28	7.6582	3.9872	3.42	0.22
1	0.50	20	90	7.6408	4.0015	3.73	0.23
2	0.50	20	90	7.6335	4.0155	3.67	0.25
3	0.50	20	90	7.6590	4.0095	3.62	0.25
1	0.50	40	7	7.5580	4.0177	3.15	0.25
2	0.50	40	7	7.6342	4.0135	2.63	0.24
3	0.50	40	7	7.5010	4.0190	2.43	0.25
1	0.50	40	14	7.6308	4.0272	2.90	0.25
2	0.50	40	14	7.6318	3.9957	2.93	0.27
3	0.50	40	14	7.5980	4.0195	2.57	0.27
1	0.50	40	28	7.5502	4.0038	2.87	0.22
2	0.50	40	28	7.5295	4.0247	3.20	0.25
3	0.50	40	28	7.5445	4.0157	2.92	0.27
1	0.50	40	90	7.7235	4.0225	2.83	0.29
2	0.50	40	90	7.5675	4.0225	2.95	0.27
3	0.50	40	90	7.7418	4.0200	3.05	0.25
1	0.50	70	7	7.6423	4.0105	1.65	0.26
2	0.50	70	7	7.6348	4.0128	1.73	0.26
3	0.50	70	7	7.6103	4.0153	1.72	0.28
1	0.50	70	14	7.6613	4.0103	1.93	0.26
2	0.50	70	14	7.6675	4.0093	1.70	0.29
3	0.50	70	14	7.6420	3.9860	1.68	0.29
1	0.50	70	28	7.6287	3.9910	1.92	0.25
2	0.50	70	28	7.5850	4.0158	1.80	0.26
3	0.50	70	28	7.7023	4.0057	1.75	0.30

Table A-7. Continued

Specimen Number	W/C	RAP-1 (%)	Curing Period (days)	Average Length (in)	Average Diameter (in)	Modulus of Elasticity ( $10^6$ psi)	Poisson's Ratio
1	0.50	70	90	7.6580	3.9948	1.93	0.28
2	0.50	70	90	7.6620	4.0087	2.03	0.26
3	0.50	70	90	7.6780	4.0050	2.06	0.30
1	0.50	100	7	7.4283	4.0168	1.15	0.20
2	0.50	100	7	7.5387	4.0043	1.08	0.26
3	0.50	100	7	7.6642	4.0092	1.12	0.28
1	0.50	100	14	7.5333	3.9992	1.20	0.28
2	0.50	100	14	7.6660	4.0108	1.22	0.29
3	0.50	100	14	7.6012	4.0168	1.35	0.30
1	0.50	100	28	7.6023	3.9973	1.30	0.32
2	0.50	100	28	7.4960	4.0168	1.30	0.33
3	0.50	100	28	7.5745	4.0185	1.18	0.29
1	0.50	100	90	7.6790	4.0058	1.13	0.28
2	0.50	100	90	7.5220	4.0318	1.35	0.30
3	0.50	100	90	7.5840	4.0190	1.23	0.30

Table A-8. Modulus of elasticity and poison's ratio test results for concrete containing RAP-2

Specimen Number	W/C	RAP-2 (%)	Curing Period (days)	Average Length (in)	Average Diameter (in)	Modulus of Elasticity ( $10^6$ psi)	Poisson's Ratio
1	0.50	20	7	7.6690	4.0098	3.08	0.24
2	0.50	20	7	7.7725	4.0235	3.35	0.21
3	0.50	20	7	7.6838	4.0168	3.28	0.25
1	0.50	20	14	7.7763	4.0305	3.55	0.26
2	0.50	20	14	7.7013	4.0020	3.42	0.26
3	0.50	20	14	7.6098	4.0345	3.42	0.24
1	0.50	20	28	7.6348	4.0148	3.53	0.24
2	0.50	20	28	7.6752	4.0120	3.72	0.28
3	0.50	20	28	7.6633	4.0175	3.82	0.26
1	0.50	20	90	7.7405	4.0147	3.88	0.24
2	0.50	20	90	7.6748	4.0338	3.90	0.25
3	0.50	20	90	7.7918	4.0302	3.85	0.24
1	0.50	40	7	7.7625	4.0300	2.58	0.25

Table A-8. Continued

Specimen Number	W/C	RAP-2 (%)	Curing Period (days)	Average Length (in)	Average Diameter (in)	Modulus of Elasticity ( $10^6$ psi)	Poisson's Ratio
2	0.50	40	7	7.7878	4.0328	2.52	0.26
3	0.50	40	7	7.8383	4.0273	2.52	0.24
1	0.50	40	14	7.6458	4.0082	2.62	0.25
2	0.50	40	14	7.7420	4.0197	2.73	0.26
3	0.50	40	14	7.6755	4.0148	2.77	0.22
1	0.50	40	28	7.7083	4.0138	2.70	0.26
2	0.50	40	28	7.6448	4.0202	2.83	0.27
3	0.50	40	28	7.7408	4.0100	2.77	0.22
1	0.50	40	90	7.8170	4.0128	2.92	0.25
2	0.50	40	90	7.6843	3.9997	2.87	0.24
3	0.50	40	90	7.7945	4.0203	2.82	0.27
1	0.50	70	7	7.6208	4.0480	1.58	0.26
2	0.50	70	7	7.6808	4.0005	1.70	0.26
3	0.50	70	7	7.6180	4.0108	1.67	0.27
1	0.50	70	14	7.7305	4.0068	1.77	0.26
2	0.50	70	14	7.7198	4.0058	1.73	0.25
3	0.50	70	14	7.6193	4.0303	1.75	0.24
1	0.50	70	28	7.8000	4.0325	1.85	0.29
2	0.50	70	28	7.7863	4.0198	1.87	0.23
3	0.50	70	28	7.6690	4.0158	1.82	0.23
1	0.50	70	90	7.6353	4.0273	1.92	0.24
2	0.50	70	90	7.7143	4.0278	1.90	0.24
3	0.50	70	90	7.6160	4.0378	2.08	0.27
4	0.50	100	7	7.6143	4.0140	1.25	0.24
5	0.50	100	7	7.7448	4.0055	1.27	0.28
6	0.50	100	7	7.7500	4.0110	1.27	0.27
4	0.50	100	14	7.6572	4.0292	1.20	0.27
5	0.50	100	14	7.6633	4.0295	1.24	0.25
6	0.50	100	14	7.7425	4.0163	1.25	0.30
4	0.50	100	28	7.6555	4.0113	1.42	0.28
5	0.50	100	28	7.8645	4.0200	1.40	0.28
6	0.50	100	28	7.6775	4.0278	1.30	0.27
4	0.50	100	90	7.9748	3.9843	1.42	0.26
5	0.50	100	90	7.7065	4.0168	1.35	0.29

Table A-9. Modulus of elasticity and poison's ratio test results for concrete containing RAP-3

Specimen Number	W/C	RAP-3 (%)	Curing Period (days)	Average Length (in)	Average Diameter (in)	Modulus of Elasticity ( $10^6$ psi)	Poison's Ratio
1	0.50	20	7	7.7120	4.0175	3.48	0.23
2	0.50	20	7	7.7288	4.0248	3.38	0.24
3	0.50	20	7	7.6768	4.0098	3.40	0.23
1	0.50	20	14	7.7620	4.0220	3.55	0.25
2	0.50	20	14	7.7740	4.0233	3.50	0.23
3	0.50	20	14	7.7365	4.0225	3.42	0.23
1	0.50	20	28	7.6748	4.0233	3.53	0.25
2	0.50	20	28	7.7378	4.0263	3.62	0.22
3	0.50	20	28	7.7855	4.0230	3.68	0.25
1	0.50	20	90	7.6765	4.0207	3.78	0.23
2	0.50	20	90	7.6413	4.0093	3.73	0.24
3	0.50	20	90	7.6783	4.0162	3.82	0.23
1	0.50	40	7	7.7533	4.0275	2.55	0.24
2	0.50	40	7	7.7365	4.0233	2.58	0.22
3	0.50	40	7	7.7498	4.0110	2.62	0.23
1	0.50	40	14	7.7315	4.0058	2.63	0.22
2	0.50	40	14	7.6585	4.0240	2.60	0.23
3	0.50	40	14	7.6405	4.0120	2.78	0.24
1	0.50	40	28	7.7275	4.0283	2.83	0.23
2	0.50	40	28	7.6803	4.0352	2.70	0.23
3	0.50	40	28	7.7590	4.0205	2.88	0.25
1	0.50	40	90	7.5965	4.0170	3.18	0.23
2	0.50	40	90	7.6845	4.0080	2.55	0.24
3	0.50	40	90	7.5885	4.0212	2.72	0.25
1	0.50	70	7	7.8115	4.0243	1.80	0.29
2	0.50	70	7	7.6578	3.9983	1.65	0.24
3	0.50	70	7	7.7595	4.0203	1.88	0.22
1	0.50	70	14	7.6868	4.0168	1.95	0.24
2	0.50	70	14	7.7563	4.0158	1.78	0.25
3	0.50	70	14	7.7305	4.0198	1.95	0.21
1	0.50	70	28	7.8208	4.0085	1.90	0.27
2	0.50	70	28	7.8105	3.9977	1.78	0.24
3	0.50	70	28	7.8173	4.0182	1.97	0.23

Table A-9. Continued

Specimen Number	W/C	RAP-3 (%)	Curing Period (days)	Average Length (in)	Average Diameter (in)	Modulus of Elasticity ( $10^6$ psi)	Poisson's Ratio
1	0.50	70	90	7.7395	4.0200	2.05	0.26
2	0.50	70	90	7.8203	4.0357	2.20	0.26
1	0.50	100	7	7.6653	3.9855	1.18	0.25
2	0.50	100	7	7.7010	4.0228	1.22	0.24
3	0.50	100	7	7.6023	4.0155	1.10	0.26
1	0.50	100	14	7.6508	4.0213	1.35	0.27
2	0.50	100	14	7.6930	4.0220	1.22	0.27
3	0.50	100	14	7.6283	4.0215	1.27	0.27
1	0.50	100	28	7.8098	4.0295	1.18	0.27
2	0.50	100	28	7.8553	4.0112	1.28	0.25
3	0.50	100	28	7.5835	3.9997	1.30	0.24
1	0.50	100	90	7.6003	4.0053	1.10	0.21
2	0.50	100	90	7.7828	4.0307	1.25	0.25
3	0.50	100	90	7.5533	4.0288	1.33	0.24

Table A-10. Modulus of elasticity and poison's ratio test results for concrete containing RAP-4

Specimen Number	W/C	RAP-4 (%)	Curing Period (days)	Average Length (in)	Average Diameter (in)	Modulus of Elasticity ( $10^6$ psi)	Poisson's Ratio
1	0.50	20	7	7.7560	4.0180	3.55	0.23
2	0.50	20	7	7.7700	4.0203	3.37	0.27
3	0.50	20	7	7.6813	4.0030	3.72	0.26
1	0.50	20	14	7.7198	4.0118	3.32	0.23
2	0.50	20	14	7.6925	4.0128	3.28	0.25
3	0.50	20	14	7.7768	4.0085	3.38	0.25
1	0.50	20	28	7.6933	4.0088	3.62	0.26
2	0.50	20	28	7.5450	3.9805	3.73	0.22
3	0.50	20	28	7.6108	4.0212	3.52	0.25
1	0.50	20	90	7.6540	4.0155	3.67	0.24
2	0.50	20	90	7.6935	4.0095	3.73	0.24
3	0.50	20	90	7.7253	4.0050	3.62	0.24
1	0.50	40	7	7.6950	4.0173	2.75	0.26

Table A-10. Continued

Specimen Number	W/C	RAP-4 (%)	Curing Period (days)	Average Length (in)	Average Diameter (in)	Modulus of Elasticity ( $10^6$ psi)	Poisson's Ratio
2	0.50	40	7	7.6800	4.0255	2.55	0.29
1	0.50	40	14	7.6283	4.0080	2.72	0.30
2	0.50	40	14	7.7240	4.0168	2.68	0.26
3	0.50	40	14	7.7218	4.0173	2.40	0.23
1	0.50	40	28	7.6278	4.0252	2.68	0.27
2	0.50	40	28	7.6215	4.0143	2.67	0.23
3	0.50	40	28	7.5740	4.0383	2.82	0.25
1	0.50	40	90	7.7020	3.9892	2.78	0.29
2	0.50	40	90	7.7103	4.0262	2.72	0.22
3	0.50	40	90	7.5668	3.9962	2.98	0.28
1	0.50	70	7	7.6053	3.9937	1.75	0.27
2	0.50	70	7	7.6828	4.0097	1.78	0.28
3	0.50	70	7	7.6645	4.0137	1.73	0.29
1	0.50	70	14	7.6180	4.0030	1.72	0.24
2	0.50	70	14	7.6125	4.0203	1.82	0.26
3	0.50	70	14	7.6930	4.0250	1.78	0.25
1	0.50	70	28	7.7028	4.0230	1.72	0.24
2	0.50	70	28	7.6375	4.0203	1.92	0.26
3	0.50	70	28	7.7130	4.0050	1.72	0.24
1	0.50	70	90	7.6660	3.9977	1.93	0.27
2	0.50	70	90	7.5580	3.9938	1.95	0.27
3	0.50	70	90	7.6705	3.9865	2.15	0.25
1	0.50	100	7	7.6515	4.0095	1.13	0.26
2	0.50	100	7	7.7155	4.0210	1.10	0.25
3	0.50	100	7	7.6475	4.0200	1.23	0.25
1	0.50	100	14	7.6320	4.0087	1.28	0.25
2	0.50	100	14	7.6238	3.9977	1.25	0.26
3	0.50	100	14	7.6678	4.0118	1.20	0.27
1	0.50	100	28	7.5380	4.0208	1.17	0.28
2	0.50	100	28	7.5968	4.0208	1.20	0.26
3	0.50	100	28	7.6303	4.0050	1.20	0.25
1	0.50	100	90	7.5783	4.0280	1.25	0.27
2	0.50	100	90	7.7695	3.9935	1.42	0.28
3	0.50	100	90	7.6370	4.0075	1.33	0.28

Table A-11. Splitting tensile strength test results for concrete containing no RAP

Specimen Number	W/C	RAP (%)	Curing Period (days)	Average Length (in)	Average Diameter (in)	Failure Load (lbs)	Splitting Tensile Strength (psi)
1	0.45	0	7	7.8400	4.0100	24270	491
2	0.45	0	7	7.7000	4.0068	25320	522
3	0.45	0	7	7.6720	4.0310	22190	457
1	0.45	0	14	8.0070	4.0190	35270	698
2	0.45	0	14	8.0350	4.0140	25460	503
3	0.45	0	14	8.0458	4.0056	29190	577
1	0.45	0	28	7.9610	4.0130	32470	647
2	0.45	0	28	7.9952	4.0250	33210	657
3	0.45	0	28	7.9672	4.0085	34460	687
1	0.45	0	90	8.0230	4.0142	32300	638
2	0.45	0	90	8.0220	4.0150	34040	673
3	0.45	0	90	8.0025	4.0150	33310	660
1	0.50	0	7	8.0850	4.0043	23190	456
2	0.50	0	7	8.0155	4.0210	24910	492
3	0.50	0	7	8.0268	4.0215	23880	471
1	0.50	0	14	7.9980	4.0096	23720	471
2	0.50	0	14	/	/	/	/
3	0.50	0	14	7.9375	4.0140	28960	579
1	0.50	0	28	8.0225	4.0310	23250	458
2	0.50	0	28	8.0167	4.0095	27320	541
3	0.50	0	28	8.0135	3.9972	24640	490
1	0.50	0	90	8.0780	4.0000	28600	563
2	0.50	0	90	8.0342	4.0370	30800	605
3	0.50	0	90	8.0000	4.0138	31510	625
1	0.55	0	7	8.0198	4.0150	25070	496
2	0.55	0	7	8.0230	4.0140	21050	416
3	0.55	0	7	7.9658	4.0126	17360	346
1	0.55	0	14	8.0111	4.0395	21800	429
2	0.55	0	14	8.0570	4.0040	21500	424
3	0.55	0	14	7.9980	4.0001	23140	460
1	0.55	0	28	8.0568	4.0163	25180	495
2	0.55	0	28	8.0760	4.0305	25970	508
3	0.55	0	28	7.9800	4.0067	26470	527
1	0.55	0	90	8.0001	4.0190	25150	498
2	0.55	0	90	7.9910	3.9983	27430	547
3	0.55	0	90	8.0046	4.0106	28550	566

Table A-12. Splitting tensile strength test results for concrete containing RAP-1

Specimen Number	W/C	RAP-1 (%)	Curing Period (days)	Average Length (in)	Average Diameter (in)	Failure Load (lbs)	Splitting Tensile Strength (psi)
1	0.50	20	7	8.0083	3.9970	17020	339
2	0.50	20	7	7.9513	3.9850	18740	377
3	0.50	20	7	8.0013	3.9895	21230	423
1	0.50	20	14	8.0400	4.0198	20990	413
2	0.50	20	14	8.0540	4.0031	22080	436
3	0.50	20	14	8.0430	4.0095	17640	348
1	0.50	20	28	8.0100	4.0290	23040	454
2	0.50	20	28	8.0447	3.9905	23480	466
3	0.50	20	28	8.0355	4.0052	22060	436
1	0.50	20	90	8.0921	4.0100	22410	440
2	0.50	20	90	8.0236	4.0200	23790	470
3	0.50	20	90	8.0525	4.0147	20750	409
1	0.50	40	7	7.9433	4.0197	16550	330
2	0.50	40	7	7.9515	4.0080	17090	341
3	0.50	40	7	7.9973	4.0156	16610	329
1	0.50	40	14	7.9865	4.0088	17160	341
2	0.50	40	14	7.9725	4.0142	18550	369
3	0.50	40	14	8.0713	4.0098	20010	394
1	0.50	40	28	8.0903	4.0108	19720	387
2	0.50	40	28	7.8960	3.9983	16860	340
3	0.50	40	28	7.9995	4.0106	19250	382
1	0.50	40	90	7.9658	3.9975	19560	391
2	0.50	40	90	8.0470	3.9965	19500	386
3	0.50	40	90	7.9328	3.9983	20460	411
1	0.50	70	7	8.0000	4.0181	12580	249
2	0.50	70	7	7.9818	3.9956	12090	241
3	0.50	70	7	7.9435	4.0108	12920	258
1	0.50	70	14	7.9600	4.0106	14240	284
2	0.50	70	14	8.0395	4.0148	14070	278
3	0.50	70	14	8.0110	4.0213	12480	247
1	0.50	70	28	8.0021	4.0193	15080	298
2	0.50	70	28	8.0075	4.0095	14740	292
3	0.50	70	28	7.9521	4.0118	15960	318
1	0.50	70	90	7.9722	4.0047	13860	276
2	0.50	70	90	8.0122	4.0106	12790	253
3	0.50	70	90	8.0155	4.0067	13130	260
1	0.50	100	7	7.8835	4.0080	9070	183
2	0.50	100	7	7.8605	4.0203	9510	192
3	0.50	100	7	7.9354	4.0070	7940	159

Table A-12. Continued

Specimen Number	W/C	RAP-1 (%)	Curing Period (days)	Average Length (in)	Average Diameter (in)	Failure Load (lbs)	Splitting Tensile Strength (psi)
1	0.50	100	14	7.9301	4.0206	9580	191
2	0.50	100	14	7.9298	4.0151	10100	202
3	0.50	100	14	7.9802	4.0001	10660	213
1	0.50	100	28	8.0580	4.0123	9730	192
2	0.50	100	28	7.9395	4.0155	9410	188
3	0.50	100	28	7.9297	4.0216	8280	165
1	0.50	100	90	8.0060	4.0073	12930	257
2	0.50	100	90	7.8600	4.0168	11900	240
3	0.50	100	90	8.0710	4.0046	11950	235

Table A-13. Splitting tensile strength test results for concrete containing RAP-2

Specimen Number	W/C	RAP-2 (%)	Curing Period (days)	Average Length (in)	Average Diameter (in)	Failure Load (lbs)	Splitting Tensile Strength (psi)
1	0.50	20	7	8.0643	4.0332	18560	363
2	0.50	20	7	8.0848	4.0200	23810	466
3	0.50	20	7	8.0995	4.0303	23220	453
1	0.50	20	14	8.0945	4.0140	23640	463
2	0.50	20	14	8.1340	4.0328	22680	440
3	0.50	20	14	8.1418	4.0253	19590	381
1	0.50	20	28	8.1815	4.0158	21930	425
2	0.50	20	28	8.0288	3.9652	23010	460
3	0.50	20	28	8.0938	3.9930	22450	442
1	0.50	20	90	8.0885	3.9965	22570	444
2	0.50	20	90	8.0498	4.0185	23530	463
3	0.50	20	90	8.0480	4.0030	26360	521
1	0.50	40	7	8.1287	4.0305	18090	352
2	0.50	40	7	8.1617	4.0345	16050	310
3	0.50	40	7	8.2152	4.0158	14440	279
1	0.50	40	14	8.0080	4.0185	16110	319
2	0.50	40	14	8.1617	4.0198	20570	399
3	0.50	40	14	8.1283	3.9990	17200	337
1	0.50	40	28	8.0953	4.0028	18090	355
2	0.50	40	28	8.0305	4.0172	18290	361
3	0.50	40	28	8.0193	4.0215	19830	391
1	0.50	40	90	8.0043	4.0043	20180	401
2	0.50	40	90	8.0780	4.0030	21790	429
3	0.50	40	90	8.0363	3.9878	20570	409

Table A-13. Continued

Specimen Number	W/C	RAP-2 (%)	Curing Period (days)	Average Length (in)	Average Diameter (in)	Failure Load (lbs)	Splitting Tensile Strength (psi)
1	0.50	70	7	7.9780	4.0203	10690	212
2	0.50	70	7	7.9793	4.0065	12520	249
3	0.50	70	7	8.1165	4.0203	12060	235
1	0.50	70	14	8.0582	4.0175	13970	275
2	0.50	70	14	8.1417	4.0107	13560	264
3	0.50	70	14	8.0607	4.0115	12570	247
1	0.50	70	28	7.9750	4.0357	14020	277
2	0.50	70	28	8.0633	4.0198	12290	241
3	0.50	70	28	8.0863	4.0250	13040	255
1	0.50	70	90	8.0393	4.0268	12490	246
2	0.50	70	90	8.0768	4.0223	13190	258
3	0.50	70	90	8.1498	4.0222	13160	256
1	0.50	100	7	8.0990	4.0093	10280	202
2	0.50	100	7	8.0243	4.0217	9890	195
3	0.50	100	7	8.1040	4.0265	10040	196
1	0.50	100	14	8.1620	4.0068	12190	237
2	0.50	100	14	8.0170	4.0077	10940	217
3	0.50	100	14	7.9950	3.9990	11390	227
1	0.50	100	28	8.1617	4.0095	10380	202
2	0.50	100	28	8.1997	4.0068	11260	218
3	0.50	100	28	8.0615	4.0140	11830	233
1	0.50	100	90	8.1815	4.0272	11970	231
2	0.50	100	90	8.1455	4.0113	10730	209
3	0.50	100	90	8.1253	4.0220	10820	211

Table A-14. Splitting tensile strength test results for concrete containing RAP-3

Specimen Number	W/C	RAP-3 (%)	Curing Period (days)	Average Length (in)	Average Diameter (in)	Failure Load (lbs)	Splitting Tensile Strength (psi)
1	0.50	20	7	8.0505	4.0228	20990	413
2	0.50	20	7	8.0555	4.0267	20800	408
3	0.50	20	7	8.0927	4.0297	17900	349
1	0.50	20	14	8.1148	4.0385	20840	405
2	0.50	20	14	8.0583	4.0053	22700	448
3	0.50	20	14	8.0573	4.0145	22530	443
1	0.50	20	28	8.1598	4.0248	21190	411
2	0.50	20	28	8.0370	4.0075	17960	355
3	0.50	20	28	8.0880	4.0370	22290	435

Table A-14. Continued

Specimen Number	W/C	RAP-3 (%)	Curing Period (days)	Average Length (in)	Average Diameter (in)	Failure Load (lbs)	Splitting Tensile Strength (psi)
1	0.50	20	90	8.1445	4.0102	24170	471
2	0.50	20	90	8.0890	4.0227	23190	454
3	0.50	20	90	8.1025	4.0205	20910	409
1	0.50	40	7	8.0430	4.0178	16450	324
2	0.50	40	7	8.0225	4.0137	18430	364
3	0.50	40	7	8.0610	4.0242	15860	311
1	0.50	40	14	8.1058	4.0143	16410	321
2	0.50	40	14	8.1260	4.0367	16760	325
3	0.50	40	14	8.1195	4.0262	16490	321
1	0.50	40	28	8.0848	4.0355	19040	372
2	0.50	40	28	8.1195	4.0128	17350	339
3	0.50	40	28	8.0045	4.0208	17210	340
1	0.50	40	90	8.0893	3.9922	19950	393
2	0.50	40	90	8.1153	4.0215	19720	385
3	0.50	40	90	8.0688	3.9945	16680	329
1	0.50	70	7	8.1430	4.0320	13100	254
2	0.50	70	7	8.0762	4.0002	13820	272
3	0.50	70	7	8.1925	4.0260	12740	246
1	0.50	70	14	8.0905	4.0173	14180	278
2	0.50	70	14	8.1040	4.0117	15110	296
3	0.50	70	14	7.9987	4.0222	13760	272
1	0.50	70	28	8.1602	4.0135	14310	278
2	0.50	70	28	8.2127	4.0147	15020	290
3	0.50	70	28	8.1817	4.0083	12830	249
1	0.50	70	90	8.0863	4.0257	14190	278
2	0.50	70	90	8.1093	4.0132	14120	276
3	0.50	70	90	8.0560	4.0157	16200	319
1	0.50	100	7	8.0685	4.0332	10510	206
2	0.50	100	7	7.9805	3.9917	10620	212
3	0.50	100	7	8.1103	4.0222	9920	194
1	0.50	100	14	8.0583	4.0068	9400	185
2	0.50	100	14	8.0620	4.0207	10260	202
3	0.50	100	14	7.9740	4.0000	11540	230
1	0.50	100	28	8.1617	4.0058	11480	224
2	0.50	100	28	8.2107	4.0200	9300	179
3	0.50	100	28	7.9795	4.0223	10200	202
1	0.50	100	90	8.0398	4.0148	12380	244
2	0.50	100	90	8.1530	4.0243	12240	237
3	0.50	100	90	8.1538	4.0427	12410	240

Table A-15. Splitting tensile strength test results for concrete containing RAP-4

Specimen Number	W/C	RAP-4 (%)	Curing Period (days)	Average Length (in)	Average Diameter (in)	Failure Load (lbs)	Splitting Tensile Strength (psi)
1	0.50	20	7	8.1220	4.0218	16830	328
2	0.50	20	7	8.0930	4.0492	18890	367
3	0.50	20	7	8.1343	4.0110	21110	412
1	0.50	20	14	8.0793	4.0132	22560	443
2	0.50	20	14	8.1065	4.0367	17700	344
3	0.50	20	14	8.0768	4.0187	19550	383
1	0.50	20	28	8.1450	4.0241	25010	486
2	0.50	20	28	8.1035	4.0120	21670	424
3	0.50	20	28	8.1118	4.0138	22600	442
1	0.50	20	90	8.1295	4.0087	24680	482
2	0.50	20	90	8.1095	4.0081	23310	457
3	0.50	20	90	8.0990	4.0330	18390	358
1	0.50	40	7	8.0185	4.0077	16490	327
2	0.50	40	7	8.1283	3.9840	14380	283
3	0.50	40	7	8.1125	3.9978	16010	314
1	0.50	40	14	8.0065	4.0257	17490	345
2	0.50	40	14	8.1768	4.0113	17460	339
3	0.50	40	14	8.0790	4.0122	19340	380
1	0.50	40	28	8.1075	4.0073	18650	365
2	0.50	40	28	8.1860	4.0105	19490	378
3	0.50	40	28	8.0655	4.0170	18850	370
1	0.50	40	90	8.1523	4.0127	16370	319
2	0.50	40	90	8.1315	4.0047	16800	328
3	0.50	40	90	8.0695	4.0017	20110	396
1	0.50	70	7	8.0915	4.0072	13420	263
2	0.50	70	7	7.9490	3.9823	10930	220
3	0.50	70	7	8.0603	4.0180	13220	260
1	0.50	70	14	8.0460	4.0218	15530	306
2	0.50	70	14	8.0367	4.0037	15800	313
3	0.50	70	14	8.0408	3.9948	14860	295
1	0.50	70	28	8.0678	4.0178	16690	328
2	0.50	70	28	8.0285	4.0005	16840	334
3	0.50	70	28	8.0180	4.0140	17500	346
1	0.50	70	90	8.0948	4.0123	15180	298
2	0.50	70	90	8.0100	4.0128	13740	272
3	0.50	70	90	8.0323	4.0138	13790	272
1	0.50	100	7	8.0425	4.0007	10320	204
2	0.50	100	7	8.0480	4.0030	12080	239
3	0.50	100	7	8.0973	4.0240	11780	230

Table A-15. Continued

Specimen Number	W/C	RAP-4 (%)	Curing Period (days)	Average Length (in)	Average Diameter (in)	Failure Load (lbs)	Splitting Tensile Strength (psi)
1	0.50	100	14	8.0595	4.0210	11700	230
2	0.50	100	14	8.1142	4.0128	12080	236
3	0.50	100	14	8.0380	4.0098	11340	224
1	0.50	100	28	8.1305	4.0003	10620	208
2	0.50	100	28	8.0503	4.0110	11630	229
3	0.50	100	28	8.0813	4.0102	11270	221
1	0.50	100	90	8.1027	4.0073	10480	205
2	0.50	100	90	8.0372	4.0157	11790	233
3	0.50	100	90	8.0058	4.0133	9540	189

Table A-16. Flexural strength test data for concrete containing no RAP

Specimen Number	W/C	RAP (%)	Curing Period (days)	Average Width (in)	Average Depth (in)	Failure Load (lbs)	Flexural Strength (psi)
1	0.45	0	7	4.0201	4.0005	3447	643
2	0.45	0	7	3.9850	4.0025	3389	637
3	0.45	0	7	4.0083	4.0020	3424	640
4	0.45	0	7	4.0175	4.0405	3930	719
5	0.45	0	7	4.0000	4.0045	3672	687
1	0.45	0	14	4.0323	4.0078	4161	771
2	0.45	0	14	3.9885	4.0148	4184	781
3	0.45	0	14	4.0870	4.0120	3640	664
4	0.45	0	14	4.0206	4.0160	4199	777
5	0.45	0	14	4.0228	4.0573	4056	735
1	0.45	0	28	3.9975	4.0316	4234	782
2	0.45	0	28	4.0800	4.0162	3559	649
3	0.45	0	28	4.0297	4.0240	4459	820
4	0.45	0	28	3.9883	4.0187	/	/
5	0.45	0	28	3.9706	4.0292	/	/
1	0.45	0	90	4.0083	4.0020	4028	753
2	0.45	0	90	4.0175	4.0405	4132	756
3	0.45	0	90	4.0000	4.0045	4009	750
4	0.45	0	90	4.0323	4.0078	/	/
5	0.45	0	90	3.9885	4.0148	/	/
1	0.50	0	7	4.0083	4.0020	3563	666
2	0.50	0	7	4.0175	4.0405	3454	632
3	0.50	0	7	4.0000	4.0045	3357	628
4	0.50	0	7	4.0323	4.0078	3222	597
5	0.50	0	7	3.9885	4.0148	/	/

Table A-16. Continued

Specimen Number	W/C	RAP (%)	Curing Period (days)	Average Width (in)	Average Depth (in)	Failure Load (lbs)	Flexural Strength (psi)
1	0.50	0	14	3.9887	4.0305	3645	675
2	0.50	0	14	4.0102	4.0108	3532	657
3	0.50	0	14	4.0063	4.0025	3337	624
4	0.50	0	14	3.9553	4.0170	3627	682
5	0.50	0	14	3.9822	4.0255	3732	694
1	0.50	0	28	4.0035	4.0150	3679	684
2	0.50	0	28	4.0160	4.0306	3686	678
3	0.50	0	28	4.0067	4.0238	3741	692
4	0.50	0	28	3.9986	4.0156	3514	654
5	0.50	0	28	3.9826	4.0145	3867	723
1	0.50	0	90	3.9880	3.9880	3677	696
2	0.50	0	90	3.9880	3.9880	3577	677
3	0.50	0	90	3.9880	3.9880	3746	709
4	0.50	0	90	/	/	/	/
5	0.50	0	90	/	/	/	/
1	0.55	0	7	4.0200	4.0200	3075	568
2	0.55	0	7	4.0195	4.0205	3297	609
3	0.55	0	7	4.0000	4.0000	3248	609
4	0.55	0	7	4.0970	4.0167	3090	561
5	0.55	0	7	4.1251	4.0161	3393	612
1	0.55	0	14	4.1145	4.0510	3618	643
2	0.55	0	14	4.1511	4.0008	3522	636
3	0.55	0	14	4.0820	4.0223	3187	579
4	0.55	0	14	4.0230	4.0381	3499	640
5	0.55	0	14	4.0085	4.0193	3502	649
1	0.55	0	28	4.0680	4.0680	4103	731
2	0.55	0	28	4.0680	4.0680	3487	622
3	0.55	0	28	4.0680	4.0680	3611	644
4	0.55	0	28	4.0680	4.0680	3703	660
1	0.55	0	90	4.0070	4.0070	3670	685
2	0.55	0	90	4.0070	4.0070	3487	650
3	0.55	0	90	4.0070	4.0070	3780	705

Table A-17. Flexural strength test data for concrete containing RAP-1

Specimen Number	W/C	RAP-1 (%)	Curing Period (days)	Average Width (in)	Average Depth (in)	Failure Load (lbs)	Flexural Strength (psi)
1	0.50	20	7	4.0205	4.0200	2741	506
2	0.50	20	7	4.0205	4.0205	2757	509
3	0.50	20	7	4.0210	4.0190	2715	502

Table A-17. Continued

Specimen Number	W/C	RAP-1 (%)	Curing Period (days)	Average Width (in)	Average Depth (in)	Failure Load (lbs)	Flexural Strength (psi)
4	0.50	20	7	4.0200	4.0200	2571	475
5	0.50	20	7	4.0195	4.0205	2635	487
1	0.50	20	14	4.0000	4.0000	3004	563
2	0.50	20	14	4.0000	4.0000	2952	554
3	0.50	20	14	4.0000	4.0000	3242	608
4	0.50	20	14	4.0000	4.0000	2510	471
5	0.50	20	14	4.0000	4.0000	2693	505
1	0.50	20	28	4.0000	4.0000	3084	578
2	0.50	20	28	4.0000	4.0000	2990	561
3	0.50	20	28	4.0000	4.0000	3022	567
4	0.50	20	28	4.0000	4.0000	2913	546
1	0.50	20	90	4.0140	4.0150	2750	510
2	0.50	20	90	4.0140	4.0150	2832	525
3	0.50	20	90	4.0140	4.0150	2824	524
4	0.50	20	90	4.0140	4.0150	2714	503
5	0.50	20	90	4.0140	4.0150	2896	537
1	0.50	40	7	4.0950	4.0950	2762	483
2	0.50	40	7	4.0950	4.0950	2729	477
3	0.50	40	7	4.0950	4.0950	2593	453
1	0.50	40	14	4.0210	4.0210	2718	502
2	0.50	40	14	4.0210	4.0210	2795	516
3	0.50	40	14	4.0210	4.0210	2636	487
4	0.50	40	14	4.0210	4.0210	3010	556
5	0.50	40	14	4.0210	4.0210	2749	507
1	0.50	40	28	4.0030	4.0030	3033	567
2	0.50	40	28	4.0030	4.0030	3102	580
3	0.50	40	28	4.0030	4.0030	3088	578
1	0.50	40	90	4.0030	4.0030	3138	587
2	0.50	40	90	4.0030	4.0030	3126	585
1	0.50	70	7	4.0115	4.0115	2060	383
2	0.50	70	7	4.0115	4.0115	1966	365
3	0.50	70	7	4.0115	4.0115	2141	398
4	0.50	70	7	4.0115	4.0115	2074	386
5	0.50	70	7	4.0115	4.0115	2035	378
1	0.50	70	14	4.0115	4.0115	2330	433
2	0.50	70	14	4.0115	4.0115	2197	408
3	0.50	70	14	4.0115	4.0115	2226	414
4	0.50	70	14	4.0115	4.0115	2270	422
5	0.50	70	14	4.0115	4.0115	2276	423
1	0.50	70	28	3.9800	3.9800	2379	453

Table A-17. Continued

Specimen Number	W/C	RAP-1 (%)	Curing Period (days)	Average Width (in)	Average Depth (in)	Failure Load (lbs)	Flexural Strength (psi)
2	0.50	70	28	3.9800	3.9800	2234	425
3	0.50	70	28	3.9800	3.9800	2520	480
4	0.50	70	28	3.9800	3.9800	2421	461
5	0.50	70	28	3.9800	3.9800	2345	446
1	0.50	70	90	3.9945	3.9945	2450	461
2	0.50	70	90	3.9945	3.9945	2742	516
3	0.50	70	90	3.9945	3.9945	2594	488
4	0.50	70	90	3.9945	3.9945	2801	527
5	0.50	70	90	3.9945	3.9945	2461	463
1	0.50	100	7	4.0275	4.0275	1567	288
2	0.50	100	7	4.0275	4.0275	1582	291
3	0.50	100	7	4.0275	4.0275	1583	291
4	0.50	100	7	4.0275	4.0275	1739	319
5	0.50	100	7	4.0275	4.0275	1724	317
1	0.50	100	14	4.0000	4.0000	1681	315
2	0.50	100	14	4.0000	4.0000	2026	380
3	0.50	100	14	4.0000	4.0000	1926	361
4	0.50	100	14	4.0000	4.0000	1693	317
5	0.50	100	14	4.0000	4.0000	/	/
1	0.50	100	28	4.0000	4.0000	2245	421
2	0.50	100	28	4.0000	4.0000	1988	373
3	0.50	100	28	4.0000	4.0000	2278	427
4	0.50	100	28	4.0000	4.0000	1905	357
5	0.50	100	28	4.0000	4.0000	/	/
1	0.50	100	90	4.0400	4.0400	2271	413
2	0.50	100	90	4.0400	4.0400	2287	416
3	0.50	100	90	4.0400	4.0400	2033	370
4	0.50	100	90	4.0400	4.0400	2323	423
5	0.50	100	90	4.0400	4.0400	2216	403

Table A-18. Flexural strength test data for concrete containing RAP-2

Specimen Number	W/C	RAP-2 (%)	Curing Period (days)	Average Width (in)	Average Depth (in)	Failure Load (lbs)	Flexural Strength (psi)
1	0.50	20	7	/	/	/	/
2	0.50	20	7	4.0330	4.0330	2700	494
3	0.50	20	7	4.0330	4.0330	2951	540
1	0.50	20	14	4.0700	4.0700	3413	607
2	0.50	20	14	4.0700	4.0700	3297	587
3	0.50	20	14	4.0700	4.0700	3367	599

Table A-18. Continued

Specimen Number	W/C	RAP-2 (%)	Curing Period (days)	Average Width (in)	Average Depth (in)	Failure Load (lbs)	Flexural Strength (psi)
1	0.50	20	28	4.0340	4.0252	3177	583
2	0.50	20	28	4.0057	4.0208	3225	598
3	0.50	20	28	3.9808	4.0337	3067	568
1	0.50	20	90	3.9293	4.0058	3572	680
2	0.50	20	90	4.0633	4.0178	3215	588
3	0.50	20	90	4.1113	4.0238	3498	631
1	0.50	40	7	4.0620	4.0620	2666	477
2	0.50	40	7	4.0620	4.0620	2573	461
3	0.50	40	7	4.0620	4.0620	2552	457
1	0.50	40	14	4.0450	4.0450	2663	483
2	0.50	40	14	4.0450	4.0450	2805	509
3	0.50	40	14	4.0450	4.0450	2509	455
1	0.50	40	28	4.0513	4.1100	2878	505
2	0.50	40	28	4.0312	4.1640	3201	550
3	0.50	40	28	4.0067	4.0330	2697	497
1	0.50	40	90	4.0550	4.0275	2850	520
2	0.50	40	90	4.0865	4.0063	2919	534
1	0.50	70	7	4.0830	4.0830	1996	352
2	0.50	70	7	4.0830	4.0830	2199	388
3	0.50	70	7	4.0830	4.0830	2272	401
1	0.50	70	14	4.0223	4.0392	2082	381
2	0.50	70	14	4.1100	4.0128	2088	379
3	0.50	70	14	4.0222	4.1655	2291	394
1	0.50	70	28	3.9750	4.0117	2162	406
2	0.50	70	28	4.1203	3.9990	2250	410
3	0.50	70	28	4.0535	4.1382	2401	415
1	0.50	70	90	4.0228	4.0068	2343	435
2	0.50	70	90	4.0768	4.0303	2335	423
3	0.50	70	90	4.1492	4.0327	2157	384
1	0.50	100	7	4.0460	4.0460	1858	337
2	0.50	100	7	4.0460	4.0460	1830	332
1	0.50	100	14	4.0400	4.1082	2117	373
2	0.50	100	14	4.0476	4.0410	1952	354
3	0.50	100	14	4.0867	4.0100	1959	358
1	0.50	100	28	4.0587	3.9953	1967	364
2	0.50	100	28	4.0405	4.0153	2031	374
3	0.50	100	28	4.0350	4.0443	2045	372
1	0.50	100	90	4.0727	4.0283	2108	383
2	0.50	100	90	4.1205	4.0477	2033	361
3	0.50	100	90	4.0633	4.0378	2000	362

Table A-19. Flexural strength test data for concrete containing RAP-3

Specimen Number	W/C	RAP-3 (%)	Curing Period (days)	Average Width (in)	Average Depth (in)	Failure Load (lbs)	Flexural Strength (psi)
1	0.50	20	7	4.0997	4.0202	2860	518
2	0.50	20	7	4.0997	4.0053	3015	550
3	0.50	20	7	4.0350	4.0223	2759	507
1	0.50	20	14	4.1565	4.0470	3075	542
2	0.50	20	14	4.0353	4.0306	2825	517
3	0.50	20	14	4.1038	4.0196	2987	541
1	0.50	20	28	4.1090	4.0086	3153	573
2	0.50	20	28	4.0570	4.0448	2870	519
3	0.50	20	28	4.0970	4.0167	3400	617
1	0.50	20	90	4.1251	4.0161	3237	584
2	0.50	20	90	4.1145	4.0510	3479	618
3	0.50	20	90	4.1511	4.0008	3214	580
1	0.50	40	7	4.0820	4.0223	2572	467
2	0.50	40	7	4.0230	4.0381	2570	470
3	0.50	40	7	4.0421	4.0185	2596	477
1	0.50	40	14	4.0538	4.0148	2617	481
2	0.50	40	14	4.0023	4.0230	2483	460
3	0.50	40	14	4.0455	4.0258	2606	477
1	0.50	40	28	4.0173	4.0183	2639	488
2	0.50	40	28	4.0580	4.0088	2558	471
3	0.50	40	28	4.0462	4.0247	2600	476
1	0.50	40	90	4.0361	3.9993	2717	505
2	0.50	40	90	3.9990	4.0371	2696	496
3	0.50	40	90	4.0376	4.0366	2990	545
1	0.50	70	7	4.0885	4.0031	2297	421
2	0.50	70	7	4.0915	4.0266	2292	415
3	0.50	70	7	4.0241	4.0001	2100	391
1	0.50	70	14	4.0213	4.0338	2119	389
2	0.50	70	14	4.0882	4.0650	2263	402
3	0.50	70	14	4.0276	4.0793	2100	376
1	0.50	70	28	4.0282	4.0087	2179	404
2	0.50	70	28	4.0323	4.0078	2049	380
3	0.50	70	28	3.9885	4.0148	2010	375
1	0.50	70	90	4.0870	4.0120	2444	446
2	0.50	70	90	4.0206	4.0160	2370	439
3	0.50	70	90	4.0228	4.0573	2422	439
1	0.50	100	7	3.9975	4.0316	1723	318
2	0.50	100	7	4.0800	4.0162	1729	315
3	0.50	100	7	4.0297	4.0240	1810	333
1	0.50	100	14	3.9883	4.0187	1661	309

Table A-19. Continued

Specimen Number	W/C	RAP-3 (%)	Curing Period (days)	Average Width (in)	Average Depth (in)	Failure Load (lbs)	Flexural Strength (psi)
2	0.50	100	14	3.9706	4.0292	1836	342
3	0.50	100	14	4.0105	4.0297	1741	321
1	0.50	100	28	3.9790	4.0063	1746	328
2	0.50	100	28	3.9732	4.0057	1804	340
3	0.50	100	28	4.0083	4.0175	1934	359
1	0.50	100	90	3.9960	4.0245	1886	350
2	0.50	100	90	4.0518	4.0245	2020	369
3	0.50	100	90	/	/	/	/

Table A-20. Flexural strength test data for concrete containing RAP-4

Specimen Number	W/C	RAP-4 (%)	Curing Period (days)	Average Width (in)	Average Depth (in)	Failure Load (lbs)	Flexural Strength (psi)
1	0.50	20	7	4.1211	4.0300	3144	564
2	0.50	20	7	4.0596	4.0391	3186	577
3	0.50	20	7	4.0815	4.0171	3023	551
1	0.50	20	14	4.0151	4.0045	3054	569
2	0.50	20	14	4.0305	4.0110	2913	539
3	0.50	20	14	4.0873	4.0240	3000	544
1	0.50	20	28	4.0760	4.0210	3346	609
2	0.50	20	28	4.0358	4.0236	3243	596
3	0.50	20	28	4.0125	4.0031	3139	586
1	0.50	20	90	4.0408	4.0190	3493	642
2	0.50	20	90	4.1495	4.0072	3270	589
3	0.50	20	90	4.0778	4.0283	3448	625
1	0.50	40	7	4.0768	4.0203	2647	482
2	0.50	40	7	4.0508	4.0065	2320	428
3	0.50	40	7	4.0396	4.0341	2555	466
1	0.50	40	14	4.0650	4.0135	2590	475
2	0.50	40	14	3.9986	4.0020	2714	509
3	0.50	40	14	4.0416	4.0165	2210	407
1	0.50	40	28	4.0058	4.0596	2889	525
2	0.50	40	28	4.0870	4.0221	2869	521
3	0.50	40	28	4.0486	3.9970	2674	496
1	0.50	40	90	4.0242	4.0228	2950	544
2	0.50	40	90	4.0482	4.0363	3177	578
3	0.50	40	90	4.0635	4.0132	2913	534
1	0.50	70	7	4.0461	4.0123	1972	363
2	0.50	70	7	4.0908	4.0140	1973	359
3	0.50	70	7	4.0785	4.0213	2092	381

Table A-20. Continued

Specimen Number	W/C	RAP-4 (%)	Curing Period (days)	Average Width (in)	Average Depth (in)	Failure Load (lbs)	Flexural Strength (psi)
1	0.50	70	14	4.0570	4.0170	2166	397
2	0.50	70	14	4.0108	4.0136	2255	419
3	0.50	70	14	4.0905	4.0735	2330	412
1	0.50	70	28	4.0778	4.0268	2267	411
2	0.50	70	28	4.0525	4.0150	2405	442
3	0.50	70	28	4.0547	4.0155	2352	432
1	0.50	70	90	4.0268	4.0090	2515	466
2	0.50	70	90	4.0645	4.0442	2713	490
3	0.50	70	90	4.0085	4.0193	2502	464
1	0.50	100	7	4.0333	4.0246	2078	382
2	0.50	100	7	4.1691	4.0155	1875	335
3	0.50	100	7	4.0100	4.0280	1899	350
1	0.50	100	14	4.0146	4.0463	1890	345
2	0.50	100	14	4.0496	4.0253	1994	365
3	0.50	100	14	4.0700	4.0130	1927	353
1	0.50	100	28	4.0693	4.0110	1992	365
2	0.50	100	28	4.0385	4.0405	1868	340
3	0.50	100	28	4.0892	4.0078	2011	367
1	0.50	100	90	4.0425	4.0037	2128	394
2	0.50	100	90	4.0067	4.0000	2221	416
3	0.50	100	90	4.0347	4.0000	2343	436

Table A-21. Modulus of toughness data for concrete containing no RAP

Specimen Number	W/C	RAP (%)	Curing Period (days)	Modulus of Toughness (lb-in/in <sup>3</sup> )
1	0.45	0	28	0.07
2	0.45	0	28	0.18
1	0.45	0	90	0.08
2	0.45	0	90	0.07
3	0.45	0	90	0.08
1	0.50	0	28	0.25
2	0.50	0	28	0.10
1	0.50	0	90	0.11
2	0.50	0	90	0.24
3	0.50	0	90	0.08
4	0.50	0	90	0.06
5	0.50	0	90	/
1	0.55	0	28	0.21
2	0.55	0	28	0.16

Table A-21. Continued

Specimen Number	W/C	RAP (%)	Curing Period (days)	Modulus of Toughness (lb-in/in <sup>3</sup> )
1	0.55	0	90	0.06
2	0.55	0	90	0.05
3	0.55	0	90	0.06

Table A-22. Modulus of toughness data for concrete containing RAP-1

Specimen Number	W/C	RAP-1 (%)	Curing Period (days)	Modulus of Toughness (lb-in/in <sup>3</sup> )
1	0.50	20	90	0.22
2	0.50	20	90	0.28
3	0.50	20	90	0.30
4	0.50	20	90	0.26
5	0.50	20	90	/
1	0.50	40	90	0.36
2	0.50	40	09	0.36
3	0.50	40	90	0.53
4	0.50	40	90	/
5	0.50	40	90	/
1	0.50	70	90	0.63
2	0.50	70	90	0.50
3	0.50	70	90	0.62
4	0.50	70	90	0.46
5	0.50	70	90	/
1	0.50	100	90	0.66
2	0.50	100	90	0.72
3	0.50	100	90	0.82
4	0.50	100	90	0.83
5	0.50	100	90	/

Table A-23. Modulus of toughness data for concrete containing RAP-2

Specimen Number	W/C	RAP-2 (%)	Curing Period (days)	Modulus of Toughness (lb-in/in <sup>3</sup> )
1	0.50	20	7	0.15
2	0.50	20	7	0.26
3	0.50	20	7	/
1	0.50	20	14	0.33
2	0.50	20	14	0.19
3	0.50	20	14	/

Table A-23. Continued

Specimen Number	W/C	RAP-2 (%)	Curing Period (days)	Modulus of Toughness (lb-in/in <sup>3</sup> )
1	0.50	20	28	0.10
2	0.50	20	28	0.26
3	0.50	20	28	0.17
1	0.50	20	90	0.29
2	0.50	20	90	0.24
3	0.50	20	90	/
1	0.50	40	7	0.33
2	0.50	40	7	0.18
3	0.50	40	7	0.18
1	0.50	40	14	0.35
2	0.50	40	14	0.25
3	0.50	40	14	0.31
1	0.50	40	28	0.32
2	0.50	40	28	0.37
3	0.50	40	28	0.30
1	0.50	40	90	0.24
2	0.50	40	90	0.44
3	0.50	40	90	0.31
1	0.50	70	7	0.66
2	0.50	70	7	0.70
3	0.50	70	7	/
1	0.50	70	14	0.55
2	0.50	70	14	0.60
3	0.50	70	14	/
1	0.50	70	28	/
2	0.50	70	28	0.60
3	0.50	70	28	0.24
1	0.50	70	90	0.38
2	0.50	70	90	0.59
3	0.50	70	90	0.29
1	0.50	100	7	0.47
1	0.50	100	14	0.77
2	0.50	100	14	0.97
3	0.50	100	14	0.52
1	0.50	100	28	0.98
2	0.50	100	28	0.55

Table A-23. Continued

Specimen Number	W/C	RAP-2 (%)	Curing Period (days)	Modulus of Toughness (lb-in/in <sup>3</sup> )
3	0.50	100	28	0.68
1	0.50	100	90	0.65
2	0.50	100	90	0.69
3	0.50	100	90	/

Table A-24. Modulus of toughness data for concrete containing RAP-3

Specimen Number	W/C	RAP-3 (%)	Curing Period (days)	Modulus of Toughness (lb-in/in <sup>3</sup> )
1	0.50	20	7	0.23
2	0.50	20	7	0.29
3	0.50	20	7	0.27
1	0.50	20	14	0.36
2	0.50	20	14	0.10
3	0.50	20	14	0.16
1	0.50	20	28	0.31
2	0.50	20	28	0.21
3	0.50	20	28	/
1	0.50	20	90	0.34
2	0.50	20	90	0.29
3	0.50	20	90	/
1	0.50	40	7	0.40
2	0.50	40	7	0.40
3	0.50	40	7	0.45
1	0.50	40	14	0.36
2	0.50	40	14	0.37
3	0.50	40	14	0.46
1	0.50	40	28	0.23
2	0.50	40	28	0.43
3	0.50	40	28	0.12
1	0.50	40	90	0.34
2	0.50	40	90	0.49
3	0.50	40	90	0.51
1	0.50	70	7	0.62
2	0.50	70	7	0.51
3	0.50	70	7	/
1	0.50	70	14	0.64

Table A-24. Continued

Specimen Number	W/C	RAP-3 (%)	Curing Period (days)	Modulus of Toughness (lb-in/in <sup>3</sup> )
2	0.50	70	14	0.22
3	0.50	70	14	/
1	0.50	70	28	0.46
2	0.50	70	28	0.38
3	0.50	70	28	0.16
1	0.50	70	90	0.46
2	0.50	70	90	0.41
3	0.50	70	90	0.57
1	0.50	100	7	1.03
2	0.50	100	7	/
3	0.50	100	7	/
1	0.50	100	14	0.33
2	0.50	100	14	0.50
3	0.50	100	14	0.69
1	0.50	100	28	1.00
2	0.50	100	28	0.92
3	0.50	100	28	0.14
1	0.50	100	90	0.56
2	0.50	100	90	0.40
3	0.50	100	90	/

Table A-25. Modulus of toughness data for concrete containing RAP-4

Specimen Number	W/C	RAP-4 (%)	Curing Period (days)	Modulus of Toughness (lb-in/in <sup>3</sup> )
1	0.50	20	7	0.18
2	0.50	20	7	0.18
3	0.50	20	7	/
1	0.50	20	14	0.13
2	0.50	20	14	0.35
3	0.50	20	14	0.38
1	0.50	20	28	0.24
2	0.50	20	28	0.44
3	0.50	20	28	0.25
1	0.50	20	90	0.26
2	0.50	20	90	0.17
3	0.50	20	90	0.35

Table A-25. Continued

Specimen Number	W/C	RAP-4 (%)	Curing Period (days)	Modulus of Toughness (lb-in/in <sup>3</sup> )
1	0.50	40	7	0.19
2	0.50	40	7	0.33
3	0.50	40	7	/
1	0.50	40	14	0.25
2	0.50	40	14	0.19
3	0.50	40	14	0.20
1	0.50	40	28	0.42
2	0.50	40	28	0.43
3	0.50	40	28	/
1	0.50	40	90	0.29
2	0.50	40	90	0.54
3	0.50	40	90	0.38
1	0.50	70	7	0.54
2	0.50	70	7	0.48
3	0.50	70	7	0.34
1	0.50	70	14	0.38
2	0.50	70	14	0.47
3	0.50	70	14	0.49
1	0.50	70	28	0.35
2	0.50	70	28	0.73
3	0.50	70	28	0.43
1	0.50	70	90	0.31
2	0.50	70	90	0.46
3	0.50	70	90	0.30
1	0.50	100	7	0.58
2	0.50	100	7	0.57
3	0.50	100	7	0.11
1	0.50	100	14	/
2	0.50	100	14	0.43
3	0.50	100	14	0.40
1	0.50	100	28	0.84
2	0.50	100	28	0.57
3	0.50	100	28	0.79
1	0.50	100	90	0.53
2	0.50	100	90	0.66
3	0.50	100	90	0.63

Table A-26. Shrinkage test data for concrete containing no RAP after air curing

Specimen Number	W/C	RAP (%)	Curing Period (days)	Shrinkage Strain ( $10^{-6}$ )
1	0.45	0	7	30
2	0.45	0	7	50
3	0.45	0	7	80
1	0.45	0	14	240
2	0.45	0	14	300
3	0.45	0	14	320
1	0.45	0	28	260
2	0.45	0	28	180
3	0.46	0	28	300
1	0.45	0	90	430
2	0.45	0	90	360
3	0.45	0	90	490
1	0.50	0	7	290
2	0.50	0	7	130
3	0.50	0	7	130
1	0.50	0	14	240
2	0.50	0	14	310
3	0.50	0	14	180
1	0.50	0	28	290
2	0.50	0	28	260
3	0.50	0	28	240
1	0.50	0	90	320
2	0.50	0	90	220
1	0.55	0	7	100
2	0.55	0	7	20
3	0.55	0	7	120
1	0.55	0	14	100
2	0.55	0	14	80
3	0.55	0	14	40
1	0.55	0	28	170
2	0.55	0	28	50
3	0.55	0	28	60
1	0.55	0	90	310
2	0.55	0	90	230
3	0.55	0	90	190

Table A-27. Shrinkage test data for concrete containing RAP-1 after air curing

Specimen Number	W/C	RAP-1 (%)	Curing Period (days)	Shrinkage Strain ( $10^{-6}$ )
1	0.50	20	7	90
2	0.50	20	7	90
3	0.50	20	7	120
1	0.50	20	14	170
2	0.50	20	14	170
3	0.50	20	14	170
1	0.50	20	28	270
2	0.50	20	28	220
3	0.50	20	28	210
1	0.50	20	90	490
2	0.50	20	90	520
3	0.50	20	90	500
1	0.50	40	7	120
2	0.50	40	7	50
3	0.50	40	7	0
1	0.50	40	14	220
2	0.50	40	14	130
3	0.50	40	14	70
1	0.50	40	28	340
2	0.50	40	28	240
3	0.50	40	28	200
1	0.50	40	90	520
2	0.50	40	90	460
3	0.50	40	90	370
1	0.50	70	7	80
2	0.50	70	7	100
3	0.50	70	7	50
1	0.50	70	14	40
2	0.50	70	14	130
3	0.50	70	14	100
1	0.50	70	28	140
2	0.50	70	28	320
3	0.50	70	28	220
1	0.50	70	90	490
2	0.50	70	90	490
3	0.50	70	90	500
1	0.50	100	7	170

Table A-27. Continued

Specimen Number	W/C	RAP-1 (%)	Curing Period (days)	Shrinkage Strain ( $10^{-6}$ )
2	0.50	100	7	200
3	0.50	100	7	190
1	0.50	100	14	280
2	0.50	100	14	320
3	0.50	100	14	320
1	0.50	100	28	500
2	0.50	100	28	540
3	0.50	100	28	540
1	0.50	100	90	880
2	0.50	100	90	930
3	0.50	100	90	520

Table A-28. Shrinkage test data for concrete containing RAP-2 after air curing

Specimen Number	W/C	RAP-2 (%)	Curing Period (days)	Shrinkage Strain ( $10^{-6}$ )
1	0.50	20	7	110
2	0.50	20	7	180
3	0.50	20	7	57
1	0.50	20	14	290
2	0.50	20	14	350
3	0.50	20	14	235
1	0.50	20	28	270
2	0.50	20	28	265
3	0.50	20	28	210
1	0.50	20	90	420
2	0.50	20	90	400
3	0.50	20	90	340
1	0.50	40	7	230
2	0.50	40	7	160
3	0.50	40	7	210
1	0.50	40	14	320
2	0.50	40	14	230
3	0.50	40	14	320
1	0.50	40	28	240
2	0.50	40	28	140
3	0.50	40	28	220
1	0.50	40	90	400

Table A-28. Continued

Specimen Number	W/C	RAP-2 (%)	Curing Period (days)	Shrinkage Strain ( $10^{-6}$ )
2	0.50	40	90	310
3	0.50	40	90	390
1	0.50	70	7	140
2	0.50	70	7	140
3	0.50	70	7	140
1	0.50	70	14	0
2	0.50	70	14	20
3	0.50	70	14	30
1	0.50	70	28	210
2	0.50	70	28	260
3	0.50	70	28	240
1	0.50	70	90	430
2	0.50	70	90	480
3	0.50	70	90	460
1	0.50	100	7	190
2	0.50	100	7	0
3	0.50	100	7	0
1	0.50	100	14	310
2	0.50	100	14	110
3	0.50	100	14	140
1	0.50	100	28	500
2	0.50	100	28	300
3	0.50	100	28	260
1	0.50	100	90	830
2	0.50	100	90	650
3	0.50	100	90	550

Table A-29. Shrinkage test data for concrete containing RAP-3 after air curing

Specimen Number	W/C	RAP-3 (%)	Curing Period (days)	Shrinkage Strain ( $10^{-6}$ )
1	0.50	20	7	140
2	0.50	20	7	110
3	0.50	20	7	120
1	0.50	20	14	240
2	0.50	20	14	220
3	0.50	20	14	200
1	0.50	20	28	360

Table A-29. Continued

Specimen Number	W/C	RAP-3 (%)	Curing Period (days)	Shrinkage Strain ( $10^{-6}$ )
2	0.50	20	28	350
3	0.50	20	28	300
1	0.50	20	90	480
2	0.50	20	90	510
3	0.50	20	90	440
1	0.50	40	7	180
2	0.50	40	7	190
3	0.50	40	7	140
1	0.50	40	14	300
2	0.50	40	14	290
3	0.50	40	14	250
1	0.50	40	28	430
2	0.50	40	28	400
3	0.50	40	28	360
1	0.50	40	90	580
2	0.50	40	90	500
3	0.50	40	90	450
1	0.50	70	7	210
2	0.50	70	7	180
3	0.50	70	7	240
1	0.50	70	14	350
2	0.50	70	14	350
3	0.50	70	14	370
1	0.50	70	28	500
2	0.50	70	28	510
3	0.50	70	28	520
1	0.50	70	90	670
2	0.50	70	90	710
3	0.50	70	90	740
1	0.50	100	7	280
2	0.50	100	7	260
3	0.50	100	7	290
1	0.50	100	14	420
2	0.50	100	14	460
3	0.50	100	14	460
1	0.50	100	28	630
2	0.50	100	28	700

Table A-29. Continued

Specimen Number	W/C	RAP-1 (%)	Curing Period (days)	Shrinkage Strain ( $10^{-6}$ )
3	0.50	100	28	660
1	0.50	100	90	810
2	0.50	100	90	920
3	0.50	100	90	880

Table A-30. Shrinkage test data for concrete containing RAP-4 after air curing

Specimen Number	W/C	RAP-4 (%)	Curing Period (days)	Shrinkage Strain ( $10^{-6}$ )
1	0.50	20	7	145
2	0.50	20	7	120
3	0.50	20	7	130
1	0.50	20	14	290
2	0.50	20	14	240
3	0.50	20	14	270
1	0.50	20	28	410
2	0.50	20	28	310
3	0.50	20	28	370
1	0.50	20	90	480
2	0.50	20	90	360
3	0.50	20	90	450
1	0.50	40	7	160
2	0.50	40	7	200
3	0.50	40	7	150
1	0.50	40	14	320
2	0.50	40	14	360
3	0.50	40	14	260
1	0.50	40	28	500
2	0.50	40	28	510
3	0.50	40	28	410
1	0.50	40	90	630
2	0.50	40	90	650
3	0.50	40	90	520
1	0.50	70	7	170
2	0.50	70	7	180
3	0.50	70	7	180
1	0.50	70	14	300
2	0.50	70	14	340

Table A-30. Continued

Specimen Number	W/C	RAP-4 (%)	Curing Period (days)	Shrinkage Strain ( $10^{-6}$ )
3	0.50	70	14	340
1	0.50	70	28	430
2	0.50	70	28	460
3	0.50	70	28	450
1	0.50	70	90	650
2	0.50	70	90	650
3	0.50	70	90	630
1	0.50	100	7	370
2	0.50	100	7	380
3	0.50	100	7	330
1	0.50	100	14	600
2	0.50	100	14	610
3	0.50	100	14	560
1	0.50	100	28	860
2	0.50	100	28	840
3	0.50	100	28	820
1	0.50	100	90	1170
2	0.50	100	90	1150
3	0.50	100	90	1160

Table A-31. Shrinkage test data for concrete containing no RAP after moist curing

Specimen Number	W/C	RAP (%)	Curing Period (days)	Shrinkage Strain ( $10^{-6}$ )
1	0.45	0	7	-50
2	0.45	0	7	30
3	0.45	0	7	70
1	0.45	0	14	120
2	0.45	0	14	70
3	0.45	0	14	-90
1	0.45	0	28	-20
2	0.45	0	28	-30
3	0.45	0	28	-80
1	0.45	0	90	30
2	0.45	0	90	-30
3	0.45	0	90	-50
1	0.50	0	7	130
3	0.50	0	7	70
3	0.50	0	7	70

Table A-31. Continued

Specimen Number	W/C	RAP (%)	Curing Period (days)	Shrinkage Strain ( $10^{-6}$ )
1	0.50	0	14	60
2	0.50	0	14	-60
3	0.50	0	14	20
1	0.50	0	28	40
2	0.50	0	28	-120
3	0.50	0	28	-70
1	0.50	0	90	-10
2	0.50	0	90	-110
3	0.50	0	90	-60
1	0.55	0	7	100
2	0.55	0	7	70
3	0.55	0	7	-20
1	0.55	0	14	-30
2	0.55	0	14	-110
3	0.55	0	14	-190
1	0.55	0	28	-40
2	0.55	0	28	-150
3	0.55	0	28	-240
1	0.55	0	90	20
2	0.55	0	90	-130
3	0.55	0	90	-160

Table A-32. Shrinkage test data for concrete containing RAP-1 after moist curing

Specimen Number	W/C	RAP-1 (%)	Curing Period (days)	Shrinkage Strain ( $10^{-6}$ )
1	0.50	20	7	-20
2	0.50	20	7	-90
3	0.50	20	7	/
1	0.50	20	14	-30
2	0.50	20	14	-80
3	0.50	20	14	/
1	0.50	20	28	-50
2	0.50	20	28	-110
3	0.50	20	28	/
1	0.50	20	90	90
2	0.50	20	90	0
3	0.50	20	90	/

Table A-32. Continued

Specimen Number	W/C	RAP-1 (%)	Curing Period (days)	Shrinkage Strain ( $10^{-6}$ )
1	0.50	40	7	-150
2	0.50	40	7	-80
3	0.50	40	7	-70
1	0.50	40	14	-200
2	0.50	40	14	-80
3	0.50	40	14	-80
1	0.50	40	28	-150
2	0.50	40	28	-40
3	0.50	40	28	-60
1	0.50	40	90	-120
2	0.50	40	90	-10
3	0.50	40	90	-90
1	0.50	70	7	-189
2	0.50	70	7	-300
3	0.50	70	7	-290
1	0.50	70	14	-180
2	0.50	70	14	-270
3	0.50	70	14	-260
1	0.50	70	28	-240
2	0.50	70	28	-330
3	0.50	70	28	-340
1	0.50	70	90	-120
2	0.50	70	90	-260
3	0.50	70	90	-290
1	0.50	100	7	-100
2	0.50	100	7	-160
3	0.50	100	7	-140
1	0.50	100	14	-160
2	0.50	100	14	-210
3	0.50	100	14	-220
1	0.50	100	28	-160
2	0.50	100	28	-230
3	0.50	100	28	-220
1	0.50	100	90	-210
2	0.50	100	90	-240
3	0.50	100	90	-280

Table A-33. Shrinkage test data for concrete containing RAP-2 after moist curing

Specimen Number	W/C	RAP-2 (%)	Curing Period (days)	Shrinkage Strain ( $10^{-6}$ )
1	0.50	20	7	170
2	0.50	20	7	150
3	0.50	20	7	90
1	0.50	20	14	190
2	0.50	20	14	270
3	0.50	20	14	170
1	0.50	20	28	-40
2	0.50	20	28	40
3	0.50	20	28	-50
1	0.50	20	90	-30
2	0.50	20	90	-20
3	0.50	20	90	-30
1	0.50	40	7	30
2	0.50	40	7	60
3	0.50	40	7	/
1	0.50	40	14	70
2	0.50	40	14	70
3	0.50	40	14	0
1	0.50	40	28	-100
2	0.50	40	28	-120
3	0.50	40	28	-220
1	0.50	40	90	-150
2	0.50	40	90	-170
3	0.50	40	90	-220
1	0.50	70	7	/
2	0.50	70	7	-50
3	0.50	70	7	-10
1	0.50	70	14	-170
2	0.50	70	14	-320
3	0.50	70	14	-290
1	0.50	70	28	-160
2	0.50	70	28	-320
3	0.50	70	28	-290
1	0.50	70	90	-150
2	0.50	70	90	-320
3	0.50	70	90	-300

Table A-33. Continued

Specimen Number	W/C	RAP-2 (%)	Curing Period (days)	Shrinkage Strain ( $10^{-6}$ )
1	0.50	100	7	-320
2	0.50	100	7	-290
3	0.50	100	7	-330
1	0.50	100	14	-300
2	0.50	100	14	-270
3	0.50	100	14	-310
1	0.50	100	28	-340
2	0.50	100	28	-300
3	0.50	100	28	-330
1	0.50	100	90	-350
2	0.50	100	90	-290
3	0.50	100	90	-330

Table A-34. Shrinkage test data for concrete containing RAP-3 after moist curing

Specimen Number	W/C	RAP-3 (%)	Curing Period (days)	Shrinkage Strain ( $10^{-6}$ )
1	0.50	20	7	-60
2	0.50	20	7	-80
3	0.50	20	7	-10
1	0.50	20	14	-50
2	0.50	20	14	-70
3	0.50	20	14	-10
1	0.50	20	28	-60
2	0.50	20	28	-90
3	0.50	20	28	-20
1	0.50	20	90	-10
2	0.50	20	90	-40
3	0.50	20	90	/
1	0.50	40	7	-10
2	0.50	40	7	-90
3	0.50	40	7	/
1	0.50	40	14	-10
2	0.50	40	14	-70
3	0.50	40	14	/
1	0.50	40	28	-20
2	0.50	40	28	-70
3	0.50	40	28	/

Table A-34. Continued

Specimen Number	W/C	RAP-3 (%)	Curing Period (days)	Shrinkage Strain ( $10^{-6}$ )
1	0.50	40	90	-30
2	0.50	40	90	-100
3	0.50	40	90	/
1	0.50	70	7	-70
2	0.50	70	7	-160
3	0.50	70	7	-40
1	0.50	70	14	-90
2	0.50	70	14	-180
3	0.50	70	14	-60
1	0.50	70	28	-60
2	0.50	70	28	-150
3	0.50	70	28	-80
1	0.50	70	90	-60
2	0.50	70	90	-140
3	0.50	70	90	-60
1	0.50	100	7	-20
2	0.50	100	7	-20
3	0.50	100	7	-10
1	0.50	100	14	-40
2	0.50	100	14	-10
3	0.50	100	14	-30
1	0.50	100	28	-30
2	0.50	100	28	-20
3	0.50	100	28	-50
1	0.50	100	90	-60
2	0.50	100	90	-20
3	0.50	100	90	-20

Table A-35. Shrinkage test data for concrete containing RAP-4 after moist curing

Specimen Number	W/C	RAP-4 (%)	Curing Period (days)	Shrinkage Strain ( $10^{-6}$ )
1	0.50	20	7	-50
2	0.50	20	7	-100
3	0.50	20	7	-30
1	0.50	20	14	-30
2	0.50	20	14	-40
3	0.50	20	14	-30

Table A-35. Continued

Specimen Number	W/C	RAP-4 (%)	Curing Period (days)	Shrinkage Strain ( $10^{-6}$ )
1	0.50	20	28	-30
2	0.50	20	28	-60
3	0.50	20	28	0
1	0.50	20	90	-60
2	0.50	20	90	-80
3	0.50	20	90	-20
1	0.50	40	7	-150
2	0.50	40	7	-70
3	0.50	40	7	-140
1	0.50	40	14	-140
2	0.50	40	14	-20
3	0.50	40	14	-100
1	0.50	40	28	-100
2	0.50	40	28	30
3	0.50	40	28	-70
1	0.50	40	90	-120
2	0.50	40	90	0
3	0.50	40	90	-90
1	0.50	70	7	-80
2	0.50	70	7	-80
3	0.50	70	7	-60
1	0.50	70	14	-40
2	0.50	70	14	-80
3	0.50	70	14	-20
1	0.50	70	28	-30
2	0.50	70	28	-90
3	0.50	70	28	-50
1	0.50	70	90	-60
2	0.50	70	90	-90
3	0.50	70	90	-60
1	0.50	100	7	40
2	0.50	100	7	50
3	0.50	100	7	20
1	0.50	100	14	30
2	0.50	100	14	0
3	0.50	100	14	-30
1	0.50	100	28	10

Table A-35. Continued

Specimen Number	W/C	RAP-4 (%)	Curing Period (days)	Shrinkage Strain ( $10^{-6}$ )
2	0.50	100	28	-20
3	0.50	100	28	-50
1	0.50	100	90	-20
2	0.50	100	90	-20
3	0.50	100	90	-50

Table A-36. Coefficient of thermal expansion test data for concrete containing no RAP

Specimen Number	W/C	RAP (%)	Curing Period (days)	Coefficient of Thermal Expansion ( $10^{-6}$ in/in/ $^{\circ}$ F)
1	0.45	0	7	4.75
2	0.45	0	7	4.46
3	0.45	0	7	4.48
1	0.45	0	14	5.04
2	0.45	0	14	4.68
3	0.45	0	14	/
1	0.45	0	28	4.67
2	0.45	0	28	5.01
3	0.45	0	28	/
1	0.45	0	90	3.92
2	0.45	0	90	3.32
3	0.45	0	90	/
1	0.50	0	7	4.42
2	0.50	0	7	4.64
3	0.50	0	7	4.85
1	0.50	0	14	3.54
2	0.50	0	14	3.82
3	0.50	0	14	/
1	0.50	0	28	4.40
2	0.50	0	28	4.30
3	0.50	0	28	/
1	0.50	0	90	4.00
2	0.50	0	90	4.08
3	0.50	0	90	/
1	0.55	0	7	/
2	0.55	0	7	/
3	0.55	0	7	/

Table A-36. Continued

Specimen Number	W/C	RAP (%)	Curing Period (days)	Coefficient of Thermal Expansion ( $10^{-6}$ in/in/°F)
1	0.55	0	14	4.74
2	0.55	0	14	4.30
3	0.55	0	14	/
1	0.55	0	28	4.40
2	0.55	0	28	3.53
3	0.55	0	28	/
1	0.55	0	90	3.80
2	0.55	0	90	3.14
3	0.55	0	90	/

Table A-37. Coefficient of thermal expansion test data for concrete containing RAP-1

Specimen Number	W/C	RAP-1 (%)	Curing Period (days)	Coefficient of Thermal Expansion ( $10^{-6}$ in/in/°F)
1	0.50	20	7	5.08
2	0.50	20	7	4.67
3	0.50	20	7	/
1	0.50	20	14	5.23
2	0.50	20	14	4.76
3	0.50	20	14	/
1	0.50	20	28	5.04
2	0.50	20	28	4.74
3	0.50	20	28	/
1	0.50	20	90	4.89
2	0.50	20	90	4.86
3	0.50	20	90	/
1	0.50	40	7	4.86
2	0.50	40	7	4.88
3	0.50	40	7	/
1	0.50	40	14	4.85
2	0.50	40	14	4.84
3	0.50	40	14	/
1	0.50	40	28	4.99
2	0.50	40	28	4.70
3	0.50	40	28	/

Table A-37. Continued

Specimen Number	W/C	RAP-1 (%)	Curing Period (days)	Coefficient of Thermal Expansion ( $10^{-6}$ in/in/°F)
1	0.50	40	90	5.00
2	0.50	40	90	4.60
3	0.50	40	90	/
1	0.50	70	7	5.22
2	0.50	70	7	5.32
3	0.50	70	7	/
1	0.50	70	14	4.98
2	0.50	70	14	4.88
3	0.50	70	14	/
1	0.50	70	28	5.64
2	0.50	70	28	5.27
3	0.50	70	28	/
1	0.50	70	90	5.04
2	0.50	70	90	5.27
3	0.50	70	90	/
1	0.50	100	7	5.48
2	0.50	100	7	5.49
3	0.50	100	7	/
1	0.50	100	14	5.80
2	0.50	100	14	6.05
3	0.50	100	14	/
1	0.50	100	28	5.94
2	0.50	100	28	6.58
3	0.50	100	28	/
1	0.50	100	90	5.94
2	0.50	100	90	5.80
3	0.50	100	90	/

Table A-38. Coefficient of thermal expansion test data for concrete containing RAP-2

Specimen Number	W/C	RAP-2 (%)	Curing Period (days)	Coefficient of Thermal Expansion ( $10^{-6}$ in/in/°F)
1	0.50	20	7	4.49
2	0.50	20	7	4.84
3	0.50	20	7	4.42

Table A-38. Continued

Specimen Number	W/C	RAP-2 (%)	Curing Period (days)	Coefficient of Thermal Expansion ( $10^{-6}$ in/in/°F)
1	0.50	20	14	4.35
2	0.50	20	14	4.97
3	0.50	20	14	4.75
1	0.50	20	28	4.24
2	0.50	20	28	5.01
3	0.50	20	28	/
1	0.50	20	90	4.50
2	0.50	20	90	5.02
3	0.50	20	90	/
1	0.50	40	7	4.67
2	0.50	40	7	4.87
3	0.50	40	7	5.08
1	0.50	40	14	4.52
2	0.50	40	14	5.16
3	0.50	40	14	4.90
1	0.50	40	28	4.95
2	0.50	40	28	4.92
3	0.50	40	28	/
1	0.50	40	90	5.33
2	0.50	40	90	5.36
3	0.50	40	90	/
1	0.50	70	7	5.83
2	0.50	70	7	5.57
3	0.50	70	7	4.99
1	0.50	70	14	5.48
2	0.50	70	14	3.98
3	0.50	70	14	/
1	0.50	70	28	4.62
2	0.50	70	28	4.59
3	0.50	70	28	5.29
1	0.50	70	90	4.68
2	0.50	70	90	4.89
3	0.50	70	90	4.72
1	0.50	100	7	5.17
2	0.50	100	7	5.21

Table A-38. Continued

Specimen Number	W/C	RAP-2 (%)	Curing Period (days)	Coefficient of Thermal Expansion ( $10^{-6}$ in/in/°F)
3	0.50	100	7	5.58
1	0.50	100	14	6.02
2	0.50	100	14	4.72
3	0.50	100	14	/
1	0.50	100	28	5.13
2	0.50	100	28	5.53
3	0.50	100	28	6.16
1	0.50	100	90	5.28
2	0.50	100	90	5.38
3	0.50	100	90	5.27

Table A-39. Coefficient of thermal expansion test data for concrete containing RAP-3

Specimen Number	W/C	RAP-3 (%)	Curing Period (days)	Coefficient of Thermal Expansion ( $10^{-6}$ in/in/°F)
1	0.50	20	7	4.65
2	0.50	20	7	4.99
3	0.50	20	7	4.75
1	0.50	20	14	4.47
2	0.50	20	14	4.75
3	0.50	20	14	4.01
1	0.50	20	28	4.64
2	0.50	20	28	4.91
3	0.50	20	28	4.55
1	0.50	20	90	/
2	0.50	20	90	/
3	0.50	20	90	/
1	0.50	40	7	4.27
2	0.50	40	7	4.55
3	0.50	40	7	4.24
1	0.50	40	14	4.15
2	0.50	40	14	4.76
3	0.50	40	14	4.31
1	0.50	40	28	4.50
2	0.50	40	28	4.82

Table A-39. Continued

Specimen Number	W/C	RAP-3 (%)	Curing Period (days)	Coefficient of Thermal Expansion ( $10^{-6}$ in/in/°F)
3	0.50	40	28	4.38
1	0.50	40	90	/
2	0.50	40	90	/
3	0.50	40	90	/
1	0.50	70	7	4.77
2	0.50	70	7	4.93
3	0.50	70	7	4.49
1	0.50	70	14	3.87
2	0.50	70	14	4.98
3	0.50	70	14	4.20
1	0.50	70	28	4.94
2	0.50	70	28	5.07
3	0.50	70	28	4.49
1	0.50	70	90	/
2	0.50	70	90	/
3	0.50	70	90	/
1	0.50	100	7	4.97
2	0.50	100	7	5.39
3	0.50	100	7	4.07
1	0.50	100	14	4.87
2	0.50	100	14	5.33
3	0.50	100	14	5.20
1	0.50	100	28	4.79
2	0.50	100	28	5.22
3	0.50	100	28	5.16
1	0.50	100	90	4.71
2	0.50	100	90	3.54

Table A-40. Coefficient of thermal expansion test data for concrete containing RAP-4

Specimen Number	W/C	RAP-4 (%)	Curing Period (days)	Coefficient of Thermal Expansion ( $10^{-6}$ in/in/°F)
1	0.50	20	7	4.22
2	0.50	20	7	4.91
3	0.50	20	7	4.22

Table A-40. Continued

Specimen Number	W/C	RAP-4 (%)	Curing Period (days)	Coefficient of Thermal Expansion ( $10^{-6}$ in/in/°F)
1	0.50	20	14	4.85
2	0.50	20	14	4.88
3	0.50	20	14	/
1	0.50	20	28	4.91
2	0.50	20	28	3.87
3	0.50	20	28	4.22
1	0.50	20	90	5.11
2	0.50	20	90	4.24
3	0.50	20	90	5.67
1	0.50	40	7	4.86
2	0.50	40	7	4.71
3	0.50	40	7	4.27
1	0.50	40	14	4.36
2	0.50	40	14	4.44
3	0.50	40	14	4.15
1	0.50	40	28	4.51
2	0.50	40	28	4.50
3	0.50	40	28	4.06
1	0.50	40	90	4.24
2	0.50	40	90	4.25
3	0.50	40	90	5.06
1	0.50	70	7	4.86
2	0.50	70	7	4.69
3	0.50	70	7	4.81
1	0.50	70	14	4.08
2	0.50	70	14	/
3	0.50	70	14	/
1	0.50	70	28	/
2	0.50	70	28	/
3	0.50	70	28	/
1	0.50	70	90	4.07
2	0.50	70	90	4.53
3	0.50	70	90	/
1	0.50	100	7	4.95
2	0.50	100	7	4.79

Table A-40. Continued

Specimen Number	W/C	RAP-4 (%)	Curing Period (days)	Coefficient of Thermal Expansion ( $10^{-6}$ in/in/°F)
3	0.50	100	7	4.78
1	0.50	100	14	4.97
2	0.50	100	14	4.75
3	0.50	100	14	4.93
1	0.50	100	28	4.40
2	0.50	100	28	4.61
3	0.50	100	28	/
1	0.50	100	90	4.68
2	0.50	100	90	4.76
3	0.50	100	90	/

## APPENDIX B STRESS-STRAIN PLOT OF RAP CONCRETE

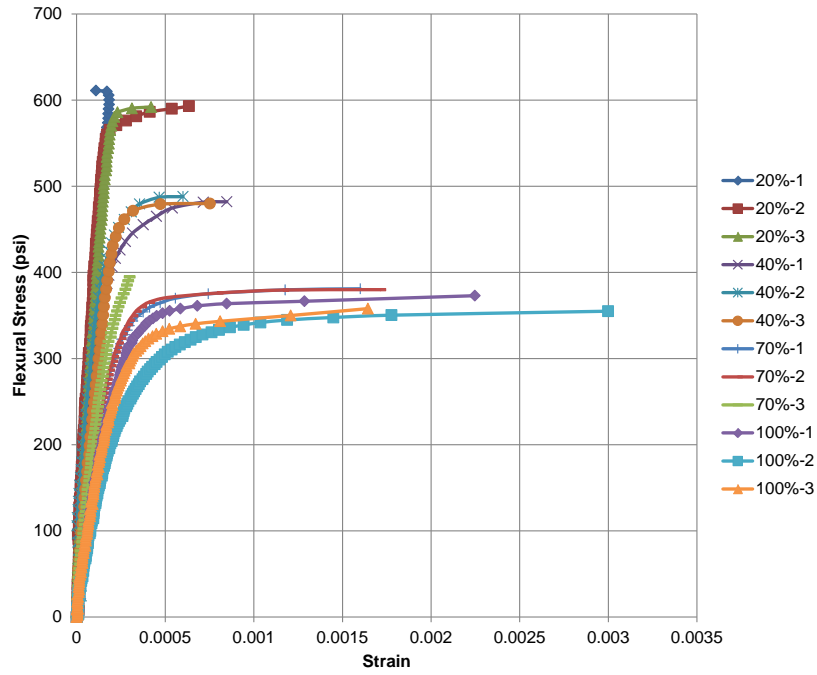


Figure B-1. Stress-strain plot for concrete mixtures with RAP-2 at 14 days of curing time

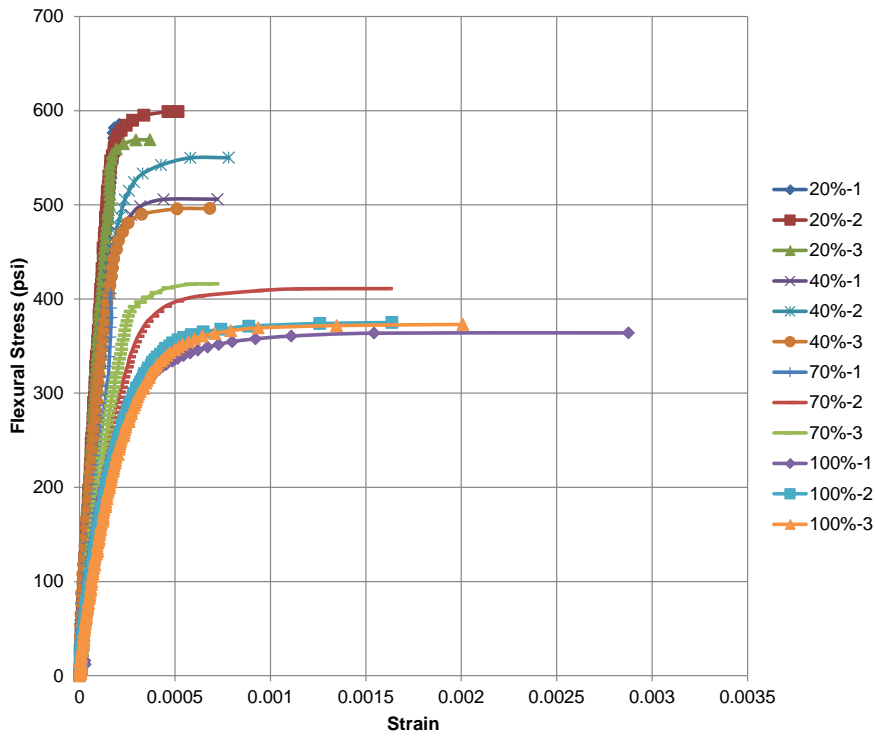


Figure B-2. Stress-strain plot for concrete mixtures with RAP-2 at 28 days of curing time

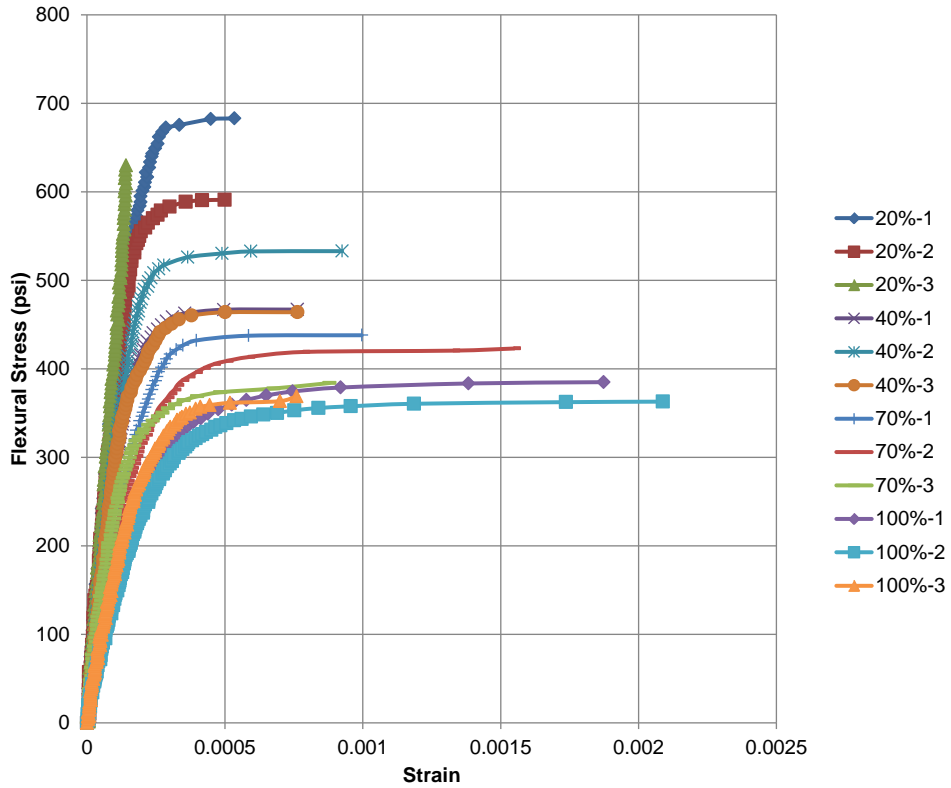


Figure B-3. Stress-strain plot for concrete mixtures with RAP-2 at 90 days of curing time

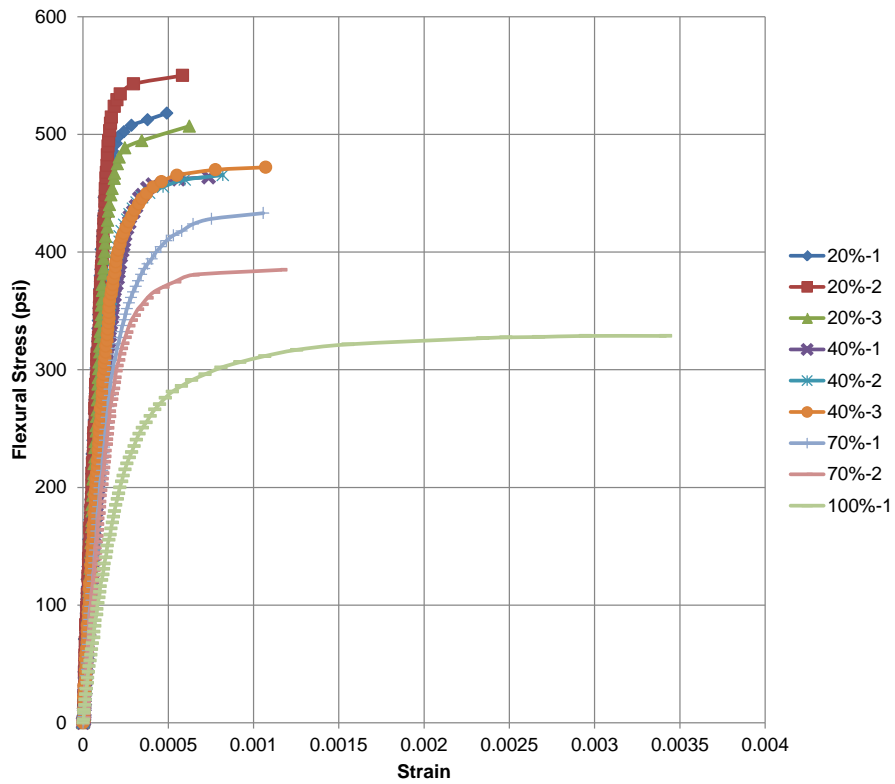


Figure B-4. Stress-strain plot for concrete mixtures with RAP-3 at 7 days of curing time

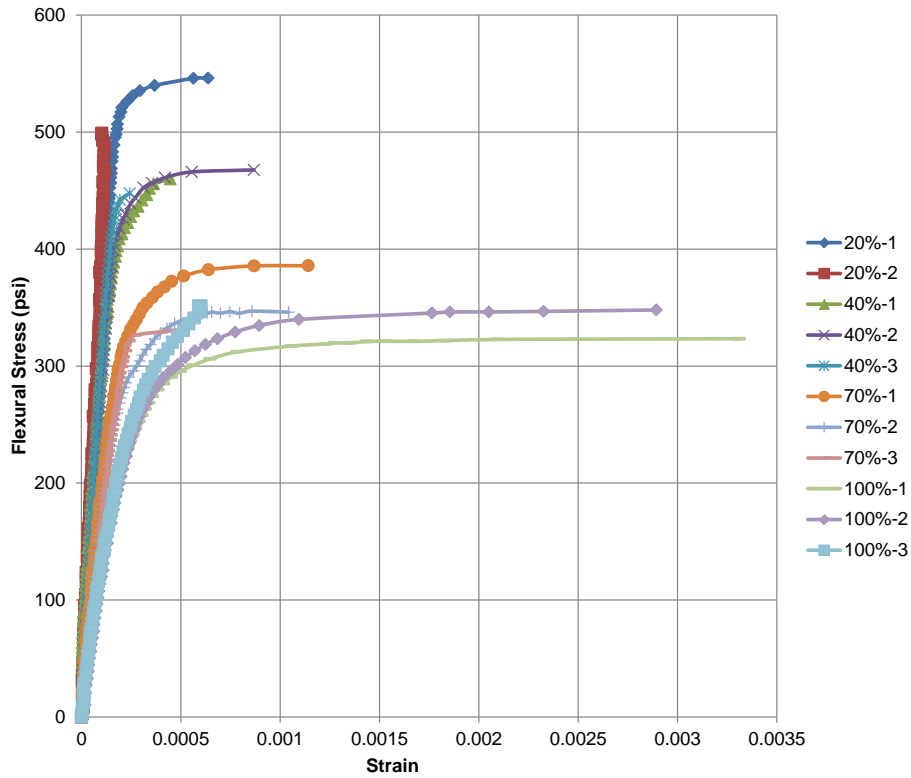


Figure B-5. Stress-strain plot for concrete mixtures with RAP-3 at 28 days of curing time

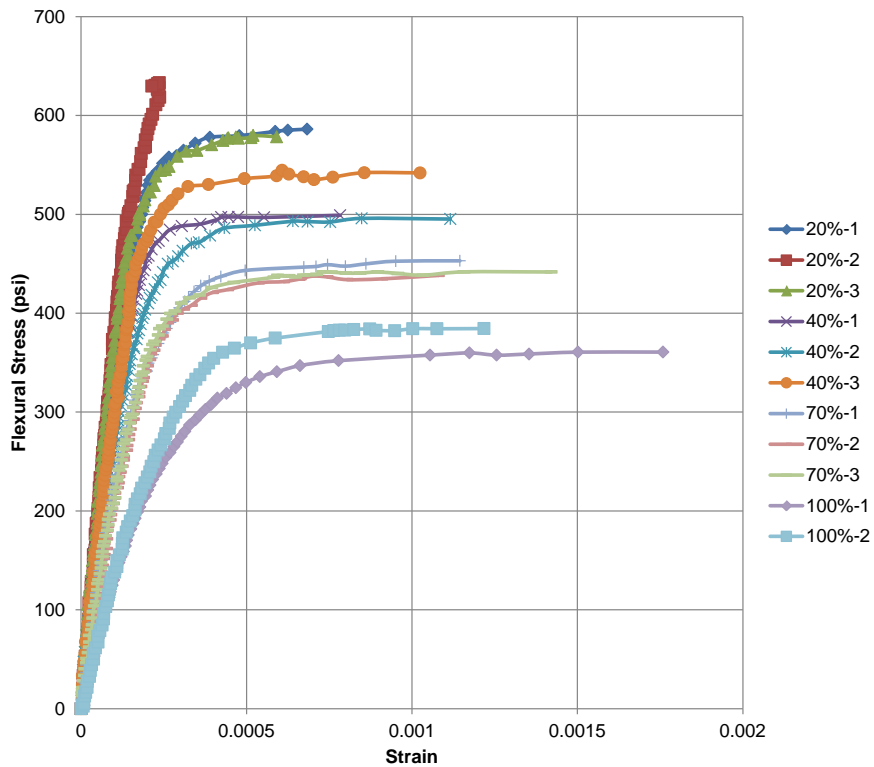


Figure B-6. Stress-strain plot for concrete mixtures with RAP-3 at 90 days of curing time

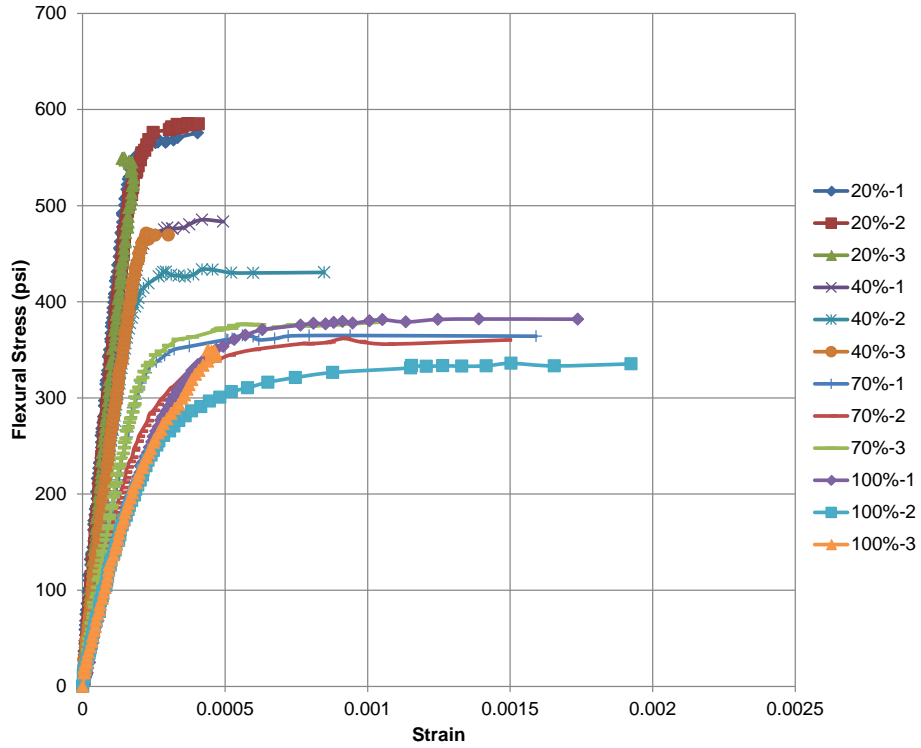


Figure B-7. Stress-strain plot for concrete mixtures with RAP-4 at 7 days of curing time

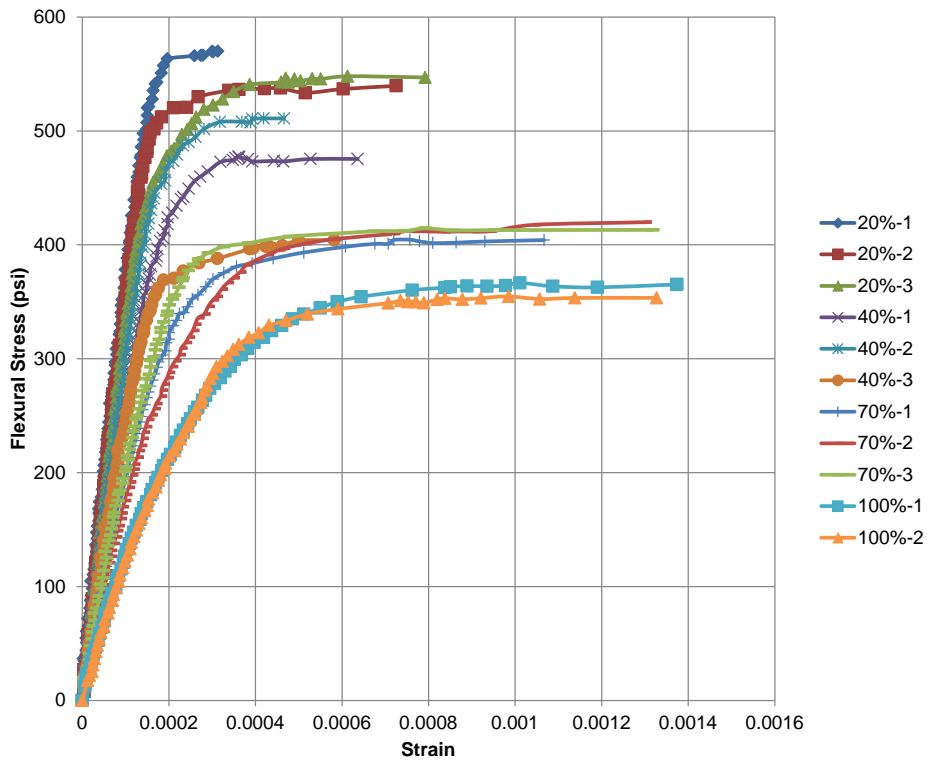


Figure B-8. Stress-strain plot for concrete mixtures with RAP-4 at 14 days of curing time

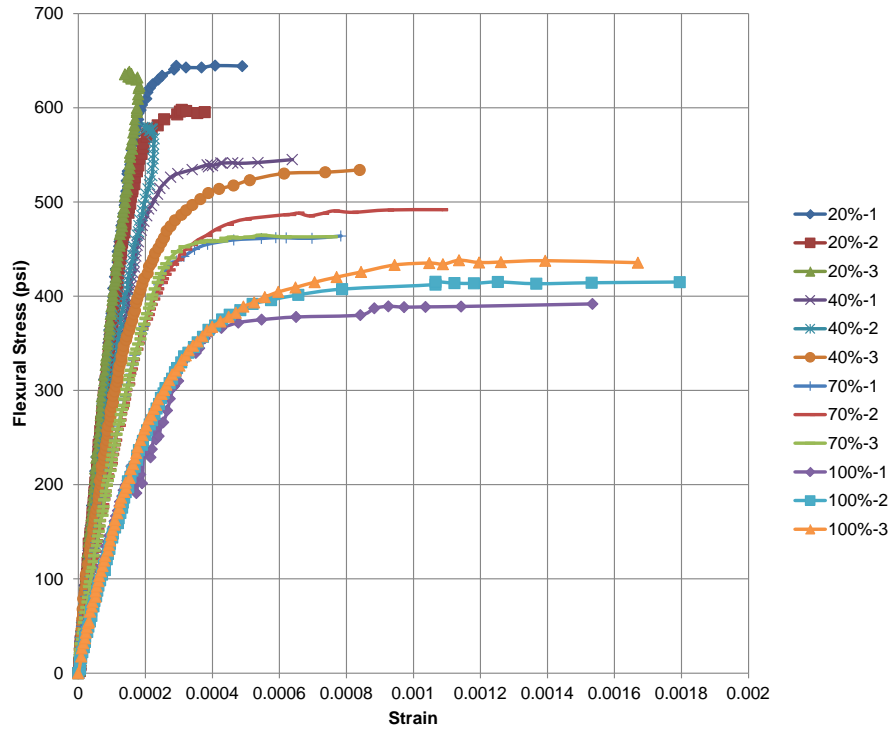


Figure B-9. Stress-strain plot for concrete mixtures with RAP-4 at 90 days of curing time

## APPENDIX C MEPDG INPUT DATA

### Traffic -- Volume Adjustment Factors

#### Monthly Adjustment Factors (Level 3, Default MAF)

Month	Vehicle Class									
	Class 4	Class 5	Class 6	Class 7	Class 8	Class 9	Class 10	Class 11	Class 12	Class 13
January	1.00	1.00	1.00	1.00	1.00	1.00	1.00	1.00	1.00	1.00
February	1.00	1.00	1.00	1.00	1.00	1.00	1.00	1.00	1.00	1.00
March	1.00	1.00	1.00	1.00	1.00	1.00	1.00	1.00	1.00	1.00
April	1.00	1.00	1.00	1.00	1.00	1.00	1.00	1.00	1.00	1.00
May	1.00	1.00	1.00	1.00	1.00	1.00	1.00	1.00	1.00	1.00
June	1.00	1.00	1.00	1.00	1.00	1.00	1.00	1.00	1.00	1.00
July	1.00	1.00	1.00	1.00	1.00	1.00	1.00	1.00	1.00	1.00
August	1.00	1.00	1.00	1.00	1.00	1.00	1.00	1.00	1.00	1.00
September	1.00	1.00	1.00	1.00	1.00	1.00	1.00	1.00	1.00	1.00
October	1.00	1.00	1.00	1.00	1.00	1.00	1.00	1.00	1.00	1.00
November	1.00	1.00	1.00	1.00	1.00	1.00	1.00	1.00	1.00	1.00
December	1.00	1.00	1.00	1.00	1.00	1.00	1.00	1.00	1.00	1.00

### Vehicle Class Distribution

(Level 3, Default Distribution)

#### AADTT distribution by vehicle class

Class 4	1.8%
Class 5	24.6%
Class 6	7.6%
Class 7	0.5%
Class 8	5.0%
Class 9	31.3%
Class 10	9.8%
Class 11	0.8%
Class 12	3.3%
Class 13	15.3%

#### Hourly truck traffic distribution

by period beginning:

Midnight	2.3%	Noon	5.9%
1:00 am	2.3%	1:00 pm	5.9%
2:00 am	2.3%	2:00 pm	5.9%
3:00 am	2.3%	3:00 pm	5.9%
4:00 am	2.3%	4:00 pm	4.6%
5:00 am	2.3%	5:00 pm	4.6%
6:00 am	5.0%	6:00 pm	4.6%
7:00 am	5.0%	7:00 pm	4.6%
8:00 am	5.0%	8:00 pm	3.1%
9:00 am	5.0%	9:00 pm	3.1%
10:00 am	5.9%	10:00 pm	3.1%
11:00 am	5.9%	11:00 pm	3.1%

Figure C-1. Traffic volume adjustment factors, vehicle class distribution, and hourly truck traffic distribution

### Traffic Growth Factor

Vehicle Class	Growth Rate	Growth Function
Class 4	2.0%	Linear
Class 5	2.0%	Linear
Class 6	2.0%	Linear
Class 7	2.0%	Linear
Class 8	2.0%	Linear
Class 9	2.0%	Linear
Class 10	2.0%	Linear
Class 11	2.0%	Linear
Class 12	2.0%	Linear
Class 13	2.0%	Linear

### Traffic -- Axle Load Distribution Factors

Level 3: Default

### Traffic -- General Traffic Inputs

Mean wheel location (inches from the lane marking): 18  
 Traffic wander standard deviation (in): 10  
 Design lane width (ft): 12

### Number of Axles per Truck

Vehicle Class	Single Axle	Tandem Axle	Tridem Axle	Quad Axle
Class 4	1.62	0.39	0.00	0.00
Class 5	2.00	0.00	0.00	0.00
Class 6	1.02	0.99	0.00	0.00
Class 7	1.00	0.26	0.83	0.00
Class 8	2.38	0.67	0.00	0.00
Class 9	1.13	1.93	0.00	0.00
Class 10	1.19	1.09	0.89	0.00
Class 11	4.29	0.26	0.06	0.00
Class 12	3.52	1.14	0.06	0.00
Class 13	2.15	2.13	0.35	0.00

### Axle Configuration

Average axle width (edge-to-edge) outside dimensions,ft): 8.5  
 Dual tire spacing (in): 12

### Axle Configuration

Tire Pressure (psi) : 120

### Average Axle Spacing

Tandem axle(psi): 51.6  
 Tridem axle(psi): 49.2  
 Quad axle(psi): 49.2

Figure C-2. Traffic growth factor, general traffic inputs, and axle configuration

### Layer 2 -- Asphalt concrete (existing)

Material type: Asphalt concrete (existing)  
Layer thickness (in): 4

#### General Properties

##### General

Reference temperature (F°): 70

##### Volumetric Properties as Built

Effective binder content (%): 11

Air voids (%): 7

Total unit weight (pcf): 148

Poisson's ratio: 0.35 (user entered)

##### Thermal Properties

Thermal conductivity asphalt (BTU/hr-ft-F°): 0.67

Heat capacity asphalt (BTU/lb-F°): 0.23

#### Asphalt Mix

Cumulative % Retained 3/4 inch sieve: 0

Cumulative % Retained 3/8 inch sieve: 15

Cumulative % Retained #4 sieve: 35

% Passing #200 sieve: 5.7

#### Asphalt Binder

Figure C-3. Layer 2 input parameters

### Layer 3 -- A-3

Unbound Material: A-3  
Thickness(in): 12

#### Strength Properties

Input Level: Level 3  
Analysis Type: ICM inputs (ICM Calculated Modulus)  
Poisson's ratio: 0.35  
Coefficient of lateral pressure, Ko: 0.5  
Modulus (input) (psi): 30000

#### ICM Inputs

##### Gradation and Plasticity Index

Plasticity Index, PI: 0  
Liquid Limit (LL): 0  
Compacted Layer: Yes  
Passing #200 sieve (%): 5  
Passing #40: 95  
Passing #4 sieve (%): 100  
D10(mm): 0.1231  
D20(mm): 0.161  
D30(mm): 0.1758  
D60(mm): 0.2289  
D90(mm): 0.3822

Figure C-4. Layer 3 input parameters

Sieve	Percent Passing
0.001mm	
0.002mm	
0.020mm	
#200	5
#100	12
#80	
#60	70
#50	
#40	95
#30	
#20	
#16	
#10	100
#8	
#4	100
3/8"	100
1/2"	
3/4"	100
1"	
1 1/2"	
2"	
2 1/2"	
3"	
3 1/2"	
4"	

Calculated/Derived Parameters

Maximum dry unit weight (pcf): 101.3 (user input)  
 Specific gravity of solids, G<sub>s</sub>: 2.70 (derived)  
 Saturated hydraulic conductivity (ft/hr): 0.005659 (derived)  
 Optimum gravimetric water content (%): 11.4 (user input)  
 Calculated degree of saturation (%): 46.4 (calculated)

Soil water characteristic curve parameters: User input

Parameters	Value
a	7.52
b	0.93
c	0.74
Hr.	100

Figure C-4. (Continued)

**Layer 4 -- A-2-4**

Unbound Material: A-2-4  
 Thickness(in): Semi-infinite

**Strength Properties**

Input Level: Level 3  
 Analysis Type: ICM inputs (ICM Calculated Modulus)  
 Poisson's ratio: 0.35  
 Coefficient of lateral pressure, Ko: 0.5  
 Modulus (input) (psi): 16500

**ICM Inputs**Gradation and Plasticity Index

Plasticity Index, PI: 6.3  
 Liquid Limit (LL) 21  
 Compacted Layer No  
 Passing #200 sieve (%): 34.1  
 Passing #40 87.9  
 Passing #4 sieve (%): 100  
 D10(mm) 0.0006968  
 D20(mm) 0.004856  
 D30(mm) 0.03384  
 D60(mm) 0.1908  
 D90(mm) 0.5561

Sieve	Percent Passing
0.001mm	
0.002mm	
0.020mm	
#200	34.1
#100	51.2
#80	
#60	69.9
#50	
#40	87.9
#30	
#20	
#16	
#10	100
#8	
#4	100
3/8"	
1/2"	
3/4"	100
1"	
1 1/2"	
2"	
2 1/2"	
3"	
3 1/2"	
4"	

Figure C-5. Layer 4 input parameters

**APPENDIX D**  
**CHARACTERIZATION OF CONCRETE CONTAINING RECLAIMED ASPHALT**  
**PAVEMENT BY SUPERPAVE INDIRECT TENSILE TEST AND X-RAY COMPUTED**  
**TOMOGRAPHY**

**D.1 Research Objectives and Scope**

The objective of this study was to assess the Superpave IDT strength test to evaluate Portland Cement Concrete (PCC) and concrete containing RAP by refining the test procedures, studying stress—strain behavior, and finding the relationship between strength test results and conventional concrete properties, as well as using X-ray CT in conjunction with the load frame, to visualize internal microstructure in concrete mixes.

Three FDOT-approved PCC mixes with  $w/c=0.45$ ,  $0.50$ , and  $0.55$  and four other concrete mixes containing 20%, 40%, 70%, and 100% of RAP-3 with  $w/c=0.5$  were produced and evaluated in this study. The hardened concrete specimens were tested conventionally and evaluated by the Superpave IDT strength test. X-ray Computed Tomography was used in conjunction with the Superpave IDT strength test to assess distribution of air voids in concrete mixes.

**D.2 Superpave<sup>®</sup> Indirect Tension Test**

**D.2.1 Development of Superpave IDT Test Apparatus**

The Superpave<sup>®</sup> indirect tensile test (IDT) was developed to satisfy the requirement of the Strategic Highway Research Program (SHRP) to determine properties of hot mix asphalt (HMA) including: resilient modulus; creep modulus; and tensile strength (Roque and Buttlar, 1992, 1994). A later study (Roque et al., 1997) was utilized to establish a data reduction system for the IDT test; this system can automatically compute resilient modulus, creep, and indirect tensile strength, as well as provide an assessment of fracture energy. AASHTO T322 has detailed

descriptions of the layout of the load frame, gage point mounting, and modulus calculations for asphalt concrete.

The common procedure is that the asphalt specimen is sliced from a cylinder six inches in diameter. Specimen thickness can be one- and one-half inches for dense-graded mixes and two inches for open-graded friction course (OGFC) mixes. Four linear variable differential transformers (LVDTs) are employed in total to measure deformations in horizontal and vertical directions on both sides of a specimen. The loading frame is a servo-hydraulic and closed-loop feedback control device, which can run in either force-control or displacement-control mode. A pre-load of ten to fifteen pounds is routinely applied, before starting the test, to avoid impact effect on the test samples. A series of testing data including testing time, axial load, axial deformation, and deformations on four gages are recorded and exported to a text file, and as such, can be used to derive a stress-strain curve for further analysis.

The analysis of the indirect tensile test can be traced back to an early study (Hondros, 1959,) that derived a full analytical solution of stress analysis for evaluating Portland Cement Concrete (PCC). For the Superpave IDT test, the distribution of tensile stress along the vertical and horizontal axis is modified and the plane stress condition near the center is as follows (Lee et al., 2011):

$$\sigma_x(x,0) = \frac{2P}{\pi ad} \left[ \frac{(1 - \frac{x^2}{R^2}) \times \sin 2\alpha}{1 + 2 \frac{x^2}{R^2} \times \cos 2\alpha + (\frac{x}{R})^4} - \tan^{-1} \frac{1 + \frac{x^2}{R^2}}{1 - \frac{x^2}{R^2}} \times \tan \alpha \right]$$

$$= \frac{2P}{\pi ad} \cdot m(x) \quad (D-1)$$

$$\sigma_y(0, y) = -\frac{2P}{\pi ad} \left[ \frac{(1 - \frac{y^2}{R^2}) \times \sin 2\alpha}{1 - 2 \frac{x^2}{R^2} \times \cos 2\alpha + (\frac{y}{R})^4} + \tan^{-1} \frac{1 + \frac{y^2}{R^2}}{1 - \frac{y^2}{R^2}} \times \tan \alpha \right]$$

$$= -\frac{2P}{\pi ad} \cdot n(y) \quad (D-2)$$

where,  $P$  = applied load, lbf.  
 $a$  = rim width of loaded section  
 $d$  = diameter of specimen  
 $x$  = radial distance from the center  
 $R$  = radius of specimen  
 $\alpha$  = angular displacement from the vertical axis

Therefore, the average stresses with the gage length  $l$  were defined as:

$$\sigma_{xAVG} = \frac{2P}{\pi ad} \times \left( \frac{1}{l} \right) \int_{-0.5}^{0.5} [m(x)] \quad (D-3)$$

$$\sigma_{yAVG} = -\frac{2P}{\pi ad} \times \left( \frac{1}{l} \right) \int_{-0.5}^{0.5} [n(y)] \quad (D-4)$$

And the horizontal and vertical strains can be derived from the strain gage measurements as:

$$\varepsilon_h = \frac{\Delta X}{l} \quad (D-5)$$

$$\varepsilon_v = \frac{\Delta Y}{l} \quad (D-6)$$

where  $\Delta X$  = horizontal strain and  $\Delta Y$  = vertical strain over the gage length  $l$ .

Three major tests: resilient modulus; creep; and indirect tensile tests are routinely performed by Superpave IDT in sequence as follows:

**Resilient modulus test.** This test is performed by applying the repeated load, resulting in horizontal deformation within the range of 200-300 microstrain. The repeated load was applied

in the form of a 0.1s loading, followed by a 0.9s rest period. The resilient modulus or MR can be calculated as follows:

$$M_R = \frac{P \times l}{\Delta X \times t \times d \times C_{CMPL}} \quad (D-7)$$

In which  $C_{CMPL}$  stands for a non-dimensional factor that varied linearly with ratio of horizontal to vertical deformation as follows:

$$C_{CMPL} = 0.6354 \times \left(\frac{X}{Y}\right)^{-1} - 0.332 \quad (D-8)$$

where  $\left(\frac{X}{Y}\right)$  = ratio of horizontal to vertical deformation.

**Creep test.** The creep compliance test is performed following the resilient modulus test on the specimen. The constant load is chosen to keep horizontal deformation within the range of 200-750 microstrain after 1000s of loading. Hence the creep compliance is computed as follows:

$$D(t) = \frac{\Delta X \times t \times d \times C_{CMPL}}{P \times l} \quad (D-9)$$

where  $D(t)$  is defined as the creep compliance at the given time.

**Indirect tensile strength test.** A constant displacement control rate of 0.5 in/min is applied to the test specimen in order to generate the stress and strain curve. In order to account for the three-dimensional effect of the stress state, the stress and strain must be multiplied by the correction factors, CSX and CBX, respectively. Both correction factors were derived from the computed Poisson's ratio obtained from the resilient modulus test.

$$\nu = -0.10 + 1.48 \times \left(\frac{X}{Y}\right)^2 - 0.0778 \times \left(\frac{X}{Y}\right)^2 \times \left(\frac{t_{AVG}}{d_{AVG}}\right) \quad (D-10)$$

where,  $t_{AVG}$  = average specimen thickness

$d_{AVG}$  = average specimen diameter

Hence, the indirect tensile strength is determined as follows:

$$\sigma(t) = \frac{2 \times (\text{FailureLoad})}{\pi \times t \times d} \times CSX \quad (\text{D-11})$$

$$\varepsilon(t) = \frac{\text{displacement}(t)}{l} \times CBX \times 1.072 \quad (\text{D-12})$$

where,  $CSX = 0.948 - 0.0114 \left( \frac{t}{d} \right) - 0.2693 \times \nu + 0.089 \times \left( \frac{t}{d} \right)^2$

$$CBX = 1.03 - 0.189 \times \left( \frac{t}{d} \right) - 0.081 \times \nu + 0.089 \times \left( \frac{t}{d} \right)^2$$

### D.2.2 Failure Load Detection and Fracture Energy in Superpave IDT

The stress state within Superpave IDT specimen was found not to be a plane stress (Heinicke et al., 1988, Roque et al., 1992, and Buttlar et al., 1996), as is shown in Figure D-1. In plane stress state (2-D), the tensile strength is constant, while the stress in the 3-D analysis varies along the axis of symmetry and will reach maximum at the vicinity of the end surface on both sides of a specimen. It was suggested that the near-surface failure load is less than the load that can break a specimen apart. Hence, the failure load was defined and determined by the stress level at the failure instant of the specimen edge. The Superpave IDT strength test, along with vertical and horizontal displacement measurements, was found to be capable of ascertaining the failure load. Figure D-2 show the detailed steps for finding the failure load. Failure load is

shown as a rapid increase in the rate of horizontal deformation at the precise instance of failure occurring on the edge of a specimen.

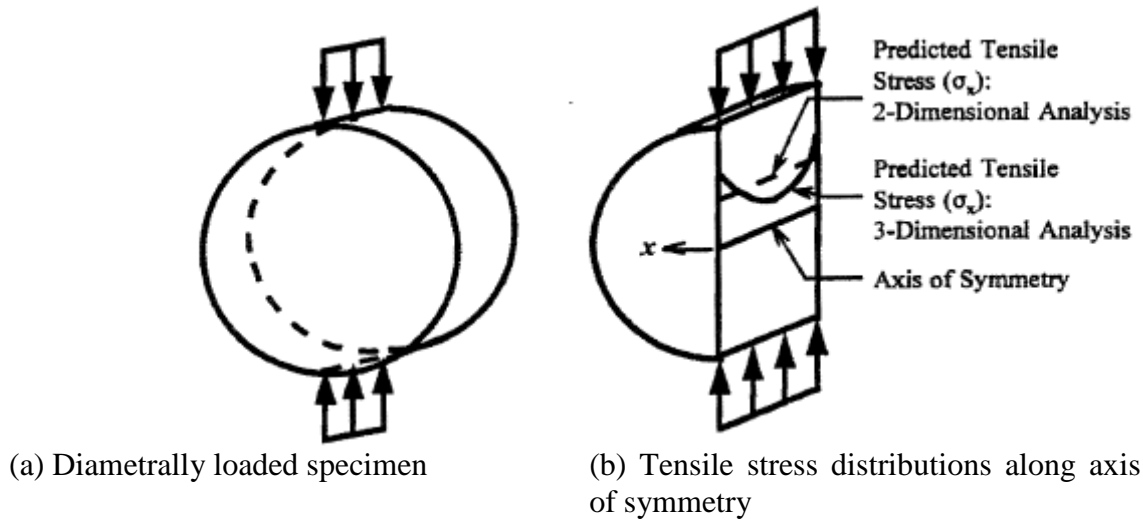


Figure D-1. Tensile stresses in a diametrically loaded specimen (after Buttlar et al., 1996)

Figure D-2 (A) presents a constantly increasing rate of applied load, Figure D-2 (B) indicates the deformations of two vertical (Y1&Y2) and two horizontal (X1&X2) gages shown against time, and Figure D-2 (C) presents two relationship lines by plotting the differences between vertical and horizontal deformations (Y-X). As the applied load increases over time, deformations of four LVDTs are increasing. It was found at the imminent occurrence of cracking, one horizontal deformation rises more than the other, which also causes the significant reduction on the (Y-X) line. Thus, the instant of failure is identified at the peak of (Y-X), and the failure load will be observed at the same time.

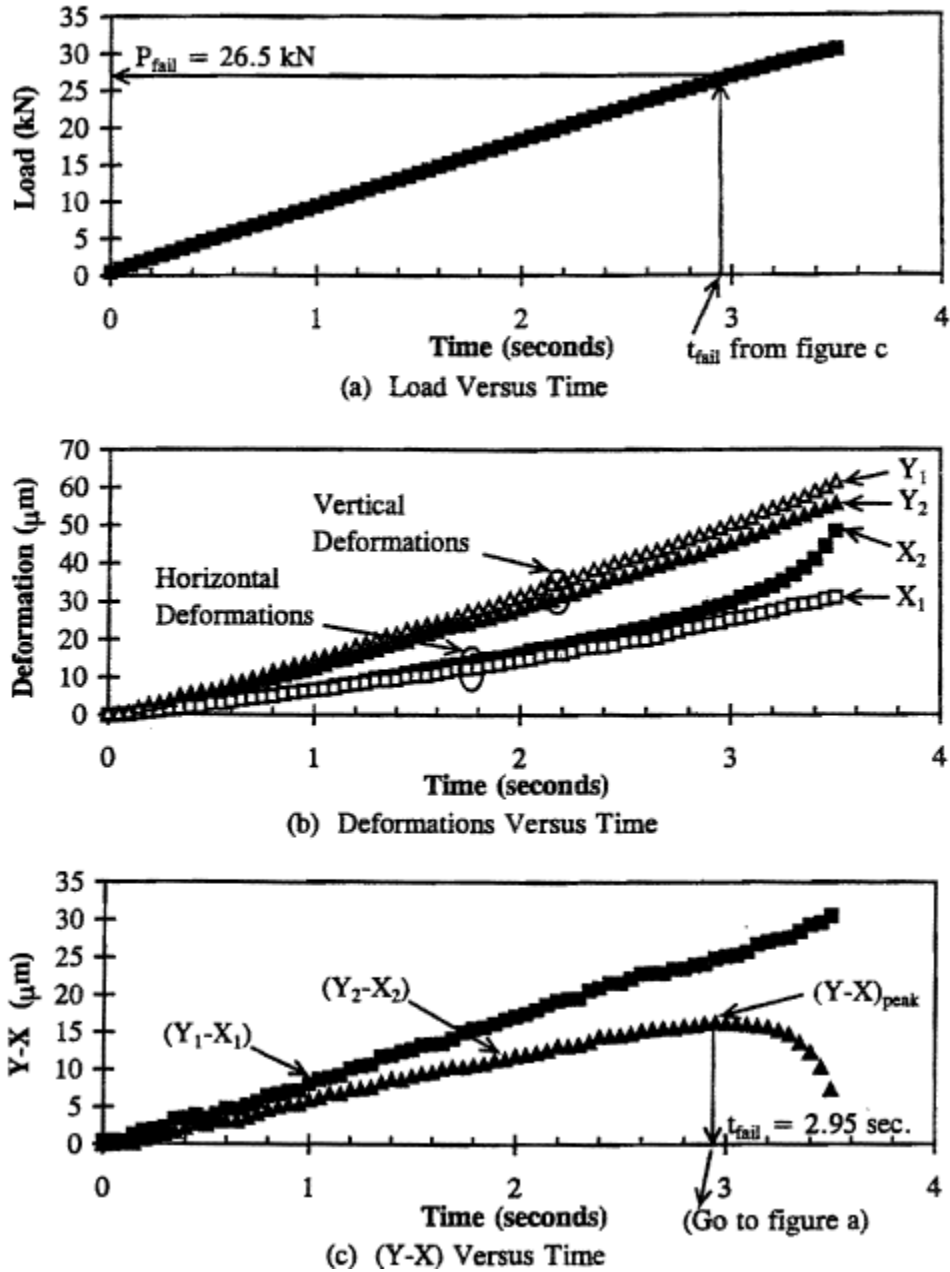


Figure D-2. Example of strength results by using Superpave IDT (after Buttlar et al., 1996)

### D.2.3 Previous Exploratory Work Using Superpave IDT on Concrete

A pilot study (Zheng, 2007) attempted to adapt the Superpave IDT strength test in conjunction with an acoustic emission (AE) device, to evaluate concrete in terms of indirect tensile strength, microdamage, and fracture properties. The researcher defined the failure load as

the “first fracture” in concrete. The secant modulus from the stress—strain curve was found to identify the onset of microdamage well, considering the integrity of concrete being affected negatively by damage. In conjunction with AE, the study also verified the onset of first fracture initiating at approximately seventy to ninety percent, and the onset of microcracking starting at about forty percent of the peak load from the Superpave IDT strength test. The researcher suggested adopting a displacement-control rate of 0.00075 in/sec (1.14 mm/min) when performing the Superpave IDT strength test on concrete.

The researcher also proposed a protocol for the Superpave IDT strength test on concrete, including specimen preparation, test procedures, and analysis, consistent with AASHTO T332. Three specimens are needed and the failure load for each specimen is the value corresponding to the instant when first peak of (Y-X) has been reached. The failure strength and strain are identified individually from each specimen, and average values are reported. The determination of Poisson’s Ratio is obtained at half of the average failure load from three specimens. However, it is the stress—strain curve up to the instant of failure load that is chosen for calculating the fracture energy for each specimen.

### **D.3 Test Sample Preparation**

#### **D.3.1 Slicing of Concrete Cylinder**

6 × 12 Inch concrete cylinders were fabricated from PCC and concrete containing RAP-3 mixes. Curing periods of 7, 14, 28, and 90 days were used. Specimens with 1.5 inches in thickness and six inches in diameter were prepared for the Superpave IDT strength test. The thin concrete specimens were sliced by a large masonry saw at the concrete laboratory of the State Materials Office in Gainesville. One cylinder could supply up to six or seven thin concrete slices. The sliced concrete specimens were subsequently transported to the asphalt laboratory at the University of Florida for further surface cleaning and fan-drying.

### D.3.2 Air Drying, Surface Cleaning, and Gage Points Attachment

The sliced concrete specimens were covered by moisture and dusts through the process of slicing. The specimens needed to be dried and cleaned before gage points could be attached. After they were taken to the asphalt laboratory, the thin concrete specimens were placed in front of a fan to be dried. The process of air drying took approximately one hour to complete. Concrete specimens were labeled using a permanent marker after air drying.

In addition, the surface of specimens were cleaned to sweep out dusts that were generated from the slicing process when the masonry saw cut through the aggregates and cement paste. The surface cleaning process was started by using steel brushes to sweep around central area of specimen in which gage points were going to be glued. Steel brushes can remove dusts or broken particles out of surface and it was followed by having paper towels soaked with acetone to wipe the same central area. The use of acetone can also take away the left-over moisture. After the surface cleaning process was finished, the thin concrete specimens were ready to be attached with strain gage points.

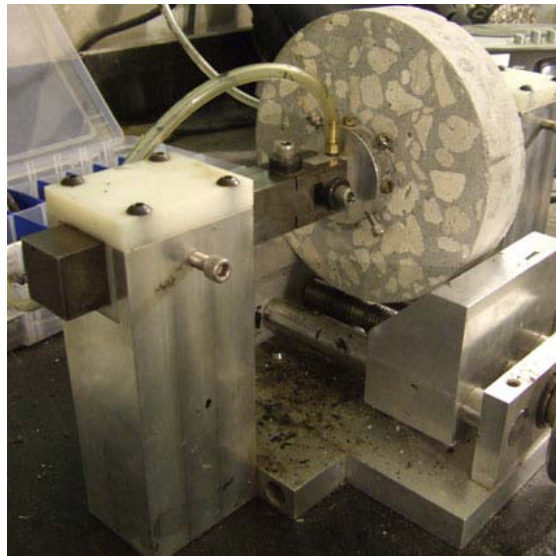


Figure D-3. Gage point mounting system (Photo courtesy of Yu-Min Su)

Four strain gage points for each surface of the thin concrete slice were attached by using Loctite Prism 454 adhesive and aligned by the gage point mounting system, shown in Figure D-3. The mounting system can place and align eight gage points (two for vertical and two for horizontal for faces) in the center of each specimen spaced at one and one-half inches on center for each direction. The purpose of attaching gage points was to provide a fixed and aligned position for later process of installing strain gages.



Figure D-4. ESPEC environment chamber (Photo courtesy of Yu-Min Su)

### **D.3.3 Temperature Conditioning**

Three temperatures were selected: -10, 23, and 60°C for Superpave IDT strength tests, representing the ambient temperature in winter, standard laboratory testing temperature, and the pavement temperature in summer in Florida, respectively. After the adhesive was dried for two hours, concrete slices with installed gage points were stored in the Advanced Materials Characterization Laboratory (AMCL) for temperature conditioning. After having been positioned in the ESPEC environment chamber (shown in Figure D-4) for low-temperature

conditioning, in a Fisher Scientific oven for high-temperature conditioning, and in ambient temperature overnight, concrete slices were ready for the Superpave IDT strength test. Three concrete slices were prepared for each testing condition; for example, three specimens for a mix with 7 days curing and being tested at 23°C.

#### **D.3.4 Installing Strain Gages**

The Superpave IDT strength test was performed using an MTS load frame. The displacement measurements from strain gages were recorded simultaneously along with the loading information. Moreover, clip-on caps were needed to be installed on gage points and subsequently aligned in the same orientation. The strain gages (or LVDTs) were hereafter attached on the aligned caps, and spacing adjustment between caps had to be calibrated as close to zero as possible based on strain gages' readings on the screen. This spacing adjustment was often a time-consuming process to perform. For low- and high- temperature conditioning situations, the specimen would be returned to the weather chamber or oven for thirty minutes reconditioning after installing caps. Gage points attachment, clip-on caps alignment, and strain gages adjustment were reported in details in a FDOT final report (Roque et al., 1997).

#### **D.3.5 Positioning Concrete Specimen**

The diameter and thickness of concrete thin specimen were measured and recorded after the temperature reconditioning. Strain gages (or LVDTs) were accurately placed on the aligned and adjusted caps before the concrete specimen was put on to the load frame. The concrete specimen had to be carefully positioning on the center of loading head in order to warrant precise loading position. Figure D-5 shows a concrete slice situated in the load frame with vertical and horizontal strain gages attached. A pre-load about ten pounds was set to hold the specimen in position without any movement. Additionally, cables connected with strain gages were arranged

to stay away from the concrete specimen to avoid damage caused by explosive concrete blast of fracture.

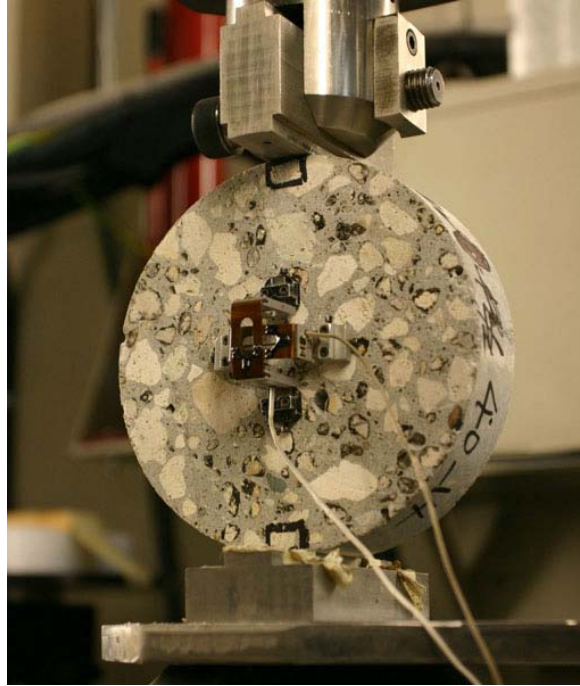


Figure D-5. Thin concrete specimen on the load frame with strain gages (Photo courtesy of Yu-Min Su)

## **D.4 The Superpave IDT Strength Test on Concrete Specimens**

### **D.4.1 Loading Condition**

In this study, both force-control and displacement-control loading conditions were used. In force-control mode, a constant load rate of 35.343 lbf/sec was used. This load rate was chosen so that it would be similar to the one used in the standard splitting tensile strength test. In the displacement-control mode, a constant displacement rate of 0.00075 in/sec was used.

## D.4.2 Data Collection and Processing

### D.4.2.1 Data collection

Two horizontal, two vertical and axial displacements, axial force, time of loading were captured in twenty data points per second. In force-control mode, it needed about 150 to 300 seconds to complete a Superpave IDT strength test on concrete specimens, while it required only 30 to 40 seconds running in the displacement-control mode. Enormous data including displacements, loads, and time were recorded to a text file which can be used for further data processing.

### D.4.2.2 Data processing

Horizontal and vertical displacements were used to compute vertical and horizontal strains on both side of the specimen with known spacing between gage points ( $l = 1.5$  inches). The corresponding indirect tensile stress also was calculated using the measured thickness (approximately 1.5 inches) and diameter (approximately 6 inches) of concrete specimen as follows:

$$T(t) = \frac{2P(t)}{\pi ld} \quad (\text{D-13})$$

where,  $T(t)$  = indirect tensile stress at time  $t$ , psi,

$P$  = axial load at time  $t$ , lbf,

$l$  = thickness of concrete thin specimen, inches,

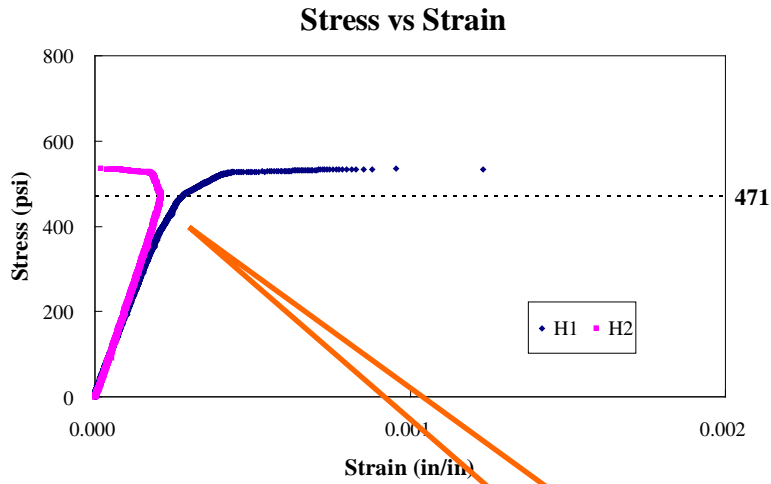
$d$  = diameter of concrete thin specimen, inches.

Two horizontal strains and the calculated tensile stress could be plotted together to generate the individual stress—strain plot containing two curves indicating the strain developments for each concrete specimen. Moreover, there were three replicate specimens evaluated for each designed mix prepared and tested by each selected temperature condition. The mean tensile stress was calculated from three axial loads and a trimmed mean strain was

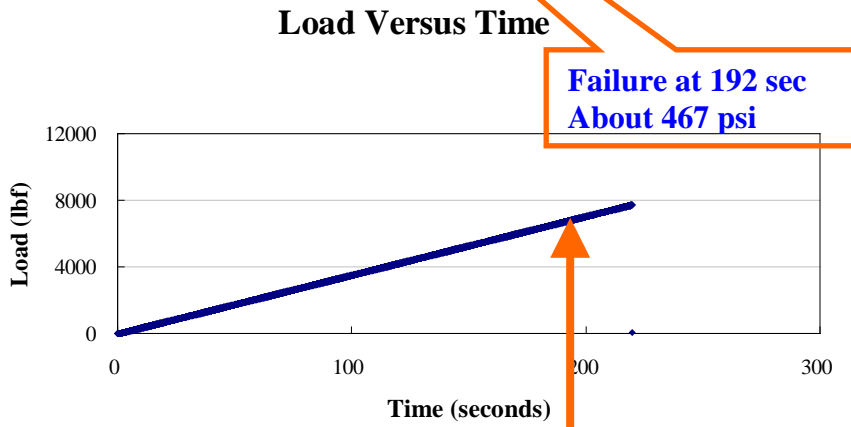
taken by computing the average strain from six faces of strains from three replicate specimens. The trimmed mean strain was obtained by ranking the highest and lowest strains but discarding the highest and lowest ones. Hence, a mean stress—strain curve was generated to each designated concrete mix for computing concrete mixture properties.

#### **D.4.2.3 Determination of failure stress and peak stress**

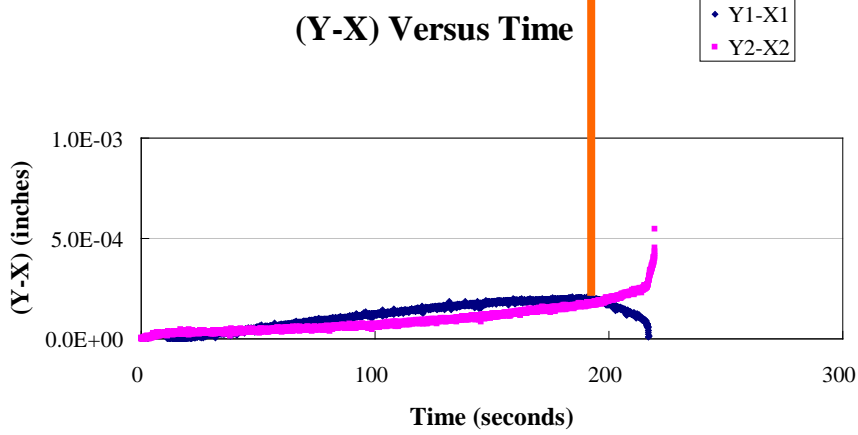
The failure stress is a vital parameter to be evaluated for adopting the Superpave IDT strength test to concrete. Conventionally, the peak stress of splitting tensile strength test is considered as the arrival of concrete failure and used for deriving the indirect tensile strength in ASTM C496. The definition of failure in HMA fracture mechanics is rather different than that in concrete. The failure of HMA is defined at the load level when the first peak of (Y-X) has been reached (Roque et al., 1996), described in Chapter 2.2. The tensile strength is calculated from the failure load and corrected by a correction factor which is affected by the Poisson's ratio. The Poisson's ratio is computed from the repeated loading condition as the Superpave IDT resilient modulus ( $M_R$ ) test. Tensile strength, resilient modulus, Poisson's ratio and fracture energy can be identified and calculated conveniently by an automation software—ITLT (Roque et al, 1997). In additional, ITLT requires consecutive Superpave IDT resilient modulus, creep, and tensile strength tests for conducting the automatic analysis.



(A)



(B)



(C)

Figure D-6. Example of determining the failure load on PCC with  $w/c=0.50$

The proposed protocol (Zheng, 2007) of the Superpave IDT strength test in testing concrete has been discussed in Chapter 2.2. Failure stress, or “first fracture”, in concrete was proposed to be determined in the same fashion as for HMA. There was no definitive description on determining the elastic modulus, while the Poisson’s ratio was proposed to be determined by strains at the half of the average failure stress from three replicate specimens. Additionally, the fracture energy was determined by calculating the area under the stress—strain curve up to the designated failure stress. Figure D-6 shows the determination process of failure load on one PCC example with  $w/c=0.50$  tested at  $23^{\circ}\text{C}$  in this study by using the proposed protocol.

The determination started from Figure 5-4(C) by identifying the first peak of Y-X from two curves. After the first peak was identified, the load could be determined for the corresponding loading time. For this example, it can be seen that the failure occurred at 192 seconds of loading, as shown in Figure 5-4(B), and the corresponding failure stress was determined to be 467 psi. Additionally, the peak stress was found to be 534 psi, which was the last data reported in the stress—strain plot in Figure 5-4(A). By observing the stress—strain curve, the peak stress by definition of conventional failure in concrete occurred clearly at the end of plastic deformation. On the other hand, the failure by definition of HMA or the proposed protocol was located about 88% of peak stress in this case.

#### **D.4.2.4 Determination of elastic modulus and Poisson’s ratio**

ASTM C469 provides the access to obtain elastic modulus (or Young’s modulus) and Poisson’s ratio by performing the compressive strength test up to 40% of peak stress to a concrete cylinder. The elastic modulus in concrete is a chord modulus and theoretically such modulus can be identical with secant modulus in elastic region. Figure D-7 (A) shows an example of secant modulus plotted with stresses under the force-control loading rate. There were two curves derived from the PCC with  $w/c=0.50$  and a concrete containing 70% RAP and

dash lines presented the occurrences of 40% of peak stress in these mixes. The secant modulus of PCC indicated a seemingly flat plateau which may imply the elastic characteristic at 40% of ultimate stress. However, the secant modulus of concrete containing 70% RAP showed a continuous declining curve that may indicate the non-elastic or plastic characteristic at this loading level. Therefore, it may be reasonably suggested that it is elastic within the 40% of peak load for PCC, though it might not be genuine for concrete containing RAP with regards to the determination of elastic modulus.

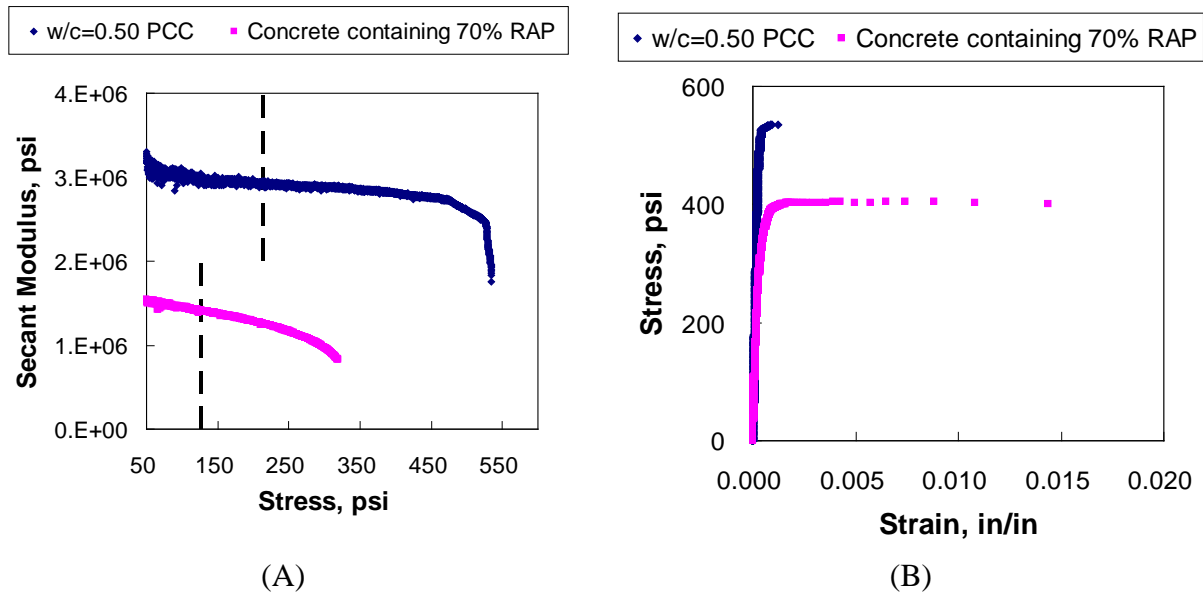


Figure D-7. Example of (A) secant modulus and (B) stress—strain curve of PCC and concrete containing 70% RAP

Similar considerations occurred for determining the Poisson's ratio whether or not the 40% of peak stress is elastic for concrete mixes. It was selected to use vertical and horizontal ratio  $\frac{Y}{X}$  at 40% of peak stress to calculate the Poisson's ratio. It has to be noted that both elastic modulus and Poisson's ratio were computed from the mean stress—strain curve of each concrete mixture in this study.

#### **D.4.2.5 Determination of fracture energy and toughness**

Fracture energy was defined in HMA fracture mechanics and proposed protocol as the area integration of stress—strain curve up to the failure stress. Figure D-6 (A) shows fairly clear that this area integration is more and less presenting the energy up to about elastic limit. Figure D-7 (B) shows the example of stress—strain curves of PCC with w/c=0.50 and concrete containing 70% RAP. The stress—strain curve of concrete containing RAP indicated a much longer plastic deformation up to 0.015 in/in horizontal strain, while the strain of PCC with w/c=0.50 only extended up to 0.001 in/in. The ductility for concrete containing RAP may be accessed effectively to include the area of plastic deformation. The toughness of concrete mix that includes overall area covering elastic and plastic regimes was used to assess the ductility of concrete containing RAP in this study.

#### **D.4.3 Computations of Concrete Properties**

In this study, individual stress—strain curve was plotted for each concrete specimen to access the failure stress, peak stress, and fracture energy (calculated up to the failure stress). In addition, the mean stress—strain curve of each concrete mix was also obtained to evaluated the elastic modulus, Poisson's ratio, and toughness (calculated up to the peak stress).

##### **D.4.3.1 Indirect tensile strength**

The average failure stress was obtained from individual stress—strain curves of three replicate concrete specimens, while the average peak stress was calculated from three axial peak loads. The indirect tension strength of concrete tested by the Superpave IDT strength test can be evaluated as follows:

$$T_{IDT}(failure) = \left( \frac{2P(failure)}{\pi dl} \right) \quad (D-14)$$

$$T_{IDT}(peak) = \left( \frac{2P(peak)}{\pi dl} \right) \quad (D-15)$$

where,  $T_{IDT}(failure)$  = indirect tensile strength of failure stress in HMA fracture mechanics, psi,  
 $T_{IDT}(peak)$  = indirect tensile strength of peak stress in conventional concrete splitting tensile test, psi,  
 $P(failure)$  = axial load at time of failure stress, lbf, and  
 $P(peak)$  = axial load at time of peak stress, lbf.

#### D.4.3.2 Elastic modulus

The mean stress—strain curve was obtained for each concrete mix. It was selected to use stress and strain at the 40% of ultimate stress to compute the secant modulus. The determination of elastic modulus by Superpave IDT strength test for concrete was defined as follow:

$$E_{IDT} = \left( \frac{T_{IDT}}{\varepsilon} \right)_{Peakstress}^{40\%} \quad (D-16)$$

where,  $E_{IDT}$  = Elastic modulus of Superpave IDT test on concrete  
 $T_{IDT}^{40\%}$  = Mean tensile stress at the 40% of peak stress, psi  
 $\varepsilon$  = Mean horizontal strain at the 40% of axial peak stress, in/in

#### D.4.3.3 Poisson's ratio

Poisson's ratio was computed from corresponding vertical to horizontal strain ratio  $\left( \frac{Y}{X} \right)$  at 40% of peak stress, associated with the equation D-10.

#### D.4.3.4 Fracture energy and toughness

The fracture energy of Superpave strength IDT test on concrete, denoted as  $J_{IDT}$ , was calculated the area under stress—strain curve up to the failure stress as follows:.

$$\Delta J_{IDT}(t_i) = \frac{1}{2} \times [\sigma(t_i) + \sigma(t_{i-1})] \times [\varepsilon(t_i) - \varepsilon(t_{i-1})] \quad (D-17)$$

$$J_{IDT}(t_{failure}) = \sum_0^{t_{failure}} \Delta J_{IDT}(t_i) \quad (D-18)$$

where,  $\Delta J_{IDT}(t_i)$  = a segment of fracture energy per one unit time  $t_i$ .

$J_{IDT}(t_{failure})$  = fracture energy (calculated up to the failure stress)

The toughness of Superpave IDT strength test on concrete was calculated the area under stress—strain curve up to the peak stress as follows:

$$J_{IDT}(t_{peak}) = \sum_0^{t_{peak}} \Delta J_{IDT}(t_i) \quad (D-19)$$

where,  $J_{IDT}(t_{peak})$  = toughness (calculated up to the peak stress)

In addition, the fracture energy were averaged from three replicate concrete specimens and the toughness was computed from the mean stress—strain curve for every concrete mixes.

## **D.5 Results of Superpave IDT Strength Test under Force-Control Loading**

### **D.5.1 Behaviors of Stress—Strain Curve**

Individual stress—strain plot of PCC and concrete containing RAP-3 at 28 and 90 days curing time were evaluated. Figure D-8 presents typical stress—strain plots for dense-graded HMA, PCC, and concrete containing RAP-3. Figure D-8(A) is a typical example of dense-graded HMA with PG 64-22 asphalt binder and tested at 10°C under a displacement-control rate—0.05 in/sec for the purpose of comparison. The plots of two horizontal strains were shown up to the peak load. After the peak load was reached, one strain was extended longer in development than the other. However, both strains were developing in the same direction.

Figure D-8(B) shows a rather different behavior of a PCC specimen with w/c=0.45 and tested at 23°C under a force-control rate. Two horizontal strains were increasing more and less at the same rate, but went apart when the peak load was approached. One strain would develop further more in the positive direction, but the other would turn in the negative direction.

Different behavior of recorded strains on both faces of a specimen suggested that one side of specimen was in tension, while the other side was in compression, due to the fact that specimen was not perfectly symmetrical.

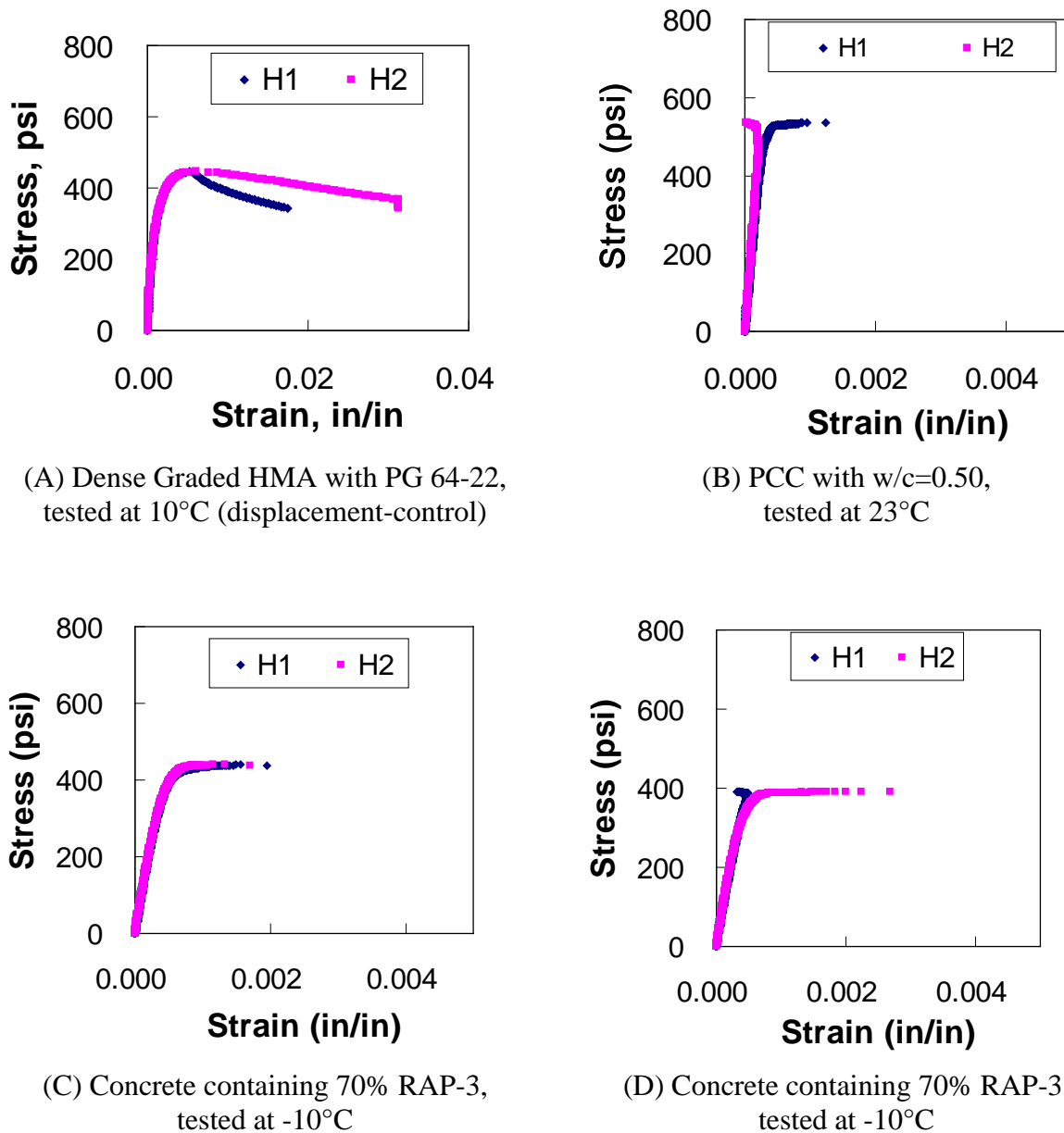


Figure D-8. Examples of stress—strain plots with two horizontal strain gages in the Superpave IDT test under force-control load rate

For concrete containing RAP-3 mixes, the stress—strain curve behaviors are shown in Figure D-8(C) and (D). Figure D-8(C) shows horizontal strains on both sides of specimen were growing uniformly in most cases for concrete mixes with higher RAP-3 replacement, such as 70% and 100%. However, there were still cases of concrete mixes containing 20% and 40% RAP-3 where the recorded horizontal strains moved in opposite directions, similar with PCC, shown in Figure D-8(D). Additionally, clear boundary limit between elastic and plastic regimes could be seen on those plots.

## **D.5.2 Results of Indirect Tensile Strength**

### **D.5.2.1 Indirect tensile strength (using peak stress)**

Concrete specimens of 7, 14, 28, and 90 days curing time were evaluated by the Superpave IDT strength test at -10, 23, and 60°C. Table 5-1 shows indirect tensile strength results of the Superpave IDT strength tests calculated from peak loads at three different testing temperatures and four different curing periods. Generally, indirect tensile strength of all PCC and concrete containing RAP-3 were higher along with the curing time and the addition of RAP-3 considerably reduced the tensile strength.

Figure D-9 shows the indirect tensile strength of all the PCC mixes. It was found that the thermal effect was indeed affecting the tensile strength of PCC mixes. The frozen internal moisture in low temperature seemed to support the early tensile strength. On the other hand, the possible accelerated drying in high temperature caused the loss in early strength. Mature concrete mixes with 28 and 90 days curing time were seemingly not to be affected by thermal effect in terms of tensile strength.

Table D-1. Results of indirect tension test (using peak stress)

Superpave IDT		Strength Tests, psi			Superpave IDT		Strength Tests, psi						
Curing Days	Mix Design	Temperature, °C			Curing Days	Mix Design	Temperature, °C						
		-10	23	60			-10	23	60				
7	w/c=0.45 PCC	474.99	602.22	470.08	7	20% RAP3	435.79	412.50	366.25				
14		544.58	552.25	360.33	14		479.28	426.12	377.69				
28		561.47	599.64	590.99	28		509.37	409.18	401.99				
90		650.62	671.25	538.41	90		504.86	459.71	419.44				
7	w/c=0.50 PCC	584.39	589.35	433.41	7	40% RAP3	393.87	389.84	302.62				
14		505.37	502.94	436.18	14		436.86	379.67	275.79				
28		497.34	550.06	554.81	28		421.72	381.02	303.53				
90		547.46	567.03	587.57	90		451.02	421.40	377.76				
7	w/c=0.55 PCC	592.23	494.40	382.33	7	70% RAP3	391.26	234.03	181.70				
14		611.48	448.24	-	14		422.84	258.42	194.64				
28		507.50	518.10	587.00	28		389.87	294.20	205.36				
90		599.67	604.28	596.85	90		415.44	360.32	234.84				
									7	100% RAP3	322.55	239.34	128.52
									14		301.81	243.95	128.87
									28		315.08	245.03	161.61
									90		381.80	304.94	169.69

\* IDT Strength test on PCC of w/c=0.55 and 14-d cured was incomplete in 60°C.

\* Water to cement ratio was 0.50 for every for concrete containing RAP-3.

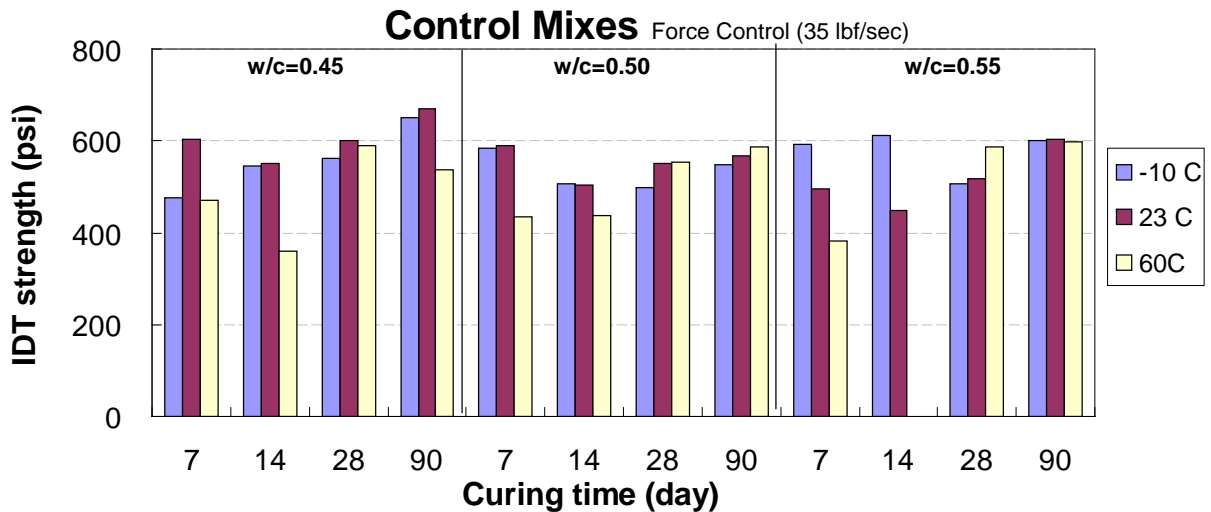


Figure D-9. Comparison of indirect tensile strength results in PCC control mixes (using peak stress)

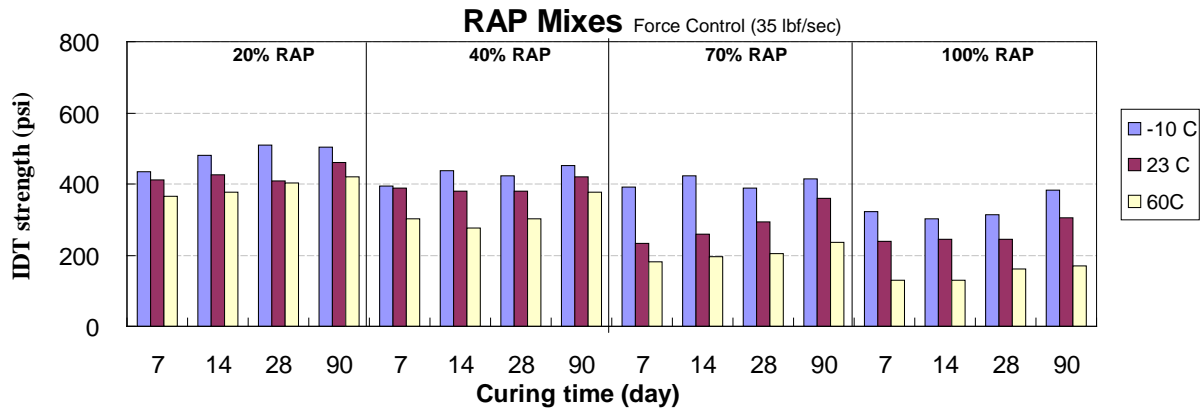


Figure D-10. Comparison of Indirect tensile strength results in concrete mixes containing RAP-3 (using peak stress)

Figure D-10 presents the indirect tensile strength of concrete mixes containing RAP-3 tested. It was found that the thermal effect clearly influenced the tensile strength of concrete mixes containing RAP-3, due to the presence of RAP. The asphalt binder played the similar role as the frozen moisture to support the tensile strength in low temperature, especially the mixes containing 70% and 100% RAP-3. However, the tensile strength loss tested in high temperature was significant on these mixes. Mature concrete mix containing 20% RAP-3 was the least one to be affected by loss of tensile strength high temperature, similarly with the observation in PCC mixes.

#### D.5.2.2 Indirect tensile strength (using failure stress)

Table D-2 shows results of the Superpave IDT strength tests computed from failure loads at three different testing temperatures and four different curing periods. Failure stresses of concrete specimens with 28 and 90 days were evaluated from the individual stress—strain curves. The tensile strength calculated from failure stress was about 74-94% of that computed from peak stress for PCC mixes, and was about 57-87% of that derived from peak stress for concrete containing RAP mixes.

Table D-2. Results of Indirect tension test (using failure stress)

Superpave IDT		Strength Tests, psi			Superpave IDT		Strength Tests, psi		
Curing Days	Mix Design	Temperature, °C			Curing Days	Mix Design	Temperature, °C		
		-10	23	60			-10	23	60
7		-	-	-	7		-	-	-
14		-	-	-	14		-	-	-
28	w/c=0.45 PCC	520.48	533.27	457.41	28	w/c=0.50 20% RAP	446.76	320.62	298.09
90		493.18	578.06	446.00	90		411.87	366.81	303.86
7		-	-	-	7		-	-	-
14		-	-	-	14		-	-	-
28	w/c=0.50 PCC	424.72	495.91	455.01	28	w/c=0.50 40% RAP	303.59	248.20	215.94
90		506.45	494.70	514.56	90		235.69	312.05	278.97
7		-	-	-	7		-	-	-
14		-	-	-	14		-	-	-
28	w/c=0.55 PCC	479.00	419.89	520.76	28	w/c=0.50 70% RAP	334.16	198.11	141.01
90		511.03	475.79	439.71	90		260.15	235.97	146.13
					7		-	-	-
					14		-	-	-
					28	w/c=0.50 100% RAP	246.94	137.35	92.77
					90		269.03	181.04	98.37

\* Stress—strain curves of concrete specimens with 7 and 14 days curing time were not included to be tested for computing failure stress.

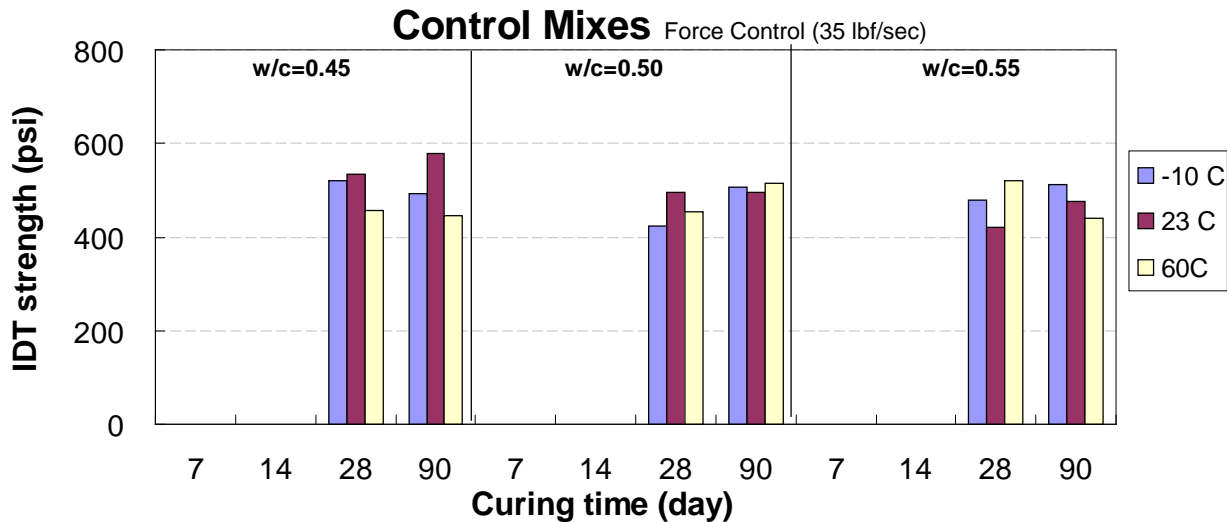


Figure D-11. Comparison of Indirect tensile strength results in PCC control mixes (using failure stress)

Figure D-11 and Figure D-12 show similar comparison as Figure D-9 and Figure D-10. For PCC mixes, the tensile strength computed from failure stress on mature concrete was not dramatically affected by the either low or high temperature, which was similar to the results calculated from peak stresses. The tensile strength of concrete mixes with low water to cement

ratio of 0.45 tested in high temperature appeared to have noticeable strength loss which may be attributed to the accelerated drying shrinkage.

For concrete containing RAP-3, tensile strength computed from failure stress presented similar trend of low temperature. The reduction of tensile strength tested at high temperature for concrete containing higher RAP-3 was significant. Nevertheless, the failure stress was generally reduced with the addition of RAP-3.

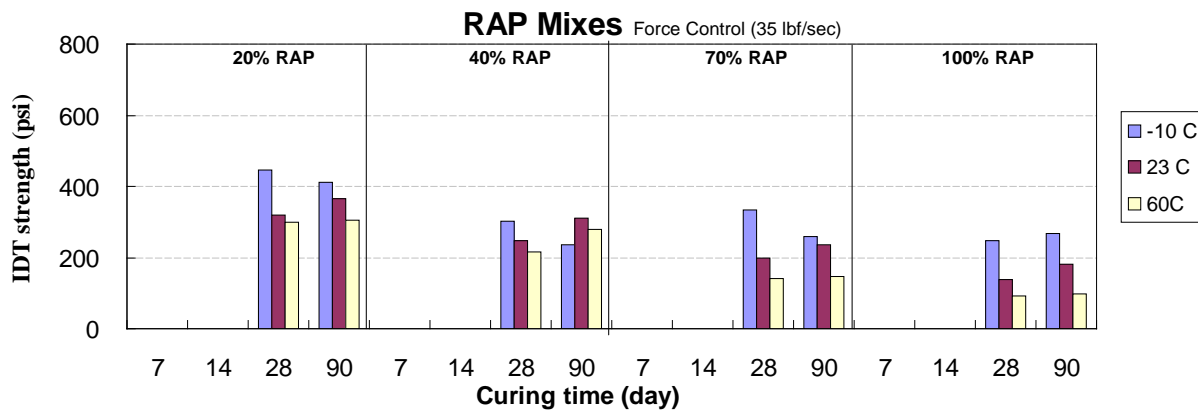


Figure D-12. Comparison of Indirect tensile strength results in concrete mixes containing RAP (failure stress)

### D.5.3 Results of Elastic Modulus, Poisson’s Ratio, and Toughness

#### D.5.3.1 Elastic modulus, Poisson’s ratio, and toughness (using peak stress)

Results of elastic modulus, Poisson’s ratio and fracture energy are shown in Table D-3.

These parameters were computed from the mean stress—strain curve of each concrete mix.

Table D-3. Results of elastic modulus, Poisson's ratio, and toughness (using peak stress)

Temperature °C	Mix Design	28-d cured					90-d cured			
		Elastic Modulus psi	Toughness		Poisson's Ratio	Elastic Modulus psi	Toughness		Poisson's Ratio	
			in*lb/in <sup>3</sup>	KJ/m <sup>3</sup>			in*lb/in <sup>3</sup>	KJ/m <sup>3</sup>		
-10	PCC	0.45	3.0712E+06	0.1765	0.0250	0.42	2.6761E+06	0.0854	0.0121	0.40
		0.50	2.6450E+06	0.0995	0.0141	0.47	2.6712E+06	0.0829	0.0117	0.55
		0.55	2.4585E+06	0.0798	0.0113	0.44	2.3970E+06	0.0716	0.0101	0.14
	RAP	20%	1.9054E+06	0.1922	0.0272	0.53	2.2948E+06	0.0988	0.0140	0.38
		40%	1.7993E+06	0.1580	0.0224	0.57	2.0157E+06	0.1377	0.0195	0.10
		70%	1.5454E+06	0.0857	0.0121	0.37	1.5734E+06	0.2257	0.0320	0.40
		100%	1.0394E+06	0.1280	0.0181	0.47	1.2428E+06	0.1461	0.0207	0.06
23	PCC	0.45	3.1190E+06	0.1319	0.0187	0.23	2.8765E+06	0.2605	0.0369	0.49
		0.50	2.9945E+06	0.2175	0.0308	0.27	2.9242E+06	0.1115	0.0158	0.39
		0.55	2.6677E+06	0.1155	0.0164	0.23	2.7121E+06	0.1190	0.0168	0.35
	RAP	20%	2.3025E+06	0.1443	0.0204	0.39	2.4203E+06	0.1550	0.0219	0.28
		40%	1.8759E+06	0.1613	0.0228	0.31	1.9935E+06	0.0840	0.0119	0.24
		70%	1.2729E+06	0.2735	0.0387	0.28	1.4077E+06	0.0800	0.0113	0.31
		100%	9.6905E+05	1.1535	0.1633	0.18	9.4949E+05	1.2894	0.1826	0.27
60	PCC	0.45	3.2879E+06	0.1450	0.0205	0.13	3.0644E+06	0.1006	0.0142	0.31
		0.50	3.4290E+06	0.1341	0.0190	0.10	2.8810E+06	0.1467	0.0208	0.32
		0.55	2.9483E+06	0.1379	0.0195	0.14	2.7737E+06	0.0499	0.0071	0.60
	RAP	20%	2.1646E+06	0.0891	0.0126	0.17	2.2332E+06	0.1553	0.0220	0.22
		40%	1.5022E+06	0.3850	0.0545	0.34	1.9805E+06	0.3011	0.0426	0.20
		70%	1.0705E+06	0.3702	0.0524	0.23	1.3186E+06	0.2263	0.0320	0.19
		100%	6.9513E+05	0.7558	0.1070	0.23	7.0755E+05	0.4041	0.0572	0.25

\* Water to cement ratio was 0.50 for every for concrete containing RAP-3.

**Elastic modulus.** Figure D-13 shows the elastic modulus of PCC and concrete mixes containing RAP-3 evaluated. It was found that the addition of RAP-3 in concrete significantly reduced the elastic modulus. In general, elastic modulus of PCC mixes were slightly reduced with longer curing time but only increased a bit along with higher test temperature. On the other hand, neither curing time nor test temperature was affecting elastic modulus of concrete containing RAP-3 significantly.

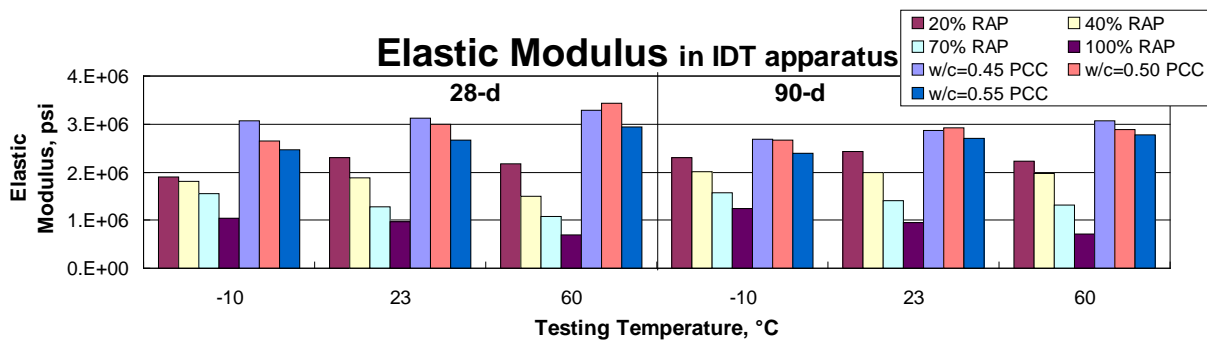


Figure D-13. Comparison of elastic modulus in PCC and concrete containing RAP

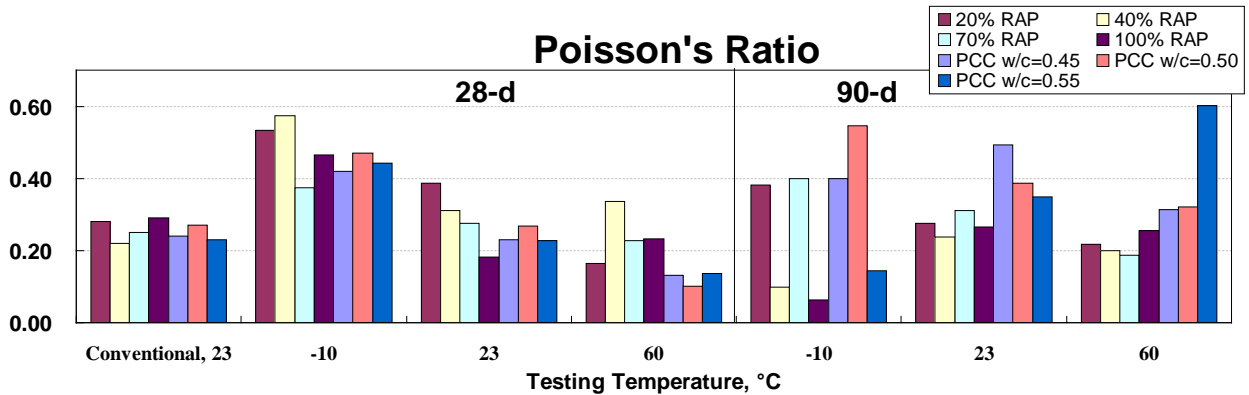


Figure D-14. Comparison of Poisson's ratio in PCC and concrete containing RAP

**Poisson's Ratio.** Figure D-14 shows that the Poisson's ratio of PCC and concrete mixes containing RAP-3 examined by Superpave IDT test as well as the conventional test results. It was found that Poisson's ratio stayed about 0.30 for both PCC and RAP-3 mixes in conventional

test. For results tested under force-control loading rate, Poisson’s ratio appeared to be abnormal, except for results of PCC mixes tested in 23°C.

**Toughness.** Figure D-15 shows toughness of PCC and concrete mixes containing RAP-3 evaluated. It was found the toughness was generally reduced along with the curing time, which may attribute to the increasing concrete brittleness from the hydration of cement.

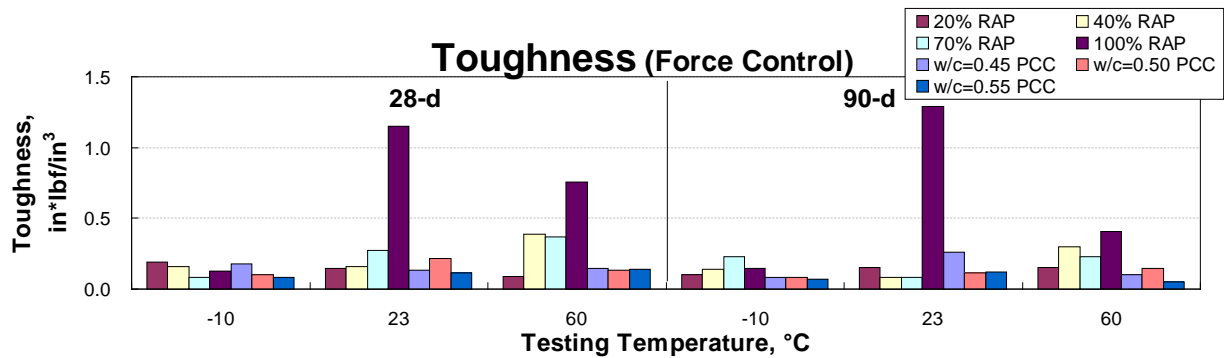


Figure D-15. Comparison of toughness in PCC and concrete containing RAP-3 (force-control)

Concrete mixes containing 40%, 70% and 100% RAP-3 developed higher toughness in high temperature than PCC and concrete containing 20% RAP-3. The concrete containing 100% RAP-3 mixes on both 28 and 90 days curing were of highest toughness, except for the low temperature test condition. Higher toughness may attribute to the ductility improved by RAP. It has to be noted that the toughness is calculated as the area under mean stress—strain curve up to the peak stress.

#### 5.4.3.2 Fracture energy (using failure stress)

Fracture energy is defined differently than the toughness. The fracture energy is the area under the stress—strain curve up to the failure stress as defined in HMA fracture mechanics in this study. Table D-4 and Figure D-16 show the fracture energy of concrete mixes of 28 and 90 days curing time.

Table D-4. Results fracture energy (using failure stress)

Temperature °C	Mix Design	28-d cured		90-d cured		
		Fracture energy in*lb/in <sup>3</sup>	KJ/m <sup>3</sup>	Fracture energy in*lb/in <sup>3</sup>	KJ/m <sup>3</sup>	
-10	PCC	w/c=0.45	0.0641	0.0091	0.0637	0.0090
		w/c=0.50	0.0471	0.0067	0.0575	0.0081
		w/c=0.55	0.0603	0.0085	0.0655	0.0093
	RAP	20%	0.0613	0.0087	0.0485	0.0069
		40%	0.0351	0.0050	0.0182	0.0026
		70%	0.0542	0.0077	0.0302	0.0043
		100%	0.0443	0.0063	0.0407	0.0058
23	PCC	w/c=0.45	0.0775	0.0110	0.0905	0.0128
		w/c=0.50	0.0566	0.0080	0.0602	0.0085
		w/c=0.55	0.0423	0.0060	0.0633	0.0090
	RAP	20%	0.0356	0.0050	0.0425	0.0060
		40%	0.0266	0.0038	0.0391	0.0055
		70%	0.0261	0.0037	0.0346	0.0049
		100%	0.0160	0.0023	0.0288	0.0041
60	PCC	w/c=0.45	0.0475	0.0067	0.0504	0.0071
		w/c=0.50	0.0602	0.0085	0.0652	0.0092
		w/c=0.55	0.0702	0.0099	0.0434	0.0061
	RAP	20%	0.0310	0.0044	0.0316	0.0045
		40%	0.0271	0.0038	0.0335	0.0047
		70%	0.0159	0.0023	0.0127	0.0018
		100%	0.0102	0.0014	0.0127	0.0018

\* Water to cement ratio was 0.50 for every for concrete containing RAP.

When compared with the toughness computed from the area of stress—strain curve up to the peak stress, all the fracture energy were less than the toughness, especially for concrete mixes containing RAP-3. Generally speaking, fracture energy of PCC mixes was higher than all concrete mixes containing RAP-3. Fracture energy of PCC mixes was not affected by testing temperatures, but higher testing temperature seemed to reduce the fracture energy of concrete containing RAP-3.

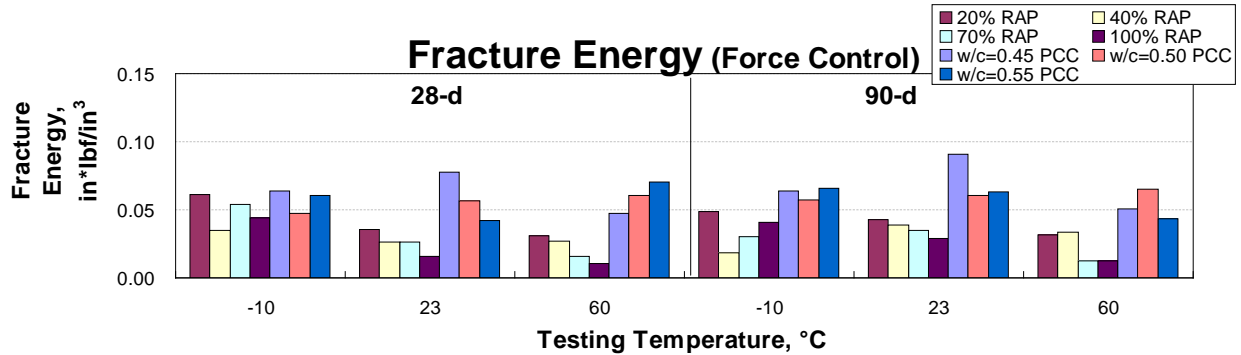


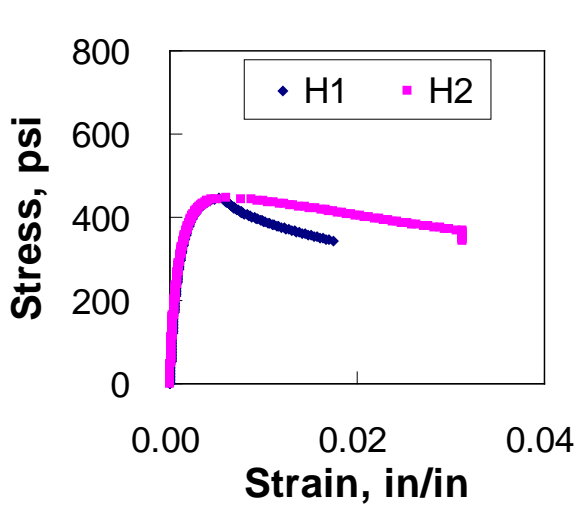
Figure D-16. Comparison of Fracture energy in PCC and concrete containing RAP-3 (using failure stress)

## D.6 Results of Superpave IDT Strength Test under Displacement-Control Loading

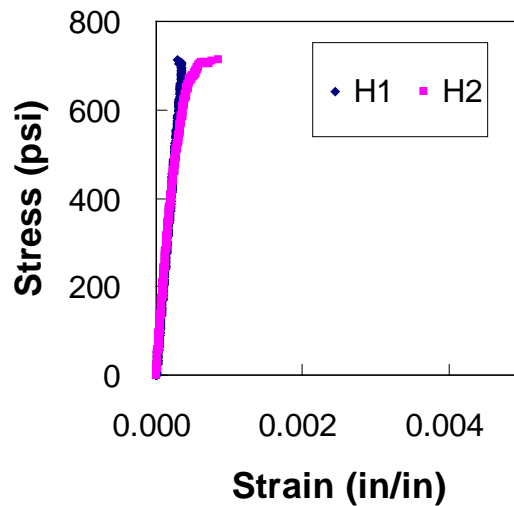
### D.6.1 Behaviors of Stress—Strain Curve

Stress—strain curve of PCC and concrete containing RAP-3 tested under displacement-control are shown in Figure D-17. Figure D-17(A) shows the same dense-graded HMA plot (same with Figure D-8(A)) for the purpose of comparison and Figure D-17(B) to (D) present example behaviors of PCC and concrete containing RAP-3.

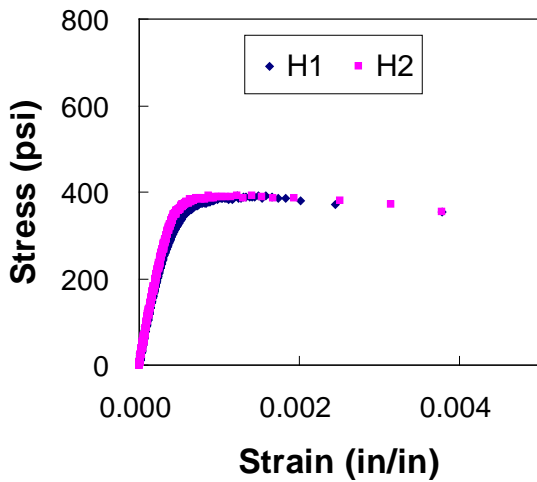
Figure D-17(B) and (D) indicated similar stress—strain behaviors with results under force-control loading rate of PCC and concrete containing RAP-3. One side of horizontal strain appeared the similar negative turning, but it was shorter than examples in force-control loading rate. Meanwhile, concrete containing 70% and 100% RAP-3 had less to none negative turning in one side of horizontal strain, shown in Figure D-17(C). The stress--strain plots of concrete containing higher RAP-3 developed similarly with the plot of HMA. All stress—strain plots had clear boundary limit in terms of elastic and plastic regimes, which was again similar with curves in force-control loading rate.



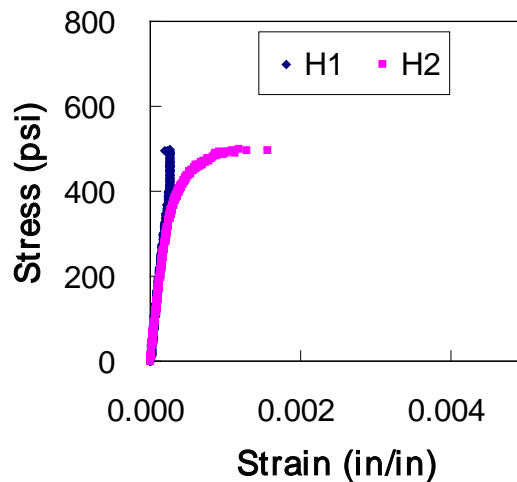
(A) Dense Graded HMA with PG 64-22, tested at 10°C



(B) PCC with w/c=0.50, tested at 60°C



(C) Concrete containing 70% RAP-3, tested at 60°C



(D) Concrete containing 20% RAP-3, tested at 60°C

Figure D-17. Examples of stress—strain plots with two horizontal strain gages in the Superpave IDT test under displacement-control load rate

### D.6.2 Indirect Tensile Strength (using peak stress)

Further effort was made to validate compare the indirect tensile strength under between the force-control rate of 35.343 lbf/sec and displacement-control rate of 0.00075 in/sec. Three PCC

and four concrete containing RAP-3 mixes of 90 days curing had been tested by the Superpave IDT under 23°C. The test results, shown in Figure D-18, appeared no significant difference for PCC and RAP-3 mixes in terms of the way of loading. It may suggest that either loading rate may yield similar indirect tensile strength.

This comparison reflected the well-known understanding about force-control and displacement-control loading rates. Mier (Mier, 1997) commented that specimen will fail in an uncontrolled manner by applying the load-control, while the displacement control with the closed-loop servo-controlled equipments can measure the post-peak softening curve of stress—strain plot. However, the load-control tests traditionally gave materials, such as concrete, ceramics, and rock, sufficient pre-peak information about the initial Young’s modulus and maximum strength.

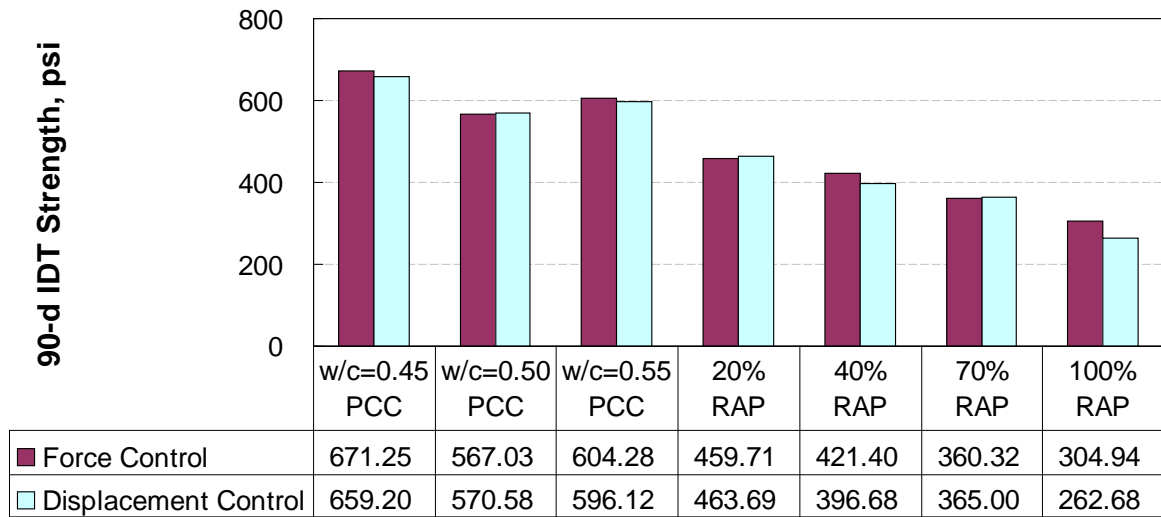


Figure D-18. Comparison of tensile strength obtained from force-control versus displacement control tests

### D.6.3 Poisson's Ratio (using peak stress)

Another endeavor was made to compare the Poisson's ratios that were determined with the displacement-control rate, shown in Figure D-19. Poisson's ratios of PCC and concrete containing RAP-3 tested under 23°C in displacement-control mode were about 0.30, similar with conventional results. In computation of tensile strength under force-control loading rate, the correction factor for correcting tensile strength (CSX, described in chapter 2.2) was omitted because of irregular Poisson's ratios. If Poisson's ratio can be reasonably assessed under the displacement-control load rate, the correction factor could be considered to correct the tensile strength.

In this study, when correction factor of CSX were to be applied, it would cause a range of 2.1% to 5.5% reduction in tensile strength from results tested by the displacement-control loading rate.

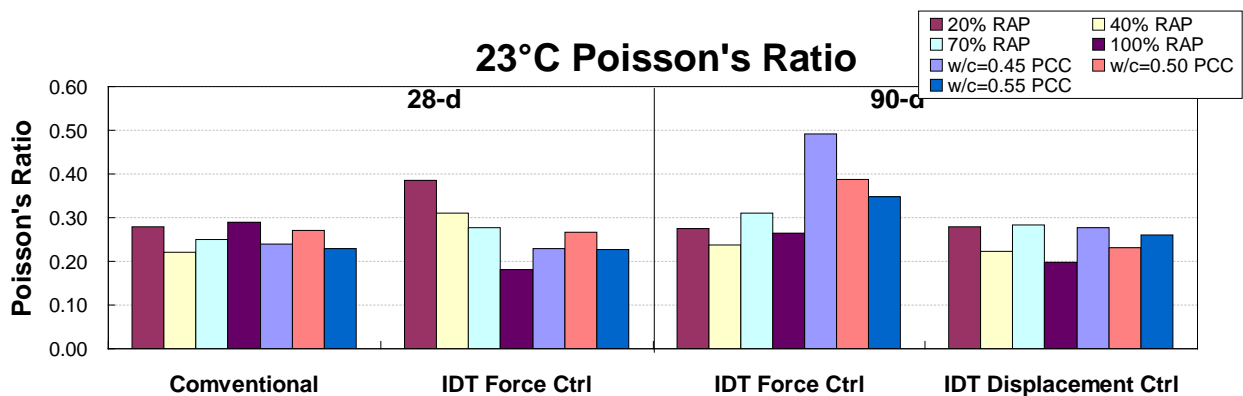


Figure D-19. Comparison of Poisson's ratio between conventional test in compression versus force-control and displacement-control in the Superpave IDT strength tests

### D.6.4 Toughness (using peak stress)

Figure D-20 shows toughness for concrete specimens of 90 days curing time tested in 23°C by force-control and displacement-control loading rates.

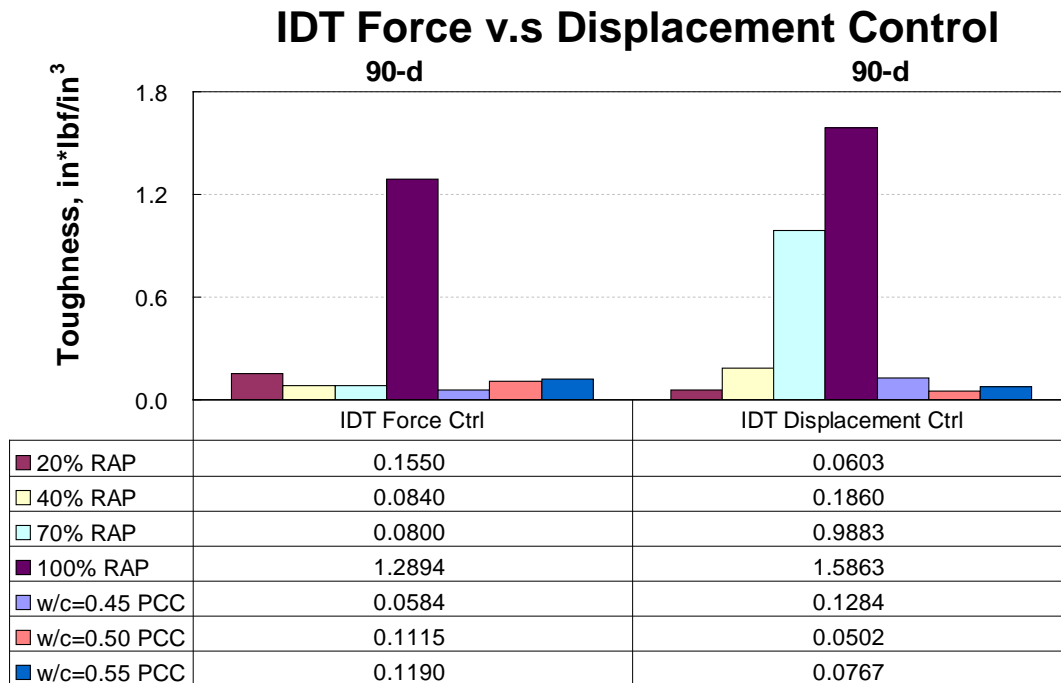


Figure D-20. Comparison of toughness obtained from force-control versus displacement control tests

The failure detection in displacement-control mode was set to stop the test when strength reduced to 50% loss of peak load, while the previous failure detection in force-control mode was set at 20%. The displacement-control mode seemed to capture noticeable toughness on 40% and 70% RAP that were not captured in the force-control mode tested in 23°C, which may proxy a better assessment in terms of toughness.

## D.7 Correlations between Conventional and Superpave IDT Strength Tests

### D.7.1 Tensile Strength

A further analysis had endeavored to establish correlations of splitting, flexural, and Superpave IDT strength, corresponding to identical curing periods, shown in Figure D-21. It was found that the splitting tensile strength correlated well with the Superpave IDT strength of 28 days curing time computed from peak stress.

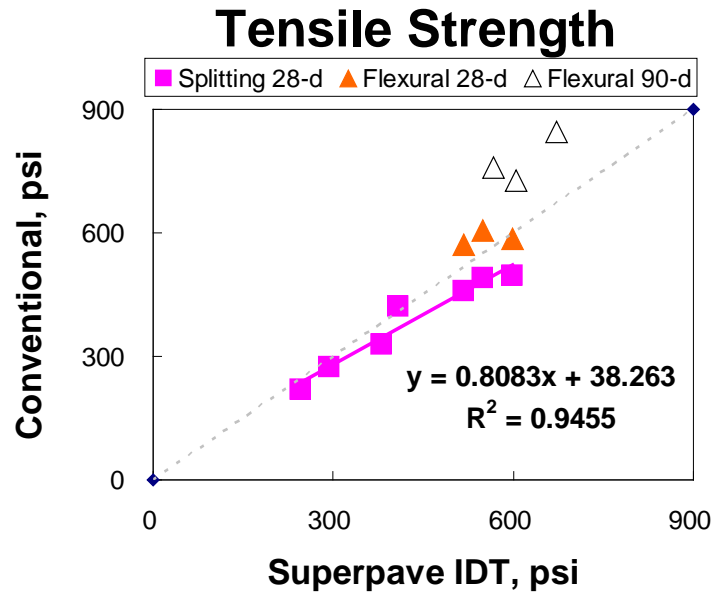


Figure D-21. Correlation of tensile strength between splitting and Superpave IDT strength test under 23°C

The linear regression between the splitting tensile ( $T_{Splitting}$ ) and the tensile strength ( $T_{IDT}(peak)$ ) computed from peak stress from the Superpave IDT strength test in this study, under 23°C, is as follows:

$$T_{Splitting} = 0.8083 \times T_{IDT}(peak) + 38.263 \quad (D-20)$$

$$R^2 = 0.9455$$

It was reasonable to see a good correlation between conventional splitting tensile and the Superpave IDT strength tests, since both tests were similar, except for the thickness of specimens. The stress state and analysis can be considered reasonably close to each other. However, none of the flexural strength data were close to the tensile strength from the Superpave IDT strength test, although this relationship may be able to be established through other well-documented correlations between splitting tensile and flexural strength.

### D.7.2 Elastic Modulus

Another attempt to correlate elastic modulus obtained from the conventional test ASTM C469 in compression and that from the Superpave IDT strength tests of concrete mixes with 28 days curing time is shown in Figure D-22. Both PCC and concrete containing RAP-3 mixes showed a high correlation between results from these two tests. The relationships of PCC and RAP-3 mixes are as follows:

$$\begin{aligned} \text{PCC mixes: } E &= 1.0983(E_{IDT}) + 1815103 & (D-21) \\ R^2 &= 0.9655 \end{aligned}$$

$$\begin{aligned} \text{Concrete containing RAP mixes: } E &= 1.6951(E_{IDT}) - 125752 & (D-22) \\ R^2 &= 0.9855 \end{aligned}$$

where,  $E$  = chord modulus of elasticity at 40% of peak stress in compression,  
 $E_{IDT}$  = secant modulus of elasticity from stress—strain curve at 40% of peak stress in Superpave IDT strength test.

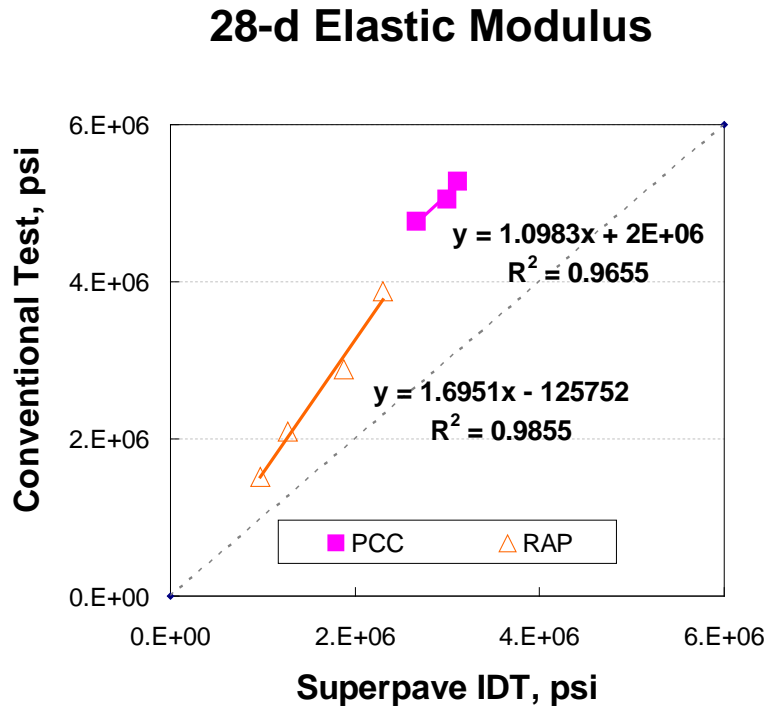


Figure D-22. Correlation of elastic modulus between conventional and the Superpave IDT strength tests

### D.7.3 Poisson's Ratio

Additional correlation between the Poisson's ratios obtained from conventional and Superpave IDT strength tests on 28-d cured mixes tested at 23°C are shown in Figure D-23. Poisson's ratio of PCC mixes obtained from these two tests related well with one another. However, the same cannot be found for concrete containing RAP mixes. The correlation of Poisson's ratios from ASTM C469 and the Superpave IDT strength test of PCC mixes is as follows:

$$\begin{aligned} \nu &= 0.9146 \times (\nu_{IDT}) + 0.0261 \\ R^2 &= 0.9702 \end{aligned} \tag{D-23}$$

where,  $\nu$  = Poisson's ratio of ASTM C469.

$\nu_{IDT}$  = Poisson's ratio of the Superpave IDT strength test.

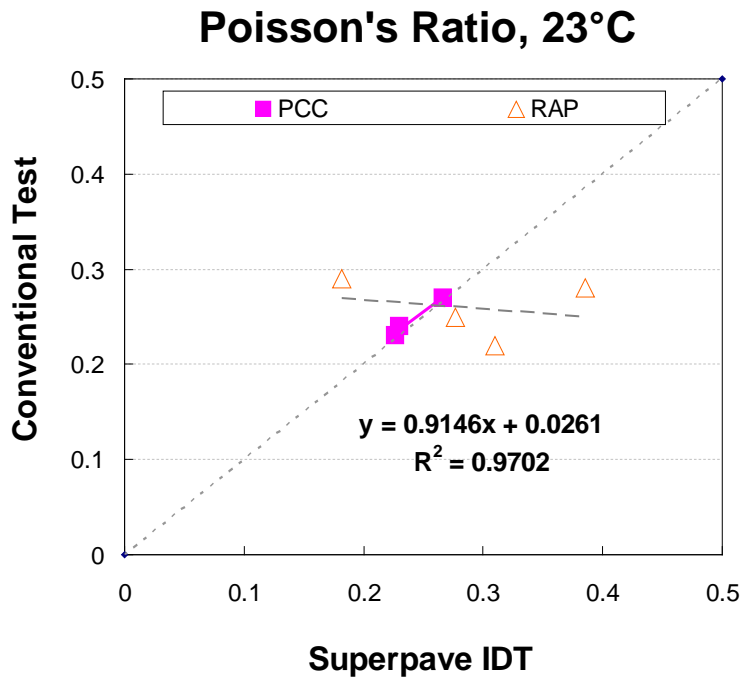


Figure D-23. Correlation of Poisson's ratio between conventional and the Superpave IDT strength tests

## **D.8 X-ray Computed Tomography Equipments at the University of Florida**

At the University of Florida, the X-ray CT facility is located in the Advanced Materials Characterization Laboratory (AMCL) in the Department of Civil and Coastal Engineering, where it was installed in 2009. It is equipped with 250 kV and 450 kV X-ray sources, a turn table, and the digital flat panel detector (FPD) inside the scanning chamber, as shown in Figure D-24 and Figure D-25 in schematic and plan views. There is also an in-situ MTS load frame that can be arranged so as to replace the turn table. Meanwhile, the 450 kV X-ray source provides a higher power to penetrate a larger object, while the 250 kV source with Micro-focus offers finer spatial resolution in scanning. The cone-beam X-ray system for both sources and the projected subject image, or so-called digital radiography (DR) image, will be recorded by the FPD. The 14 bit (i.e.  $2^{14}=16384$  gray levels) FPD is made of amorphous silicon (a-Si) with a  $2240 \times 3200$  pixel display, and 127 microns in pixel pitch. Both X-ray sources and FPD can be adjusted on the Y-axis. The definition of orientations is shown in the lower left corner of Figure 6-1. Additionally, the turn table or the load frame, controlled by joysticks or the proprietary software, can provide accurate segment turns for acquiring DR images. The resolution in “voxel” size is determined not only by the pixel pitch of the FPD, but also by the geometry between locations of the X-ray source, the test object on either the turn table or load frame, and the FPD. The geometric positioning of turn table, in-situ load frame, or FPD to X-ray sources can be arranged to optimize the contrast of DR images as well as achieve the geometric magnification.

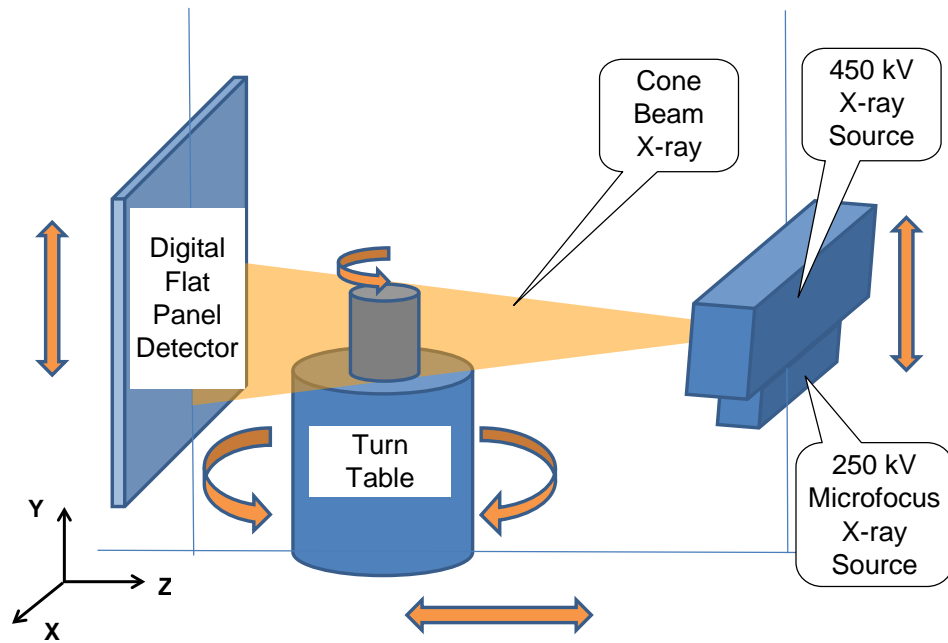


Figure D-24. Major components of X-ray CT facility at UF

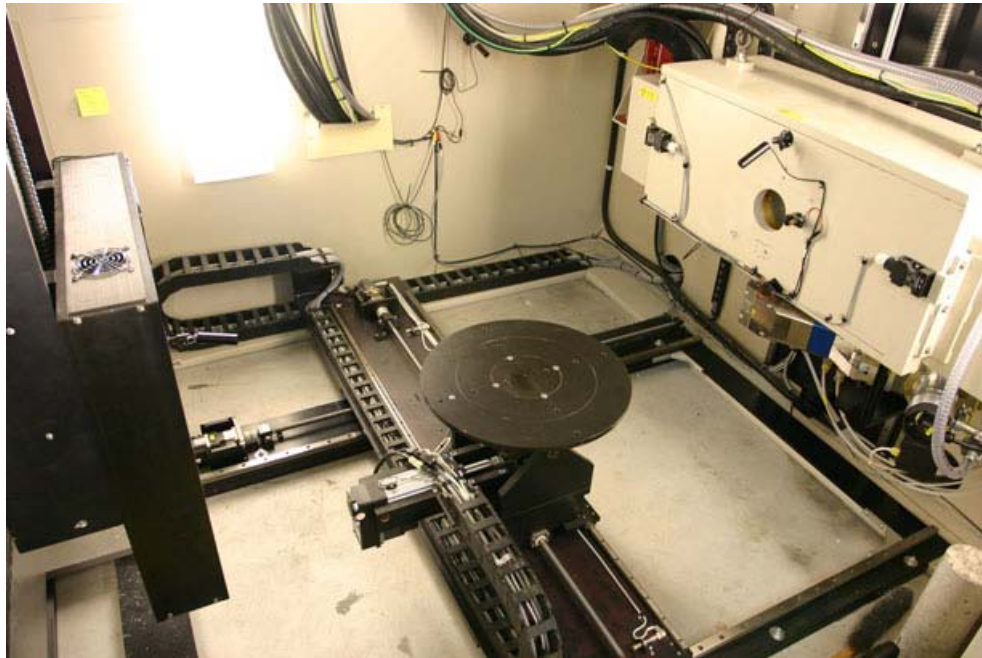


Figure D-25. Diagonal plan view of CT scan chamber

## **D.9 Procedures of X-ray Computed Tomography**

To start with, both X-ray sources require a warm-up routine every other day. A large lead block is placed in front of the X-ray source to prevent the emission of X-rays. If the X-ray CT scan is to be employed on a given day, the warm-up process on the designated X-ray source must take place. The warm-up process is controlled by the “FXE-Control” software for 225 kV X-ray source, while it is necessary to operate the warm-up process manually for 445kV X-ray source. Several steps involved in performing an X-ray CT scan at UF are as follows.

### **D.9.1 Calibration of Digital Flat Panel Detector**

The manufacturer suggests that the flat panel detector be calibrated every time that a new subject is to be scanned. There are three steps: “dark field”; “light field”; and “middle field” to be performed.

Dark field calibration ensures the condition of the detector, and the suggested target value is approximately 16000, which is about the limit of 14 bit gray levels. There is no X-ray emission when this calibration is running. The dark field calibration also offers a clean background and compensates the malfunctioning pixels on the detector. The light field calibration works to make certain that the detector could capture sufficient X-ray flux of the lowest gray levels—1500 to 3500. The least desirable gray level on the acquired DR image requires 2500, which means that the gray level on the “darkest” area of the targeted sample needs to have enough X-ray transverse to ensure the details that the DR image may carry. The middle field calibration requires medium gray levels, from 4000 to 8000. Both calibrations need the X-ray to be powered on, with the filter placed in front of the X-ray source, if the following X-ray CT scan may require that. The voltage and amperage will be recorded for future reference, in case of some abnormality occurring in the detector.

### **D.9.2 Position of Test Sample**

Either turn table or in-situ load frame is capable of being arranged between the X-ray source and the detector. Test sample needs to be fixed in its position to prevent undesired movement while the turn table is turning the segment during scanning. Additionally, the manufacturer suggests that it is convenient to scan a raised sample on the turn table. A plastic foam or low-density material is suggested, to help elevate the test sample. Additionally, duct tape is usually used to hold the test sample and plastic foam together. It is also important to place the test sample with the plastic foam carefully in the center of turn table. The duct tape can also help in fixing the specimen's position on the load frame without the hydraulic attenuator. When using the load frame, it is also a good idea to set a pre-load, to hold the specimen still.

### **D.9.3 Contrast Optimization in DR Images**

The manufacturer suggests adjusting the voltage (kV) and amperage ( $\mu\text{A}$ ) to optimize the contrast of DR images. The combination of kV and  $\mu\text{A}$  for CT scan can be varied. The rule of thumb (NSI training materials, 2009) suggests to firstly ramping up the voltage high enough, while not saturating the circular edge of concrete sample. Secondly, adjust amperage to determine a sufficient gray level (more than 2500) by observing the longest route (thickest portion) of the specimen, where the X-rays penetrate completely. Selection of X-ray source, geometric positioning, and the use of filter may influence the clarity of DR image. A trial run obtaining quality DR images is necessary.

### **D.9.4 Acquisition of DR Images**

The proprietary software, "X-View IW CT" is used for acquiring DR images at UF. It is necessary to have the scanning degrees of angle (number of view steps) assigned for each revolution scan of 360 degrees. For instance, if six degrees per segment turn was assigned, there are sixty DR images to be scanned and acquired. The larger the number of DR images scanned,

the more details of the targeted subject can be captured for later 3-D reconstruction. Common numbers of view steps in the X-ray CT facility at UF are 120, 360, 720, and 1440. However, it is time-consuming to acquire more DR images. For example, a 120-image scan on a concrete slice with 1.5 inches in thickness and 6 inches in diameter will consume approximately one hour, or about three hours per 360-image scan to collect DR images. It is necessary to determine how many view steps are sufficient for the test sample. The manufacturer suggests view steps of 720, or a half degree per segment turn, for a revolution scan.

#### **D.9.5 Reconstruction of 3-D Virtual Model**

The collected DR images will be transferred to the workstation computer with the proprietary software, “efX-CT” that is used to gather DR images, acquire the spatial information, and stack DR images into the 3-D virtual model. A special medium calibration rod with spheres spaced at 5 mm is designed to capture the spatial information where the test specimen was positioned. The purpose of obtaining this spatial information is to provide a volume reference, for software to establish the reconstruction. It is normal to capture 60 images with the same voltage used for a test specimen uses, but the amperage needs to be turned down in order to capture DR images on the calibration tools with sufficient contrast. It is easier to complete this task with the 225 kV X-ray source, and it may take many trials to finish this calibration with the 450 kV X-ray source. The definition issue is usually the main reason associated with the geometric positioning of the test sample. An adjustment using other amperages or an enhancement of contrast on acquired DR images may sometimes facilitate the process. A repetition of the scan from the beginning to obtain a better geometric positioning may be needed. It has been said that this 3-D calibration is crucial but may take many attempts to complete the process. Figure D-26 shows a completed process of obtaining the cylindrical spatial information.

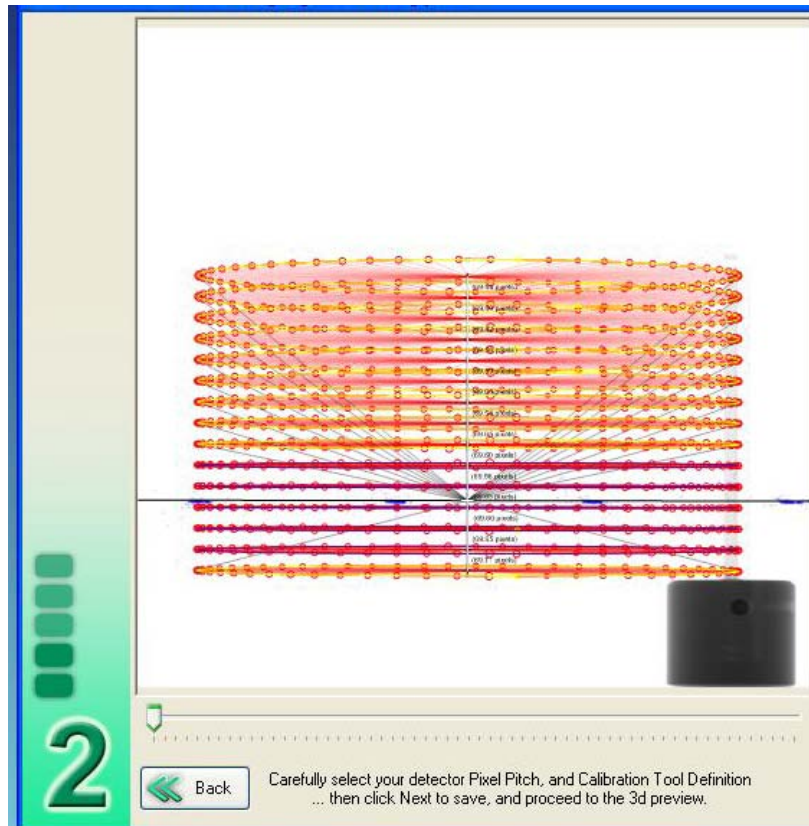


Figure D-26. Acquisition of spatial information by 3-D calibration tool

After acquiring 60 DR images of the calibration tool, the system is ready to assemble the collected DR images of test sample and of the calibration images to reconstruct the 3-D virtual model. Similar to the process of collecting DR images, the system requires about one hour for a 120-image scan or three hours for a 360-image scan for reconstruction process. However, it must be noted that the overall time span for completing an X-ray CT scan depends on the specimen thickness, the pixel size of the DR image, and the number of view steps. Figure D-27 depicts a 3-D virtual reconstructed model of a concrete specimen.

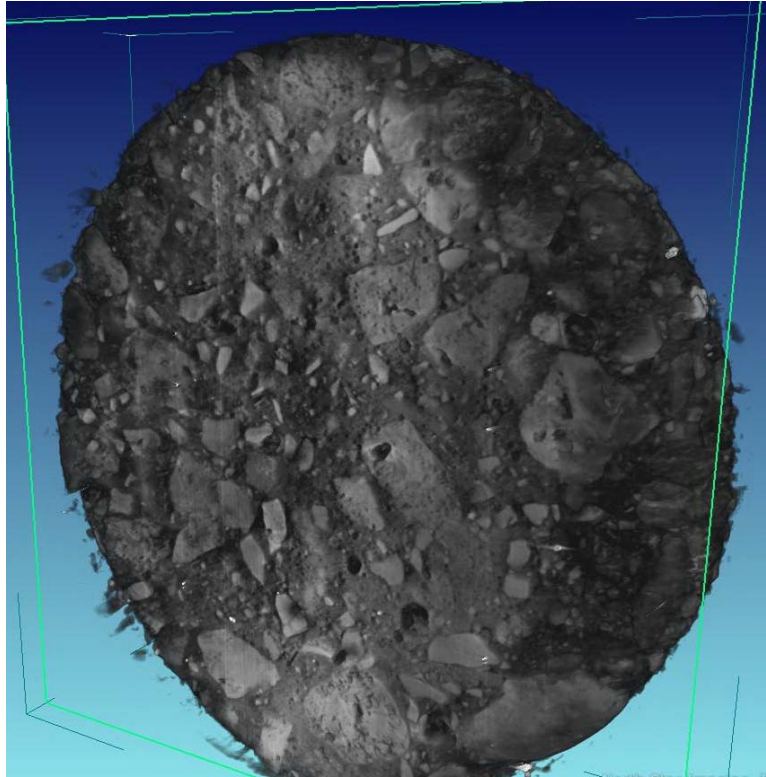
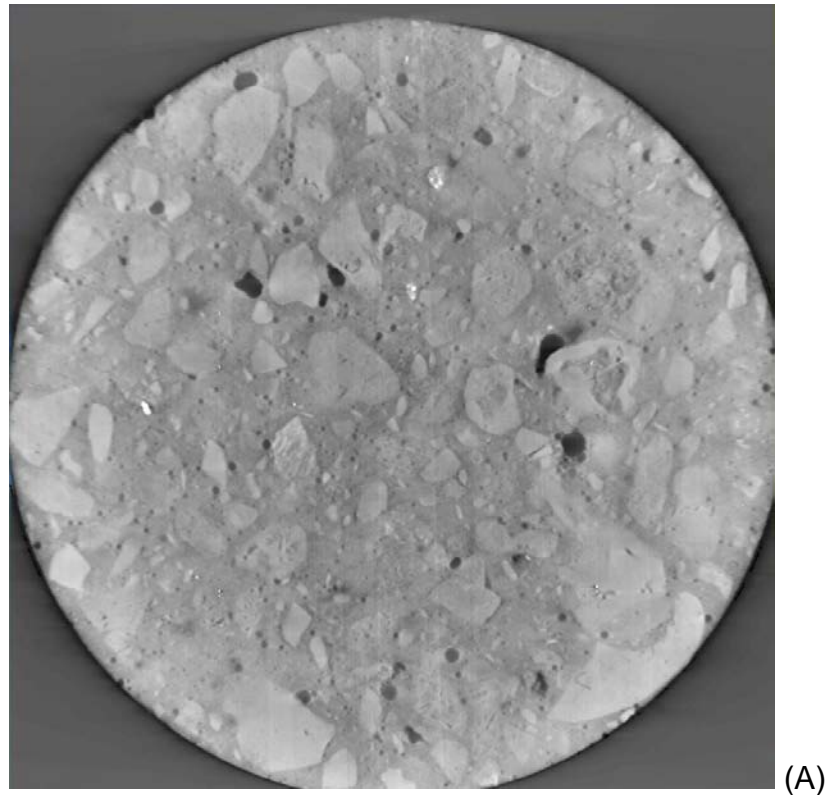


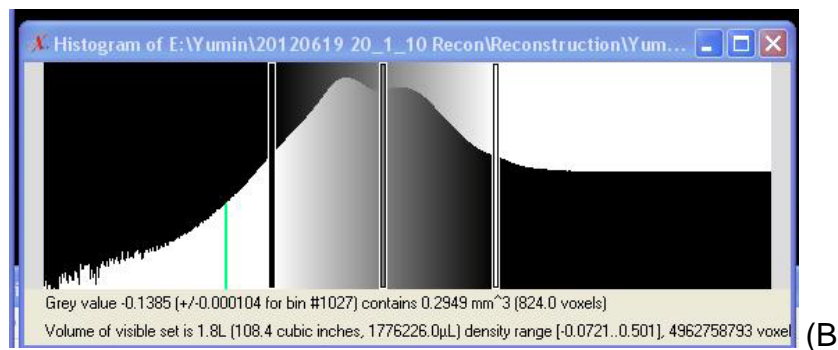
Figure D-27. 3-D reconstructed model of a concrete specimen

#### **D.9.6 Export of 2-D Images of Virtual Slice**

When the process of reconstruction is finished, a virtual 3-D will be virtually available within the window created by the software “efX-CT”. It has been mentioned that the advantage of X-ray CT is the ability to observe and to investigate the properties or phenomena of interest within the test specimen. The software is capable of recording video clips of the user’s manipulation on a test sample or of exporting the virtual-sliced images on the desired axis or angle.



(A)



(B)

Figure D-28. (A) A cross-sectional image of reconstructed 3-D model in concrete after process of window-leveling on Z-axis (B) Histogram of the 3-D model

A histogram is built associated with the reconstructed 3-D model. The histogram is a distribution or presentation that plots the accumulated number of pixels by specific gray levels. A technique of so-called “window-leveling”, by confining the histogram to certain gray levels, can result in segmentation or a divided view of each element separately. For example, a reconstructed model of concrete can apply window-leveling to separate aggregates, cement paste,

and voids. Figure D-28 (A) shows a cross-sectional image of a 3-D reconstructed model in concrete after the process of window-leveling. Figure D-28 (B) presents the histogram of the 3-D reconstructed model. The observer pulls the left and right bars to adjust the central bar, so that it falls more or less on the trough between two crests on the histogram. The whole cross-sectional virtual slice is visible on the computer monitor by carefully tuning these bars.

Once the area of interest is clearly observed, the process of exporting 2-D images of virtual slices can be performed. The software designates the default three axes, X, Y, and Z to export such cross-sectional slices. The spacing between slices is based on the resolution of the 3-D reconstructed model. For example, if the reconstructed model has the resolution of 71 microns in voxel size, the distance between two virtual slices is 71 microns, or 0.003 inches. Hence, the location of a specific virtual slice may be located for further investigations.

In short, it is feasible to perform X-ray CT scan to acquire 2-D DR images and to subsequently reconstruct the virtual 3-D model. By performing the window-leveling technique on the histogram enables the observer to reveal the area of interest. The 2-D images of virtual slices on the test sample can be exported, with the spacing distance identical with the resolution size, for further analysis.

## **D.10 X-ray CT in Conjunction with the Superpave IDT Strength Test**

### **D.10.1 Test Program**

The Superpave IDT Strength Test has been adopted to test concrete specimens as described in Chapter 5. A displacement-control loading rate of 0.00075 inches/sec with the closed-loop servo-controlled was selected for this task. It was decided to employ the loading program to apply an incremental load/unload pattern using the concrete mixes with 90 days curing, by the Superpave IDT strength test, namely from 0% (before loading), 10%, 20%, and up to the initiation of crack or failure. The test was performed in ambient temperature, approximately

23°C. The X-ray CT scan was performed after applying ten pounds of pre-loading to hold the test specimen. After the first scan was completed, a 10% load was then applied to the specimen and sustained for ten seconds. After ten seconds, the force was adjusted back to pre-load, and another X-ray CT scan was performed. It was assumed that the specimen had been damaged as much as necessary in ten seconds by the 10% incremental load. The loading and unloading pattern was to prevent the creep effect from adversely affecting the cause of microcrack initiation. The loading and unloading pattern continued until a failure was detected.

### **D.10.2 Concrete Mixes Evaluated**

Two PCC mixes ( $w/c=0.45$  and  $w/c=0.55$ ) and four  $w/c=0.50$  concrete mixes containing different levels of RAP replacement (20%, 40%, 70%, and 100%) were tested under the load/unload loading pattern, while X-ray CT scans were performed at the unloading mode. RAP material was obtained from Vero Beach, Florida, where its aggregate composition had been verified as mostly Florida limestone. Concrete cylinders were subjected to 100% moisture for 90 days of curing, and concrete specimens with 1.5 inches in thickness were prepared. The preparation of concrete specimens was identical with the descriptions of preparation for the Superpave IDT strength test described in Chapter 5.

### **D.10.3 Test Procedures**

#### **D.10.3.1 Geometry of load frame**

The in-situ load frame with force range of 22 kip (100 kN) is located inside the chamber and can be arranged in a chosen position between X-ray sources and FPD. Under such an arrangement, it is possible to apply loads to a specimen without moving its position, before and after a test. The geometrical positioning was set where the center of specimen was about three feet away from the X-ray source and two feet away from the FPD. This geometry offered resolution to 71 micron in voxel size. The X-ray source of 225 kV with Microfocus was selected

for this task. The smaller focal spot (< 6 micron) of the 225 kV tube can help minimize the unnecessary loss of definition and facilitate the efficiency of the later process of 3-D reconstruction. It was decided to use 120 kV and 550  $\mu$ A for scanning the concrete specimen, and 120 kV and 130  $\mu$ A for 3-D calibration of reconstruction under this geometry throughout this task. For 3-D calibration of reconstruction, the kV had to remain the one used for scanning concrete (i.e., 120 kV). The adjustment of amperage was used to observe black dots along the calibration rod clearly and to saturate the wrapped plastic materials.

#### **D.10.3.2 Positioning of test sample on the load frame**

An aligning steel bar was required to be attached to the turn table of the loading frame, as shown in Figure D-29, in order to synchronize the movement between the top hydraulic actuator and the turn table on the bottom, when the X-ray CT scan was performed.

Additionally, there is a limitation in synchronizing both compartments. It was found that the revolution X-ray CT scan can be completed when than 2500 pounds is applied at the same time. However, a pre-load of ten to fifteen pounds was chosen to secure the concrete specimen in the same location before and after the test, which was far less than this limitation of applied load.

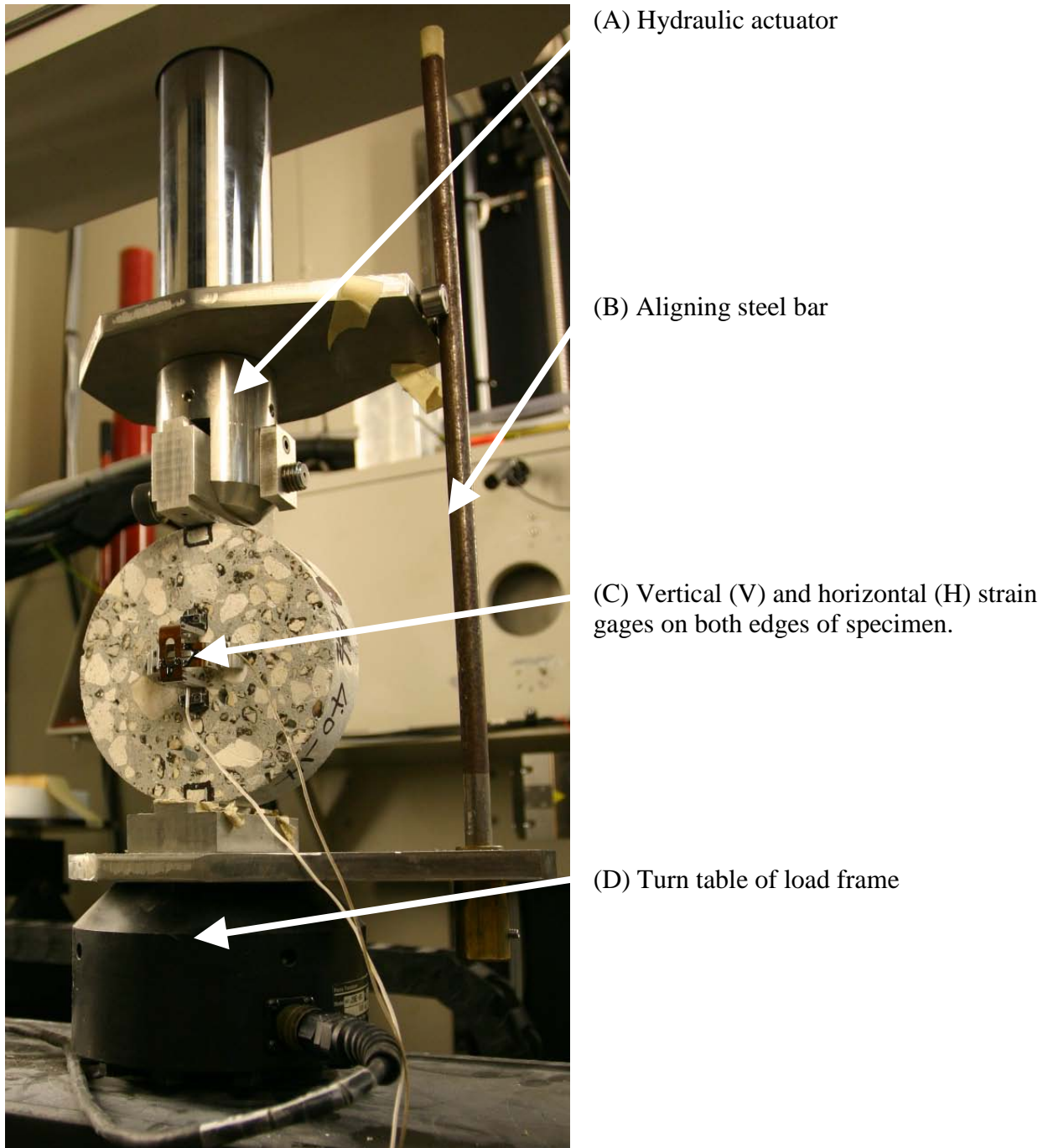


Figure D-29. The load frame set-up under Superpave IDT apparatus (Photo courtesy of Yu-Min Su)

### D.10.3.3 Performing an X-ray CT scan on concrete

The X-ray CT scan set to acquire 120 DR images was selected in this task. It has to be noted that the CT scan in conjunction with the load frame took a longer time for acquiring each

DR image, because shadows of the top hydraulic actuator and the bottom turn table, appearing nearly black as shown in Figure D-30, comprised more volume information for the acquisition system to handle. It took 45 minutes to complete an acquisition of 120 DR images.

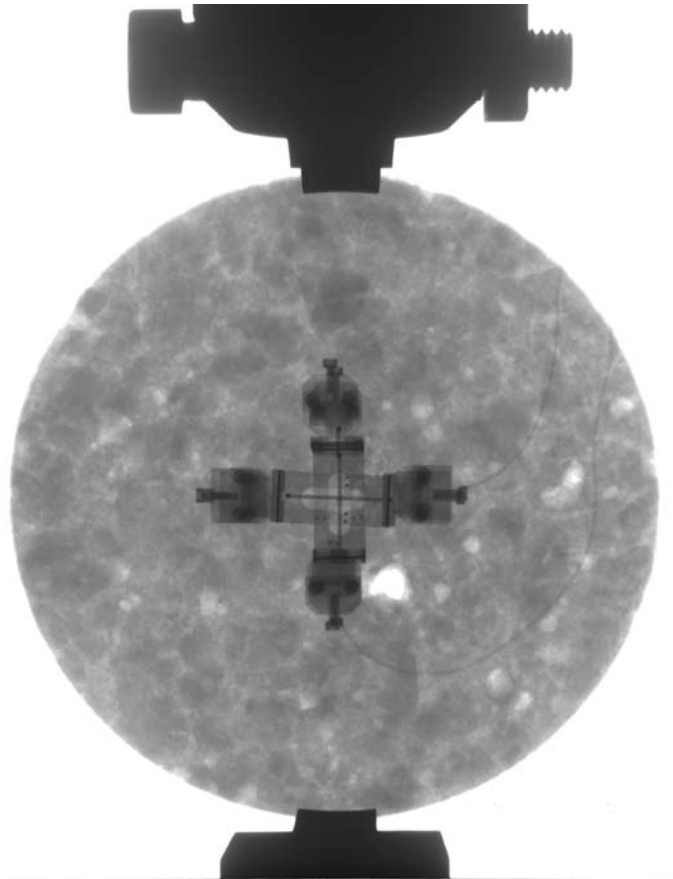


Figure D-30. DR image of the Superpave IDT concrete specimen with strain gages

Moreover, if the scan of the 3-D calibration tool for reconstruction could be acquired properly, the reconstruction could be established within about an hour on the workstation computer by 120 DR images. Detailed procedures for obtaining DR images, reconstructing 3-D virtual model, and exporting virtual slices have been discussed in Chapters D.9.4 to D.9.6..

#### **D.10.3.4 Exporting virtual slices on concrete**

The reconstructed 3-D model can be manipulated to export virtual slices at the designated angle. In this study, hundreds of virtual slices were exported on the Z-axis (i.e., along the axis of sample thickness). The spacing between two virtual slices was 71 microns (0.003 inches), identical with the voxel size, resulting in about 530 effective slices for a concrete specimen 1.5 inches in thickness. However, the usable slices usually were lower. The position, orientation, and surface condition of a specimen, as well as artifacts of a reconstructed 3-D model can reduce usable images for analysis. There were either 411 or 441 effective virtual slices of any mix found suitable for further analysis.

#### **D.10.4 Development of Image-Processing Technique of Analyzing Air Voids**

An image-processing protocol for perceiving air voids had been developed and will be introduced in this chapter. By examining the exported virtual slices, the “cupping” or so-called “beam hardening” effect had been found, which caused the area close to the circular edges that appeared to be higher density. However, the attenuation in the central area was rather uniform. Since the concrete specimen was tested under the indirect tension mode, the most interesting area was in the center. Theoretically, the crack would initiate approximately in the central area under this loading condition. Thus, a 1.5 inch square area of interest was determined for this task, where it also would more or less fit in with the strain gage measurement of the Superpave IDT test apparatus used to measure horizontal and vertical displacements on both surfaces of concrete specimen. Several image processing techniques were introduced as follows:

- Cropping the interest area;
- Applying proper threshold of gray level to isolate voids;
- Calculating area of air voids;
- Performing the analysis of air void distribution.

#### D.10.4.1 Crop the interested area

Figure D-31 shows a real virtual slice cut from a reconstructed 3-D model by a quick CT scan with 120 DR images.

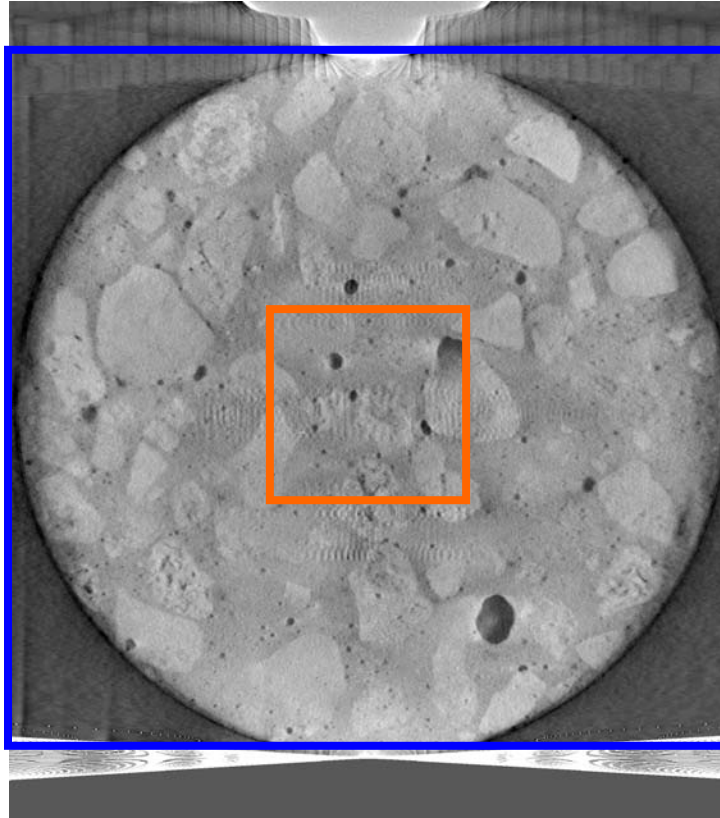


Figure D-31. Cropping the interested area from a virtual slice

Several artificial defects were found on both top and bottom, and also near central area. The central artifacts were induced by four gage points designated for measuring vertical and horizontal displacements in Superpave IDT. Several image-processing softwares exist that can crop images to the desired area, and it was decided to use Adobe® Photoshop® CS5 in this study.

Firstly, the blue square was designated manually to include the whole visible concrete specimen. After selecting this six-inch area, a similar way of cropping one segment one quarter that size from the center can be chosen to accurately receive the central 1.5 inch square area.

The unit can be manipulated by pixel numbers or by operator's preferences. The cropped area of interest can thereafter be saved into a new image file, shown in Figure D-32.

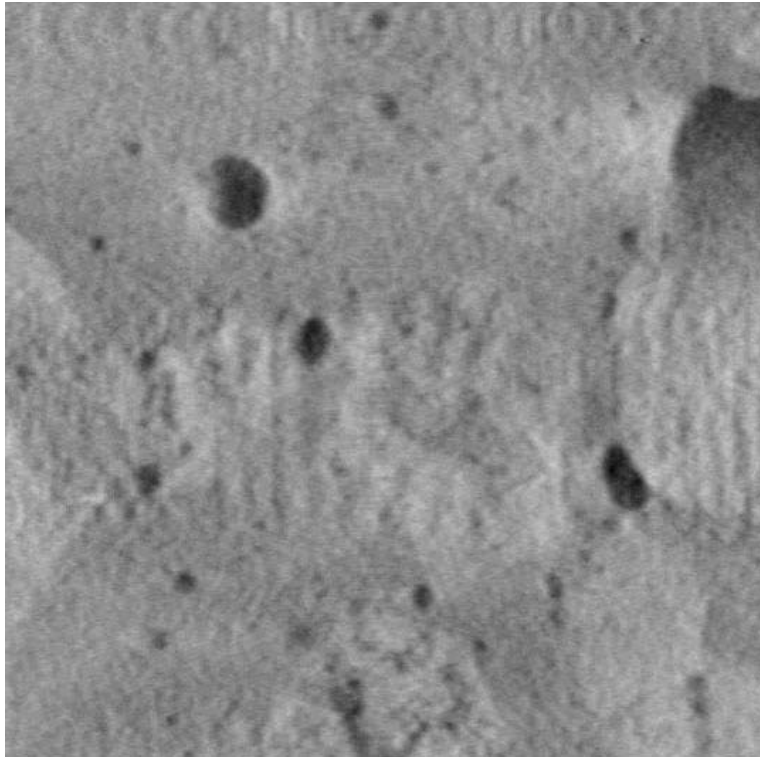


Figure D-32. Cropped image 1.5 inches square on each slice

#### **D.10.4.2 Apply proper threshold of gray level to isolate voids**

The next step was to isolate voids from aggregates and cement paste. A “binary” process had been adopted by taking advantage of considering voids and pores as air having a density of zero. Therefore, by adjusting the histogram of image, or so-called “window-leveling”, the operator can obtain this information. Most image analysis software has the image adjusting function of “threshold”, which can provide access to the binary process. It was determined to use threshold of gray levels of 87 in this study, which could fit well to isolate voids from other elements, as shown in Figure D-33.

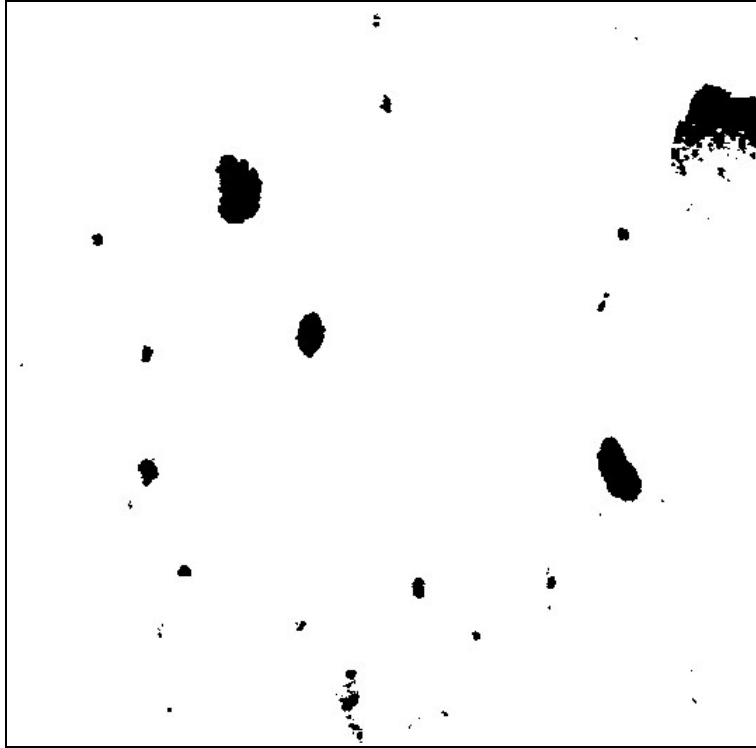


Figure D-33. Cropped image after binary process (threshold=87)

The areas appearing as black or near black were voids and pores, and it can be seen that the rest of the elements, such as aggregates, cement paste, and certain artifacts were whited-out. However, it must be remarked that the voids inside Florida limestone, artifacts from the reconstruction process, and noise signals from gage points were inevitably included. A trial and error process was extensively performed to avoid these issues and the threshold was used throughout this analysis.

Moreover, a fixed position of the load frame without changing the X-ray emission power (i.e. kV and  $\mu\text{A}$ ) was suggested in order to constantly produce similar DR images for 3-D reconstruction as well as to maintain nearly identical contrast of exported slices. The resulting image was saved in an independent folder for the next process. An automatic order “batch” with

selected actions was compiled to find, crop, binary, and save resulting images in the chosen folder up to this step in the software.

#### **D.10.4.3 Calculating area of air voids**

More than four hundred images for each mix were needed for further analysis to calculate the void or area of nearly black pixels. There was a need to develop an automatic process to calculate the area of voids. The MATLAB<sup>®</sup> R2011b with signal process and image analysis toolboxes was selected for this study. The MATLAB code was developed and compiled to calculate total pixel numbers, determine numbers of nearly white pixels, and save these data in a Microsoft<sup>®</sup> Excel<sup>®</sup> file in this cropped binary image. The concept can be reversed, calculating numbers of quasi-black pixels as well.

#### **D.10.4.4 Performing the analysis of air voids distribution**

The air voids distribution from all virtual slices can be estimated and recorded in the same Excel file. A plot of percentage of air voids versus the location along the Z-axis (i.e., axis of sample thickness) for each mix was established.

### **D.11 Analysis of Air Voids Distribution in Different Load Levels**

#### **D.11.1 Effects of Loading and Unloading on Concrete Mixes**

Table 6-1 shows the loading/unload pattern of concrete mixes. The load level was designated and incrementally increased by ten percent, based on the peak load of a concrete specimen after 90 days of curing in the Superpave IDT strength test. In Table D-5, for instance the w/c=0.45 mix, with 10% load level, it was stopped at a load 1223 pounds, which reflected 13.2% (1223/9268) of final failure load.

Almost every mix was tested up to 80 percent of the failure load, with the only exception being the concrete mix containing 100% RAP-3. Every tested concrete mix had a lower final failure load, compared with the 90-d strength test, with the exception of w/c=0.45 mix. This may

suggest that the 80% load level may not initiate damage to w/c=0.45 mix. However, a rather clear strength reduction can be observed for w/c=0.55 PCC and for all four mixes of concrete containing RAP-3.

Table D-5. Load/unload pattern used in Superpave IDT strength test

Load Level lbf	PCC w/c=0.45	PCC w/c=0.55	Concrete 20%RAP	Concrete 40%RAP	Concrete 70%RAP	Concrete 100%RAP
10%	1223 (13.2%)	980 (15.3%)	683 (12.8%)	600 (12.0%)	600 (17.0%)	480 (11.1%)
20%	2097 (22.6%)	1751 (27.3%)	1350 (25.3%)	1000 (21.8%)	1180 (33.5%)	860 (25.5%)
30%	3100 (33.4%)	2474 (38.6%)	1960 (36.7%)	1750 (35.0%)	1550 (44.0%)	1350 (40.1%)
40%	4300 (46.4%)	3500 (54.5%)	2750 (51.5%)	2300 (45.9%)	2020 (57.3%)	1620 (48.1%)
50%	4956 (53.5%)	4217 (65.7%)	3280 (61.4%)	2800 (56.0%)	2500 (71.0%)	2050 (60.9%)
60%	5979 (64.5%)	5094 (79.4%)	3890 (72.8%)	3500 (69.9%)	3000 (85.2%)	--
70%	6762 (71.7%)	5742 (89.5%)	4520 (83.3%)	4050 (80.9%)	--	--
80%	7778 (83.9%)	--	5200 (97.4%)	--	--	--
Failure Load (Peak Load)	9268.9 (9489.6)	6417.7 (8544.5)	5341.4 (6500.3)	5006.8 (5958.6)	3523.1 (5094.9)	3368.6 (4311.8)

### D.11.2 Average Air Voids under Different Loading Level

The air void distribution had been used to analyze two PCC mixes and four concrete mixes containing RAP-3, as shown in Figure D-34 to Figure D-39 and Table D-6. Each curve presented an internal distribution of air voids through the Z-axis under corresponding load level. Each figure contains the distribution curve before loading in gray color, namely zero percentage of loading, and other color curves with four load levels for the purpose of observation. It was assumed that the variation of void distribution would be manifest as the indication of microcracking occurrence internally.

Table D-6. Average air voids under different load levels

Mixes	PCC				Concrete Containing RAP							
	w/c=0.45		w/c=0.55		20%		40%		70%		100%	
Load Level	Ave.	Diff.	Ave.	Diff.	Ave.	Diff.	Ave.	Diff.	Ave.	Diff.	Ave.	Diff.
0%	1.19%	0.00%	0.77%	0.00%	1.10%	0.00%	1.40%	0.00%	1.01%	0.00%	1.15%	0.00%
10%	1.25%	0.05%	0.39%	-0.39%	1.28%	0.19%	1.42%	0.02%	1.07%	0.07%	1.16%	0.01%
20%	1.40%	0.21%	0.84%	0.07%	1.00%	-0.10%	1.40%	0.00%	1.17%	0.16%	1.21%	0.06%
30%	1.29%	0.09%	0.71%	-0.06%	1.20%	0.11%	1.43%	0.03%	1.08%	0.07%	0.92%	-0.23%
40%	1.19%	0.00%	0.42%	-0.35%	1.08%	-0.01%	1.42%	0.02%	1.14%	0.13%	0.92%	-0.23%
50%	1.24%	0.05%	0.60%	-0.17%	1.14%	0.05%	1.57%	0.17%	1.19%	0.19%	1.28%	0.13%
60%	1.38%	0.19%	0.71%	-0.06%	0.81%	-0.28%	1.61%	0.21%	1.21%	0.20%	-	-
70%	1.43%	0.24%	0.53%	-0.24%	0.93%	-0.16%	1.59%	0.19%	-	-	-	-
80%	1.47%	0.28%	-	-	1.23%	0.13%	-	-	-	-	-	-
BREAK	6.57%	5.37%	4.00%	3.23%	-	-	3.96%	2.56%	-	-	3.01%	1.86%

For analyzing void differential among all tested mixes, the maximum variation did not exceed  $\pm 0.3\%$  of air voids. Void distribution of w/c=0.45 PCC, concrete mixes containing 40% and 70% RAP-3 were more or less in an increasing trend. A relative large number of voids growing at 60% load level (corresponding with 64.5% of peak load) in PCC with w/c=0.45 PCC, 50% to 70% load level (corresponding with 56.0% of peak load) in concrete containing 40% RAP, and 40% to 60% load level (corresponding with 57.3% of peak load) in concrete containing 70% RAP-3 were noticeable. Void distribution in 100% RAP-3 had great void variation at 30% load level (corresponding with 40.1% of peak load), while air void distributions in w/c=0.55 PCC and 20% RAP-3 mixes appeared to be irregular, or not noticeably exact in any manner.

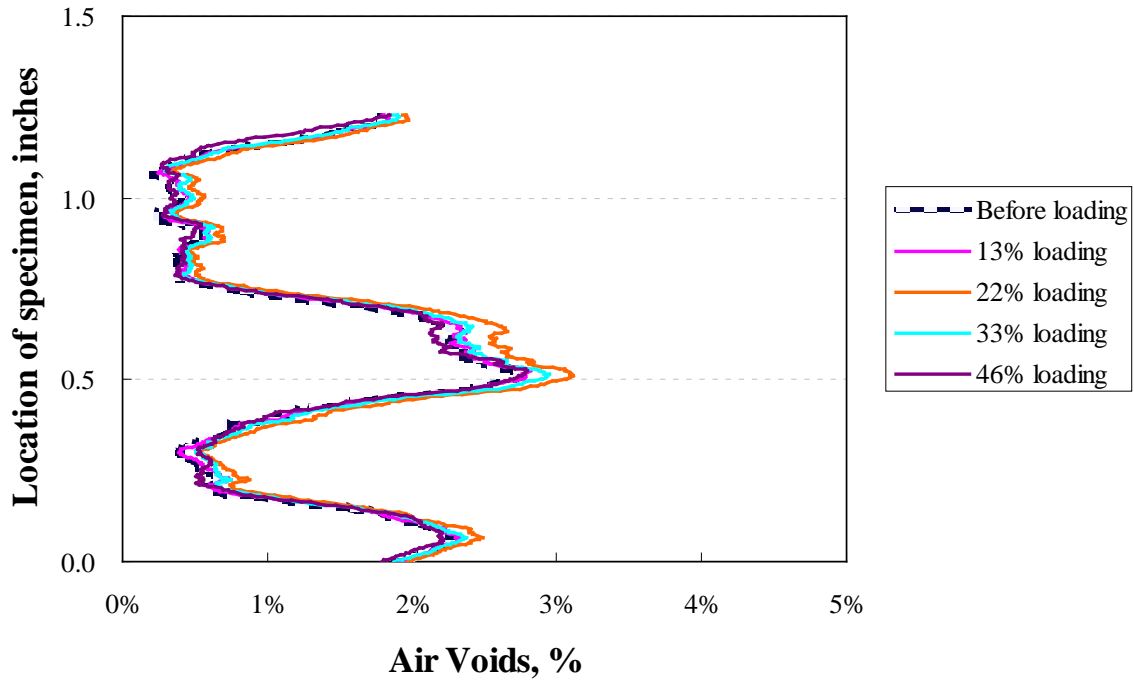
A drop in air voids was also observed in the early stage of loading, such as 10% load level at w/c=0.55 (corresponding with 15.3% of peak load) and 20% load level at w/c=0.45 PCC (corresponding with 22.6% of peak load), 20% RAP-3 (corresponding with 25.3% of peak load), 70% RAP-3 (corresponding with 33.5% of peak load), and 100% RAP-3 (corresponding with 25.5% of peak load). This reduction can be attributed to the well-known debonding of concrete

layers caused by relatively low loads. Such debonding or microcracks will not propagate and the microstructure is considered intact (Mier 1997).

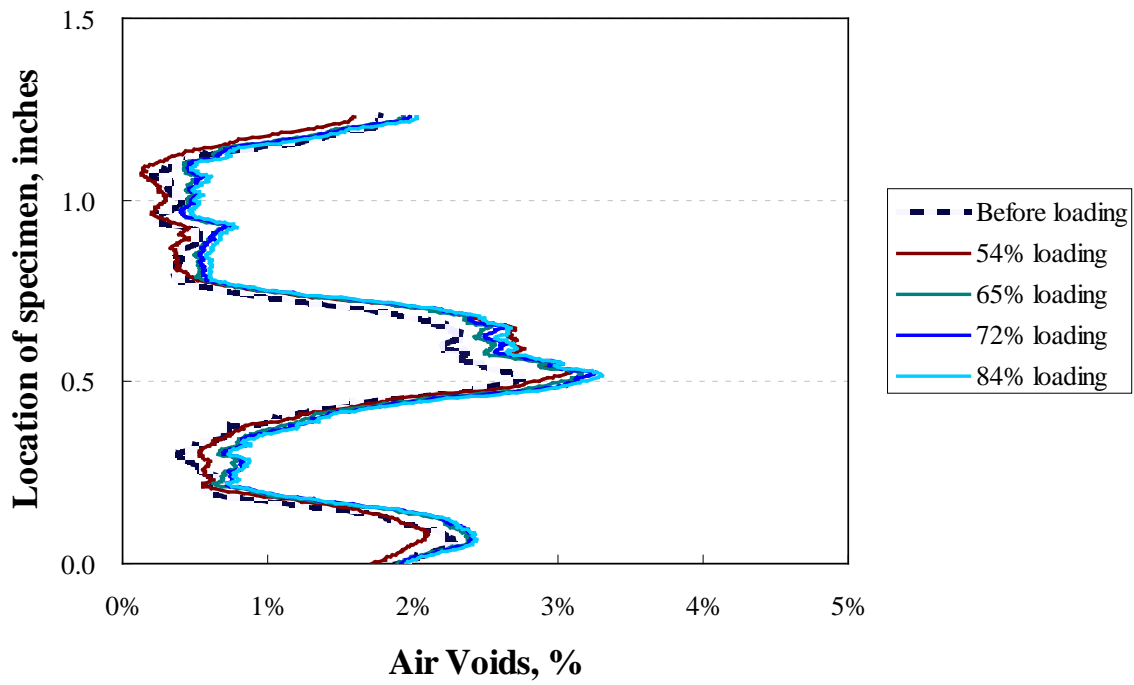
### **D.11.3 Average Air Voids in Concrete containing RAP during Fracture**

There were two concrete containing 40% and 70% RAP-3 that proved subject to the condition wherein the failure was detected without breaking the specimen apart. The distributions of air voids at the point of fracture were more or less captured without moving the sample from the load frame. Two attempts were made to recover PCC specimens after fracture; the specimens were duct-taped to perform the CT scan. However, the loss of concrete materials during rupture increased the average percentage of air voids. It was rather difficult to match up the distribution of air voids after the specimen was removed from the original place. Nevertheless, it was fairly noticeable that the fracture would cause a dramatic jump in air voids, shown in Figure D-40 and Figure D-41.

Another attempt was made to evaluate the void variation during fracture. There was a dot curve with orange-color shifted by the magnitude of difference in percentage of air voids before loading and in fracture. It was found in the shape of an Arabic numeral “8” or a double “S”, which indicated that voids on one side grew more than on the other on the concrete specimen during fracture, compared with the shifted distribution. PCC mixes had more apparent cracks opening than was the case with RAP-3 mixes, which may also suggest the explosive nature of failure in PCC. This phenomenon may be related to the similar observation on stress—strain curve in this study, in chapter 5. The crack initiation and growing horizontal displacement occurred on the same side of specimen, while a snap or a negative displacement on the other side of specimen happened, simultaneously. The near-fracture “bending” of concrete specimens under the Superpave IDT strength test worked differently than regular asphalt specimens.

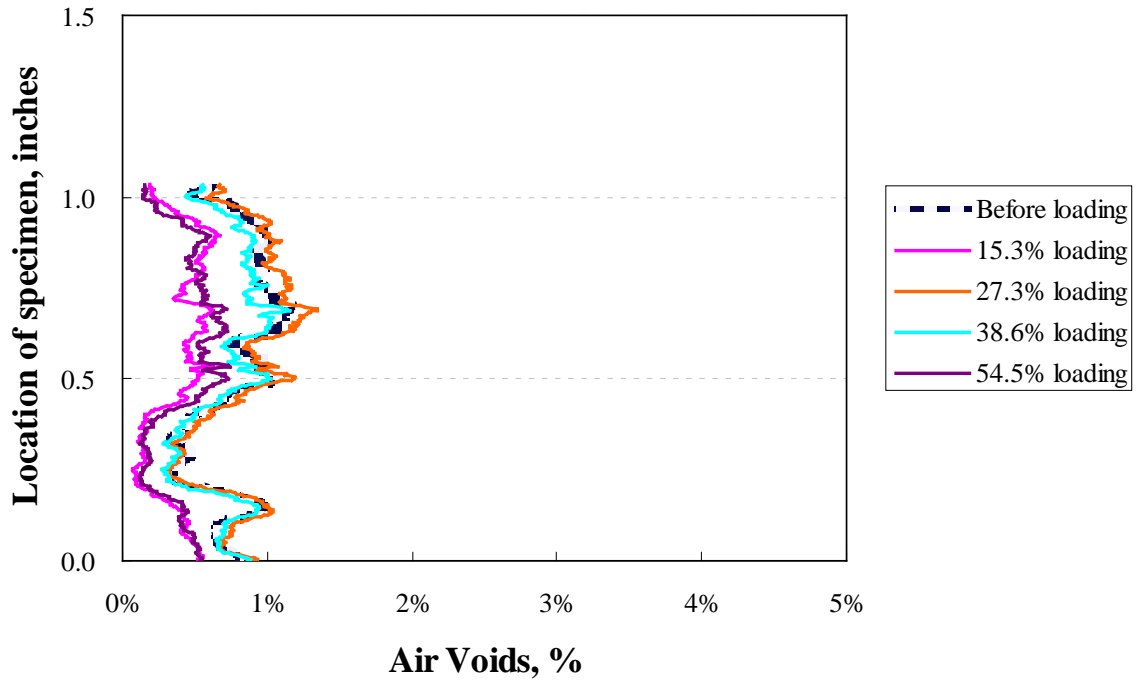


(A)

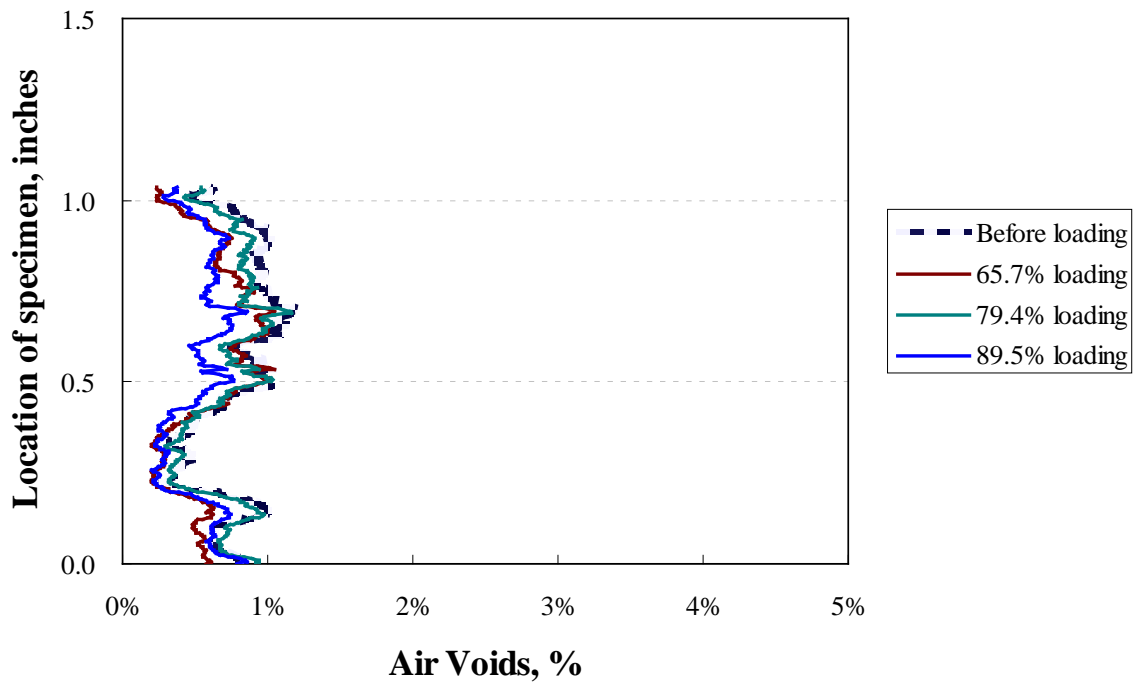


(B)

Figure D-34. Air void distribution of w/c=0.45 PCC mix

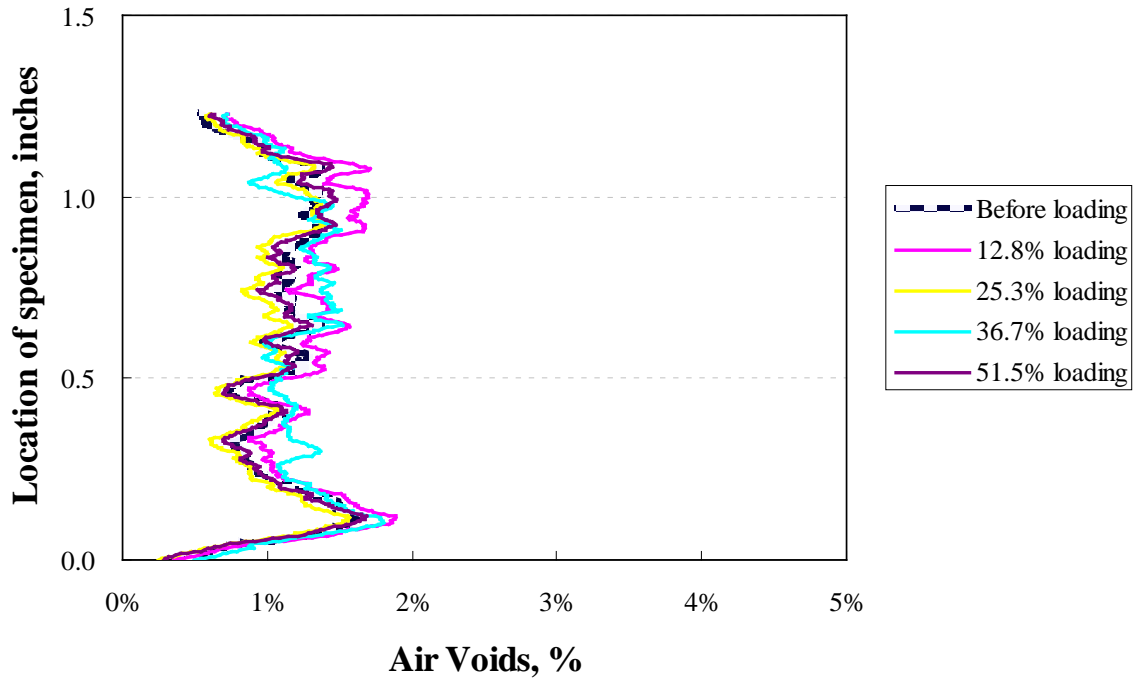


(A)

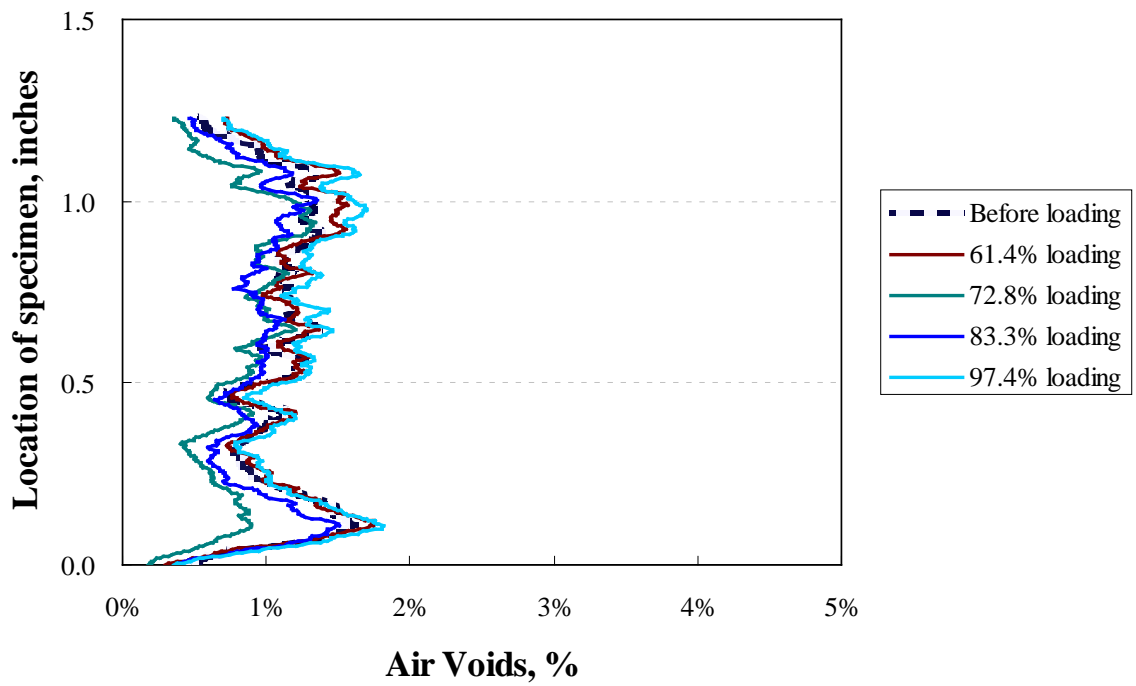


(B)

Figure D-35. Air void distribution of w/c=0.55 PCC mix

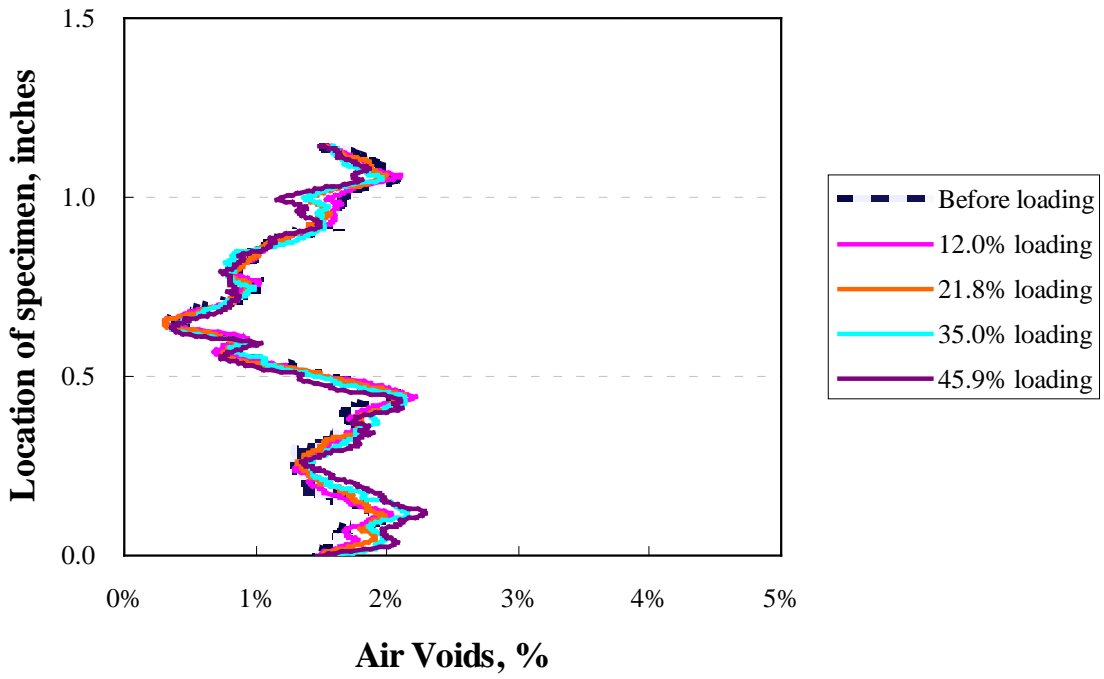


(A)

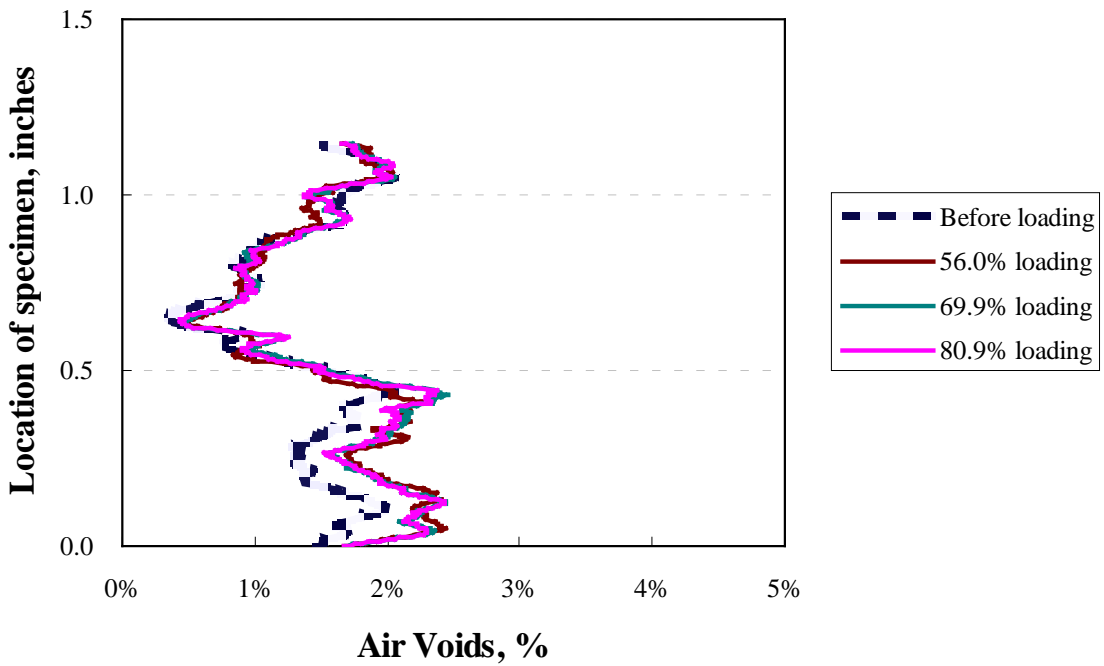


(B)

Figure D-36. Air void distribution of concrete mix containing 20% RAP

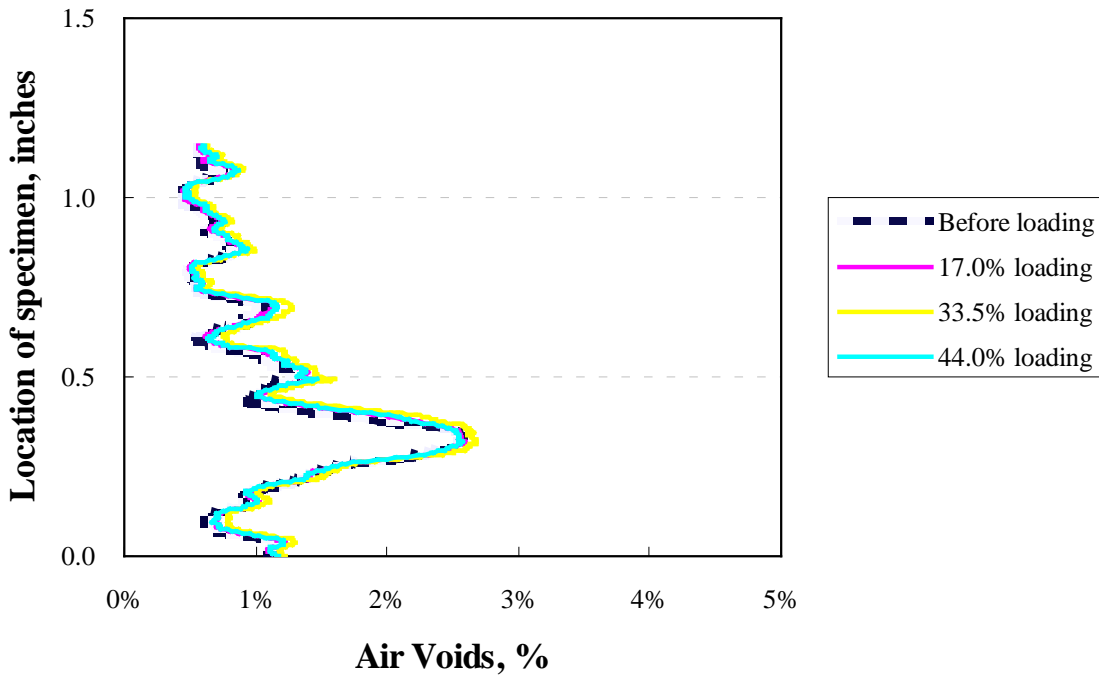


(A)

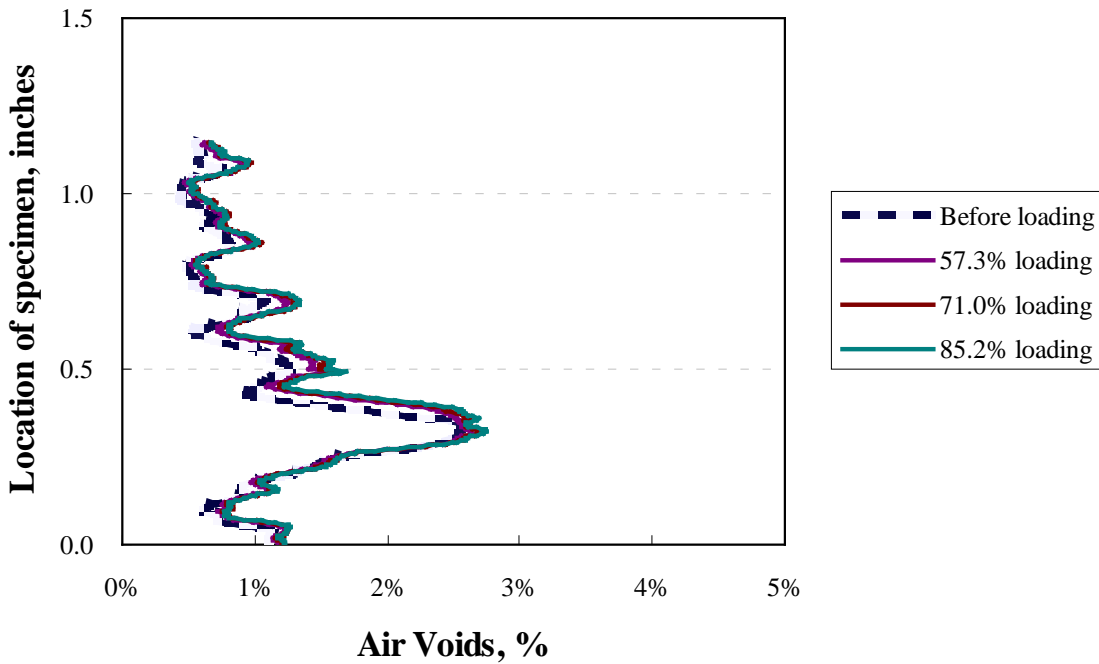


(B)

Figure D-37. Air void distribution of concrete mix containing 40% RAP

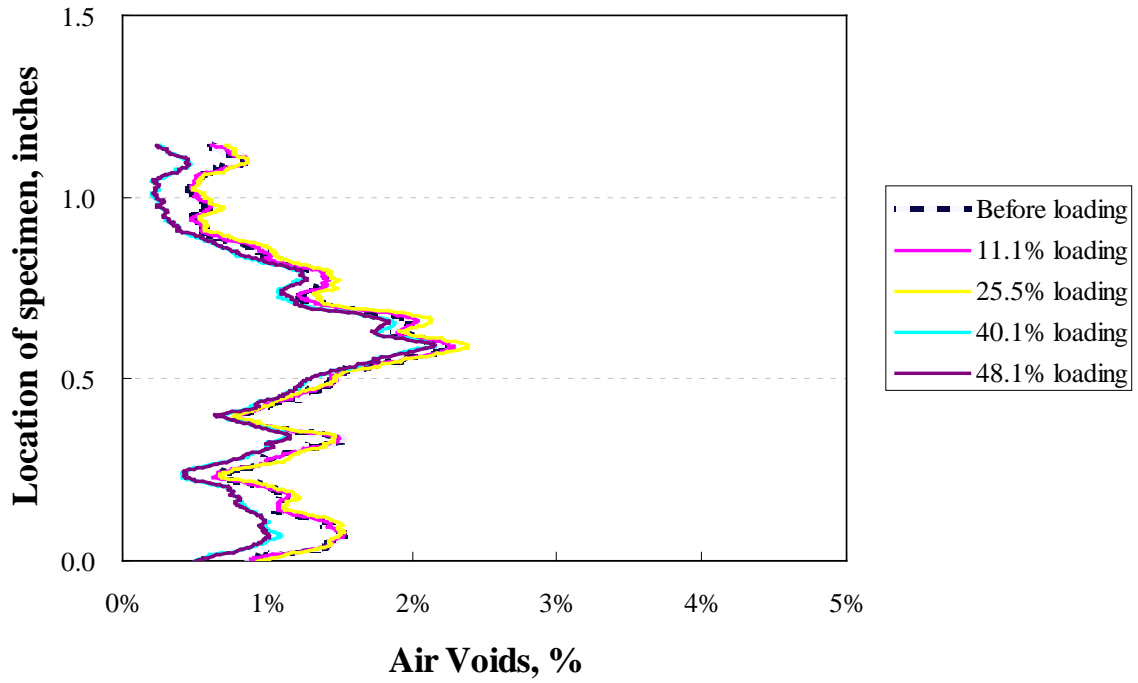


(A)

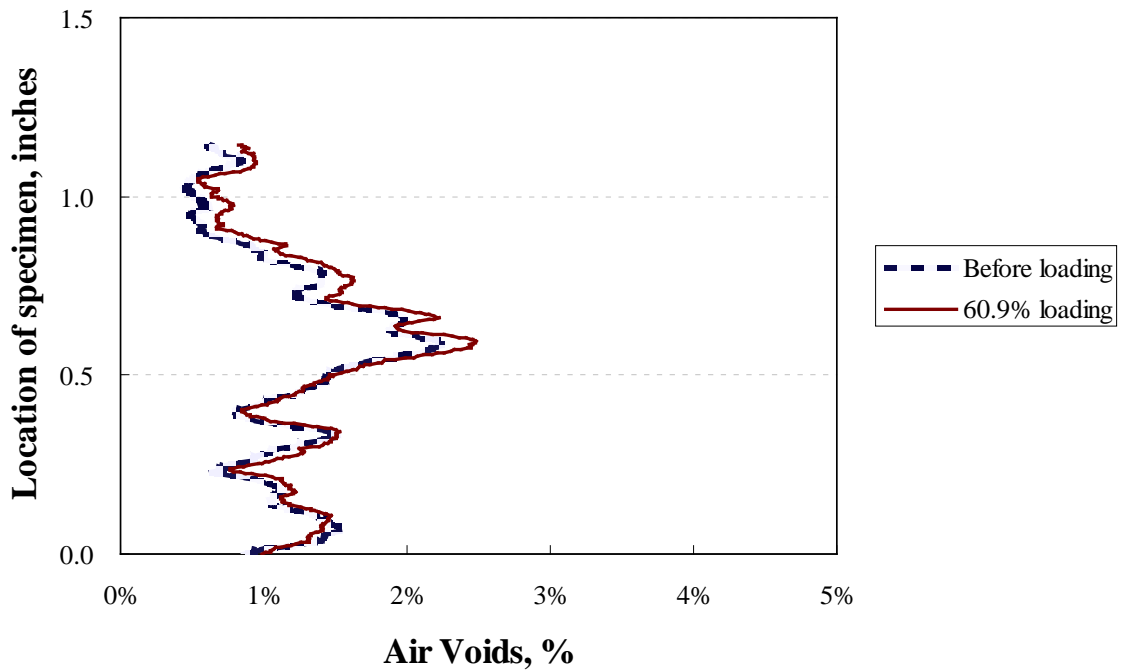


(B)

Figure D-38. Air void distribution of concrete mix containing 70% RAP

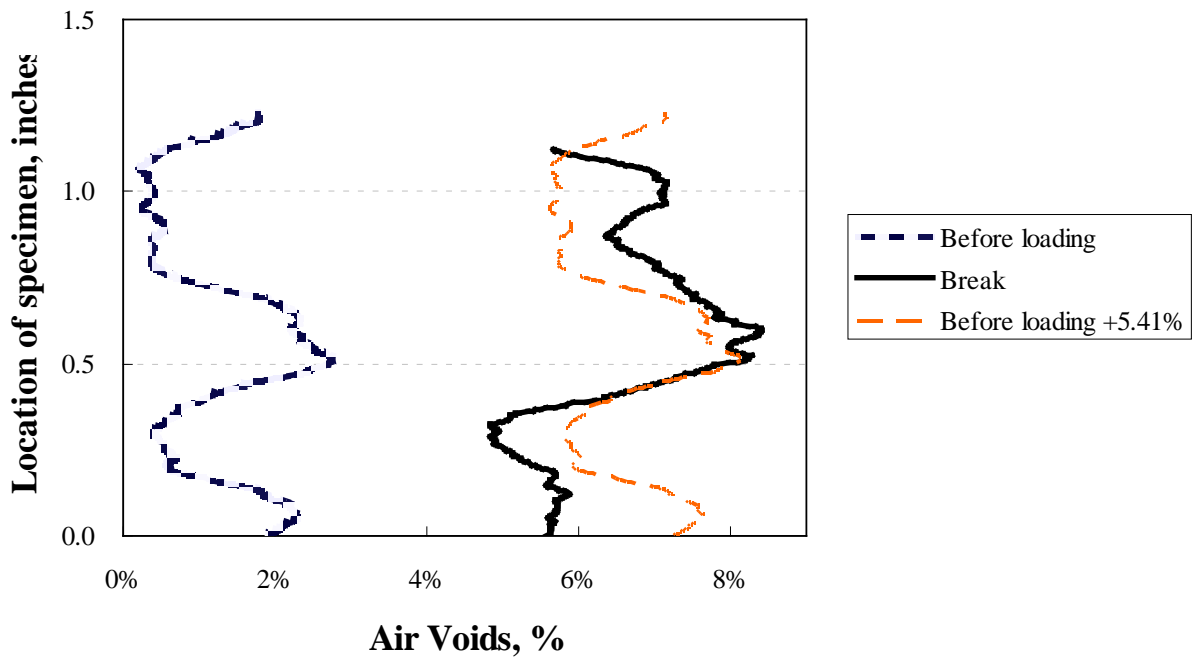


(A)

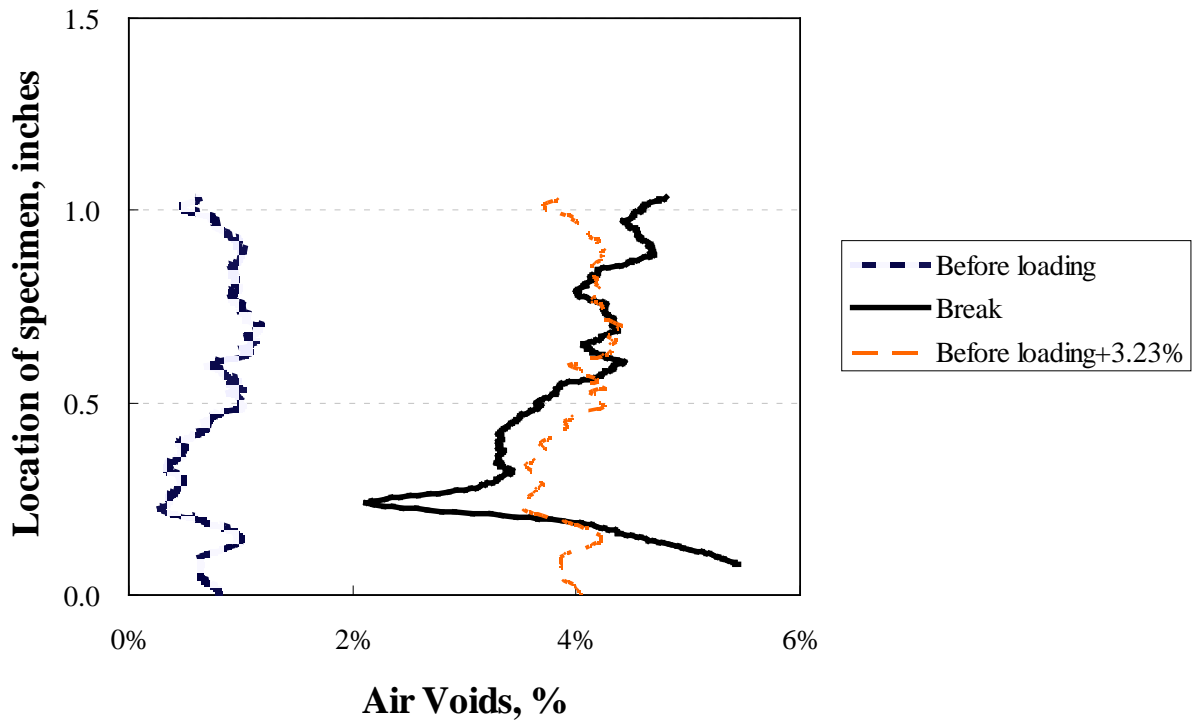


(B)

Figure D-39. Air void distribution of concrete mix containing 100% RAP

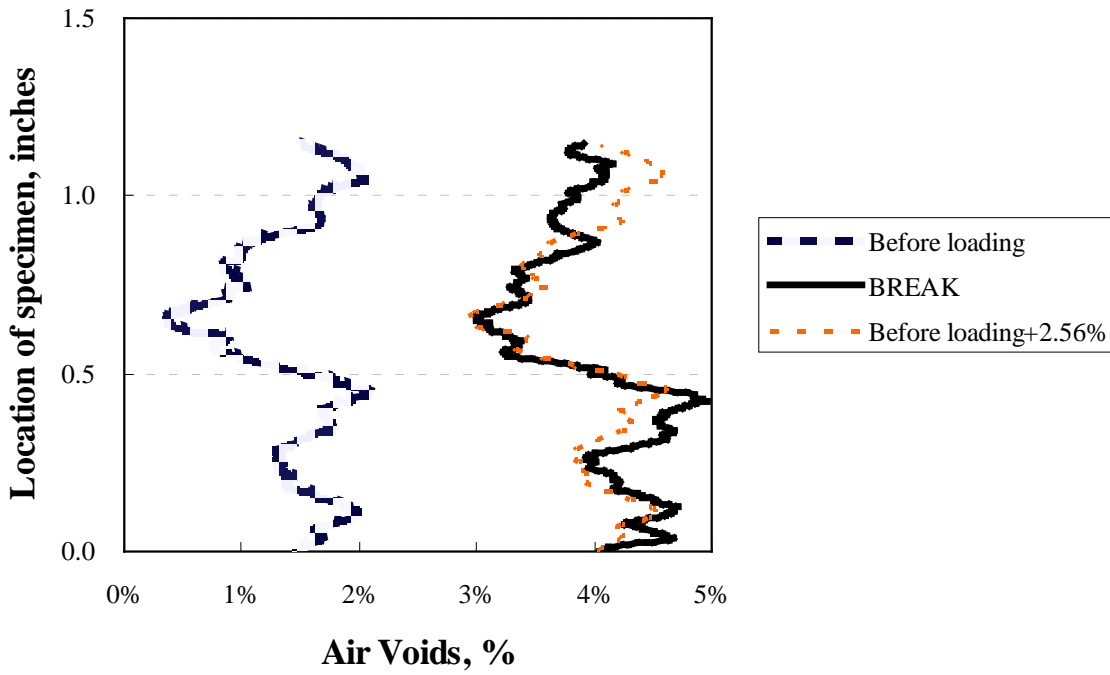


(A) w/c=0.45 PCC

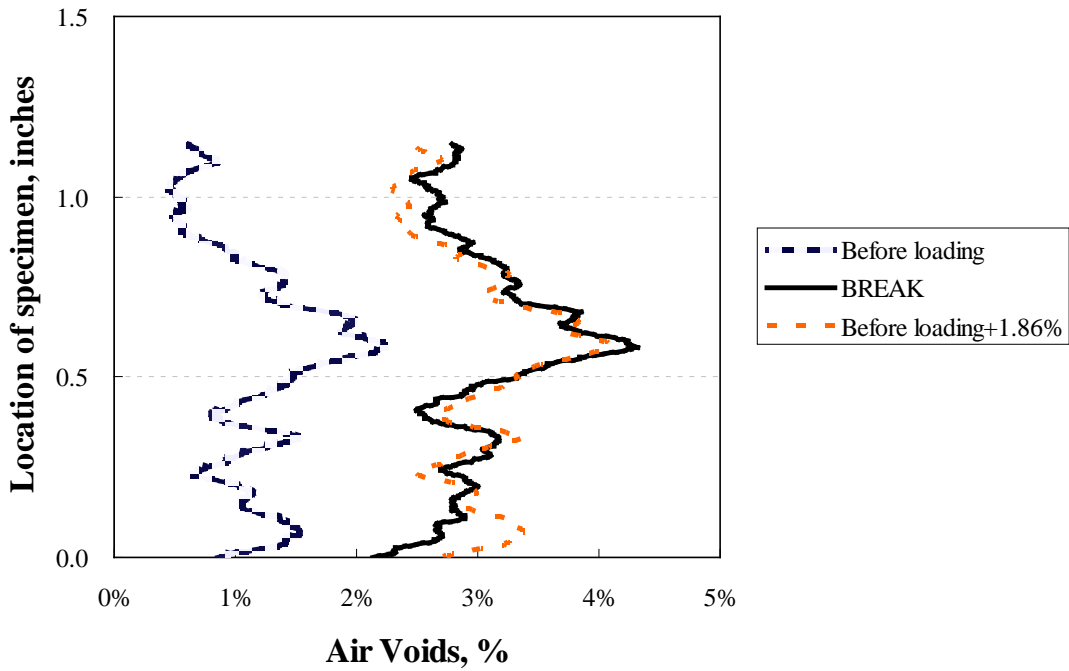


(B) w/c=0.55 PCC

Figure D-40. Voids distributions after fracture of w/c=0.45 and 0.55 PCC mixes



(A) concrete containing 40% RAP



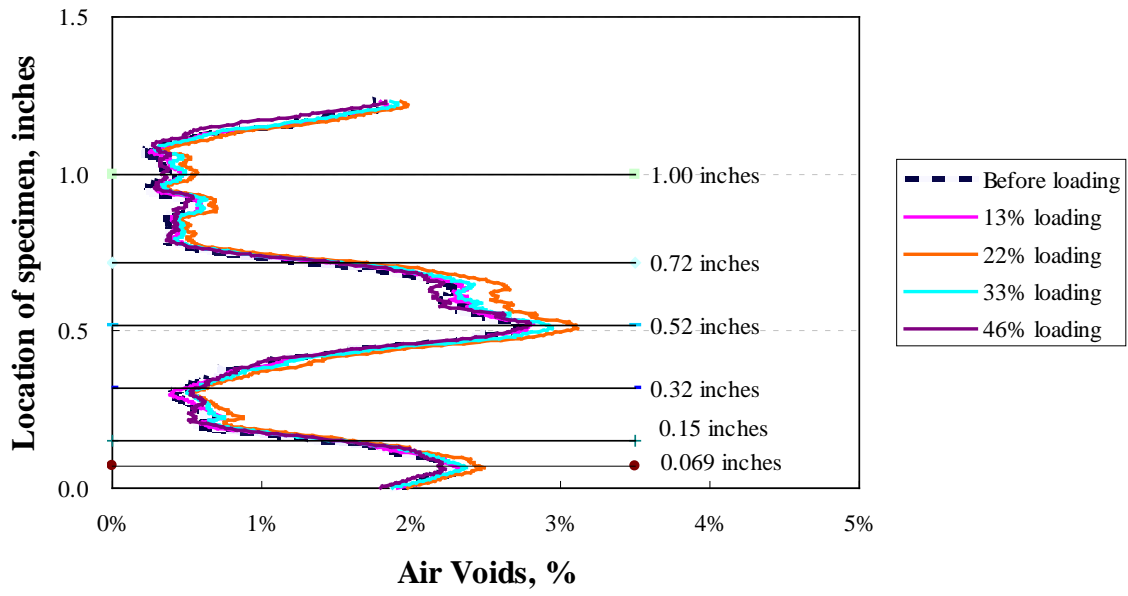
(B) concrete containing 100% RAP

Figure D-41. Voids distributions after fracture of concrete mixes containing 40% and 100% RAP

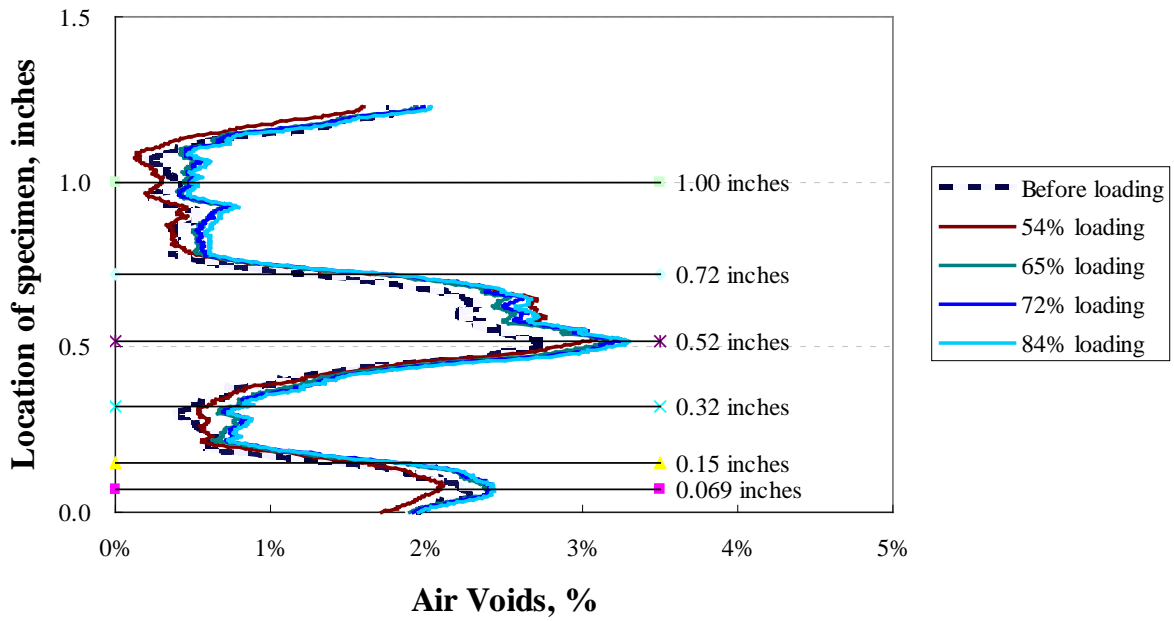
## D.12 Visualization of Microcracking in Concrete

### D.12.1 Visualization of Concrete Microcracking under Load/Unload Pattern

A detailed side-by-side comparison in virtual slices was performed for w/c=0.45 PCC mix to approximate visualization of microcracking. The intent was to examine how distributions of air void varied along with the incremental load level. Figure D-42 shows identical air void distribution, as Figure D-34, with several locations of interest from one surface. By observing the curves compared with the distribution before loading, there were locations at 0.069 and 0.52 inches with higher average air voids, while locations of 0.32 and 1.0 inches developed lower air voids. Locations at 0.15 and 0.72 inches were in a transition zone of void reduction. Figure D-43 to Figure D-48 provided a side-by-side comparison of slices under different load levels. For lower load levels, the variation of void distribution seemed to be insignificant, except for the one of 22% (i.e., debonding of concrete layer). However, for higher load levels, it appeared that the internal structure with large air voids, such as 0.069 and 0.52 inches, and with lower air voids, for instance 0.32 and 1.00 inches, had the tendency of enlarging the average air voids. By carefully examining the slices on these locations (marked in orange circles), the new microcracks were occurring on the cement paste. Some existing voids were seemingly enlarging the size of voids or the shape of voids had been deformed, due to the loading. At some narrow tips of cement paste in between aggregates (marked in blue circles) of locations of 0.15 and 0.72 inches, it was found that previous discrete microcracks became “channelized” to be connected to each other. The tiny new microcracks or flow movement in terms of voids can be arguably detected under this quick X-ray CT scan protocol. However, it was not found that the microcracks were specifically generated around aggregates in this mix, nor upon additional examination of concrete mix containing 100% RAP-3, shown in Figure D-49.

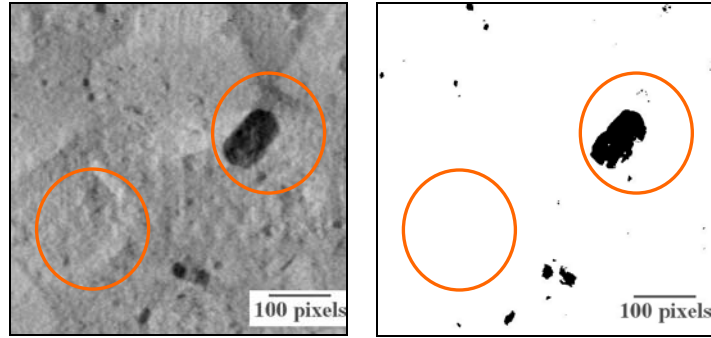


(A)

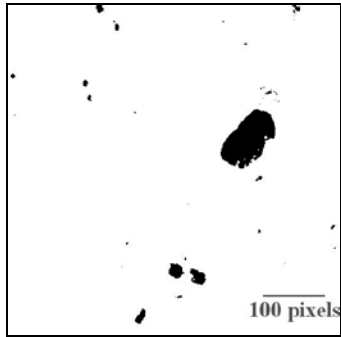


(B)

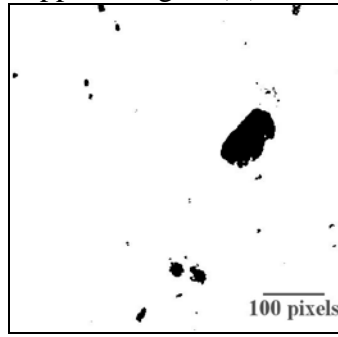
Figure D-42. Air voids distribution in w/c=0.45 PCC with locations of interest



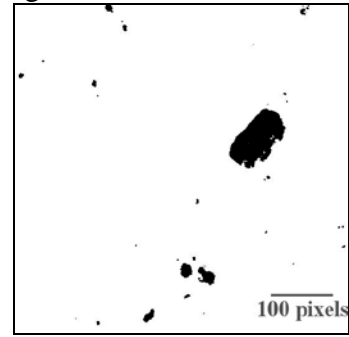
(A) Cropped image (B) before loading



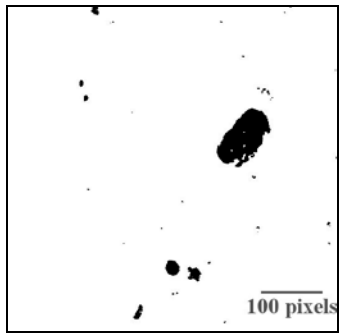
(C) 13.2% of peak load



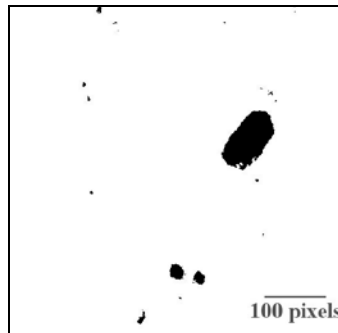
(D) 22.6% of peak load



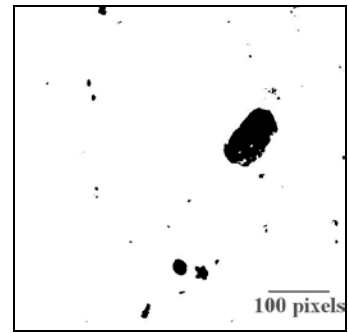
(E) 33.4% of peak load



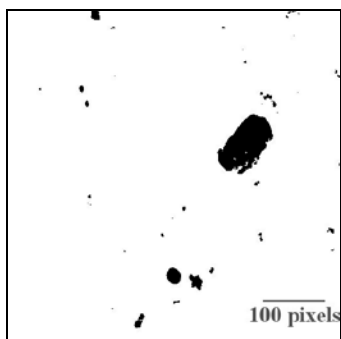
(F) 46.4% of peak load



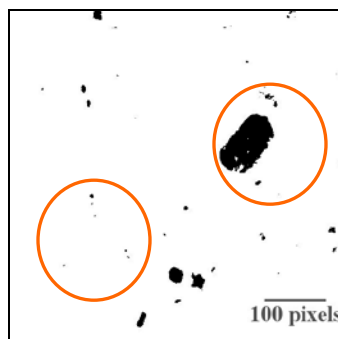
(G) 53.5% of peak load



(H) 64.5% of peak load

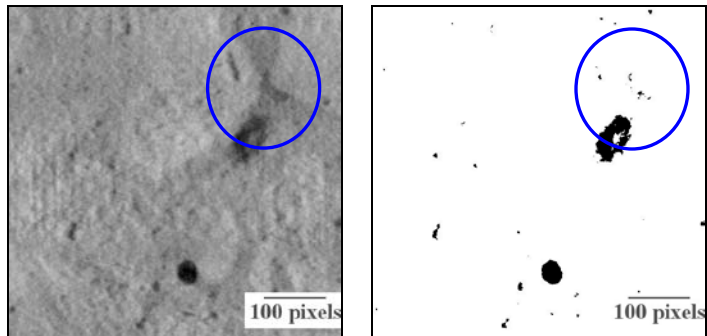


(I) 71.7% of peak load

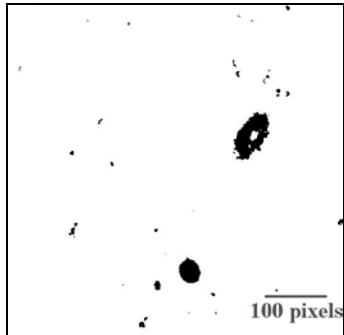


(J) 83.9% of peak load

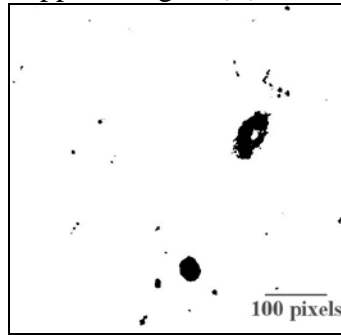
Figure D-43. Air voids at the location of 0.069 inches



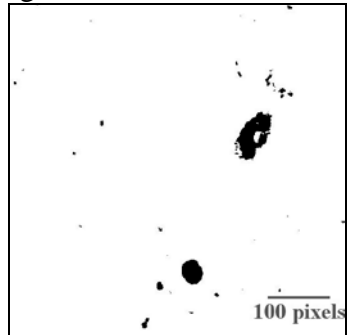
(A) Cropped image (B) before loading



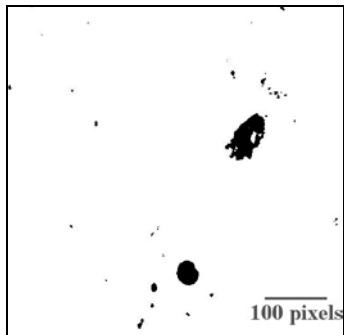
(C) 13.2% of peak load



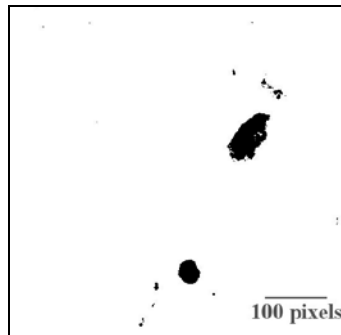
(D) 22.6% of peak load



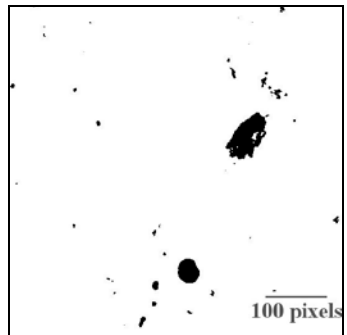
(E) 33.4% of peak load



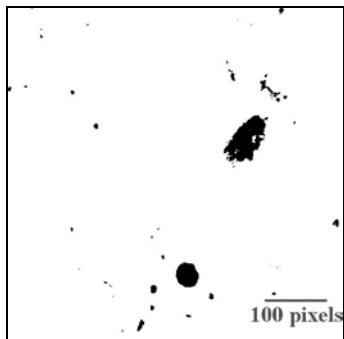
(F) 46.4% of peak load



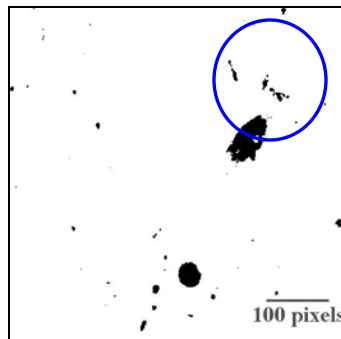
(G) 53.5% of peak load



(H) 64.5% of peak load

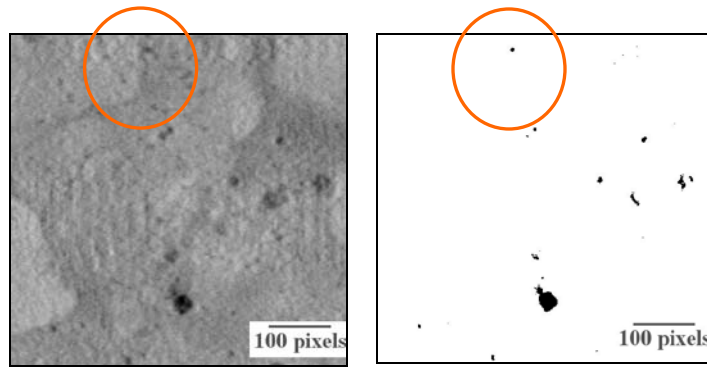


(I) 71.7% of peak load

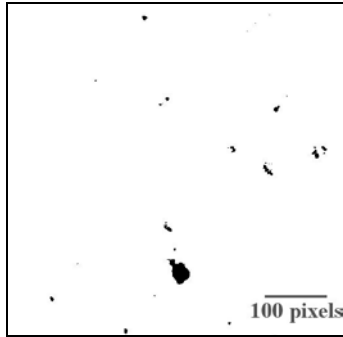


(J) 83.9% of peak load

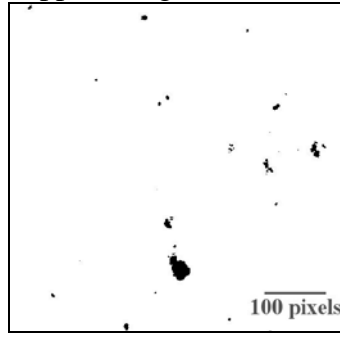
Figure D-44. Air voids at the location of 0.15 inches



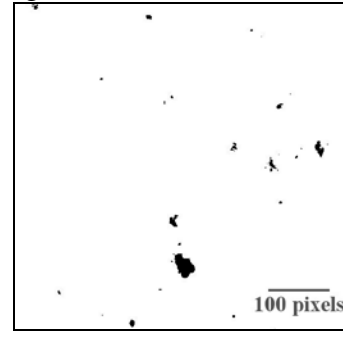
(A) Cropped image (B) before loading



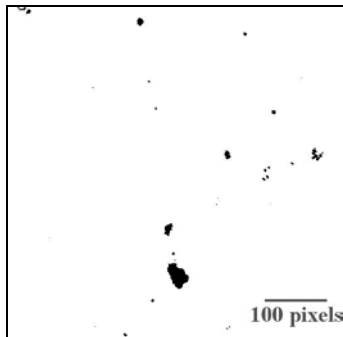
(C) 13.2% of peak load



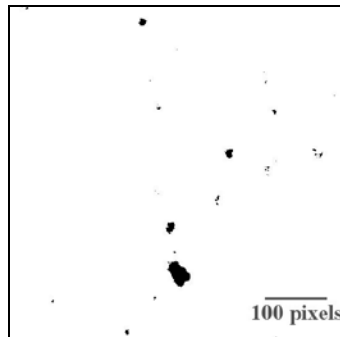
(D) 22.6% of peak load



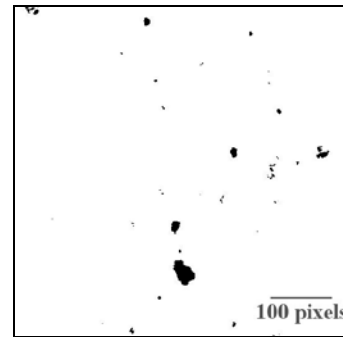
(E) 33.4% of peak load



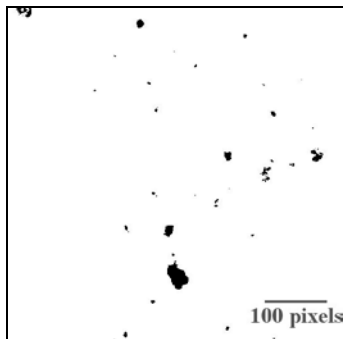
(F) 46.4% of peak load



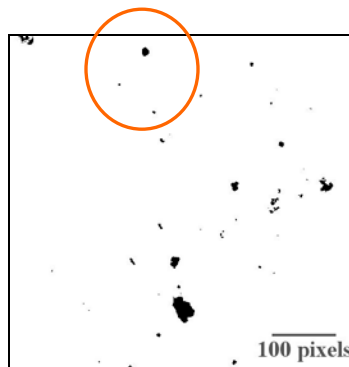
(G) 53.5% of peak load



(H) 64.5% of peak load

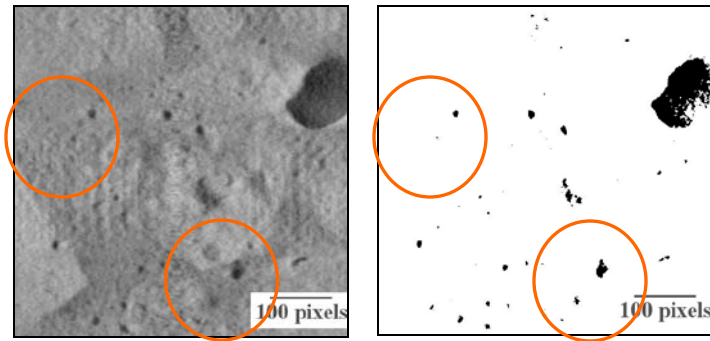


(I) 71.7% of peak load

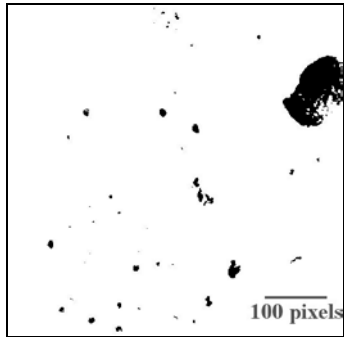


(J) 83.9% of peak load

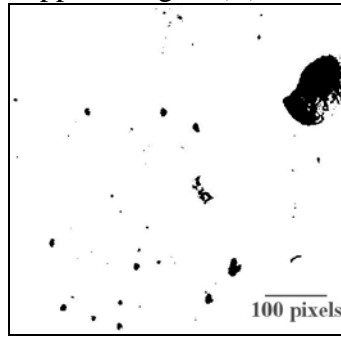
Figure D-45. Air voids at the location of 0.32 inches



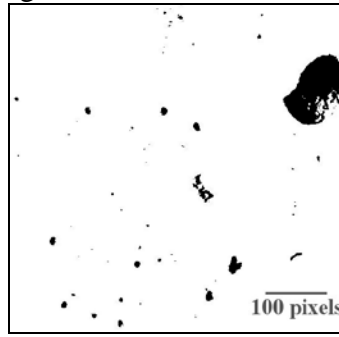
(A) Cropped image (B) before loading



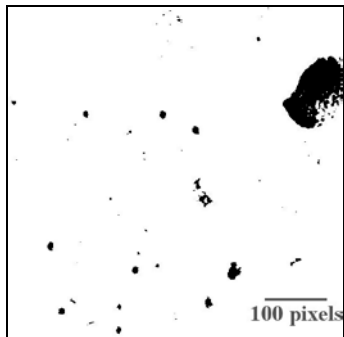
(C) 13.2% of peak load



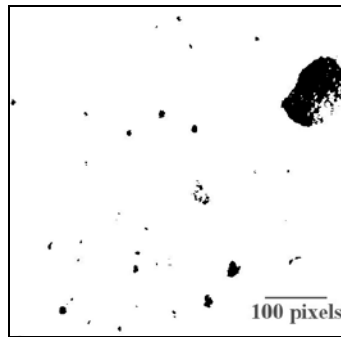
(D) 22.6% of peak load



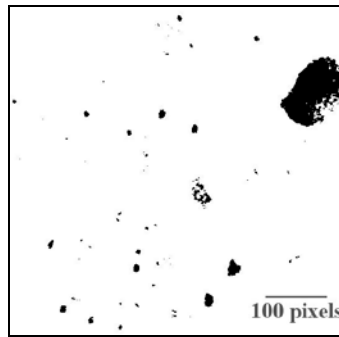
(E) 33.4% of peak load



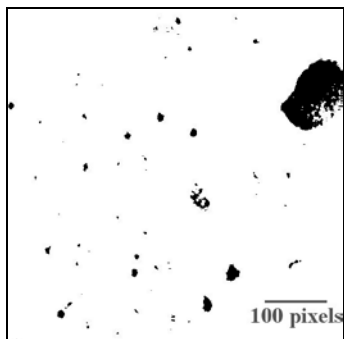
(F) 46.4% of peak load



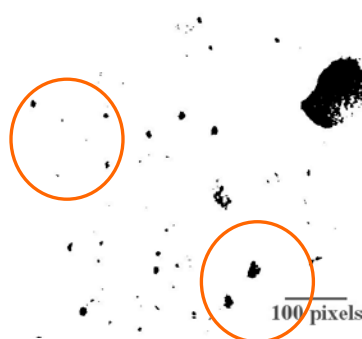
(G) 53.5% of peak load



(H) 64.5% of peak load

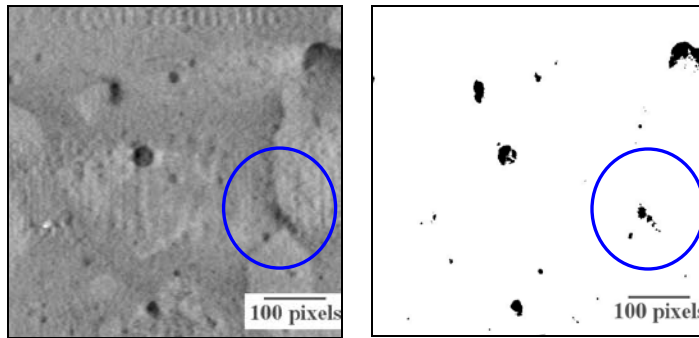


(I) 71.7% of peak load

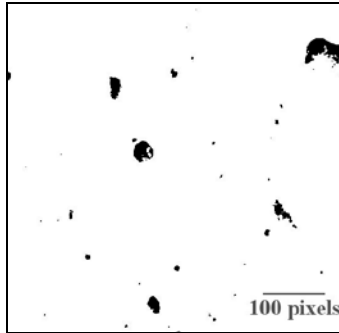


(J) 83.9% of peak load

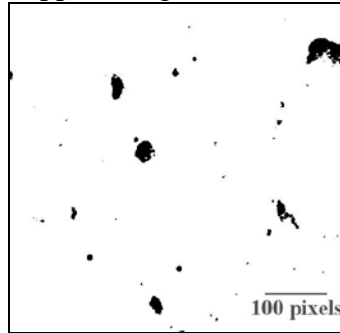
Figure D-46. Air voids at the location of 0.52 inches



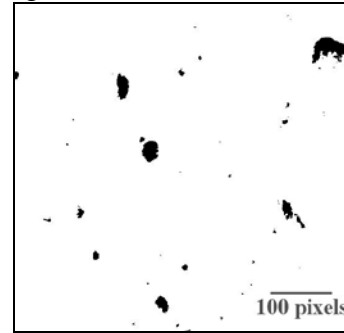
(A) Cropped image (B) before loading



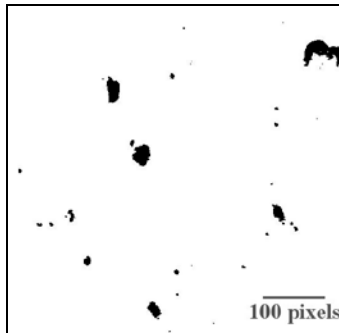
(C) 13.2% of peak load



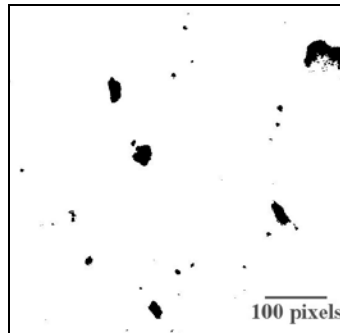
(D) 22.6% of peak load



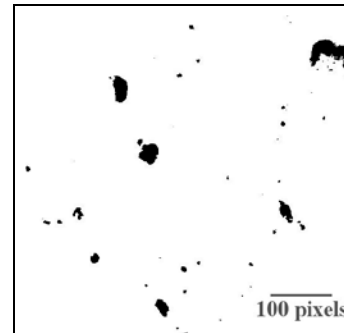
(E) 33.4% of peak load



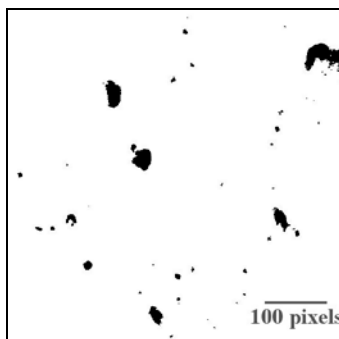
(F) 46.4% of peak load



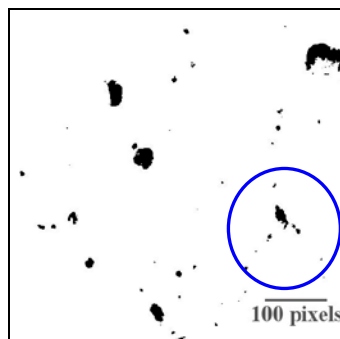
(G) 53.5% of peak load



(H) 64.5% of peak load



(I) 71.7% of peak load



(J) 83.9% of peak load

Figure D-47. Air voids at the location of 0.72 inches

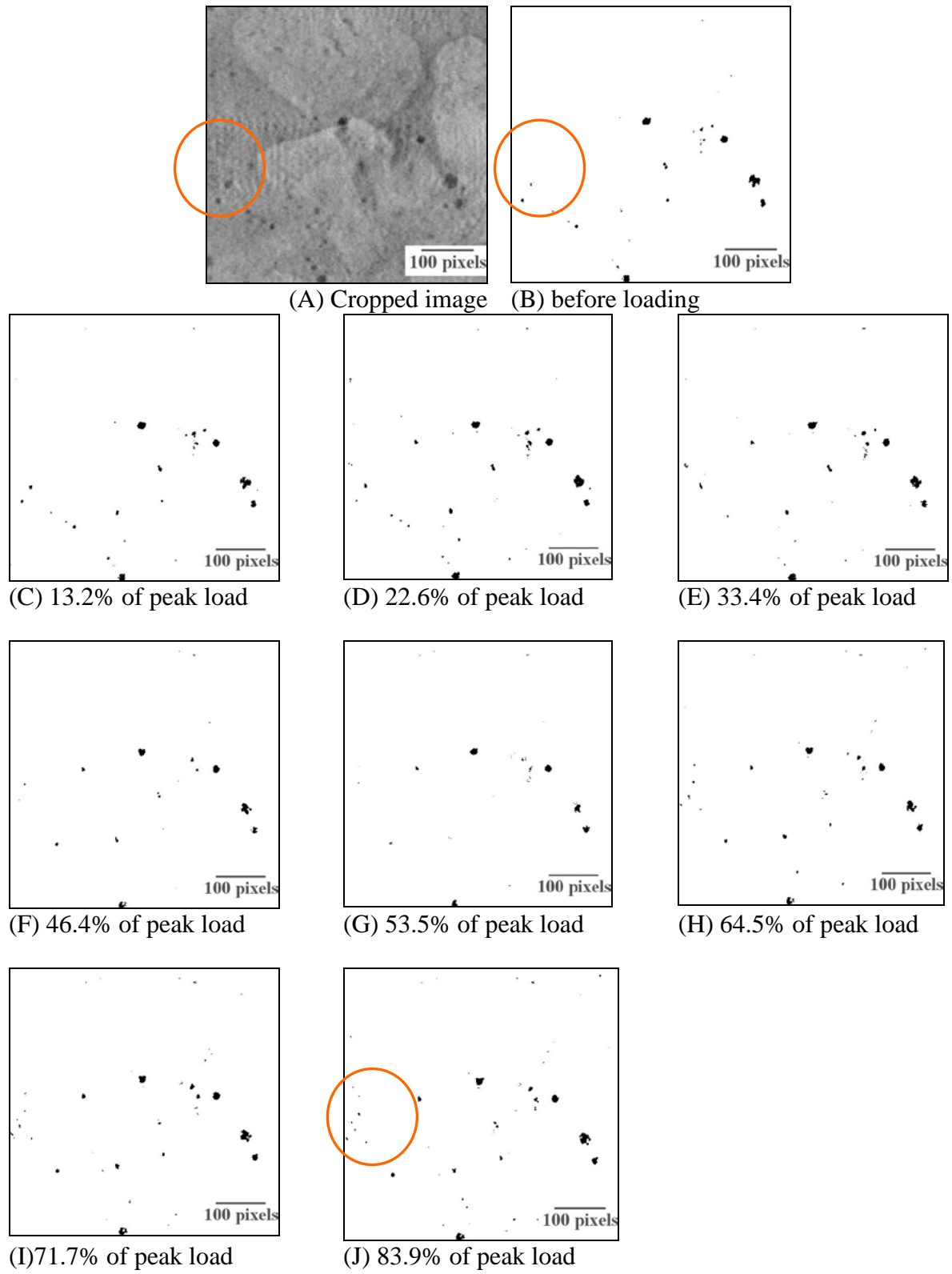


Figure D-48. Air voids at the location of 1.00 inches

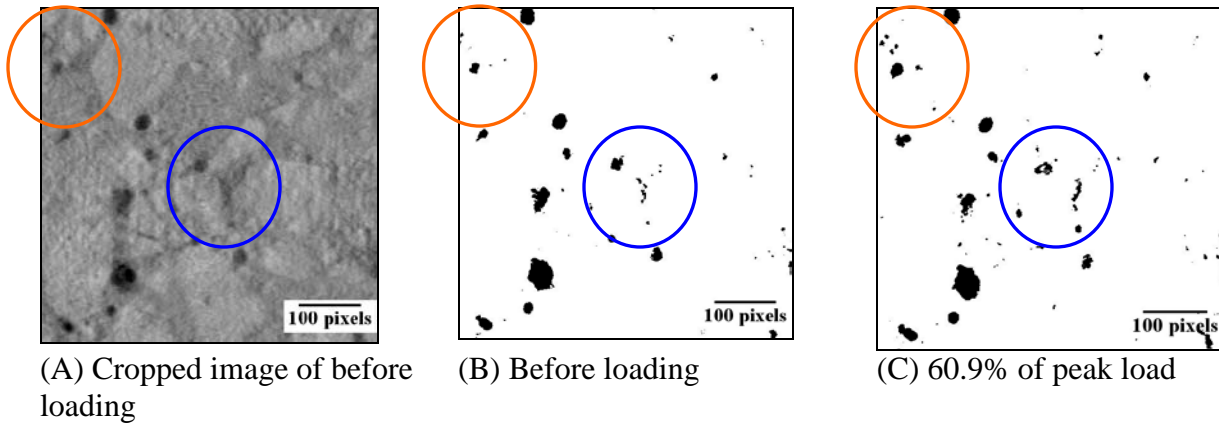


Figure D-49. Air voids at the location of 0.60 inches

### D.12.2 Visualization of Concrete Microcracking during Fracture

Moreover, a further assessment of void distribution was attempted to evaluate the air void distribution. As has been discussed in Chapter D.11, the percentage of air voids on one surface was growing positively more than the other side, during fracture. Voids on the other side actually grew less than average, for instance in Figure D-39 of 100% RAP-3 mix. Three locations at 0.09, 0.60, and 1.00 inches slices, before loading and fracture, had been pulled out for the side-by-side comparison, shown in Figure D-50 to D-52.

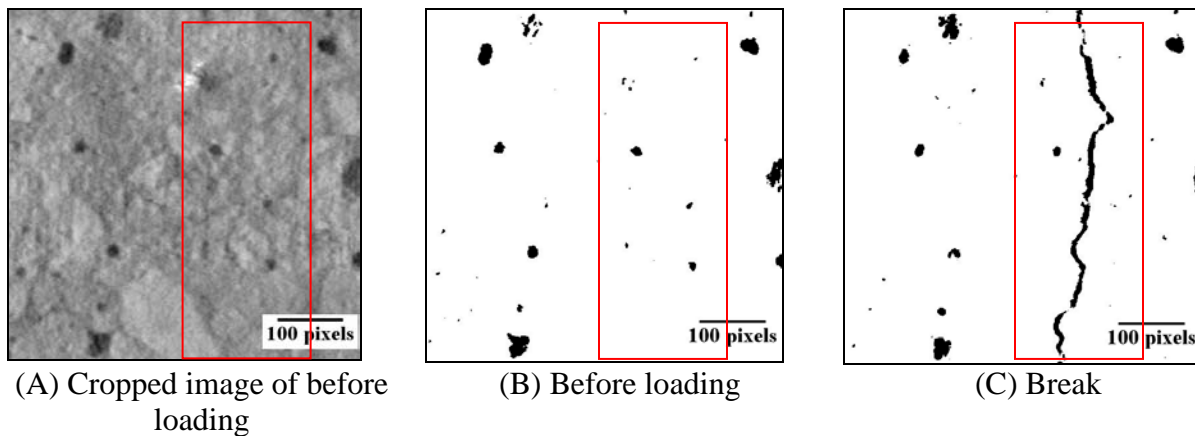


Figure D-50. Air voids at the location of 0.09 inches of 100% RAP-3 (voids reduction)

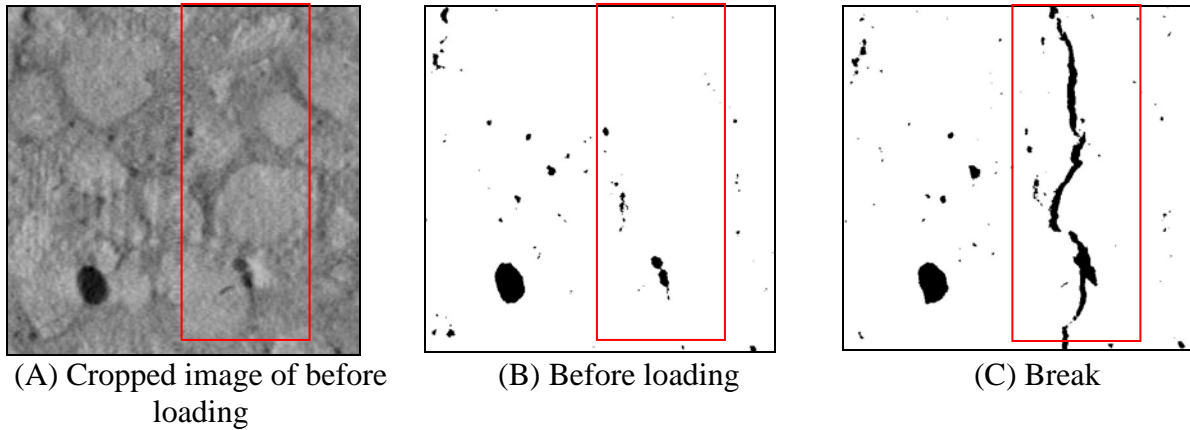


Figure D-51. Air voids at the location of 0.60 inches of 100% RAP-3 (voids dull)

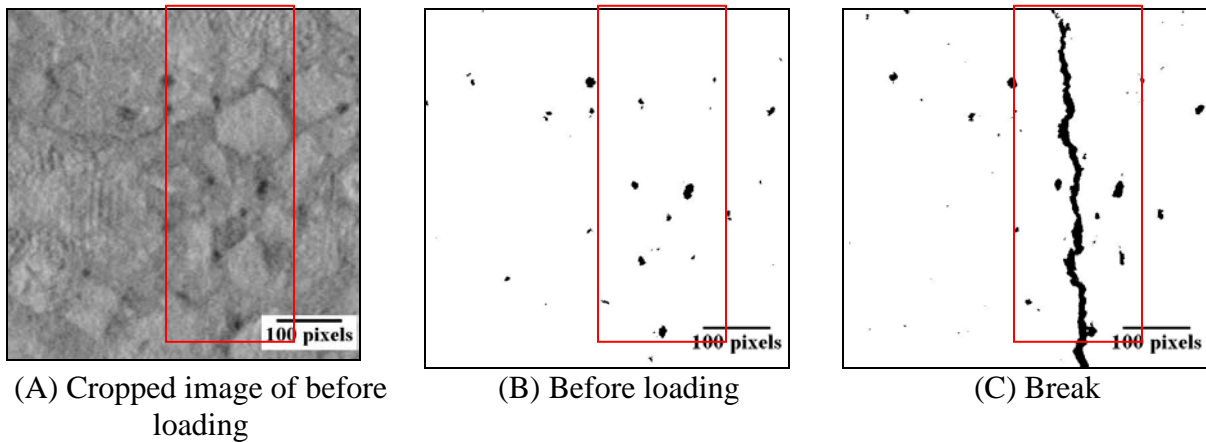


Figure D-52. Air voids at the location of 1.00 inches of 100% RAP-3 (voids growing)

The location at 0.09 inches found the air void distribution, compared with the shifted average, showing a reduction of voids; the location at 0.60 inches showed no voids variation; and the location at 1.0 indicated a slight growth in voids. The fracture pattern and voids variation can be seen on all (C) images with red marks. Air voids around both cliffs of fracture were visually less at location of 0.09 inches, seemingly no activities at the location of 0.60 inches, but slight enlargement at the location of 1.00 inches. It was obvious that the fracture itself had created a relatively enormous amount of voids and also pushed both plateaus away from each

other. It has to be assumed here that this separation only caused a trivial derivative error of air voids distribution.

Since it could be now recognized that the crack started from the vicinity of surface farther from the location of zero, propagating through the other end, the closing cracks may be explicable by the well-known crack analysis first proposed by Hillerborg (Hillerborg et al., 1976). It was described for the mode I crack—the opening due to the tensile stress. Due to the plasticization or tensile softening around the crack-tip, cracks around the tip may be closing by the lateral force generated along with the crack propagation. On the other hand, the rupture behavior of concrete may rip the microstructure apart instantaneously without softening both regions, hence no closing voids. In the concrete mix containing 100% RAP, the reduction in air voids around the fracture plane can be found between locations of zero to 0.60 inches, which may suggest the location of onset crack-tip.

Figure D-53 presents the fracture pattern of  $w/c=0.45$  PCC, which exhibited a rather straight vertical fracture plane, which also resembled similar observations of fracture plane in testing thin specimens with Superpave IDT strength test or flexural beam test of conventional ASTM C78. Additionally, the right-bottom air void appeared to siphon the fracture plane toward its vicinity, and eventually that plane connected with void. When compared with Figure D-50 (A) and (C), fracture in RAP concrete mixes developed a longer route than PCC and also noticeably propagated around aggregates. The more meanders in the route of the fracture plane, the more energy dissipates, which can support the result of higher toughness in concrete mixes containing RAP.

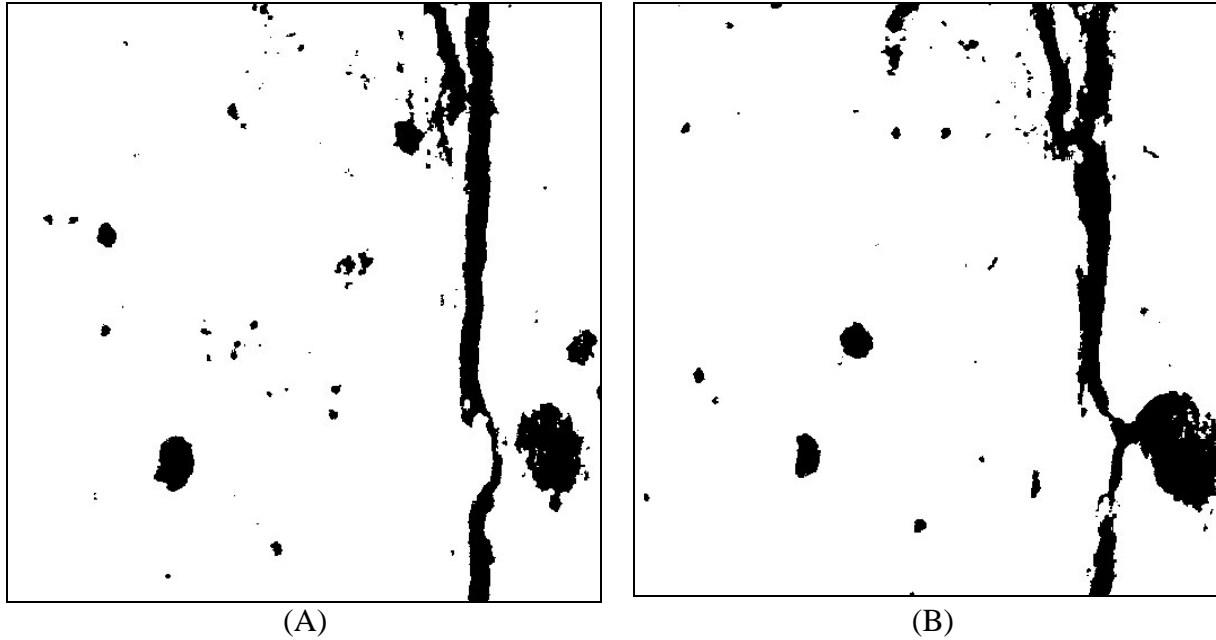


Figure D-53. Fracture pattern in w/c=0.45 PCC mix

### **D.13 Summary of Findings and Recommendations**

Portland Cement Concrete (PCC) and concrete incorporating RAP as aggregate were evaluated by the Superpave Indirect Tensile (IDT) strength test in this study. Concrete mixture properties were obtained from the IDT test using a constant force-control and a displacement-control rate. The properties obtained included tensile strength, elastic modulus, Poisson's ratio, and fracture energy. Stress—strain behavior of the concrete were also studied. The effects of temperature and different curing time to concrete properties were also investigated.

Relationships between the conventional and Superpave IDT tests were studied using the limited data obtained. Major research findings with regards to use the Superpave IDT strength test on concrete mixes are as follows:

- When the maximum load obtained from the Superpave IDT strength test was used to calculate the tensile strength of the concrete at 28 days curing time, the computed tensile strength from the Superpave IDT strength test correlated well with the corresponding splitting tensile strength from the conventional splitting tensile strength test.

- The elastic modulus and Poisson's ratio of the concrete obtained at 40% of its ultimate stress in the Superpave IDT strength test correlated well with the corresponding values obtained from the conventional compressive test.
- When the toughness is calculated by determining the area under the stress-strain plot up to the maximum stress, it can be used to differentiate between concretes containing different percentage of RAP.
- The tensile strength and Poisson's ratio of concrete as obtained from the Superpave IDT strength test using a displacement-control mode were very close to those obtained from the Superpave IDT strength test using a force-control mode.
- In running the Superpave IDT strength test on concrete specimens, when the concrete specimen was loaded beyond its elastic limit, the horizontal strain on one of the specimen face tended to go in the negative direction while the horizontal strain on the other face increased in the positive direction. However, this problem was not observed when concrete containing high percentage of RAP was tested.
- The tensile strength of concrete without RAP at early age was seen to increase as the temperature decreased. However, this effect of temperature was not seen among the concrete at later ages.
- The tensile strength of concrete containing RAP was seen to decrease as the %RAP increased. The tensile strength of concrete containing RAP was seen to decrease as the temperature increased.
- The addition of RAP in concrete noticeably reduced the elastic modulus of the concrete.
- Toughness of concrete was seen to increase as the %RAP in concrete increased.

Furthermore, the test procedures of X-ray Computed Tomography (CT) in conjunction with the Superpave IDT were developed. An image-processing technique was established to assess the distribution of air voids and to visualize the microcracking in concrete. The following are the main findings from this investigation:

- An image-processing technique for analyzing air voids was developed. For the test configuration used, the use of a threshold value of 87 gray levels (out of  $2^8=256$ ) was found to give good results in differentiating between air voids and non-air voids in the X-ray images of the concrete surface. The computer code for automatic processing of the X-ray image for calculation of air voids was successfully developed.

- It was found that there was very small variation in air voids for concrete with or without RAP. The maximum variation of air voids measured from the central area of the specimen was within  $\pm 0.3\%$  for all the concrete mixes tested.
- The volume of air voids in the concrete was observed to increase significantly when a concrete specimen was loaded to fracture.
- The air voids developed more on the specimen face where a crack initiated, but grew less on the other face.
- As a concrete specimen was loaded and unloaded, air voids which were formed tended to develop in the cement paste. This observation applies to both concrete with or without RAP.
- The path of crack propagation in concrete containing 100% RAP was found to be longer than that in concrete without RAP, as examined on virtual slices from X-ray CT scan. This explained the higher toughness in the concrete containing RAP.

Based on the research findings, the following recommendations are made:

- It is recommended to adopt the Superpave IDT strength test using a constant displacement-control rate of 0.00075 in/sec to test concrete mixtures in tension. More replicate tests are needed to obtain sufficient data to establish the relationships between the properties obtained by conventional tests and those by the Superpave IDT strength test.
- A protocol of fatigue test using the Superpave IDT test on concrete mixtures needs to be evaluated and established.
- The image-processing software to identify internal structural properties on the 3-D reconstructed model or the exported 2-D virtual slices needs to be developed.
- A technique to compensate for the beam-hardening effect around the edges of a specimen in a X-ray CT scan needs to be developed, so that the distribution of air voids on a whole concrete specimen could be properly determined. More trials on different combinations of geometry, voltage, and amperage are needed.
- The use of the Superpave IDT strength test in conjunction with the X-ray CT technique for the study of the stress-strain behavior of concrete beyond the elastic limit and crack initiation needs to be further studied.

## D.14 References

- AASHTO T322 (2007). *Standard Method of Test for Determining the Creep Compliance and Strength of Hot-Mix Asphalt (HMA) Using the Indirect Tensile Test Device*. American Association of State Highway and Transportation Officials, Washington DC.
- Alshibli, K. and Reed A. (2010). "Advances in Computed Tomography for Geomaterials." *GeoX 2010*, 28 February- 3 March, 2010, New Orleans, United States of America. London: ISTE, 2010. Print.
- ASTM C469 (2010). *Standard Test Method for Static Modulus of Elasticity and Poisson's Ratio of Concrete in Compression*. ASTM International, West Conshohocken, PA.
- ASTM C496 (2011). *Standard Test Method for Splitting Tensile Strength of Cylindrical Concrete Specimens*. ASTM International, West Conshohocken, PA.
- ASTM E 1411 (2011). *Standard Guide for Computed Tomography (CT) Imaging*. ASTM International, West Conshohocken, PA.
- Buttlar, W. G., and Roque, R. (1994). "Experimental Development and Evaluation of the Strategic Highway Research Program Measurement and Analysis for Indirect Tensile Testing at Low Temperature." *Trans. Res. Rec. 1454*, Transportation Research Board, National Research Council, Washington, D.C., 163–171.
- Desrues, J, Viggiani G., and Besuelle P. (2006). "Advances in X-Ray Tomography for Geomaterials." *GeoX 2006*, 4-7 October, 2006, Aussois, France. London: ISTE, Print.
- Farcas, F. A. (2012). "Evaluation of Asphalt Field Cores with Simple Performance Tester and X-ray Computed Tomography", *Licentiate Thes.*, Div. of Highway and Railway Eng., Dep. Tran. Sci., KTH Royal Institute of Technology, SE-110 44 Stockholm, Sweden.
- Hillerborg, A., Modéer, M., and Petersson, P. –E. (1976). "Analysis of crack formation and crack growth in concrete by means of fracture mechanics and finite elements." *Cem. Concr. Res.*, 6, 773-782.
- Hondros, G. (1959). "The Evaluation of Poisson's Ratio and the Modulus of Materials of a Low Tensile Resistane by the Brazilian (Indirect Tensile) test with particular reference to Concrete." *Australian J. App. Sci.*, 10(3), 243-268.
- Kim, S. (2005). "Direct Measurement of Asphalt Binder Thermal Cracking." *J. Mater. Civ. Eng.*, 17(6), 632–639.
- Landis, E. N. and Bolander J. E. (2010). "Integration of 3D Imaging and Discrete Element Modeling for Concrete Fracture Problems." *GeoX 2010*, 28 February- 3 March, 2010, New Orleans, United States of America. London: ISTE, Print, 117-123.
- Lane, E. (1987). *Guide to rocks and minerals of Florida*. Florida Geological Survey Special Publications 8, Tallahassee, Florida, 61.

- Lee, H, Kim, S., and Choubane, B. (2011). "Construction of Dynamic Modulus Master Curves Using Resilient Modulus and Creep Test Data." *Res. Rep. Num. FL/DOT/SMO/11-544*, State Material Office, Florida Department of Transportation, Gainesville, Florida.
- Mier, J G. M. (1997). *Fracture Processes of Concrete: Assessment of Material Parameters for Fracture Models*. Boca Raton: CRC Press.
- Ōtani, J. and Obara, Y. (2004). X-ray Ct for Geomaterials: Soils, Concrete, Rocks : Proceedings of the International Workshop on X-Ray Ct for Geomaterials. *Geox2003*, 6-7 November, 2003, Kumamoto, Japan. Lisse, the Netherlands: A.A. Balkema, Print.
- Roque R, Birgisson B, Sangpetngam B, Zhang Z. (2002). "Hot Mix Asphalt Fracture Mechanics: A Fundamental Crack Growth Law for Asphalt Mixtures." *J. Asso. Asph. Pav. Tech.*, 71, 816-827.
- Roque, R. and Buttlar, W. G. (1992). "The Development of a Measurement and Analysis System to Accurately Determine Asphalt Concrete Properties Using the Indirect Tension Mode." *J. Asso. Asph. Pav. Tech.*, 61, 304-332.
- Roque, R. Buttlar, W. G., Tia, M., Dickison, S. W. and Reid, B. (1997). "Evaluation of SHRP Indirect Tension Tester to Mitigate Cracking in Asphalt Concrete Pavements and Overlays." Final Rep., FDOT Project #0510755 (B9885), Department of Civil Engineering, Gainesville, Florida, 32611-6580
- Zhang, Z. (2000). "Identification of Suitable Crack Growth Law for Asphalt Mixtures Using the Superpave Indirect Tensile Test (IDT)." *Ph. D. dissertation*, Department of Civil Engineering, University of Florida, Gainesville, Florida 32611-6580
- Zhang, Z., Roque, R., Birgisson, B., and Sangpetngam, B. (2001). "Identification and Verification of a Suitable Crack Growth Law." *J. Asso. Asph. Pav. Tech.*, 70, 206-241.